# THE COMPUTATION OF WAVEGUIDE VECTOR FIELDS AND THE GENERATION OF FIELD PATTERNS USING COMPUTER GRAPHICS

by

M.L.X. dos Santos, Eng.; M.Sc.

Thesis submitted to the University of Leicester for the degree of Doctor of Philosophy.

April, 1979.

UMI Number: U622277

All rights reserved

INFORMATION TO ALL USERS
The quality of this reproduction is dependent upon the quality of the copy submitted.

In the unlikely event that the author did not send a complete manuscript
and there are missing pages, these will be noted. Also, if material had to be removed,
a note will indicate the deletion.

UMI®
Dissertation Publishing

UMI U622277
Published by ProQuest LLC 2015. Copyright in the Dissertation held by the Author.
Microform Edition © ProQuest LLC.
All rights reserved. This work is protected against
unauthorized copying under Title 17, United States Code.

ProQuest®

ProQuest LLC
789 East Eisenhower Parkway
P.O. Box 1346
Ann Arbor, MI 48106-1346

THESIS
582407
8 8 79

LEICESTER UNIVERSITY LIBRARY

X752977023

## SUMMARY

This thesis reports on the numerical evaluation of waveguide vector field distributions and on the display of vector results by means of computer graphics. The waveguide scalar functional is derived from the least action principle and a unified theory directed towards the numerical determination of waveguide propagation characteristics is presented. The application of the finite element method to the minimization of the waveguide scalar functional is also discussed. Numerical comparative results between the first-order finite element nodal equation and the five-point finite difference operator are produced to illustrate the dependence of these algebraic distributions on mesh length and mode complexity. The graphic techniques commonly employed to display waveguide mode patterns are analysed and a method of displaying general vector fields using an assembly of 3-dimensional oriented arrows is developed and described in detail. Examples of application of the proposed computerized graphic technique to a typical rectangular waveguide and to numerical results describing the electromagnetic field inside one-port rectangular waveguide junctions containing simple discontinuities are given.

M.L.X. dos SANTOS Ph.D. THESIS 1979

M. L. X. DOS SANTOS:
THE COMPUTATION OF WAVEGUIDE VECTOR FIELDS AND THE GENERATION OF FIELD PATTERNS USING COMPUTER GRAPHICS

This thesis reports on the numerical evaluation of waveguide vector field distributions and on the display of vector results by means of computer graphics. The waveguide scalar functional is derived from the least action principle and a unified theory directed towards the numerical determination of waveguide propagation characteristics is presented. The application of the finite element method to the minimization of the waveguide scalar functional is also discussed. Numerical comparative results between the first-order finite element nodal equation and the five-point finite difference operator are produced to illustrate the dependence of these algebraic distributions on mesh length and mode complexity. The graphic techniques commonly employed to display waveguide mode patterns are analysed and a method of displaying general vector fields using an assembly of 3-dimensional oriented arrows is developed and described in detail. Examples of application of the proposed computerized graphic technique to a typical rectangular waveguide and to numerical results describing the electromagnetic field inside one-port rectangular waveguide junctions containing simple discontinuities are given.

## ACKNOWLEDGEMENTS

It is a pleasure to be able to acknowledge my debt to Mr. A. J. Baden Fuller, for his patient guidance and many helpful suggestions throughout the research project and preparation of this thesis and for reading and commenting upon my work in all its stages. I have also profited much from my professional contacts with the staff of the Department of Engineering of the University of Leicester and of the University of Leicester Computer Laboratory. I would like to take this opportunity to express my gratitude to all of them.

As always, I owe the most to my family, especially my wife Myriam who not only provided me with encouragement and moral support throughout the many joys and trials of postgraduate research but who also typed this thesis with the utmost care and dedication.

I would gratefully acknowledge my indebtedness to the C. N. Pq. - Conselho Nacional de Desenvolvimento Cientifico e Tecnologico - for the research grant on the strength of which this work was carried out.

M.L.X.S.

Leicester, 1979.

CONTENTS

CHAPTER 1 INTRODUCTION . . . . . 1

1.1 Purpose . . . . . 1

1.2 Numerical Approach to Waveguide . . . . . 1

1.3 Unified Mathematical Treatment . . . . . 3

1.4 Comparative Results . . . . . 4

1.5 Field Patterns . . . . . 4

1.6 Original Contributions . . . . . 6

1.7 Nomenclature, Terminology and Symbols . . . . . 7

1.8 Conclusions and Future Developments . . . . . 7

CHAPTER 2 FUNDAMENTAL THEORY OF WAVEGUIDES . . . . . 8

2.1 Introduction . . . . . 8

2.2 Conditions for the Electromagnetic Potentials . . . 8

2.3 Maxwell's Equations and Boudary Conditions . . . . 14

2.4 Normal Mode Field Equations . . . . . 17

2.5 Orthogonality and Completeness of the Transverse Normal Mode Electric Field Intensities . . . . . 23

2.6 Variational Expression for the Propagation Function 26

2.7 Normal Mode Classification . . . . . 29

2.7.1 TEM Modes . . . . . 33

2.7.2 TE Modes . . . . . 35

2.7.3 TM Modes . . . . . 39

2.8 Cut-Off, Wave Impedance and Mode Duality . . . . . 40

2.9 Orthogonality and Completeness of the Normal Mode Field Intensities . . . . . 44

2.10 Power Flow and Power Orthogonality . . . . . 44

2.11 Field Expandability . . . . . 48

2.12 Complete Solution for Ideal Waveguides . . . . . 58

2.13 Scalar Waveguide Functional . . . . . 59

2.14 Non-Ideal Waveguides . . . . . 64

CHAPTER 3 THE FINITE ELEMENT METHOD FOR WAVEGUIDES . . . . . 65

3.1 Introduction . . . . . 65

3.2 The Finite Element Model of the Cross-Section . . . 66

3.3 Formalism of the First-Order Finite Element Model . 67

3.3.1 Finite Element Matrices . . . . . 72

3.3.2 Comparison with the Finite Difference Method 74

3.4 Higher Order Approximations and Other Applications 75

3.5 Calculation of the First-Order Finite Element Matrix Components . . . . . 75

3.6 Algebraic Form of the Coefficients $k_{ij}$ . . . . . 83

3.7 TEM Propagation and the Angular Form of the Coefficients $k_{ij}$ . . . . . 83

3.8 Compact Form of the Nodal Equation . . . . . 84

3.9 Approximations to the First-Order Finite Element Nodal Equation and the Five Point Finite Difference Operator . . . . . 85

3.10 A Simple Numerical Experiment in Rectangular Waveguide . . . . . 90

3.10.1 Method . . . . . 91

3.10.2 Boundary Values and Natural Boundary Conditions . . . . . 93

3.10.3 Results . . . . . 96

3.10.4 Conclusions . . . . . 119

3.11 Interpretation of the First-Order Finite Element Approximation in Terms of Triangle Area Co-ordinates . . . . . 120

3.12 Higher-Order Elements . . . . . 124

3.13 Formalism of the Higher-Order Finite Element Models 125

3.14 Calculation of the Matrices [ $S^e$ ] and [ $T^e$ ] . . . 131

3.15 Program Package for 2-D Field Problems . . . . . 133

3.15.1 Description . . . . . 133

3.15.2 Implementation . . . . . 134

3.15.3 Examples of Nodal Value Distributions . . . 135

3.15.4 Comparative Results . . . . . 139

3.16 Extension of the Higher-Order Finite Element Model to Solve d-Dimensional Helmholtz's Equations. . . . 146

3.17 Application of the Finite Element Minimization Technique to 3-D Vector Problems . . . . . 150

CHAPTER 4 WAVEGUIDE FIELD PATTERNS . . . . . 151

4.1 Introduction . . . . . 151

4.2 Basic Limitation of Waveguide Mode Patterns . . . . 153

4.3 Difficulties in the Interpretation of Field Intensity Variations by Means of Field Lines. . . . 154

4.3.1 Conventional Diagrams . . . . . 154

4.3.2 Automatically Generated Contour Diagrams . . 158

4.4 Regions of Pseudo Intense Field . . . . . 164

4.5 Perspective View of Waveguide Fields . . . . . 165

4.6 Phase and Polarization . . . . . 168

4.7 Alternative Graphic Techniques for Vector Field Representation . . . . . 168

4.8 3-Dimensional Representation of Vectors . . . . . 171

4.8.1 Plane Sample of a Vector Field . . . . . 174

4.8.2 Geometric Definitions . . . . . 176

4.8.3 Image of a Point on the Slice Surface . . . 181

4.8.4 3-Dimensional Representation and Frontal Image of a Vector . . . . . 183

4.8.5 General Image Co-Ordinates . . . . . 190

4.8.6 Picture Generation . . . . . 192

4.8.7 Segment Visibility and Image Degeneration . 196

4.8.8 Transverse Fields and Null Degenerated Images . . . . . 201

4.8.9 Specialized Image . . . . . 207

4.8.10 First Examples . . . . . 215

4.8.10.1 Transverse Field Diagrams . . . . 219

4.8.10.2 Non-Transverse Fields . . . . . 219

4.8.10.3 Electric and Magnetic Fields . . . 226

4.8.10.4 Polarization . . . . . 227

4.8.10.5 Phase Relationships,Longitudinal Variations and the Pseudo Increase in Field Intensity Effect . . . . 227

4.9 Visual Approximation to Field Lines . . . . . 231

4.10 Dynamic Diagrams . . . . . 240

4.11 Representation of General Volume Fields . . . . . 256

4.12 Field Information from the Scalar Nodal Value Distribution . . . . . 275

4.13 Direct Calculation of the Vector Component Distributions of General Cross-Section Waveguides . 288

CHAPTER 5 CONCLUSION . . . . . 291

5.1 Critique . . . . . 291

5.2 Results . . . . . 292

5.3 Future Developments . . . . . 293

APPENDICES . . . . . 295

APP.1 Integration of Eq.(3.39) and the Angular Form of the Coefficients $k_{0j}$ and $k_{ij}$ . . . . . 295

APP.2 Program Description : MXSNEX . . . . . 303

APP.3 Scalar Finite Element Program Package (Cambridge Version):Examples of Access and Use from Leicester. 310

APP.4 Orthogonal Projection of a Point onto a Plane . . . 340

APP.5 Program Description : MXSGUIA . . . . . 346

NOTATION . . . . . 363

BIBLIOGRAPHY . . . . . 395

# FIGURES


2.1 Finite Volume and the Electromagnetic Potentials . . . . . 11

2.2 Boundary Conditions for Perfect Dielectric . . . . . 16

2.3 Boundary Conditions on a Perfect Conducting Surface . . . 18

2.4 Waveguide Cross-Section. . . . . 20

3.1 Waveguide Cross-Section and Nodal Points . . . . . 69

3.2 Finite Element Cross-Section Model . . . . . 70

3.3 The Element J Adjoining Node $N_0$ . . . . . 76

3.4 Finite Element Division of a Regular Mesh . . . . . 86

3.5 Rectangular Waveguide Cross-Section for Numerical Experimentation . . . . . 92

3.6 Area Co-Ordinates . . . . . 122

3.7 $4^{th}$ Order Element . . . . . 126

3.8 Single Subscript Numbering System . . . . . 127

4.1 $TE_{10}$ Electric Field Lines (5 lines) . . . . . 156

4.2 $TE_{10}$ Electric Field Lines (19 lines) . . . . . 157

4.3 $TE_{10}$ Contour Map . . . . . 161

4.4 $TM_{11}$ Contour Map . . . . . 162

4.5 $TE_{11}$ Contour Map . . . . . 163

4.6 $TM_{11}$ Pseudo Intense Field Region . . . . . 166

4.7 $TE_{11}$ Pseudo Intense Field Region . . . . . 167

4.8 Perspective Field Plotting . . . . . 169

4.9 $TE_{10}$ 3-D Field Line Display . . . . . 172

4.10 $TM_{11}$ 3-D Field Line Display . . . . . 173
4.11 Bounded Region and Plane Sample . . . . . 175
4.12 Sample Points . . . . . 177
4.13 Reference Systems . . . . . 179
4.14 Advancing and Elevating Angles . . . . . 180
4.15 Local Reference System. . . . . 182
4.16 3-Dimensional Arrow Representing the Vector Quantity $\underline{V}_c$ . 185
4.17 Orthogonal Image of the 3-D Arrow onto the Sampling Plane 186
4.18 Image Segments . . . . . 189
4.19 Drawing Sequence . . . . . 193
4.20 Examples of Positive and Negative Frontal Images . . . . 198
4.21 Plane Arrow . . . . . 203
4.22 Specialized Image . . . . . 214
4.23 $TE_{10}$ Transverse Field Display . . . . . 220
4.24 $TM_{11}$ Transverse Field Display . . . . . 221
4.25 $TM_{21}$ Transverse Field Display . . . . . 222
4.26 $TE_{10}$ Non-Transverse Field Display . . . . . 223
4.27 $TM_{11}$ Non-Transverse Field Display . . . . . 224
4.28 $TM_{21}$ Non-Transverse Field Display . . . . . 225
4.29 $TM_{21}$ Electromagnetic Field Distribution Display . . . . . 228
4.30 $TM_{22}$ Electromagnetic Field Distribution Display . . . . . 229
4.31 Circular Polarization . . . . . 230
4.32 Plane Samples in a Rectangular Waveguide . . . . . 232
4.33 Rectangular Waveguide Sample Sequence (1) . . . . . 233
4.34 Rectangular Waveguide Sample Sequence (2) . . . . . 234
4.35 Rectangular Waveguide Sample Sequence (3) . . . . . 235
4.36 Rectangular Waveguide Sample Sequence (4) . . . . . 236
4.37 Rectangular Waveguide Sample Sequence (5) . . . . . 237

4.38 Rectangular Waveguide Sample Sequence (6) . . . . . 238
4.39 Field Behaviour Along the Longitudinal Direction . . . . 239
4.40 Dynamic Display Sequence (1) . . . . . 243
4.41 Dynamic Display Sequence (2) . . . . . 244
4.42 Dynamic Display Sequence (3) . . . . . 245
4.43 Dynamic Display Sequence (4) . . . . . 246
4.44 Dynamic Display Sequence (5) . . . . . 247
4.45 Dynamic Display Sequence (6) . . . . . 248
4.46 Dynamic Display Sequence (7) . . . . . 249
4.47 Dynamic Display Sequence (8) . . . . . 250
4.48 Dynamic Display Sequence (9) . . . . . 251
4.49 Dynamic Display Sequence (10) . . . . . 252
4.50 Dynamic Display Sequence (11) . . . . . 253
4.51 Dynamic Display Sequence (12) . . . . . 254
4.52 Dynamic Display Sequence (13) . . . . . 255
4.53 Microwave Junction and Sampling Planes . . . . . 257
4.54 Plane Sample (1) . . . . . 258
4.55 Plane Sample (2) . . . . . 259
4.56 Plane Sample (3) . . . . . 260
4.57 Plane Sample (4) . . . . . 261
4.58 Plane Sample (5) . . . . . 262
4.59 Plane Sample (6) . . . . . 263
4.60 Plane Sample (7) . . . . . 264
4.61 Plane Sample (8) . . . . . 265
4.62 Plane Sample (9) . . . . . 266
4.63 Plane Sample (10) . . . . . 266
4.64 Plane Sample (11) . . . . . 267
4.65 Microwave Junction and Sampling Planes . . . . . 268

4.66 Plane Sample (1) . . . . . 269

4.67 Plane Sample (2) . . . . . 270

4.68 Plane Sample (3) . . . . . 271

4.69 Plane Sample (4) . . . . . 272

4.70 Plane Sample (5) . . . . . 273

4.71 Plane Sample (6) . . . . . 274

4.72 $TE_{10}$ Field Distribution from the Nodal Values . . . . . 289

A1.1 Local Co-Ordinate System for Integration of Eq.(3.39) . . 296

A1.2 Vertices and Angles of an Element . . . . . 302

A3.1 Finite Element Division of the Cross-Section . . . . . 311

A3.2 Nodal Distribution on the Cross-Section . . . . . 315

A4.1 Orthogonal Projection . . . . . 341

A5.1 Geometry of the Waveguide Sample . . . . . 348

A5.2 Output Format and Mapping . . . . . 349

A5.3 Program Organization . . . . . 361

## MAPS AND TABLES

2.1 Method for constructing the finite element model of a primitive region . . . . . 68

3.1 Results obtained when estimating the central node values of the $TE_{10}$ generating function (36 internal points). . . 99

3.2 Percentual errors when estimating the central node values of the $TE_{10}$ distribution using the finite difference formula (36 internal points) . . . . . 99

3.3 Percentual errors when estimating the central node values of the $TE_{10}$ distribution using the finite element and the symmetric finite element formulae (36 internal points). . 101

3.4 Analytical node values of the $TM_{11}$ generating function (36 internal points). . . . . 102

3.5 Central node values estimated by the finite difference formula for the $TM_{11}$ mode (36 internal points). . . . . 103

3.6 Central node values estimated by the finite element formula for the $TM_{11}$ mode (36 internal points) . . . . . 104

3.7 Central node values estimated by the symmetric finite element formula for the $TM_{11}$ mode (36 internal points). . 105

3.8 Percentual errors when estimating the central node values of the $TM_{11}$ distribution using the finite difference formula (36 internal points) . . . . . 106

3.9 Percentual errors when estimating the central node values of the $TM_{11}$ distribution using the finite element formula (36 internal points) . . . . . 107

3.10 Percentual errors when estimating the central node values of the $TM_{11}$ distribution using the symmetric element formula (36 internal points) . . . . . 108

3.11 Results obtained when estimating the central node values of the $TE_{10}$ generating function (78 internal points). . . 109

3.12 Percentual errors when estimating the central node values of the $TE_{10}$ distribution using the finite difference formula (78 internal points) . . . . . 110

3.13 Percentual errors when estimating the central node values of the $TE_{10}$ distribution using the finite element formula (78 internal points). . . . . 111

3.14 Analytical node values of the $TM_{11}$ generating function (78 internal points). . . . . 112

3.15 Central node values estimated by the finite difference formula for the $TM_{11}$ mode (78 internal points) . . . . . 113

3.16 Central node values estimated by the finite element formula for the $TM_{11}$ mode (78 internal points) . . . . . 114

3.17 Central node values estimated by the symmetric finite element formula for the $TM_{11}$ mode (78 internal points). . 115

3.18 Percentual errors when estimating the central node values of the $TM_{11}$ distribution using the finite difference formula (78 internal points) . . . . . 116

3.19 Percentual errors when estimating the central node values of the $TM_{11}$ distribution using the finite element formula (78 internal points). . . . . 117

3.20 Percentual errors when estimating the central node values of the $TM_{11}$ distribution using the symmetric finite element formula (78 internal points). . . . . 119

3.21 Nodal values of the generating function of the $TE_{10}$ mode obtained by using the finite element program package. . . 136

3.22 Nodal values of the generating function of the $TM_{11}$ mode obtained by using the finite element program package. . . 137

3.23 Nodal values of the generating function of the $TE_{11}$ mode obtained by using the finite element program package. . . 138

3.24 Nodal values of the generating function of the $TE_{10}$ mode obtained by using the analytical expression . . . . . 140

3.25 Nodal values of the generating function of the $TM_{11}$ mode obtained by using the analytical expression . . . . . 141

3.26 Percentual errors in the nodal value distribution of the $TE_{10}$ mode, obtained by using the finite element program package . . . . . 142

3.27 Percentual errors in the nodal value distribution of the $TM_{11}$ mode, obtained by using the finite element program package . . . . . 143

3.28 Nodal values of the generating function of the $TE_{11}$ mode obtained by using the analytical expression . . . . . 144

3.29 Percentual errors in the nodal value distribution of the $TE_{11}$ mode, obtained by using the finite element program package . . . . . 145

4.1 Image segment visibility (Table) . . . . . 202

4.1 x-Component of $\nabla_T G_{10}$ obtained from the nodal value distribution (Map) . . . . . 278

4.2 y-Component of $\nabla_T G_{10}$ obtained from the nodal value distribution . . . . . 279

4.3 Distribution of the normalized $h_z$ component for the $TE_{10}$ mode . . . . . 283

4.4 Distribution of the normalized $h_y$ component for the $TE_{10}$ mode . . . . . 284

4.5 Distribution of the normalized $h_x$ component for the $TE_{10}$ mode . . . . . 285

4.6 Distribution of the normalized $e_x$ component for the $TE_{10}$ mode . . . . . 286

4.7 Distribution of the normalized $e_y$ component for the $TE_{10}$ mode . . . . . 287

A2.1 Input variables in the program MXSNEX . . . . . 306

A2.2 Routines in the program MXSNEX. . . . . 309

A3.1 Constraints (sides on boundary) . . . . . 320

A3.2 Constraints (sides inside cross-section). . . . . 320

A3.3 Scale factors . . . . . 320

A3.4 Node identification and positioning . . . . . 321

A3.5 Element identification and properties (TE modes). . . . . 321

A3.6 Element identification and properties (TM modes). . . . . 321

A3.7 Data cards. . . . . 322

A3.8 Default conditions . . . . . 323

A3.9 Error indicator . . . . . 324

Error indicator (continue) . . . . . 325

A5.1 Input variables (MXSGUIA) . . . . . 351

A5.2 Variables SHAPE, CUT and IORDM . . . . . 352

A5.3 Program organization (MXSGUIA). . . . . 360

# CHAPTER 1

# INTRODUCTION

## 1.1 PURPOSE

The object of this chapter is to provide a brief outline of the thesis and the context in which it was developed. The main topics are presented in summarized form to give a global perspective of its contents. The main original contributions are highlighted.

## 1.2 THE NUMERICAL APPROACH TO WAVEGUIDES

The technological improvement in digital computation over the last few years has been accompanied by renewed interest in the numerical solution of microwave problems. Among these, the determination of basic mode characteristics of arbitrarily shaped waveguides, such as cut-off wave-number and field configuration, has been extensively treated(1). Using the fast improving computer facilities, it is possible to apply the finite difference method very efficiently. The method was no novelty and had already been applied by MOTZ(2) in 1946 to analyse klystron cavities.

The scalar Helmholtz equation was solved for a variety of cross-section shapes as, for example, the conventional rectangular and ridged waveguides treated by COLLINS and DALY(3) and the lunar and

T-Septate circular waveguides studied by BEAUBIEN and WEXLER[4]. The first general purpose program using finite difference methods[5] was reported by DAVIES and MUILWYK[6]. The applications, however , displayed some shortcomings of the finite difference technique, namely:

a) - equispaced distribution of nodal values over the cross-section;

b) - difficulty of approximating complicated curved boundaries;

c) - need to introduce "image points" to establish the boundary conditions for TE modes.

The foregoing difficulties would not occur if the finite element method, used for example by COURANT[7] in 1943 to solve problems of equilibrium and vibrations, were employed. In this respect the early works of ZIENKIEWICZ[8], DALY[9] and SILVESTER[10] were significant. These works were then followed by successive relevant contributions by SILVESTER culminating with the publication, together with KONRAD, of an extremely useful and versatile program package for two-dimensional field problems[11]. Many other relevant publications appeared and the application of numerical techniques for modeling passive microwave devices expanded quickly. SILVESTER and CSENDES[5] reckon that it produced, up to the beginning of 1974, approximately 10 000 papers covering various mathematical formulations including the finite difference and finite element analysis. Half of these papers could, then, be regarded as recent. Nowadays, the application of the finite element method occupies a prominent place in waveguide analysis and can be regarded as a well established technique. Chapter 3 is devoted to this technique.

## 1.3 UNIFIED MATHEMATICAL TREATMENT

The variational method used to formulate the finite element approach to waveguide problems shifts the emphasis from the field curvature inside the structure to the extremization of a functional. Here, contrary to what happens with the finite difference method, which discretizes the differential equation governing the field distributions, the finite element method brings attention to the energy relationships prevailing in the propagation. The scalar Helmholtz equation comes up being the Euler-Lagrange equation of the functional. In order to understand the solution of the waveguide problem by the finite element method, it is necessary to relate the functional to a physical principle from which it can be obtained.

In general, the literature takes explicitly the waveguide functional as related to the electromagnetic energy but does not precisely establish the physical grounds of the formulation. It is on those grounds, however, that this energy relationship and the functional itself can be understood.

A precise interpretation of the waveguide functional and its formulation based on a physical principle governing the waveguide field is presented in this work. The development of the theory leading to the expression of the functional has been based on the work of MORISHITA and KUMAGAI[12]. They have shown that the variational expressions for guided propagation can rigorously be obtained from the least action principle. Extensive use of the works of KUROKAWA[13][14][15] enabled the presentation, in Chapter 2, of a unified mathematical treatment directed towards the numerical determination of the waveguide propagation characteristics.

## 1.4 COMPARATIVE RESULTS

A theoretical comparison between the finite difference and the first-order finite element operators is presented. The material is largely influenced by the excellent paper by KINSNER and TORRE[16]. It goes further, however, to provide computed results for both operators compared with the exact values of the potential function of a typical rectangular waveguide. The exact values are to be understood here as the values computed through the analytical expression for the potential function.

Numerical evidence in the form of percentual error maps is produced. They show that, for low order modes, a good accuracy can be expected from both operators. Also, the accuracy of the nodal value distribution obtained by using the finite element operator (and of the finite difference operator)is shown to deteriorate when higher modes are considered. The need to increase the order of the finite element polynomial interpolation of the potential function is, therefore, numerically demonstrated.

Finally, a brief description of the program package[11] used to generate finite element results for the first modes inside a typical rectangular waveguide is presented. Percentual error maps for those modes are produced. The examples obtained are used later in order to illustrate the generation of field patterns from numerically evaluated nodal value distributions.

## 1.5 FIELD PATTERNS

A set of numbers is only meaningful when interpreted in terms of the quantities it relates to. In the case of waveguides, the set

of numbers appearing on the print-out gives the value of the longitudinal component of the non-transverse propagating field on prescribed points over the cross-section. The direct obtainable information about the field distribution inside the structure is, therefore, quite restricted. In order to appreciate the results, further operations need to be performed on the output values. These operations must lead to the characterization of the electromagnetic behaviour of the structure in a convenient form. Because there is no analytical expression to characterize the space dependence of the field distribution, a graphic image or diagram ought to be produced to convey this information.

Usually the graphic image of the field distribution over the waveguide cross-section is obtained by contouring the nodal value distributions(17). It is shown in this thesis that contour maps are not, however, always convenient for describing the electromagnetic field distribution. The difficulties in the generation and interpretation of such field maps are discussed. Also, the conventional field line diagrams used in microwave engineering for the purpose of describing waveguide fields are questioned. The inadequacy of such diagrams for electrodynamical situations is fully characterized.

An alternative method for representing waveguide fields in particular and vector fields in general, using computer graphics, is proposed. It consists of generating field patterns for which the vector quantity is precisely and uniquely represented by oriented 3-dimensional arrows at representative points of the space. It is shown that the resulting diagrams constitute a complete representa-

tion of the vector quantity. Information about intensity, direction, polarization and phase can be displayed by using these diagrams. Examples of field patterns obtained from the analytical expressions for the electric and magnetic fields of low order modes in a typical rectangular waveguide are presented. Dynamical computerized film displays of rectangular waveguide fields are being experimentally generated and pertinent comments are also made.

The generation of the proposed field patterns from the scalar nodal value distributions obtained by the finite element method is discussed and an example provided. This involves the numerical differentiation of the nodal value distribution , and the stability of the process is discussed.

Finally, the difficulty of interpreting 3-dimensional vector finite element results is dealt with. Examples of the application of the field pattern technique to 3-dimensional numerically evaluated waveguide discontinuity fields are presented to show the adequacy and simplicity of the method. This material appears in Chapter 4.

## 1.6 ORIGINAL CONTRIBUTIONS

The main original contributions to the knowledge of the computation and display of waveguide fields presented in this thesis can be summarized as follows:

- Presentation of a unified mathematical treatment of waveguides, directed towards numerical computation.

- Proposal of a computer graphic technique for displaying vector fields in general and waveguide fields in particular.

Other original contributions appear in the text. They are regarded as consequential to the development of the topics listed above.

## 1.7 NOMENCLATURE, TERMINOLOGY AND SYMBOLS

Wherever possible, the terminology and nomenclature in this thesis have been used in accordance with the commom practice in the literature. However, when attachment to the usual terminology would conflict with well established concepts, the author used his personal judgement to replace names. This is clearly indicated in the text. A list of symbols is incorporated.

## 1.8 CONCLUSIONS AND FUTURE DEVELOPMENTS

The conclusions arrived at during the development of the research work reported in this thesis and suggestions for possible future developments on the subjects treated are presented in Chapter 5.

# CHAPTER 2

# FUNDAMENTAL THEORY OF WAVEGUIDES

## 2.1 INTRODUCTION

The field configuration inside ideal waveguides can be obtained numerically through the minimization of a functional[8][9][10] associated with the electromagnetic energy. The functional is developed by using variational methods, either:

a) by performing operations into a known satisfied differential equation for a suitable scalar potential function[18][19][20]

or,

b) by producing by trial and error the relevant stationary expression[13][21]

or,

c) by resorting to a fundamental physical principle enabling its systematic derivation[12][22][23].

The first approach is formally consistent but leads to complementary or transpose quantities which are difficult to interprete while the second depends on ingenuity and labour and will not be considered here. The third alternative will be adopted in the present work as a proposal for the presentation of the fundamental theory of waveguides.

The objective of the chapter is to present a theory where the numerical solution of the field equations appears naturally from a physical principle governing the electromagnetic field rather than as a mathematical diversion avoiding the solution of differential equations. The validity and simplicity of the usual practice of starting by stating the ideal waveguide problem as a functional minimization problem is not being questioned. However, it seems to the author that in Microwave Engineering considerable enlightment of the formalism is gained by placing the emphasis on physical principles.

This chapter has been written to demonstrate that such treatment can be presented mostly by adapting and bringing together derivations available in the literature (see references) into a logical order. Furthermore, it will be shown in the chapter that, as the scalar functional expression for the waveguide is derived from the least action principle for electromagnetic quantities, its association to the electromagnetic energy is not direct, but established through the action integral. Also, it will be demonstrated that an interpretation of the functional in terms of the error in estimating the field configuration is consistent with the physical principle governing the fields.

Finally, some well known waveguide normal mode properties are introduced into the chapter for the purpose of achieving a global comprehension of the matter.

## 2.2 CONDITIONS FOR THE ELECTROMAGNETIC POTENTIALS

Consider the Lagrange function for electromagnetic quantities[24]:

$$Lg = \frac{1}{2} \iiint [\, \underline{E}(\underline{r},t) \cdot \underline{D}(\underline{r},t) - \underline{H}(\underline{r},t) \cdot \underline{B}(\underline{r},t) \,]\, dV$$

$$+ \iiint [\, \underline{A}(\underline{r},t) \cdot \underline{J}(\underline{r},t) - Q(\underline{r},t) \;\; F(\underline{r},t) \,]\, dV \qquad (2.1)$$

where

$$\underline{E}(\underline{r},t) = - [\, \frac{\delta}{\delta t} \;\; \underline{A}(\underline{r},t) + \text{grad } F(\underline{r},t) \,] \qquad (2.2)$$

$$\underline{B}(\underline{r},t) = \text{curl } \underline{A}(\underline{r},t) \qquad (2.3)$$

V is a volume enclosed by the surface S, t the time and $\underline{r}$ the position vector of a point in V as illustrated in Fig.(2.1). The electric charge density and the electric current density are denoted respectively by $Q(\underline{r},t)$ and $\underline{J}(\underline{r},t)$. The functions $F(\underline{r},t)$ and $\underline{A}(\underline{r},t)$ are the scalar and vector electromagnetic potentials satisfying the pertinent gauge condition[25]:

$$\text{div } \underline{A}(\underline{r},t) = G_t \; (F(\underline{r},t)) \qquad (2.4)$$

where $G_t$ is a function of time to be specified later.

The electric and magnetic field intensities are $\underline{E}(\underline{r},t)$ and $\underline{H}(\underline{r},t)$, related to the electric and magnetic flux densities $\underline{D}(\underline{r},t)$ and $\underline{B}(\underline{r},t)$ by the constitutive relations

$$\underline{D}(\underline{r},t) = \varepsilon \; \underline{E}(\underline{r},t) \qquad (2.5)$$

$$\underline{B}(\underline{r},t) = \mu \, \underline{H}(\underline{r},t) \qquad (2.6)$$

where $\varepsilon$ and $\mu$ are the permittivity and the permeability of the

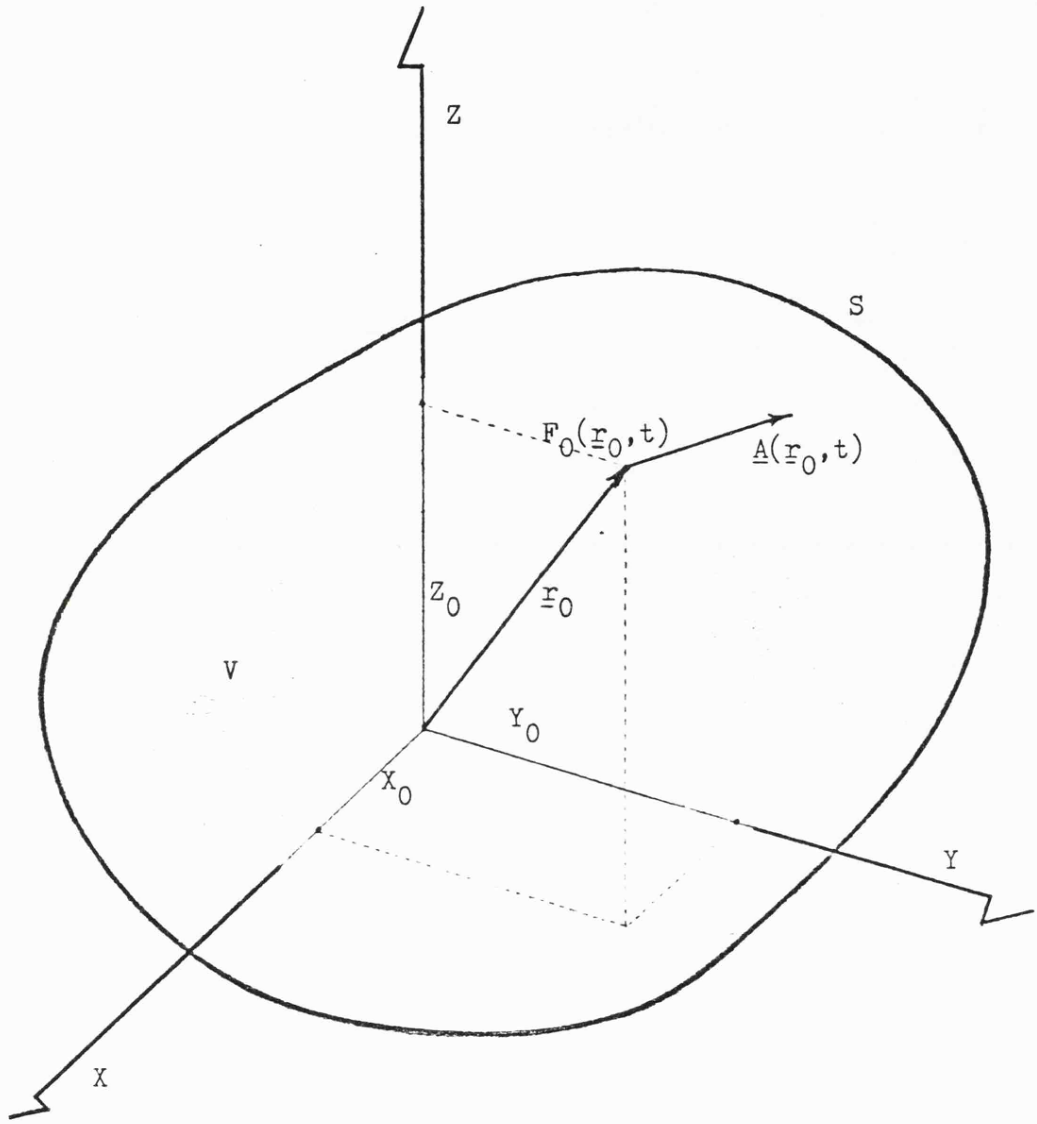


FIG.2.1 FINITE VOLUME AND THE ELECTROMAGNETIC POTENTIALS

The electromagnetic potentials involved in calculating the Lagrange function for the electromagnetic field.

medium enclosed by S of V, assumed to be perfect, i.e., lossless , linear, isotropic and homogeneous.

The least action principle for electromagnetic quantities states that the electromagnetic fields which may exist in V during the time interval $(t_i, t_f)$ are those related to the potentials $\underline{A}(\underline{r},t)$ and $F(\underline{r},t)$ for which the action

$$I_t = \int_{t_i}^{t_f} Lg \, dt \tag{2.7}$$

is stationary.

Extending the time interval from $(-\infty)$ to $(+\infty)$ and introducing the Fourier transforms (FT [ ] ) of the electromagnetic quantities in eq.(2.1), denoted by

$$\mathrm{FT}\,[\, s(\underline{r},t)\,] = s(\underline{r},\omega) \tag{2.8}$$

$$\mathrm{FT}\,[\, \underline{v}(\underline{r},t)\,] = \underline{v}(\underline{r},\omega) \tag{2.9}$$

the action given by eq.(2.7) can be written in the form:

$$I_\omega = \frac{1}{2\pi} \int_{-\infty}^{\infty} \frac{1}{2} \iiint [\underline{E}(\underline{r},\omega) \cdot \underline{D}^*(\underline{r},\omega) - \underline{H}(\underline{r},\omega) \cdot \underline{B}^*(\underline{r},\omega)] \, dV \, d\omega$$

$$+ \frac{1}{2\pi} \int_{-\infty}^{\infty} \iiint [\underline{A}(\underline{r},\omega) \cdot \underline{J}^*(\underline{r},\omega) - Q(\underline{r},\omega) \, F^*(\underline{r},\omega)] \, dV \, d\omega \tag{2.10}$$

where $\omega$ is the angular frequency, $\underline{D}^*(\underline{r},t)$ and $\underline{B}^*(\underline{r},t)$ are the complex conjugates of $\underline{D}(\underline{r},t)$ and $\underline{B}(\underline{r},t)$ etc. The frequency domain counterparts of eq.(2.2),(2.3),(2.5) and (2.6) are given by:

$$\underline{E}(\underline{r},\omega) = - [\ i\omega\, \underline{A}(\underline{r},\omega) + \text{grad}\ F(\underline{r},\omega)\ ] \tag{2.11}$$

$$\underline{B}(\underline{r},\omega) = \text{curl}\ \ \underline{A}(\underline{r},\omega) \tag{2.12}$$

$$\underline{D}(\underline{r},\omega) = \varepsilon\, \underline{E}(\underline{r},\omega) \tag{2.13}$$

$$\underline{B}(\underline{r},\omega) = \mu\, \underline{H}(\underline{r},\omega) \tag{2.14}$$

Denoting the first order variation of $I_\omega$ due to a small variation in $F(\underline{r},\omega)$ by $\delta_F I_\omega$ and similarly denoting by $\delta_A I_\omega$ the first-order variation of $I_\omega$ due to a small variation in $\underline{A}(\underline{r},\omega)$ the use of the least action principle and the frequency domain counterpart of eq.(2.4) yields:

$$\text{div}\ \underline{A}(\underline{r},\omega) = G_\omega\ (F(\underline{r},\omega\ )) \tag{2.15}$$

$$\delta_F I_\omega = 0 \tag{2.16}$$

$$\delta_A I_\omega = 0 \tag{2.17}$$

## 2.3 MAXWELL'S EQUATIONS AND BOUNDARY CONDITIONS

The electromagnetic quantities in V must be real functions of time and so eq.(2.8) and eq.(2.9) can be written in the form:

$$FT\,[\,s(\underline{r},t)\,] = s^*(\underline{r},-\omega) \tag{2.18}$$

$$FT\,[\,\underline{v}(\underline{r},t)\,] = \underline{v}^*(\underline{r},-\omega) \tag{2.19}$$

Substituting eq.(2.13) and eq.(2.14) into eq.(2.10) and taking into account eq.(2.18) and eq.(2.19) it can be shown that the unilateral expression for the frequency domain action is given by[12]:

$$I = \frac{1}{2\pi}\int_0^\infty \iiint \left[\frac{\varepsilon}{2}(\underline{E}^*\cdot\underline{E} + \underline{E}\cdot\underline{E}^*) - \frac{\mu}{2}(\underline{H}^*\cdot\underline{H} + \underline{H}\cdot\underline{H}^*)\right] dV\, d\omega$$

$$+ \frac{1}{2\pi}\int_0^\infty \iiint \left[(\underline{A}^*\cdot\underline{J} + \underline{A}\cdot\underline{J}^*) - (QF^* + Q^*F)\right] dV\, d\omega \tag{2.20}$$

with $\underline{E}$, $\underline{H}$, $\underline{A}$, F, etc., denoting hereafter, unless otherwise specified implicit dependence of the quantities upon space and angular frequency.

The first-order variations of the action in eq.(2.20) due to a small change $\delta F$ in F and due to a small change $\delta\underline{A}$ in $\underline{A}$ are given by

$$\delta_F I = \frac{1}{2\pi}\int_0^\infty \iiint \delta F^*\,(\mathrm{div}\,\varepsilon\,\underline{E} - Q)\, dV\, d\omega$$

$$+ \frac{1}{2\pi}\int_0^\infty \iiint \delta F\,(\mathrm{div}\,\varepsilon\,\underline{E} - Q)^*\, dV\, d\omega \tag{2.21}$$

$$\delta_A \; I_\omega = \frac{1}{2\pi} \int_0^\infty \iiint \delta \underline{A}^* \cdot (i\omega\varepsilon \underline{E} - \text{curl } \underline{H} + \underline{J}) \, dV \, d\omega$$

$$+ \frac{1}{2\pi} \int_0^\infty \iiint \delta \underline{A} \cdot (i\omega\varepsilon \underline{E} - \text{curl } \underline{H} + \underline{J})^* \, dV \, d\omega \qquad (2.22)$$

Applying the least action conditions for the electromagnetic potentials given by eq.(2.16) and eq.(2.17) to eq.(2.21) and (2.22) respectively, calculating the curl of eq.(2.11), the divergence of eq.(2.12) and using the constitutive relations, Maxwell's equations for time harmonic fields are obtained:

$$\text{div } \underline{D} = Q \qquad (2.23)$$

$$\text{curl } \underline{H} = \underline{J} + i\omega\varepsilon \underline{E} \qquad (2.24)$$

$$\text{curl } \underline{E} = - i\omega\mu \underline{H} \qquad (2.25)$$

$$\text{div } \underline{B} = 0 \qquad (2.26)$$

The boundary conditions for the electromagnetic vectors are established by applying Maxwell's equations on the interface between two perfect media $M_1(\varepsilon_1, \mu_1)$ and $M_2(\varepsilon_2, \mu_2)$, characterized by permittivities $\varepsilon_1$ and $\varepsilon_2$ and permeabilities $\mu_1$ and $\mu_2$, as illustrated in Fig.(2.2), in the form:

$$\underline{n} \times (\underline{E}_2 - \underline{E}_1) = 0 \qquad (2.27)$$

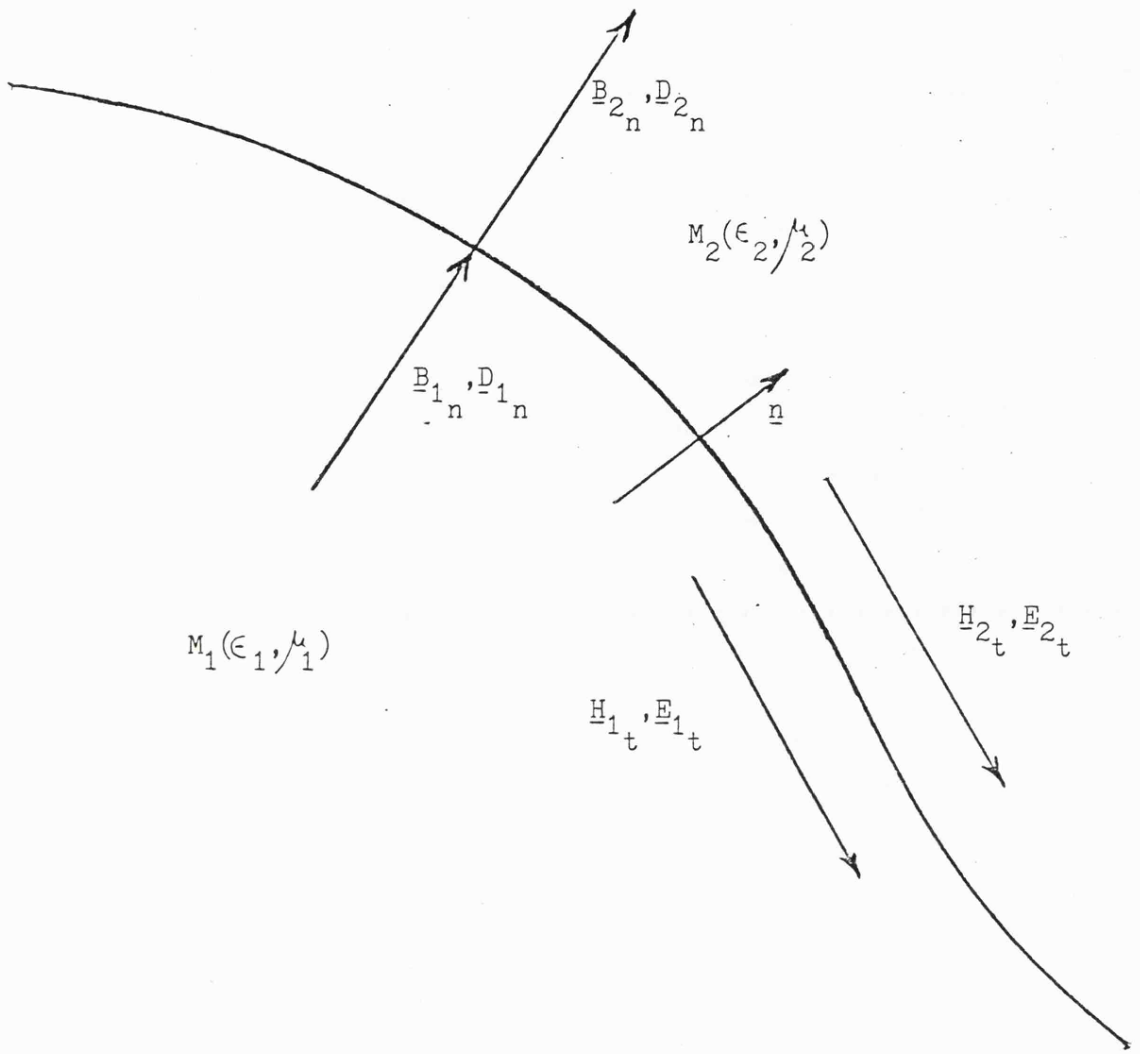


FIG.2.2 BOUNDARY CONDITIONS FOR PERFECT DIELECTRICS

Schematic representation of the continuity of the normal components of the flux densities and tangential components of the field intensities on the interface between two media.

$$\underline{n} \times (\underline{H}_2 - \underline{H}_1) = 0 \tag{2.28}$$

$$\underline{n} \cdot (\underline{D}_2 - \underline{D}_1) = 0 \tag{2.29}$$

$$\underline{n} \cdot (\underline{B}_2 - \underline{B}_1) = 0 \tag{2.30}$$

When the interface between $M(\varepsilon, \mu)$ and a perfect conducting medium $M_c$ is considered the boundary conditions for the electromagnetic vectors become

$$\underline{n} \times \underline{E} = 0 \tag{2.31}$$

$$\underline{n} \times \underline{H} = \underline{J}_s \tag{2.32}$$

$$\underline{n} \cdot \underline{D} = Q_s \tag{2.33}$$

$$\underline{n} \cdot \underline{B} = 0 \tag{2.34}$$

where $\underline{J}_s$ and $Q_s$ are the surface current and surface charge densities. The situation is depicted in Fig.(2.3).

## 2.4 NORMAL MODE FIELD EQUATIONS

Consider a general loss-free cylindrical region confined by a finite number of closed perfect conducting surfaces $S_1$, $S_2$, ... $S_n$ extending indefinitely along the axial direction ($\underline{u}_z$) having a constant cross-section defined by the closed curves $C_1$, $C_2$, ... $C_n$ generated by its intersection with the plane $z$ = constant as

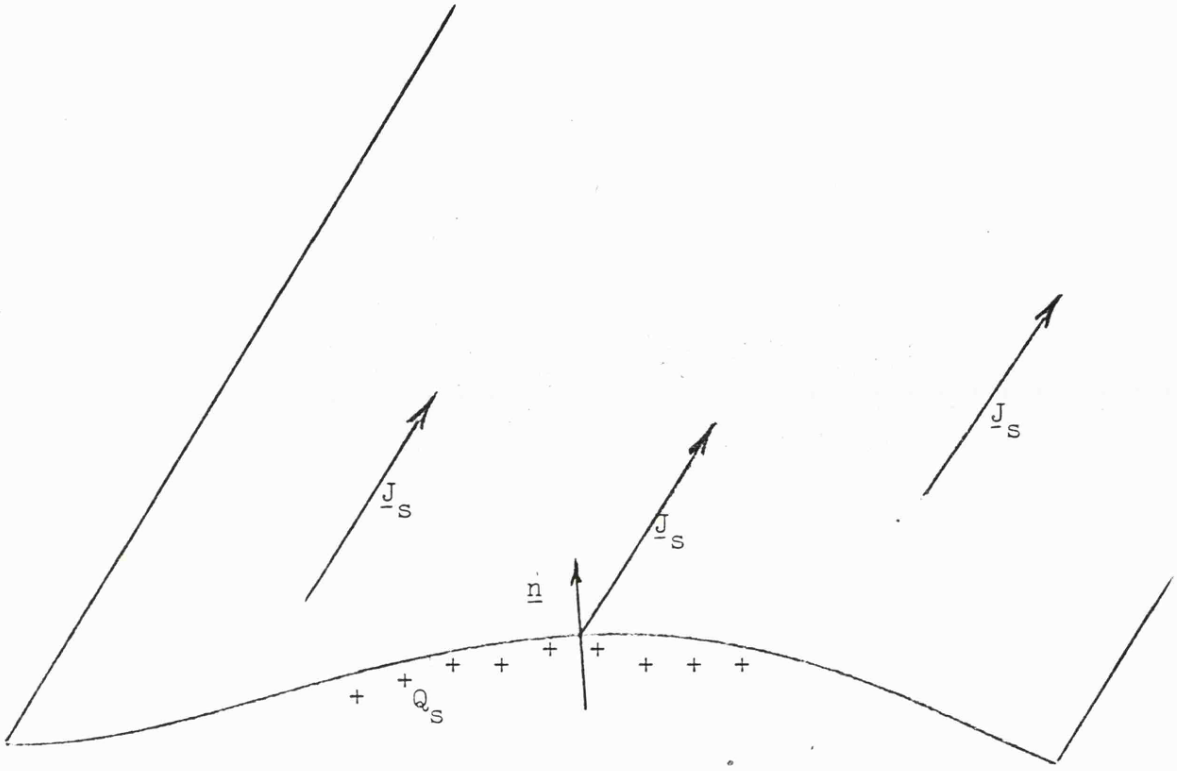


FIG.2.3 BOUNDARY CONDITIONS ON A PERFECT CONDUCTING SURFACE

Schematic representation of the charge and current densities on the interface between a perfect conducting surface and a perfect dielectric.

illustrated in Fig.(2.4).

The electric and magnetic field intensities of a normal mode wave propagating along the positive longitudinal direction in the current and charge free medium within the region can be described respectively by the equations:

$$\underline{E} = \underline{E}_0 \exp(i\omega t - \gamma z) \tag{2.35}$$

$$\underline{H} = \underline{H}_0 \exp(i\omega t - \gamma z) \tag{2.36}$$

where $\gamma$ is the propagation function* of the structure and $\underline{E}_0$ and $\underline{H}_0$ are vectorial functions of the transverse co-ordinates x and y only.

As the region extends indefinitely in the longitudinal direction it is convenient to decompose the field vectors in eq.(2.35) and eq.(2.36) into transverse and longitudinal components in the form:

$$\underline{E} = (\underline{E}_T + \underline{u}_z E_L) \exp(i\omega t - \gamma z) \tag{2.38}$$

---

* The propagation function $\gamma$ is usually called "propagation constant" ("phase constant" for ideal waveguides), but this nomenclature in the author's opinion is somewhat equivocal since it depends in general on the wave frequency, on the electric and magnetic properties of the medium and on the waveguide geometry.

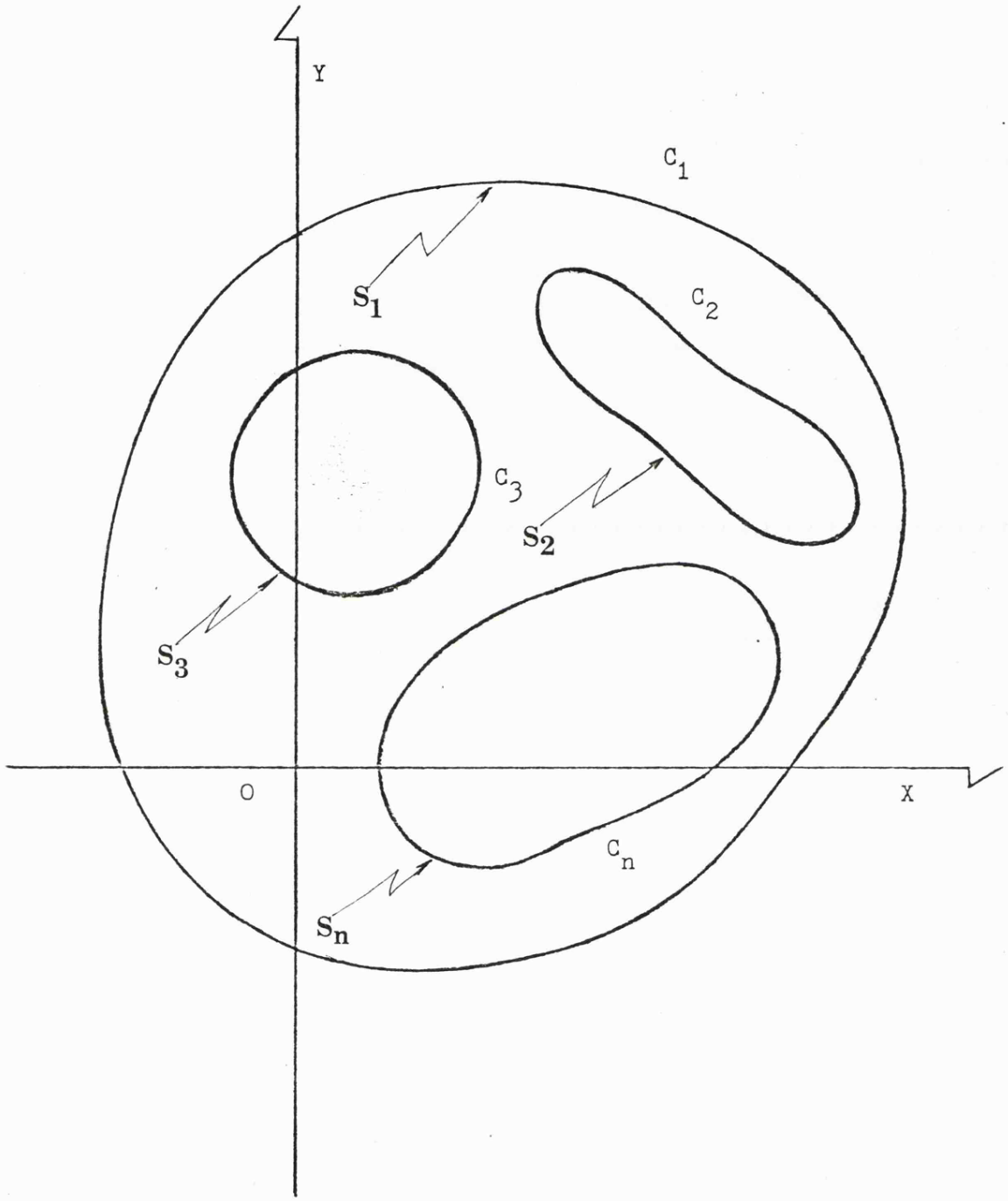


FIG.2.4 WAVEGUIDE CROSS-SECTION

The waveguide is the confined dielectric space between the surfaces $S_1$, $S_2$, ... $S_n$. The cut of the region by a plane z = constant generates the cross-section shown.

$$\underline{H} = (\underline{H}_T + \underline{u}_z H_L) \exp(i\omega t - \gamma z) \tag{2.39}$$

Substitution of eq.(2.38) and eq.(2.39) into eq.(2.26) and eq.(2.25) results:

$$\text{curl}\,[(\underline{E}_T + \underline{u}_z E_L) \exp(-\gamma z)] = -i\omega\mu(\underline{H}_T + \underline{u}_z H_L) \exp(-\gamma z) \tag{2.40}$$

$$\text{curl}\,[(\underline{H}_T + \underline{u}_z H_L) \exp(-\gamma z)] = i\omega\varepsilon(\underline{E}_T + \underline{u}_z E_L) \exp(-\gamma z) \tag{2.41}$$

Separation of the transverse and the longitudinal parts of eq.(2.40) and eq.(2.41) leads to[13]:

$$\text{curl}\ \underline{E}_T = -i\omega\mu\underline{u}_z H_L \tag{2.42}$$

$$\underline{u}_z \times \text{grad}\ E_L + \gamma\,\underline{u}_z \times \underline{E}_T = i\omega\mu\underline{H}_T \tag{2.43}$$

$$\text{curl}\ \underline{H}_T = i\omega\varepsilon\,\underline{u}_z E_L \tag{2.44}$$

$$\underline{u}_z \times \text{grad}\ H_L + \gamma\,\underline{u}_z \times \underline{H}_T = -i\omega\varepsilon\underline{E}_T \tag{2.45}$$

Substitution of eq.(2.38) into eq.(2.24) and eq.(2.39) into eq.(2.27) yields

$$\text{div}\ \underline{E}_T = \gamma E_L \tag{2.46}$$

$$\text{div } \underline{H}_T = \gamma H_L \tag{2.47}$$

Calculation of the curl of eq.(2.42) and the use of eq.(2.45) give:

$$\text{curl curl } \underline{E}_T - \omega^2 \mu \varepsilon \underline{E}_T = i\omega\mu\gamma \, \underline{u}_z \times \underline{H}_T \tag{2.48}$$

The subtraction of the gradient of eq.(2.46) from both sides of eq.(2.48) yields:

$$\text{curl curl } \underline{E}_T - \text{grad div } \underline{E}_T - \omega^2 \mu \varepsilon \underline{E}_T$$

$$= - (i\omega\mu\gamma \underline{u}_z \times \underline{H}_T + \text{grad } E_L) \tag{2.49}$$

Cross-multiplication of eq.(2.43) by $\underline{u}_z \gamma$ and the expansion of the triple vector products show that:

$$i\omega\mu\gamma \, \underline{u}_z \times \underline{H}_T = - \gamma ( \gamma \underline{E}_T + \text{grad } E_L) \tag{2.50}$$

Substitution of eq.(2.50) into eq.(2.49) gives the vector differential equation for the transverse electric field intensity in the waveguide, in the form:

$$\nabla^2 \underline{E}_T + ( \gamma^2 + \omega^2 \mu \varepsilon ) \underline{E}_T = 0 \tag{2.51}$$

Similarly the elimination of all field variables except $\underline{H}_T$ shows that the transverse magnetic field intensity satisfies

$$\nabla^2 \underline{H}_T + ( \gamma^2 + \omega^2 \mu \varepsilon ) \underline{H}_T = 0 \tag{2.52}$$

Comparison of those results shows that the waveguide transverse field intensity vectors for normal mode propagation are solutions of the homogeneous vector Helmholtz equation

$$( \nabla^2 + k_{cn}^2 ) \underline{v}_n = 0 \tag{2.53}$$

subjected to the pertinent boundary conditions.

## 2.5 ORTHOGONALITY AND COMPLETENESS OF THE TRANSVERSE NORMAL MODE ELECTRIC FIELD INTENSITIES

According to eq.(2.31) and eq.(2.46) the boundary conditions to be applied to eq.(2.53) for the electric field intensity are

$$\begin{aligned} \underline{n} \times \underline{E}_T &= 0 \\ \operatorname{div} \underline{E}_T &= 0 \end{aligned} \tag{2.54}$$

$$(\text{on } S_1, S_2, \ldots S_n)$$

The orthogonality and completeness properties of the transverse electric field intensities are developed by considering two independent solutions of eq.(2.53), $\underline{E}_{Tm}$ and $\underline{E}_{Tn}$, together with the boundary conditions given by eq.(2.54).

Let eq.(2.53) be identically satisfied by the transverse vector function $\underline{E}_{Tm}$, that is

$$\text{curl curl } \underline{E}_{Tm} - \text{grad div } \underline{E}_{Tm} - k_{cm}^2 \underline{E}_{Tm} = 0 \qquad (2.55)$$

Dot-multiplication of eq.(2.55) by the complex conjugate of $\underline{E}_{Tm}$ and integrating over the waveguide cross-section gives:

$$\iint \underline{E}_{Tm}^* \cdot \text{curl curl } \underline{E}_{Tm} \, dS - \iint \underline{E}_{Tm}^* \cdot \text{grad div } \underline{E}_{Tm} \, dS$$

$$= k_{cm}^2 \iint \underline{E}_{Tm}^* \cdot \underline{E}_{Tm} \, dS \qquad (2.56)$$

Substitution of the vector identities

$$\iint \underline{A} \cdot \text{grad div } \underline{B} \, dS = \iint \text{div } \underline{A} \text{ div } \underline{B} \, dS + \int (\underline{n} \cdot \underline{A}) \text{ div } \underline{B} \, dL \qquad (2.57)$$

$$\iint \underline{A} \cdot \text{curl curl } \underline{B} \, dS = \iint \text{curl } \underline{A} \cdot \text{curl } \underline{B} \, dS - \int \underline{A} \times \text{curl } \underline{B} \cdot \underline{n} \, dL \qquad (2.58)$$

into eq.(2.56), taking into account eq.(2.54), yields

$$k_{cm}^2 = \frac{\iint (\text{curl } \underline{E}_{Tm})^2 \, dS + \iint (\text{div } \underline{E}_{Tm})^2 \, dS}{\iint (\underline{E}_{Tm})^2 \, dS} \qquad (2.59)$$

Therefore all the eigenvalues associated with normal mode propagation along the structure are real and non-negative.

On the other hand , if $\underline{E}_{Tn}$ is another field solution of eq.(2.53) subjected to eq.(2.54) then

$$\text{curl curl } \underline{E}_{Tn} - \text{grad div } \underline{E}_{Tn} - k_{cn}^2 \underline{E}_{Tn} = 0 \qquad (2.60)$$

Dot-multiplication of eq.(2.55) by $\underline{E}_{Tn}$ and eq.(2.60) by $\underline{E}_{Tm}$, subtracting the results and integrating across the cross-section gives[26]

$$(k_{cm}^2 - k_{cn}^2) \iint \underline{E}_{Tm} \cdot \underline{E}_{Tn} \, dS = 0 \tag{2.61}$$

showing that the orthogonality relation

$$\iint \underline{E}_{Tm} \cdot \underline{E}_{Tn} \, dS = 0 \tag{2.62}$$

$$(m \neq n)$$

holds for non-degenerate modes.

The solutions of eq.(2.51) constitute a complete set when it is possible to represent any arbitrary vector function satisfying the boundary conditions by means of a series of those solutions. In that case, the truncated series produces an error which tends to zero when the number of terms is increased indefinitely.

It can be shown that the error $e_N^2$ when approximating an arbitrary transverse field configuration satisfying the boundary conditions on the waveguide perfect conducting walls, $\underline{E}_{TA}$, by a finite series of transverse electric fields, $\underline{E}_{Ti}$, corresponding to the normal mode waves of eq.(2.38), in the form

$$\underline{E}_{TA} \approx \sum_{i=1}^{N} c_i \, \underline{E}_{Ti} \tag{2.63}$$

where

$$\iint ( \underline{E}_{Ti} )^2 \, dS = 1 \tag{2.64}$$

$$c_i = \iint \underline{E}_{TA} \cdot \underline{E}_{Ti} \, dS \tag{2.65}$$

satisfies [26]

$$\lim_{N \to \infty} e_N^2 = \lim_{N \to \infty} \left[ \iint (\underline{E}_{TA})^2 \, dS - \sum_{i=1}^{N} c_i^2 \right] = 0 \tag{2.66}$$

Consequently, the set of transverse normal mode electric field intensities is an orthogonal complete set.

## 2.6 VARIATIONAL EXPRESSION FOR THE PROPAGATION FUNCTION

Considering the gauge condition in eq.(2.15) given by

$$\text{div} \; \underline{A}(\underline{r},\omega) = 0 \tag{2.67}$$

and using eq.(2.11) the scalar potential and the electric field intensity within the waveguide region can be written as:

$$F(\underline{r}, \omega) = 0 \tag{2.68}$$

$$\underline{E}(\underline{r}) = - i\omega \underline{A}(\underline{r}) \tag{2.69}$$

Substitution of eq.(2.69) into eq.(2.20), taking into account Maxwell's equations and constitutive relations, gives the Lagrange function in the form:

$$Lg\ (\underline{E}) = \iiint\ (\varepsilon\ \underline{E}^*(\underline{r})\ .\ \underline{E}(\underline{r}) - \frac{1}{\mu\omega^2}\ (\text{curl}\ \underline{E}(\underline{r}))^*\ .\ \text{curl}\ \underline{E}(\underline{r}))\ dV \tag{2.70}$$

Decomposing the volume integral in eq.(2.70) into a surface integral over the cross-section and an integral along the symmetry axis results:

$$Lg\ (\underline{E}) = \int_{-\infty}^{\infty} [\iint(\varepsilon\ \underline{E}^*(\underline{r})\ .\ \underline{E}(\underline{r}) - \frac{1}{\mu\omega^2}\ (\text{curl}\ \underline{E}(\underline{r}))^*.\ \text{curl}\ \underline{E}(\underline{r}))dS]dz \tag{2.71}$$

Using Fourier transformation, eq.(2.71) can be written in the form:

$$Lg\ (\underline{E}_\beta) = \frac{1}{2\pi}\ \int_{-\infty}^{\infty}\ \iint(\ \varepsilon\underline{E}_\beta^*\ .\ \underline{E}_\beta - \frac{1}{\mu\omega^2}\ \text{curl}\ \underline{E}_\beta^*\ .\ \text{curl}\ \underline{E}_\beta)\ dS\ d\beta \tag{2.72}$$

where $\underline{E}_\beta$ is the Fourier transform of $\underline{E}(\underline{r})$ with transverse component satisfying the Helmholtz equation on the cross-section:

$$(\ \nabla_T^2\ +\ k_{cn}^2\ )\ \underline{E}_{\beta T}\ =\ 0 \tag{2.73}$$

with the subscript T to the operator denoting transverse derivatives. The longitudinal component $E_{\beta L}$ of $\underline{E}_\beta$ is given by

$$E_{\beta L}\ =\ i\ \frac{1}{\beta}\ \nabla_T\ .\ \underline{E}_{\beta T} \tag{2.74}$$

Substitution of eq.(2.73) and eq.(2.74) into eq.(2.72) gives:

$$Lg(\underline{E}_\beta) = \frac{1}{2\pi} \int_{-\infty}^{\infty} \iint [\epsilon ( \underline{E}_{\beta T}^2 + \frac{1}{\beta^2} ( \nabla_T \cdot \underline{E}_{\beta T})^2$$

$$- \frac{1}{\mu\omega^2} (\nabla_T \times \underline{E}_{\beta T})^2 + \frac{1}{\mu\omega^2\beta^2} (\nabla_T \times \nabla_T \times \underline{E}_{\beta T} - \omega^2\mu\epsilon\underline{E}_{\beta T})^2] dS d\beta \tag{2.75}$$

Because the normal mode transverse electric field intensities form a complete set, and $\underline{E}_{\beta T}$ satisfies eq.(2.73) it is possible to write, assuming propagation in the z direction[12]:

$$\underline{E}_{\beta T} = \sum_j \delta ( \beta + \beta_j) \underline{E}_{Tj}(x,y) \tag{2.76}$$

where $\underline{E}_{Tj}(x,y)$ represents the tranverse electric field intensity of the $j^{th}$ mode with propagation function $\gamma_j = i\beta_j$ and $\delta$ is the Dirac function.

Substitution of eq.(2.76) into eq.(2.75) and the integration with respect to $\beta$ [12] gives the variational expression for the propagation function[14], in the form*:

$$\gamma^2(\underline{E}_T) = \frac{\iint(\nabla_T \times \nabla_T \times \underline{E}_T(x,y) - \omega^2\mu\epsilon\underline{E}_T(x,y))^2 dS - \omega^2\mu\epsilon\iint(\nabla_T \cdot \underline{E}_T(x,y))^2 dS}{\iint(\nabla_T \times \underline{E}_T(x,y))^2 dS - \omega^2\mu\epsilon\iint(\underline{E}_T(x,y))^2 dS}$$

$$= - \beta^2 (\underline{E}_T) \tag{2.77}$$

---

*The expressions in references (12) and (14) coincide with eq.(2.77) when ideal waveguides are considered.

Once the variational expression has been obtained it is possible to derive the infinite set of normal mode transverse electric field intensities. Assuming that there has been found a function $\underline{E}_{Tp}$ satisfying the boundary conditions and for which eq.(2.77) is stationary, another eigenfunction $\underline{E}_{Tq}$ satisfying the boundary conditions and making eq.(2.77) stationary can be found by using the orthogonality relationship. All the eigenvalues can be obtained since the procedure holds for any $p \neq q$ and therefore, conceptionally, the problem of normal mode propagation in waveguides is solved.

## 2.7 NORMAL MODE CLASSIFICATION

The complete normal mode transverse electric field intensity set can be decomposed into three primary subsets:

$$\text{i)}\ [\ \underline{E}_T^{(1)}\ ] = \underline{E}_{T1}^{(1)},\ \underline{E}_{T2}^{(1)},\ \ldots\ \underline{E}_{Tn}^{(1)},\ \underline{E}_{Tn+1}^{(1)} \tag{2.78}$$

for which the general vector function $\underline{E}_{Tj}^{(1)}$, $(j = 1,2,\ldots n,n+1)$has:

$$\text{curl}\ \underline{E}_{Tj}^{(1)} = 0 \tag{2.79}$$

$$\text{div}\ \underline{E}_{Tj}^{(1)} = 0 \tag{2.80}$$

$$\text{ii)}\ [\ \underline{E}_T^{(2)}\ ] = \underline{E}_{T1}^{(2)},\ \underline{E}_{T2}^{(2)},\ \ldots\ \underline{E}_{Tn}^{(2)},\ \underline{E}_{Tn+1}^{(2)},\ \ldots \tag{2.81}$$

for which the general vector function $\underline{E}_{Tj}^{(2)}$, $(j = 1,2,..n,n+1\ldots)$has:

$$\text{curl } \underline{E}_{Tj}^{(2)} \neq 0 \tag{2.82}$$

$$\text{div } \underline{E}_{Tj}^{(2)} = 0 \tag{2.83}$$

and

$$\text{iii) } [\ \underline{E}_{T}^{(3)}\ ] = \underline{E}_{T1}^{(3)},\ \underline{E}_{T2}^{(3)},\ \ldots\ \underline{E}_{Tn}^{(3)},\ \underline{E}_{Tn+1}^{(3)}\ ,\ldots \tag{2.84}$$

for which the general vector function $\underline{E}_{Tj}^{(3)}$ has:

$$\text{curl } \underline{E}_{Tj}^{(3)} = 0 \tag{2.85}$$

$$\text{div } \underline{E}_{Tj}^{(3)} \neq 0 \tag{2.86}$$

Consideration of a vector function in a set $[\ \underline{E}_{T}^{(4)}]$ with neither curl nor divergence equal to zero implies the possibility of defining the non-vanishing functions

$$\underline{E}_{Tj}^{(a)} = c^{(a)} \text{ curl curl } \underline{E}_{Tj}^{(4)} \tag{2.87}$$

within set $[\ \underline{E}_{T}^{(1)}]$ or set $[\ \underline{E}_{T}^{(2)}]$ and

$$\underline{E}_{Tj}^{(b)} = c^{(b)} \text{ grad div } \underline{E}_{Tj}^{(4)} \tag{2.88}$$

within the set $[\ \underline{E}_{T}^{(1)}]$ or set $[\ \underline{E}_{T}^{(3)}]$ .

Substitution of eq.(2.87) and eq.(2.88) into eq.(2.51)results:

$$\underline{E}_{Tj}^{(4)} = (c^{(b)}\ \underline{E}_{Tj}^{(a)} - c^{(a)}\ \underline{E}_{Tj}^{(b)}) \ /\ c^{(a)}c^{(b)}k_{cj}^{2} \tag{2.89}$$

As $\underline{E}_{Tj}^{(4)}$ is assumed to be a normal mode transverse electric field intensity it satisfies eq.(2.51), then

$$\begin{aligned} &\text{curl curl}\ \ (c^{(b)}\ \underline{E}_{Tj}^{(a)} - c^{(a)}\ \underline{E}_{Tj}^{(b)}) \ /\ c^{(a)}c^{(b)}k_{cj}^{2} \\ &- \text{grad div}\ \ (c^{(b)}\ \underline{E}_{Tj}^{(a)} - c^{(a)}\ \underline{E}_{Tj}^{(b)}) \ /\ c^{(a)}c^{(b)}k_{cj}^{2} \\ &- k_{cj}^{2}\ (c^{(b)}\ \underline{E}_{Tj}^{(a)} - c^{(a)}\ \underline{E}_{Tj}^{(b)}) \ /\ c^{(a)}c^{(b)}k_{cj}^{2} = 0 \end{aligned} \tag{2.90}$$

Manipulation of eq.(2.90) yields:

$$\begin{aligned} &\frac{1}{c^{(a)}k_{cj}^{2}}\ (\text{curl curl}\ \underline{E}_{Tj}^{(a)} - \text{grad div}\ \underline{E}_{Tj}^{(a)} - k_{cj}^{2}\ \underline{E}_{Tj}^{(a)} \\ &- \frac{1}{c^{(b)}k_{cj}^{2}}\ (\text{grad div}\ \underline{E}_{Tj}^{(b)} - k_{cj}^{2}\ \underline{E}_{Tj}^{(b)}\ ) = 0 \end{aligned} \tag{2.91}$$

From eq.(2.88) and eq.(2.89) we get

$$\text{grad div}\ \underline{E}_{Tj}^{(4)} = \frac{1}{c^{(b)}}\ \underline{E}_{Tj}^{(b)} \tag{2.92}$$

$$\text{div}\ \underline{E}_{Tj}^{(b)} = -\ c^{(b)}\ k_{cj}^{2}\ \text{div}\ \underline{E}_{Tj}^{(4)} \tag{2.93}$$

Substitution of eq.(2.92) and eq.(2.93) into eq.(2.91) gives

$$\text{curl curl } \underline{E}_{Tj}^{(a)} - \text{grad div } \underline{E}_{Tj}^{(a)} - k_{cj}^2 \, \underline{E}_{Tj}^{(a)} = 0 \qquad (2.94)$$

and therefore the function $\underline{E}_{Tj}^{(a)}$ is a solution of eq.(2.51).Taking the cross-product of eq.(2.94) by the unit vector normal to the cross-section boundary, $\underline{n}$ , and noting that $\underline{E}_{Tj}^{(a)}$ is divergenceless it can be shown that:

$$\underline{n} \times \underline{E}_{Tj}^{(a)} = \frac{1}{k_{cj}^2} \underline{n} \times (\text{curl} [ \frac{1}{c^{(a)} k_{cj}^2} \text{ curl } \underline{E}_{Tj}^{(4)} ] ) \qquad (2.95)$$

As $\underline{E}_{Tj}^{(4)}$ is a solution of eq.(2.51) subjected to the boundary conditions of eq.(2.54) it follows from eq.(2.95) and eq.(2.87) that:

$$\begin{aligned} \underline{n} \times \underline{E}_{Tj}^{(a)} &= 0 \\ \text{div } \underline{E}_{Tj}^{(a)} &= 0 \end{aligned} \qquad (2.96)$$

However, from eq.(2.94) and eq.(2.96) $\underline{E}_{Tj}^{(4)}$ and $\underline{E}_{Tj}^{(a)}$ are solutions of the same equation subjected to the same boundary conditions and so, from eq.(2.89) , $\underline{E}_{Tj}^{(b)}$ is also a solution under the same conditions. Therefore any function within subset $[ \underline{E}_{T}^{(4)} ]$ can be described by the superposition of the previous primary subsets and the following mode classification applies.

2.7.1 TEM MODES

For normal modes belonging to the first subset $[\ \underline{E}_T^{(1)}]$ , eq.(2.46) and eq.(2.47) show that

$$E_L = 0$$
$$H_L = 0 \qquad (2.97)$$

and the propagating electromagnetic field lies entirely on the transverse plane. The modes are denominated TEM modes from the initials of Transverse Electric and Magnetic fields. The transverse electric field intensities for this group of solutions can be obtained through the gradient of a generating scalar function $G_n^{(1)}(x,y)$ satisfying

$$\text{div grad } G_n^{(1)}(x,y) = 0 \qquad (2.98)$$

$$\underline{n} \times \text{grad } G_n^{(1)}(x,y) = 0 \qquad (2.99)$$

$$(\text{on } S_1, S_2, \ldots S_n)$$

in the form

$$\underline{E}_{Tn}^{(1)} = \text{grad } G_n^{(1)}(x,y) \qquad (2.100)$$

From eq.(2.99) it follows that on any closed curve on the boundary surfaces

$$\frac{\delta}{\delta \ell} \left[ G_n^{(1)}(x,y) \right] = 0 \tag{2.101}$$

and therefore $G_n^{(1)}(x,y)$ is single-valued over any closed conducting surface of the region.

For a single-connected boundary $G_n^{(1)}(x,y)$ is a constant, $G_0$ , and so

$$\iint \text{div } G_n^{(1)}(x,y) \text{ grad } G_n^{(1)}(x,y) \, dS =$$

$$= G_0 \iint \text{div grad } G_n^{(1)}(x,y) \, dS \tag{2.102}$$

Using Green's first identity and eq.(2.102) it follows that

$$\iint (\text{grad } G_n^{(1)}(x,y))^2 \, dS = 0 \tag{2.103}$$

and therefore no TEM propagation may occur inside single-connected waveguides. For N-connected waveguides, however, there are (N - 1) possibilities of assigning constant values for $G_n^{(1)}(x,y)$ and (N - 1) TEM modes may propagate. In this case the generating function is obtained by solving Laplace's equation over the waveguide cross-section:

$$\nabla_T^2 G_n^{(1)}(x,y) = 0 \tag{2.104}$$

subjected to the boundary condition

$$G_n^{(1)}(x,y) = \text{constant} \tag{2.105}$$

over the N closed curves.

The single eigenvalue resulting from eq.(2.59) shows that the propagation is non-dispersive with a propagation function given by

$$\gamma = i\omega(\mu\varepsilon)^{\frac{1}{2}} \tag{2.106}$$

In Microwave Engineering, guiding structures supporting TEM waves are, in general, called transmission lines rather than waveguides and have applications, usually, in cabling and low-power techniques. Conventional methods can be applied to analyse the properties of transmission lines[27] and only non-TEM propagating structures will remain under the denomination "waveguides" and will hereupon be treated*.

2.7.2 TE MODES

The transverse electric field intensities belonging to the second set $[\ \underline{E}_T^{(2)}]$ are divergenceless and according to eq.(2.42) and eq.(2.46) the normal modes are classified as Transverse Electric.

On the other hand, as

$$\underline{u}_z \times \text{curl}\ \underline{E}_{Tn}^{(2)} = 0 \tag{2.107}$$

it is possible to write:

---

* Higher-order modes in multi-connected guiding structures included.

$$\text{curl } \underline{E}_{Tn}^{(2)} = \underline{u}_z \, G_n^{(2)}(x,y) \tag{2.108}$$

where $G_n^{(2)}(x,y)$ is a scalar function of the transverse co-ordinates.

Substitution of eq.(2.108) into eq.(2.51) shows that the function $G_n^{(2)}(x,y)$ is a solution of:

$$(\nabla_T^2 + k_{cn}^2) \, G_n^{(2)}(x,y) = 0 \tag{2.109}$$

The boundary condition for the divergence on the conducting walls is automatically satisfied by this group of functions and, as

$$\underline{n} \times \underline{E}_T^{(2)} = \underline{u}_z \frac{1}{k_{cn}^2} (\underline{n} \cdot \text{grad } G_n^{(2)}(x,y)) \tag{2.110}$$

the boundary conditions for TE modes reduce to either

$$\underline{n} \cdot \text{grad } G_n^{(2)}(x,y) = 0 \tag{2.111}$$

$$(\text{on } S_1, S_2, \ldots S_n)$$

or

$$\frac{\delta}{\delta n} [ G_n^{(2)}(x,y) ] = 0 \tag{2.112}$$

$$(\text{on } C_1, C_2, \ldots C_n)$$

where $\frac{\delta}{\delta n} [\ ]$ indicates a derivative calculated in the direction normal to the boundary.

If $G_i^{(2)}(x,y)$ and $G_j^{(2)}(x,y)$ are solutions of eq.(2.109) subjected to the condition in eq.(2.112), then

$$G_j^{(2)}(x,y) \text{ div grad } G_i^{(2)}(x,y) - G_i^{(2)}(x,y) \text{ div grad } G_j^{(2)}(x,y) =$$

$$= (k_{ci}^2 - k_{cj}^2)\, G_i^{(2)}(x,y)\; G_j^{(2)}(x,y) \qquad (2.113)$$

Integration over the cross-section and the use of Green's second identity gives:

$$\int_C \left( G_j^{(2)}(x,y) \frac{\delta}{\delta n} [G_i^{(2)}(x,y)] - G_i^{(2)}(x,y) \frac{\delta}{\delta n} [G_j^{(2)}(x,y)] \right) dL =$$

$$= (k_{ci}^2 - k_{cj}^2) \iint G_i^{(2)}(x,y)\; G_j^{(2)}(x,y)\, dS \qquad (2.114)$$

Substitution of eq.(2.112) into eq.(2.114) leads to the orthogonality relation:

$$\iint G_m^{(2)}(x,y)\; G_n^{(2)}(x,y)\, dS = 0 \qquad (2.115)$$

$$(m \neq n)$$

When degenerate modes occur, that is, in the occurrence of two distinct scalar functions $G_p^{(2)}(x,y)$ and $G_q^{(2)}(x,y)$, having the same eigenvalue $k_{cp} = k_{cq}$, the subset $[\underline{E}_T^{(2)}]$ can be modified by replacing $G_q^{(2)}(x,y)$ by the function

$$G_{pq}^{(2)}(x,y) = A\, G_p^{(2)}(x,y) + G_q^{(2)}(x,y) \tag{2.116}$$

where

$$A = - \frac{\iint G_p^{(2)}(x,y)\, G_q^{(2)}(x,y)\, dS}{\iint (\, G_p^{(2)}(x,y))^2\, dS} \tag{2.117}$$

in order to preserve the orthogonality within the set.[26]

The longitudinal magnetic field intensity components are determined using eq.(2.42) and eq.(2.108). This gives:

$$\underline{H}_{Ln}^{(2)} = i\, \underline{u}_z \frac{1}{\omega\mu} G_n^{(2)}(x,y) \tag{2.118}$$

The transverse magnetic field intensity components are obtained by combining eq.(2.44); eq.(2.52) and eq.(2.118) in the form:

$$\underline{H}_{Tn}^{(2)} = - i\, (\, \gamma_n / \omega\mu) \frac{1}{k_{cn}^2} \text{ grad } G_n^{(2)}(x,y) \tag{2.119}$$

Cross-multiplication of eq.(2.43) by $\underline{u}_z$ and the expansion of the triple vector product gives:

$$\underline{E}_{Tn}^{(2)} = - i \frac{\omega\mu}{\gamma_n} \underline{u}_z \times \underline{H}_{Tn} \tag{2.120}$$

Substitution of eq.(2.119) into eq.(2.120) leads to the deter-

mination of the transverse electric field intensities in terms of $G_n^{(2)}(x,y)$, in the form:

$$\underline{E}_{Tn}^{(2)} = -\underline{u}_z \times \frac{1}{k_{cn}^2} \text{ grad } G_n^{(2)}(x,y) \tag{2.121}$$

2.7.3 TM MODES

The magnetic field intensities corresponding to the functions within the irrotational subset $[\underline{E}_T^{(3)}]$ are transverse (eq.(2.42)). The vectors $\underline{E}_{Tn}^{(3)}$ can be obtained from the scalar function $G_n^{(3)}(x,y)$ through the expression:

$$\underline{E}_{Tn}^{(3)} = \text{grad } G_n^{(3)}(x,y) \tag{2.122}$$

with $G_n^{(3)}(x,y)$ satisfying

$$(\nabla_T^2 + k_{cn}^2)\, G_n^{(3)}(x,y) = 0 \tag{2.123}$$

subjected to the boundary condition

$$G_n^{(3)}(x,y) = 0 \qquad (\text{on } C_1,\ C_2,\ \ldots\ C_n) \tag{2.124}$$

The boundary condition $\underline{n} \times \underline{E}_{Tn}^{(3)}$ is automatically satisfied by the subset. Following a procedure similar to that employed for TE modes it can be shown that the functions $G_n^{(3)}(x,y)$ are orthogo-

nal, that is:

$$\iint G_m^{(3)}(x,y)\, G_n^{(3)}(x,y)\, dS = 0 \qquad (m \neq n) \tag{2.125}$$

In case of degeneracy between functions $G_p^{(3)}(x,y)$ and $G_q^{(3)}(x,y)$ the latter can be replaced by

$$G_{pq}^{(3)}(x,y) = G_q^{(3)}(x,y) - \left( \frac{\iint G_p^{(3)}(x,y)\, G_q^{(3)}(x,y)\, dS}{\iint (G_p^{(3)}(x,y))^2\, dS} \right) G_p^{(3)}(x,y) \tag{2.126}$$

to keep orthogonality[26].

Once the solutions to eq.(2.123) and eq.(2.122) have been obtained, the remainder of the electromagnetic vectors are developed analogously to TE modes, in the form:

$$\underline{E}_{Ln}^{(3)} = \underline{u}_z \frac{k_{cn}^2}{\gamma_n} G_n^{(3)}(x,y) \tag{2.127}$$

$$\underline{H}_{Tn}^{(3)} = -i\,(\omega\varepsilon/\gamma_n)\, \underline{u}_z \times \text{grad}\, G_n^{(3)}(x,y) \tag{2.128}$$

## 2.8 CUT-OFF, WAVE IMPEDANCE AND MODE DUALITY

The propagation functions $\gamma_n$ can be written in terms of the eigenvalues $k_{cn}$ in the form:

$$\gamma_n = (k_{cn}^2 - k^2)^{\frac{1}{2}} \tag{2.129}$$

where $k$ is the space wave-number:

$$k = \omega(\mu\varepsilon)^{\frac{1}{2}} \tag{2.130}$$

The eigenvalue $k_{cn}$ is called the cut-off wave-number since it determines the wavelength for which $\gamma_n$ becomes real and the fields are exponentially attenuated instead of propagating along the structure.

The space wavelength for which cut-off occurs is called cut-off wavelength, being given by:

$$\lambda_{cn} = \frac{2\pi}{k_{cn}} \tag{2.131}$$

The guided wavelength is defined as the distance the wave must propagate to undergo a phase shift of $2\pi$ radians, that is:

$$\lambda_g = \frac{2\pi}{\beta} \tag{2.132}$$

$$(\gamma_n = i\beta)$$

Combination of eq.(2.130), eq.(2.131) and eq.(2.132) gives:

$$\lambda_g = 2\pi \frac{1}{k\left[1 - \left(\frac{k_{cn}}{k}\right)^2\right]^{\frac{1}{2}}} \tag{2.133}$$

Fields for which $k < k_{cn}$ have real propagation function and are referred to as evanescent modes.

The phase and group velocities, $v_p$ and $v_g$, are given by

$$v_p = c \frac{1}{\left[ 1 - \left(\frac{k_{cn}}{k}\right)^2 \right]^{\frac{1}{2}}} \tag{2.134}$$

$$v_g = c \left[ 1 - \left(\frac{k_{cn}}{k}\right)^2 \right]^{\frac{1}{2}} \tag{2.135}$$

where

$$c = \frac{1}{(\mu\varepsilon)^{\frac{1}{2}}} \tag{2.136}$$

On the other hand, by considering the projection of a general vector quantity $\underline{v}$ onto a transverse plane $\underline{v}_T$ and the vector resulting from rotating $\underline{v}_T$ through $\pi/2$ rad., $\underline{v}_T^o$, it can be shown[28] that the wave impedance $Z_n^{(i)}$ can be written formally as:

$$Z_n^{(i)} = \frac{\left|E_{Tj}^{(i)}\right|}{\left|H_{Tj}^{(i)}\right|} = \frac{\left|E_{Tj}^{(i)}\right|}{\left|H_{Tj}^{o(i)}\right|}$$

$$= \frac{\gamma_n \nabla_T E_{Ln} - i\omega\mu \nabla_T^o H_{Ln}}{\gamma_n \nabla_T^o H_{Ln} - i\omega\varepsilon \nabla_T E_{Ln}} \tag{2.137}$$

Substitution of $H_{Ln} = 0$ for TE modes and $E_{Ln} = 0$ for TM modes into eq.(2.137) and the use of eq.(2.118), eq.(2.119), eq.(2.121),

eq.(2.122), eq.(2.127) and eq.(2.129) show that, except for a scaling factor, the field configuration inside waveguides can be written as:

$$\underline{E}_{Tn}^{(2)} = Z_n^{(2)} \, \underline{u}_z \times \underline{H}_{Tn}^{(2)} \tag{2.138}$$

$$\underline{E}_{Ln}^{(2)} = 0 \tag{2.139}$$

$$\underline{H}_{Tn}^{(2)} = -\gamma_n \, \nabla_T \, G_n^{(2)}(x,y) \tag{2.140}$$

$$\underline{H}_{Ln}^{(2)} = \underline{u}_z \, k_{cn}^2 \, G_n^{(2)}(x,y) \tag{2.141}$$

$$\underline{E}_{Tn}^{(3)} = \gamma_n \, \nabla_T \, G_n^{(3)}(x,y) \tag{2.142}$$

$$\underline{E}_{Ln}^{(3)} = \underline{u}_z \, k_{cn}^2 \, G_n^{(3)}(x,y) \tag{2.143}$$

$$\underline{H}_{Tn}^{(3)} = -\frac{1}{Z_n^{(3)}} \, \underline{u}_z \times \underline{E}_{Tn}^{(3)} \tag{2.144}$$

$$\underline{H}_{Ln}^{(3)} = 0 \tag{2.145}$$

where

$$Z_n^{(2)} = i \, \frac{\omega\mu}{\gamma_n} \tag{2.146}$$

$$Z_n^{(3)} = - i \frac{\gamma_n}{\omega \varepsilon} \tag{2.147}$$

The dual characteristic of the propagation in ideal waveguides is established from eq.(2.142) to eq.(2.147) and the space orthogonality of the electromagnetic fields for a given mode reduces to the transverse relation

$$\underline{E}_{Tn}^{(i)} \cdot \underline{H}_{Tn}^{(i)} = 0 \tag{2.148}$$

## 2.9 ORTHOGONALITY AND COMPLETENESS OF THE NORMAL MODE FIELD INTENSITIES

It can be shown, for instance by following a derivation similar to that adopted previously for the electric field intensities, that the relation

$$\iint \underline{H}_{Tm} \cdot \underline{H}_{Tn} \, dS = 0 \qquad (m \neq n) \tag{2.149}$$

holds for any two non-degenerate waveguide normal modes.

It can also be shown that the normal mode transverse magnetic field intensities constitute a complete set. Therefore, the normal mode field intensities form complete orthogonal sets and can be used for the expansion of arbitrary waveguide field configurations[29].

## 2.10 POWER FLOW AND POWER ORTHOGONALITY

The time average power flow in the structure is given by the

integral of the complex Poynting vector over the cross-section, in the form:

$$P = \frac{1}{2} \mathrm{Re} \left[ \iint (\underline{E} \times \underline{H}^*) \cdot \underline{u}_z \, dS \right] \tag{2.150}$$

For a single propagating TE mode, substitution of eq.(2.132), to eq.(2.141) into eq.(2.150) and the use of Green's first identity give:

$$P_n^{(2)} = -\frac{1}{2} Z_n^{(2)} \beta_n^2 \iint G_n^{(2)}(x,y) \nabla_T^2 G_n^{(2)}(x,y) \, dS$$

$$+ \frac{1}{2} Z_n^{(2)} \beta_n^2 \int_C G_n^{(2)}(x,y) \frac{\delta}{\delta n} [G_n^{(2)}(x,y)] \, dL \tag{2.151}$$

$$(\gamma = i\beta)$$

The line integral in eq.(2.151) vanishes (eq.(2.112), therefore, considering eq.(2.109) the power for a single propagating TE mode is given by:

$$P_n^{(2)} = \frac{1}{2} Z_n^{(2)} \beta_n^2 k_{cn}^2 \iint (G_n^{(2)}(x,y))^2 \, dS \tag{2.152}$$

When a single propagating TM mode is considered, similar derivation leads to:

$$P_n^{(3)} = \frac{1}{2} \frac{1}{Z_n^{(3)}} \beta_n^2 k_{cn}^2 \iint (G_n^{(3)}(x,y))^2 \, dS \tag{2.153}$$

Application of eq.(2.25) for two independent propagating modes with fields given respectively by $\underline{E}_p^{(i)}$, $\underline{H}_p^{(i)}$ and $\underline{E}_q^{(j)}$, $\underline{H}_q^{(j)}$ gives:

$$\text{curl } \underline{E}_p^{(i)} = - i\omega\mu \underline{H}_p^{(i)} \tag{2.154}$$

$$\text{curl } \underline{E}_q^{(j)} = - i\omega\mu \underline{H}_q^{(j)} \tag{2.155}$$

Dot-multiplication of eq.(2.154) by $\underline{H}_q^{(j)}$ and eq.(2.155) by $\underline{H}_p^{(i)}$ and the subtraction of the results give:

$$\underline{H}_q^{(j)} \cdot \text{curl } \underline{E}_p^{(i)} - \underline{H}_p^{(i)} \cdot \text{curl } \underline{E}_q^{(j)} = 0 \tag{2.156}$$

Following a similar procedure but using eq.(2.24), it can be shown equally that:

$$\underline{E}_q^{(j)} \cdot \text{curl } \underline{H}_p^{(i)} - \underline{E}_p^{(i)} \cdot \text{curl } \underline{H}_q^{(j)} = 0 \tag{2.157}$$

Addition of eq.(2.156) and eq.(2.157) and subsequent simplification give:

$$\text{div} \left[ \underline{E}_p^{(i)} \times \underline{H}_q^{(j)} - \underline{E}_q^{(j)} \times \underline{H}_p^{(i)} \right] = 0 \tag{2.158}$$

The quantities in eq.(2.158) are fields of waves propagating along the waveguide depending on the longitudinal co-ordinate as $e^{-i\beta_p z}$ and $e^{-i\beta_q z}$. After some manipulation , eq.(2.158) can be

written as:

$$\nabla_T \cdot [\, \underline{E}_p^{(i)} \times \underline{H}_q^{(j)} - \underline{E}_q^{(j)} \times \underline{H}_p^{(i)} \,]$$

$$= i\,(\beta_p + \beta_q)\, \underline{u}_z \cdot (\underline{E}_p^{(i)} \times \underline{H}_q^{(j)} - \underline{E}_q^{(j)} \times \underline{H}_p^{(i)}) \quad (2.159)$$

Application of Gauss's theorem and substitution of the boundary condition for the tangential electric field intensities gives the result:

$$i\,(\beta_p + \beta_q) \iint \underline{u}_z \cdot (\underline{E}_p^{(i)} \times \underline{H}_q^{(j)} - \underline{E}_q^{(j)} \times \underline{H}_p^{(i)})\, dS = 0 \quad (2.160)$$

The result in eq.(2.160) is general and can be applied when the $q^{th}$ mode has propagation direction reversed, then:

$$i\,(\beta_p - \beta_q) \iint \underline{u}_z \cdot (-\underline{E}_p^{(i)} \times \underline{H}_q^{(j)} - \underline{E}_q^{(j)} \times \underline{H}_p^{(i)})\, dS = 0 \quad (2.161)$$

Addition and subtraction of eq.(2.160) and eq.(2.161) give:

$$\iint (\underline{E}_{Tq}^{(j)} \times \underline{H}_{Tp}^{(i)}) \cdot \underline{u}_z \, dS = 0 \quad (2.162)$$

$$\iint (\underline{E}_{Tp}^{(i)} \times \underline{H}_{Tq}^{(j)}) \cdot \underline{u}_z \, dS = 0 \quad (2.163)$$

$$(\beta_p \neq \beta_q)$$

On the other hand, for ideal waveguides, the eigenvalues $k_{cn}$

are real (eq.(2.59)) and therefore the solutions to eq.(2.53) can be chosen to be real. Consequently eq.(2.162) and eq.(2.163) may now be written in the form:

$$\iint (\underline{E}_p^{(i)} \times \underline{H}_q^{*(j)}) \cdot \underline{u}_z \, dS = 0 \qquad (2.164)$$

$$(\beta_p \neq \beta_q)$$

Combination of eq.(2.150) and eq.(2.164) gives:

$$P_{pq}^{(i)(j)} = \tfrac{1}{2} \, \mathrm{Re} \left[ \iint (\underline{E}_p^{(i)} \times \underline{H}_q^{*(j)} \cdot \underline{u}_z \, dS \right] = 0 \qquad (2.165)$$

$$(p \neq q)$$

where $P_{pq}^{(i)(j)}$ represents the time average power flow due to the interaction of two non-degenerate propagating modes.

From eq.(2.165) the total time average power flow, $P_t$, inside ideal waveguides, in the absence of degeneracy, can be written as:

$$P_t = \sum_n P_n \qquad (2.166)$$

where $P_n$ is the time average power flow due to each propagating mode. The power carried by any mode is, therefore, independent of the presence of other modes.

## 2.11 FIELD EXPANDIBILITY

The normal mode solutions to the waveguide problem are obtained by assuming exponential dependence of the field variables, in the

form given by eq.(2.35) and eq.(2.36). Such a priori assumption on the functional dependence of the field configuration is, in principle, very restrictive.

However, using the orthogonality and completeness properties of the normal modes, a general expression involving no a priori assumption on the field vectors (other than meeting the requirements on the boundary) can be obtained[13][15].

The technique used for developing the general solution consists of representing an arbitrary propagating field by a linear combination of normal modes. The expansion coefficients are determined making use of Maxwell's equations, as follows.

Consider an arbitrary electromagnetic field satisfying the boundary conditions on the waveguide walls, with electric and magnetic field intensities $\underline{E}$ and $\underline{H}$. Using eq.(2.63), eq.(2.64) and eq.(2.65) the arbitrary field can be expanded in terms of the normal mode fields in the form:

$$\underline{E} = \sum_{n=1}^{\infty} \left[ \underline{E}_{Tn} \iint \underline{E} \cdot \underline{E}_{Tn} \, dS \right] + \sum_{n=1}^{\infty} \left[ \underline{u}_z E_{Ln} \iint (\underline{u}_z \cdot \underline{E}) E_{Ln} \, dS \right] \tag{2.167}$$

$$\underline{H} = \sum_{n=1}^{\infty} \left[ \underline{H}_{Tn} \iint \underline{H} \cdot \underline{H}_{Tn} \, dS \right] + \sum_{n=1}^{\infty} \left[ \underline{u}_z H_{Ln} \iint (\underline{u}_z \cdot \underline{H}) H_{Ln} \, dS \right] \tag{2.168}$$

where the normal mode base vectors are orthonormal, that is, orthogonal and normalized such that:

$$\iint |\underline{E}_{Tn}|^2 \, dS = 1 \quad ; \quad \iint E_{Ln}^2 \, dS = 1 \tag{2.169}$$

$$\iint |\underline{H}_{Tn}|^2 \, dS = 1 \quad ; \quad \iint H_{Ln}^2 \, dS = 1 \tag{2.170}$$

Noting that in Maxwell's equation curl $\underline{E}$ behaves as a magnetic field, its expansion can be carried out in terms of $\underline{H}_n$, i.e., substitute for $\underline{H}$ in eq.(2.168):

$$\text{curl } \underline{E} = \sum_{n=1}^{\infty} \left[ \underline{H}_{Tn} \iint \text{curl } \underline{E} \cdot \underline{H}_{Tn} \right] dS$$

$$+ \sum_{n=1}^{\infty} \left[ \underline{u}_z \, H_{Ln} \iint ( \underline{u}_z \cdot \text{curl } \underline{E}) \, H_{Ln} \, dS \right] \tag{2.171}$$

On the other hand, the integrand in the first term of eq.(2.171) can be written in the form:

$$\text{curl } \underline{E} \cdot \underline{H}_{Tn} = \frac{\delta}{\delta z} ( \underline{u}_z \times \underline{E}_T) \cdot \underline{H}_{Tn} - ( \underline{u}_z \times \text{grad } E_L) \cdot \underline{H}_{Tn} \tag{2.172}$$

Because , for the normal mode, the function $\underline{u}_z \times \underline{E}_{Tn}$ behaves as $\underline{H}_{Tn}$, the function div $\underline{E}_{Tn}$ behaves like $E_{Ln}$ and the previous comment about curl $\underline{E}$ can be extended to curl $\underline{E}_{Tn}$ , eq.(2.167) to eq.(2.172) can be written in terms of the normal mode transverse electric field intensities alone:

$$\underline{E} = \sum_{n=1}^{\infty} \left[ \underline{E}_{Tn} \iint \underline{E} \cdot \underline{E}_{Tn} \, dS \right]$$

$$+ \sum_{n=1}^{\infty} \left[ \underline{u}_z \frac{\text{div } \underline{E}_{Tn}}{Nn} \iint ( \underline{u}_z \cdot \underline{E}) \frac{\text{div } \underline{E}_{Tn}}{Nn} \, dS \right] \qquad (2.173)$$

$$\underline{H} = \sum_{n=1}^{\infty} \left[ ( \underline{u}_z \times \underline{E}_{Tn}) \iint \underline{H} \cdot ( \underline{u}_z \times \underline{E}_{Tn}) \, dS \right]$$

$$+ \sum_{n=1}^{\infty} \left[ \frac{\text{curl } \underline{E}_{Tn}}{Mn} \iint \underline{H} \cdot \frac{\text{curl } \underline{E}_{Tn}}{Mn} \, dS \right] \qquad (2.174)$$

$$\text{curl } \underline{E} = \sum_{n=1}^{\infty} \left[ ( \underline{u}_z \times \underline{E}_{Tn}) \iint \text{curl } \underline{E} \cdot ( \underline{u}_z \times \underline{E}_{Tn}) \, dS \right]$$

$$+ \sum_{n=1}^{\infty} \left[ \frac{\text{curl } \underline{E}_{Tn}}{Mn} \iint \text{curl } \underline{E} \cdot \frac{\text{curl } \underline{E}_{Tn}}{Mn} \, dS \right] \qquad (2.175)$$

$$\text{curl } \underline{E} \cdot ( \underline{u}_z \times \underline{E}_{Tn}) = \left[ \frac{\delta}{\delta z} ( \underline{u}_z \times \underline{E}_T) - \underline{u}_z \times \text{grad } E_L \right] \cdot ( \underline{u}_z \times \underline{E}_{Tn}) \qquad (2.176)$$

where Nn and Mn are normalizing factors introduced to keep the base functions orthonormal as before.

Operation of the dot-product, integration and application of the Gauss's theorem into eq.(2.176) and taking into account that $\underline{E}$ satisfies the boundary conditions give:

$$\iint \text{curl } \underline{E} \cdot (\underline{u}_z \times \underline{E}_{Tn})\, dS = \frac{\delta}{\delta z} \iint \underline{E}_T \cdot \underline{E}_{Tn}\, dS$$

$$+ \iint \underline{u}_z \cdot \underline{E} \text{ div } \underline{E}_{Tn}\, dS \qquad (2.177)$$

Similarly, after some manipulation, we get:

$$\iint \text{curl } \underline{E} \cdot \text{curl } \frac{\underline{E}_{Tn}}{Mn}\, dS = k_{cn}^2 \iint \underline{E} \cdot \frac{\underline{E}_{Tn}}{Mn}\, dS \qquad (2.178)$$

Substitution of eq.(2.177) and eq.(2.178) into eq.(2.175) gives the expansion of curl $\underline{E}$ in the form:

$$\text{curl } \underline{E} = \sum_{n=1}^{\infty} \left[ (\underline{u}_z \times \underline{E}_{Tn}) \left( \frac{\delta}{\delta z} \iint \underline{E}_T \cdot \underline{E}_{Tn}\, dS + \iint \underline{u}_z \cdot \underline{E} \text{ div } \underline{E}_{Tn} dS \right) \right]$$

$$+ \sum_{n=1}^{\infty} \left[ \frac{\text{curl } \underline{E}_{Tn}}{Mn} k_{cn}^2 \iint \underline{E} \cdot \frac{\underline{E}_{Tn}}{Mn}\, dS \right] \qquad (2.179)$$

Similar procedure allows curl $\underline{H}$ to be written as:

$$\text{curl } \underline{H} = \sum_{n=1}^{\infty} \left[ \underline{E}_{Tn} \left( - \frac{\delta}{\delta z} \iint \underline{H} \cdot (\underline{u}_z \times \underline{E}_{Tn}) dS + \iint \underline{H} \cdot \text{curl } \underline{E}_{Tn}\, dS \right) \right]$$

$$+ \sum_{n=1}^{\infty} \left[ \underline{u}_z \frac{\text{div } \underline{E}_{Tn}}{Nn} k_{cn}^2 \iint \underline{H} \cdot \frac{(\underline{u}_z \times \underline{E}_{Tn})}{Nn}\, dS \right] \qquad (2.180)$$

Substitution of eq.(2.179) and eq.(2.174) into eq.(2.25) and eq.(2.180) and eq.(2.173) into eq.(2.24) equating the coefficients

yields

$$i\,\omega\varepsilon \iint \underline{E} \cdot \underline{E}_{Tn}\, dS = -\frac{\delta}{\delta z} \iint \underline{H} \cdot (\underline{u}_z \times \underline{E}_{Tn})\, dS + \iint \underline{H} \cdot \text{curl}\, \underline{E}_{Tn}\, dS \tag{2.181}$$

$$i\,\omega\varepsilon \iint (\underline{u}_z \cdot \underline{E})\, \text{div}\, \underline{E}_{Tn}\, dS = k_{cn}^2 \iint \underline{H} \cdot (\underline{u}_z \times \underline{E}_{Tn})\, dS \tag{2.182}$$

$$(\text{div}\, \underline{E}_{Tn} \neq 0)$$

$$-i\,\omega\mu \iint \underline{H} \cdot (\underline{u}_z \times \underline{E}_{Tn})\, dS = \frac{\delta}{\delta z} \iint \underline{E} \cdot \underline{E}_{Tn}\, dS + \iint (\underline{u}_z \cdot \underline{E})\, \text{div}\, \underline{E}_{Tn}\, dS \tag{2.183}$$

$$-i\,\omega\mu \iint \underline{H} \cdot \text{curl}\, \underline{E}_{Tn}\, dS = k_{cn}^2 \iint \underline{E} \cdot \underline{E}_{Tn}\, dS \tag{2.184}$$

$$(\text{curl}\, \underline{E}_{Tn} \neq 0)$$

For TE propagation, div $\underline{E}_{Tn} = 0$ and the combination of eq.(2.179) to eq.(2.184) results:

$$\frac{\delta^2}{\delta z^2} \left[ \iint \underline{E} \cdot \underline{E}_{Tn}\, dS \right] + (\omega^2\mu\varepsilon - k_{cn}^2) \left[ \iint \underline{E} \cdot \underline{E}_{Tn}\, dS \right] = 0 \tag{2.185}$$

The general solution of eq.(2.185) is given by:

$$\iint \underline{E} \cdot \underline{E}_{Tn}\, dS = A_n\, e^{-\gamma_n z} + B_n\, e^{\gamma_n z} \tag{2.186}$$

$$(\gamma_n \neq 0)$$

$$\iint \underline{E} \cdot \underline{E}_{Tn}\, dS = C_n + D_n z \qquad (2.187)$$

$$(\gamma_n = 0)$$

Substitution of eq.(2.186) and eq.(2.187) into the original equations taking into account eq.(2.146) results:

$$\iint \underline{H} \cdot (\underline{u}_z \times \underline{E}_{Tn})\, dS = \frac{1}{Z_n^{(2)}} \left[ A_n e^{-\gamma_n z} - B_n e^{\gamma_n z} \right] \qquad (2.188)$$

$$(\gamma_n \neq 0)$$

$$\iint \underline{H} \cdot \text{curl}\, \underline{E}_{Tn}\, dS = \frac{k_{cn}^2}{Z_n^{(2)} \gamma_n} \left[ A_n e^{-\gamma_n z} + B_n e^{\gamma_n z} \right] \qquad (2.189)$$

$$(\gamma_n \neq 0)$$

$$\iint \underline{H} \cdot (\underline{u}_z \times \underline{E}_{Tn})\, dS = i \frac{1}{\omega\mu} D_n \qquad (2.190)$$

$$(\gamma_n = 0)$$

$$\iint \underline{H} \cdot \text{curl}\, \underline{E}_{Tn}\, dS = i \frac{k_{cn}^2}{\omega\mu} (C_n + D_n z) \qquad (2.191)$$

$$(\gamma_n = 0)$$

Similarly, consideration that, for TM modes curl $\underline{E}_{Tn} = 0$ together with the use of eq.(2.147) leads to:

$$\iint \underline{E} \cdot \underline{E}_{Tn} \, dS = A_n \, e^{-\gamma_n z} + B_n \, e^{\gamma_n z} \qquad (2.192)$$

$$(\gamma_n \neq 0)$$

$$\iint \underline{H} \cdot (\underline{u}_z \times \underline{E}_{Tn}) \, dS = \frac{1}{Z_n^{(3)}} \left[ A_n \, e^{-\gamma_n z} - B_n \, e^{\gamma_n z} \right] \qquad (2.193)$$

$$(\gamma_n \neq 0)$$

$$\iint (\underline{u}_z \cdot \underline{E}) \, \mathrm{div} \, \underline{E}_{Tn} \, dS = \frac{k_{cn}^2}{\gamma_n} \left[ A_n \, e^{-\gamma_n z} - B_n \, e^{\gamma_n z} \right] \qquad (2.194)$$

$$(\gamma_n \neq 0)$$

$$\iint \underline{E} \cdot \underline{E}_{Tn} \, dS = i \, \frac{1}{\omega \varepsilon} \, D_n \qquad (2.195)$$

$$(\gamma_n = 0)$$

$$\iint \underline{H} \cdot (\underline{u}_z \times \underline{E}_{Tn}) \, dS = C_n + D_n z \qquad (2.196)$$

$$(\gamma_n = 0)$$

$$\iint (\underline{u}_z \cdot \underline{E}) \, \mathrm{div} \, \underline{E}_{Tn} \, dS = - i \, \frac{k_{cn}^2}{\omega \varepsilon} \, (C_n + D_n z) \qquad (2.197)$$

$$(\gamma_n = 0)$$

Considering that none of the $\gamma_n$ is zero, eq.(2.173) and eq.(2.174) can now be written respectively as:

$$\underline{E} = \sum_{n=1}^{\infty} [\underline{E}_{Tn} ( A_n e^{-\gamma_n z} + B_n e^{\gamma_n z} ) ]$$

$$+ \sum_{n=1}^{\infty} [ \underline{u}_z \frac{k_{cn}^2}{\gamma_n Nn} \text{ div } \underline{E}_{Tn} ( A_n e^{-\gamma_n z} - B_n e^{\gamma_n z} ) ] \qquad (2.198)$$

$$\underline{H} = \sum_{n=1}^{\infty} [ (\underline{u}_z \times \underline{E}_{Tn}) \frac{1}{Z_n} ( A_n e^{-\gamma_n z} - B_n e^{\gamma_n z} ) ]$$

$$- \sum_{n=1}^{\infty} [ \frac{k_{cn}^2}{Z_n \gamma_n Mn} \text{ curl } \underline{E}_{Tn} ( A_n e^{-\gamma_n z} + B_n e^{\gamma_n z} ) ] \qquad (2.199)$$

Noting that

$$\frac{1}{k_{cn} k_{cm}} \iint \text{curl } \underline{E}_{Tn} \cdot \text{curl } \underline{E}_{Tm} \, dS = \frac{k_{cm}}{k_{cn}} \iint \underline{E}_{Tn} \cdot \underline{E}_{Tm} \, dS \qquad (2.200)$$

$$\frac{1}{k_{cn} k_{cm}} \iint \text{div } \underline{E}_{Tn} \text{ div } \underline{E}_{Tm} \, dS = \frac{k_{cm}}{k_{cn}} \iint \underline{E}_{Tn} \cdot \underline{E}_{Tm} \, dS \qquad (2.201)$$

the normalizing factors are given by

$$Mn = Nn = k_{cn}^2 \qquad (2.202)$$

Substitution of eq.(2.202) into eq.(2.198) and eq.(2.199) gives the field expansion in the form:

$$\underline{E} = \sum_{n=1}^{\infty} \left[ \underline{E}_{Tn} \left( A_n e^{-\gamma_n z} + B_n e^{\gamma_n z} \right) \right]$$

$$+ \underline{u}_z \sum_{n=1}^{\infty} \left[ \frac{\operatorname{div} \underline{E}_{Tn}}{\gamma_n} \left( A_n e^{-\gamma_n z} - B_n e^{\gamma_n z} \right) \right] \qquad (2.203)$$

$$\underline{H} = \sum_{n=1}^{\infty} \left[ \underline{u}_z \times \frac{\underline{E}_{Tn}}{Z_n} \left( A_n e^{-\gamma_n z} - B_n e^{\gamma_n z} \right) \right]$$

$$- \sum_{n=1}^{\infty} \left[ \frac{1}{Z_n \gamma_n} \operatorname{curl} \underline{E}_{Tn} \left( A_n e^{-\gamma_n z} + B_n e^{\gamma_n z} \right) \right] \qquad (2.204)$$

Finally, the introduction of eq.(2.138) to eq.(2.145) into eq.(2.203) and eq.(2.204) shows that an arbitrary field configuration propagating along the waveguide can be written as*:

$$\underline{E} = \sum_{n=1}^{\infty} \left[ \underline{E}_{Tn} + \underline{u}_z E_{Ln} \right] A_n e^{-\gamma_n z} + \sum_{n=1}^{\infty} \left[ \underline{E}_{Tn} - \underline{u}_z E_{Ln} \right] B_n e^{\gamma_n z}$$

$$(\gamma_n \neq 0) \qquad (2.205)$$

---

* Adopting the usual convention[25] for waves travelling along the positive and negative direction, eq.(2.205) and eq.(2.206) can be written:

$$\underline{E} = \sum_n \left( \underline{E}_n^+ e^{-i\beta_n z} + \underline{E}_n^- e^{i\beta_n z} \right)$$

$$(\gamma = i\beta)$$

$$\underline{H} = \sum_n \left( \underline{H}_n^+ e^{-i\beta_n z} + \underline{H}_n^- e^{i\beta_n z} \right)$$

$$\underline{H} = \sum_{n=1}^{\infty} \left[ \underline{H}_{Tn} + \underline{u}_z H_{Ln} \right] A_n e^{-\gamma_n z} + \sum_{n=1}^{\infty} \left[ - \underline{H}_{Tn} + \underline{u}_z H_{Ln} \right] B_n e^{\gamma_n z}$$

$$(\gamma_n \neq 0) \qquad (2.206)$$

If some of the propagating functions are zero the coefficients in eq.(2.205) and eq.(2.206) are replaced by using eq.(2.187), eq.(2.190) and eq.(2.191); or eq.(2.195), eq.(2.196) and eq.(2.197) depending on the normal modes concerned.

## 2.12 COMPLETE SOLUTION FOR IDEAL WAVEGUIDES

Once the transverse electromagnetic field configuration on the cross-section $z = 0$ of the waveguide is known, the constants in eq.(2.205) and eq.(2.206) are uniquely determined by the relations:

$$A_n = \tfrac{1}{2} \left[ \iint \underline{E}_T (0) \cdot \underline{E}_{Tn} \, dS + \iint \underline{H}_T (0) \cdot (\underline{u}_z \times \underline{E}_{Tn}) \, dS \right] \quad (2.207)$$

$$B_n = \tfrac{1}{2} \left[ \iint \underline{E}_T (0) \cdot \underline{E}_{Tn} \, dS - \iint \underline{H}_T (0) \cdot (\underline{u}_z \times \underline{E}_{Tn}) \, dS \right] \quad (2.208)$$

As the normal mode transverse electric field intensities can be obtained by using eq.(2.77) and since the other field components can be derived from $\underline{E}_{Tn}$, the waveguide solution is conceptionally com - plete*. The completeness of the solution still holds when either $\underline{E}_T$ or $\underline{H}_T$ are specified on two different cross-sections $z = z_1, z_2$ provided that none of the exponents $\gamma_n(z_2-z_1)$ equals $iK\pi$ (K=0,1,2..).

---

* Analogous treatment can be presented for the transverse magnetic field intensity.

## 2.13 SCALAR WAVEGUIDE FUNCTIONAL

As the waveguide solutions can be expanded into normal mode solutions, a scalar variational expression involving the normal mode generating functions $G_n^{(i)}$ is desirable. Once this scalar functional is obtained its minimization will produce the correct generating functions from which the electromagnetic field can be calculated. Furthermore, as the trial functions become scalar functions the numerical minimization process is simplified.

To develop the scalar functional from the least action principle consider the variation of the variational expression for the propagation function in eq.(2.77) due to a small change in the transverse electric field, $\delta\, \underline{E}_T$, in the form:

$$\delta\, \gamma^2\, (\underline{E}_T) \left( \tfrac{1}{2} \iint [(\text{curl } \underline{E}_T(x,y))^2 - \omega^2 \mu \varepsilon\, \underline{E}_T^2(x,y)]\, dS \right)$$

$$= \iint \Big( [\ \text{curl curl } \underline{E}_T(x,y) - \text{grad div } \underline{E}_T(x,y)$$

$$- \ (\omega^2 \mu \varepsilon + \gamma^2(\underline{E}_T))\ \underline{E}_T(x,y)\ ]$$

$$.\ [\ \text{curl curl } \delta\, \underline{E}_T - \omega^2 \mu \varepsilon\, \delta\, \underline{E}_T\ ] \Big)\, dS$$

$$+ \int_C \left( \underline{n}\ \text{div } \underline{E}_T\ .\ [\ \text{curl curl } \delta\, \underline{E}_T - \omega^2 \mu \varepsilon\, \delta\, \underline{E}_T\ ] \right) dL$$

$$- \ \gamma^2\, (\underline{E}_T) \int_C [\ (\ \underline{n} \times \underline{E}_T(x,y)\ .\ \text{curl } \delta\, \underline{E}_T\ ]\, dL \qquad (2.209)$$

As the variation $\delta\, \gamma^2(\underline{E}_T)$ must vanish, the transverse electric field satisfies simultaneously the waveguide field equation and the boundary conditions or, in other words, any trial vector function

extremizing eq.(2.77) can be obtained, as shown before, through some scalar generating function $G^{(i)}(x,y)$, solution of the homogeneous scalar Helmholtz equation

On the other hand, for any transverse electric field the relation

$$\iint [ ( \text{curl } \underline{E}_T(x,y))^2 - \omega^2\mu\varepsilon \underline{E}_T^2(x,y) ] \, dS \neq 0 \qquad (2.210)$$

holds.

Application of eq.(2.77) respectively for TE and TM modes gives:

$$\gamma^2(\underline{E}_T) = \frac{\iint [ \text{curl curl } \underline{E}_T^{(2)}(x,y) - \omega^2\mu\varepsilon \underline{E}_T^{(2)}(x,y) ]^2 \, dS}{\iint [ (\text{curl } \underline{E}_T^{(2)}(x,y))^2 - ( \omega^2\mu\varepsilon \underline{E}_T^{(2)}(x,y))^2] \, dS} \qquad (2.211)$$

$$\gamma^2(E_T) = \frac{- \omega^2\mu\varepsilon \iint [ (\text{div } \underline{E}_T^{(3)}(x,y))^2 + (\omega^2\mu\varepsilon)^2(\underline{E}_T^{(3)}(x,y))^2] \, dS}{- \omega^2\mu\varepsilon \iint (\underline{E}_T^{(3)}(x,y))^2 \, dS} \qquad (2.212)$$

Simplification of eq.(2.211) by introducing eq.(2.51) yields:

$$\iint ( \text{curl } \underline{E}_T^{(2)}(x,y))^2 \, dS = k_{cn}^2 \iint (\underline{E}_T^{(2)}(x,y))^2 \, dS \qquad (2.213)$$

while the introduction of eq.(2.51) into eq.(2.212) results:

$$\iint ( \text{div } \underline{E}_T^{(3)}(x,y))^2 \, dS = k_{cn}^2 \iint (\underline{E}_T^{(3)}(x,y))^2 \, dS \qquad (2.214)$$

Substitution of eq.(2.108) and eq.(2.121) into eq.(2.213) gives:

$$k_{cn}^2 \iint (G_n^{(2)}(x,y))^2 \, dS = \iint (\text{grad } G_n^{(2)}(x,y))^2 \, dS \qquad (2.215)$$

Similarly, substitution of eq.(2.122) and eq.(2.123) into eq.(2.214) gives :

$$k_{cn}^2 \iint (G_n^{(3)}(x,y))^2 \, dS = \iint (\text{grad } G_n^{(3)}(x,y))^2 \, dS \qquad (2.216)$$

When the generating functions are not the exact solutions but trial functions, $G^{(t)}(x,y)$, satisfying the boundary conditions associated with its mode type, reference to eq.(2.215) and eq.(2.216) suggests the definition of an error functional for the approximation in the form :

$$F(G^{(t)}) = \iint (\text{grad } G^{(t)}(x,y))^2 \, dS - k_{cn}^2 \iint (G^{(t)}(x,y))^2 \, dS \qquad (2.217)$$

The variation of $F(G^{(t)})$ due to a small variation $\delta \, G_n^{(i)}(x,y)$ in $G_n^{(i)}(x,y)$ is given by:

$$\begin{aligned} \delta \, F(G^{(t)}) = & \iint ( \text{grad } (G_n^{(i)}(x,y) + \delta \, G_n^{(i)}(x,y))^2 \, dS \\ & - \iint ( \text{grad } G_n^{(i)}(x,y))^2 \, dS \\ & - 2 \, k_{cn}^2 \iint \delta \, G_n^{(i)}(x,y) \, G_n^{(i)}(x,y) \, dS \\ & - k_{cn}^2 \iint ( \delta \, G_n^{(i)}(x,y))^2 \, dS \qquad (2.218) \end{aligned}$$

Application of Green's first identity to eq.(2.216) gives:

$$F(G^{(t)}) = - \iint [(G_n^{(i)}(x,y) + \delta G_n^{(i)}(x,y))\ \nabla_T^2\ (G_n^{(i)}(x,y) + \delta G_n^{(i)}(x,y))]\ dS$$

$$- \iint (\text{grad}\ G_n^{(i)}(x,y))^2 - 2\ k_{cn}^2 \iint \delta G_n^{(i)}(x,y)\ G_n^{(i)}(x,y)\ dS$$

$$- k_{cn}^2 \iint (\delta\ G_n^{(i)}(x,y))^2\ dS$$

$$+ \int_C [(G_n^{(i)}(x,y) + \delta G_n^{(i)}(x,y))\ \nabla_T (G_n^{(i)}(x,y) + \delta G_n^{(i)}(x,y))].\underline{n}\ dL \tag{2.219}$$

Under either TE or TM boundary conditions, the line integral in eq.(2.219) vanishes. Therefore, neglecting second order terms we have:

$$\delta F(G^{(t)}) = - \iint G_n^{(i)}(x,y)\ \nabla_T^2\ \delta G_n^{(i)}(x,y)\ dS$$

$$- \iint \delta\ G_n^{(i)}(x,y)\ \nabla_T^2\ G_n^{(i)}(x,y)\ dS$$

$$- 2\ k_{cn}^2 \iint G_n^{(i)}(x,y)\ \delta\ G_n^{(i)}(x,y)\ dS \tag{2.220}$$

Application of Green's second identity to eq.(2.220) gives:

$$\delta F(G^{(t)}) = - 2 \iint \delta\ G_n^{(i)}(x,y)\ [\ \nabla_T^2 + k_{cn}^2\ ]\ G_n^{(i)}(x,y)\ dS$$

$$+ \int_C \delta\ G_n^{(i)}(x,y)\ \nabla_T\ G_n^{(i)}(x,y)\ .\ \underline{n}\ dL$$

$$+ \int_C G_n^{(i)}(x,y)\ \nabla_T\ \delta\ G_n^{(i)}(x,y)\ .\ \underline{n}\ dL \tag{2.221}$$

On the boundary, the trial function satisfies the boundary conditions, and the line integral in eq.(2.221) vanishes. Therefore the functional is stationary for any small variation when the trial function equals the exact solution.

Furthermore, from eq.(2.217) the Rayleigh quotient[6]

$$k_{cn}^2 \leqslant - \frac{\iint G_n^{(i)}(x,y)\ \nabla_T^2\ G_n^{(i)}(x,y)\ dS}{\iint (\ G_n^{(i)}(x,y))^2\ dS} \tag{2.222}$$

is obtained for any $G_n^{(i)}(x,y)$ satisfying the boundary condition

$$G_n^{(i)}(x,y)\ \text{grad}\ G_n^{(i)}(x,y)\ .\ \underline{n}\ =\ 0 \tag{2.223}$$

Consequently, under TE or TM boundary conditions any trial function G will produce a positive F(G)[19][20], that is:

$$F\ (\ G^{(t)}\ )\ \geqslant\ 0 \tag{2.224}$$

It can be concluded from the previous results that:

a) The minimization of the scalar functional

$$F(G) = \iint [(\text{grad}\ G)^2 - k_{cn}^2\ G^2\ ]\ dS$$

where G is a function of the transverse co-ordinates satisfying the boundary conditions, determines the normal mode field configuration.

b) The functional F(G) has a minimum zero value when the exact solution is obtained and could be interpreted as a measure of the error for a given estimate of the field distribution.

c) The electromagnetic energy of the exact field configuration corresponds to a stationary value of the action integral.

## 2.14 NON-IDEAL WAVEGUIDES

In practical waveguides the attenuation and coupling due to the wall impedance associated with the non-perfect characteristics of the medium may give rise to situations where the ideal treatment presented in this chapter does not apply. These are, however, particular situations, outside the scope of this work. In general, the field configuration within waveguides of practical interest can be investigated assuming idealistic conditions[30] and consistent results can be expected.

# CHAPTER 3

# THE FINITE ELEMENT METHOD FOR WAVEGUIDES

## 3.1 INTRODUCTION

Chapter 3 describes the application of a specialized version of the Ritz-Garlekin method[31] to the minimization of the waveguide scalar functional

$$F(G) = \iint (\text{grad } G_n(x,y))^2 - k_{cn}^2 \iint (G_n(x,y))^2 \, dS \qquad (3.1)$$

known as the Finite Element Method[32][33].

The central idea of the method consists of approximating the waveguide cross-section by an assembly of small triangular areas in which a suitable dependence of the scalar function $G_n(x,y)$ is assumed. This allows the determination of the nodal values of the functions $G_n(x,y)$ for which $F(G)$ is stationary[34]. A detailed development of the method from the first to higher-order finite element approximation is presented.

A simple numerical experiment involving some of the first propagating modes in a rectangular waveguide and the five-point finite difference operator is used in the chapter to show the limitations of the first-order finite element approximation. Higher-order fini-

te element models are then constructed by resorting to triangle area co-ordinates which provide a natural extension of the method to problems in 3-D spaces.

A brief description of a computer program[11][35] which became available in Leicester and has been used during this research work is presented. Examples of generating function nodal values obtained using the program are given. The use of a finite element technique to solve 3-D vector field problems in waveguides[36] is also briefly described in this chapter.

## 3.2 THE FINITE ELEMENT MODEL OF THE CROSS-SECTION

The process of discretizing the continuum waveguide cross-section by the finite element method in order to proceed to the minimization of the scalar functional can be summarized as follows.

Let S be either a simply or multiply connected bounded region of the cartesian plane with boundary C. Let the boundary C consist of a finite number of closed non-intersecting curves $C_1, C_2, \ldots C_n$, included in the region S. Finally define a general set of functions $[\ G_n(x,y)\ ]$ for which eq.(3.1) has a unique value on S.

Instead of finding the true functions $G_n(x,y)$ within the set $[\ G_n(x,y)\ ]$ for which the scalar functional has its minimum value , the finite element formulation employs finite subdomains $S_D$ defined in S to construct a model region $S_M$ where an approximation to the true functions, $G_{Mn}(x,y)$ , can be obtained.

Any proper assembly of subdomains or elements into a connected model region gives an approximate global solution over the primitive region. Because it is possible to use and arrange different subdomains $S_D$ for the same model region $S_M$ it is possible to develop

different finite element models for the primitive region S.

The process of dividing S into subdomains $S_D$ is known as "finite element mesh generation" and although playing a very important part when accuracy and the interpretation of results are concerned, will not be considered in detail here. It constitutes a research topic outside the scope of the present thesis. Rather , for the purpose of this work and without loss of generality the model region $S_M$ is assumed to be constructed by following the steps given in table T (3.1)[16]. An example of application of the procedure described by table T (3.1) to a general waveguide cross-section to obtain its finite element model is depicted in Fig(3.1) and Fig(3.2).

## 3.3 FORMALISM OF THE FIRST-ORDER FINITE ELEMENT MODEL

The transformation of the waveguide integro-differential problem into an algebraic problem by the discretization of the cross-section using first-order elements will now be discussed.

Consider, in the model region, the subdomain defined by the nodal points $N_i, N_j$ and $N_k$. Assume that the function $G_{Mn}(x,y)$ which minimizes eq.(3.1) when the integration is carried over the model region has at those nodal points the values $G_i, G_j$ and $G_k$.

Further, assume that the function $G_{Mn}(x,y)$ can be described over the element by the following equation:

$$G^e_{Mn}(x,y) = P^e_1(x,y) \tag{3.2}$$

where $P^e_1$ is a complete first-order polynomial expression[37] uniquely defined for each element. The polynomial $P^e_1$ characterizes the

| | |
|---|---|
| STEP 1 : | A finite number N of points of S are identified as nodal points and labelled $N_g (g = 1,2,\ldots,N)$ |
| STEP 2 : | A finite number M of triangular elements $T_g$ are defined on the nodal points. This step actually creates the M closed disjoint elements $T_g (g = 1,2,\ldots,M)$ |
| STEP 3 : | The nodal points associated with a given element are called local nodes and labelled $N_\ell (\ell = 1,2,3)$ |
| STEP 4 : | The elements are assembled, creating the model $S_M$ of the primitive region S. The assembly is done by grouping the m elements adjacent to a specific node. |

TABLE T 2.1 : Method for constructing the finite element model $S_M$ of a primitive region S.

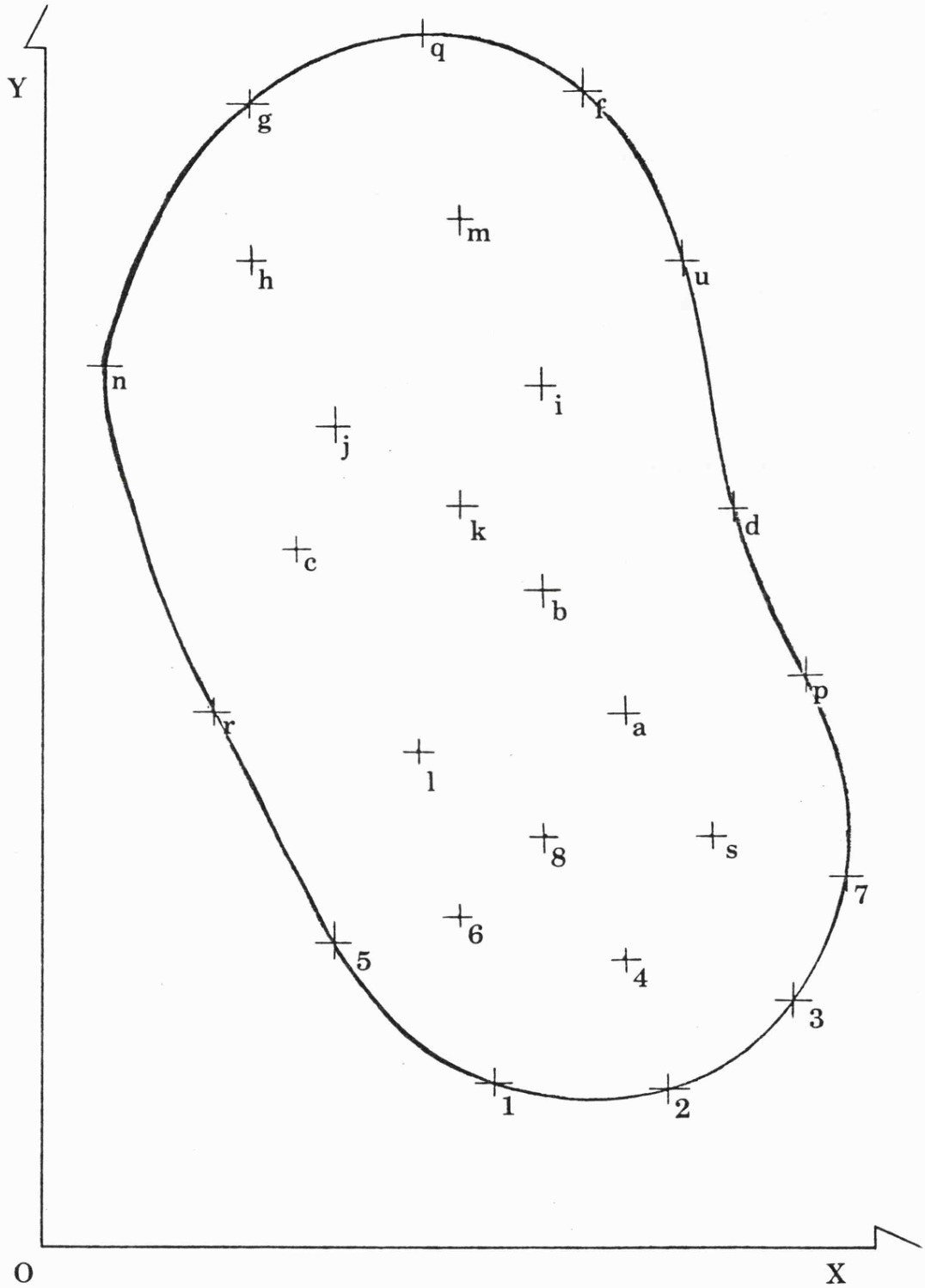


FIG.3.1 WAVEGUIDE CROSS-SECTION AND NODAL POINTS

Nodal points are defined and labelled on the waveguide cross-section.

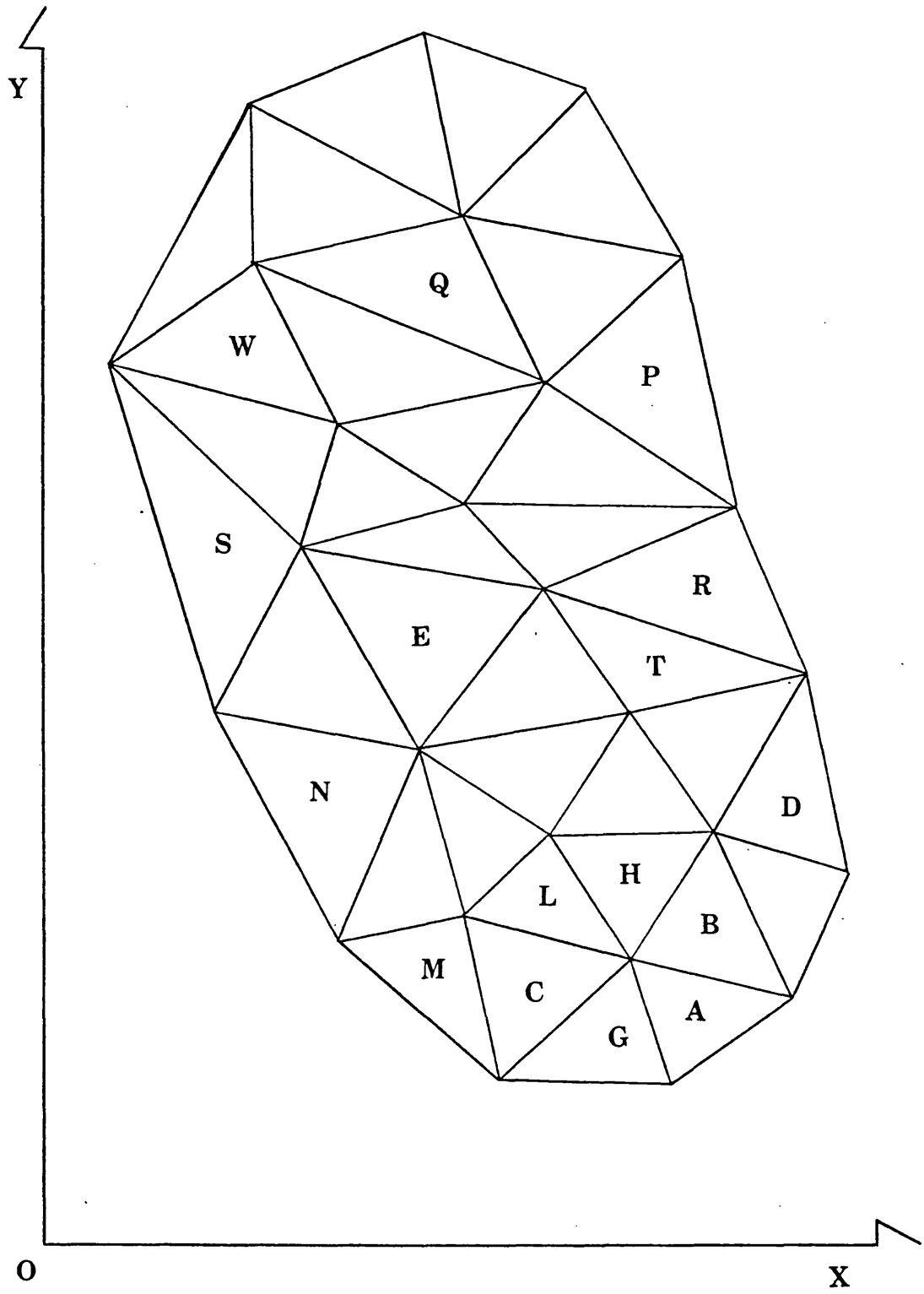


FIG. 3.2 FINITE ELEMENT CROSS-SECTION MODEL

The cross-section model is formed by grouping the triangle elements.

order of the approximation of the generating function* inside the element and is made to vanish at any point outside the element boundaries. The domain of the generating function when the variables x and y assume values which are enclosed by the element boundaries is represented in eq.(3.2) by $G^{e}_{Mn}(x,y)$.

Substitution of eq.(3.2) into eq.(3.1) transforms the scalar variational expression for normal mode propagation in waveguides within each element into a function of the nodal values $G_{\ell}$. Because N nodes have been defined over the model region and the integration over the cross-section corresponds to the summation of the integrals over each individual element, the functional F(G) can be written as a function H of the nodal values:

$$F(G) = H\,(G_1, G_2, \ldots G_n) \tag{3.3}$$

---

* The nomenclature here differs from the usual. This has been done deliberately by the author, fearing that the usual terminology would possibly obscure the way in which the matter is being treated. For instance, it is usual to call the functions $G_{Mn}(x,y)$ "potential functions". This has not been done here as the term "potential" has been used in Chapter 2 with a specific meaning which would not be applicable to $G_{Mn}(x,y)$. It was decided to call those functions "generating functions" because the field distribution is derived[26] from them. In fact, this terminology has already been used in Chapter 2, but, there, the usual practice in the literarure is to use the longitudinal components of the field in place of $G_{Mn}(x,y)$ and the question on what to call the function did not appear pertinent.

Finally, the optimum set of values $G_\ell$ is obtained by solving the N-equations system given by:

$$\frac{\delta H}{\delta G_\ell} = 0 \tag{3.4}$$

3.3.1 FINITE ELEMENT MATRICES

The algebraic problem represented by eq.(3.4) can be described in a compact form by resorting to matrix notation. To do so, the dependence of the generating function on the element nodal values is written in the form:

$$G^e_{Mn}(x,y) = [\, N^e \,]\ [\, G^e \,] \tag{3.5}$$

where

$$[\, N^e \,] = [\, N^e_i(x,y) \quad N^e_j(x,y) \quad N^e_k(x,y) \,] \tag{3.6}$$

is a function of the element geometry, called"shape" function and

$$[\, G^e \,] = \begin{bmatrix} G_i \\ G_j \\ G_k \end{bmatrix} \tag{3.7}$$

On the other hand, within an element, the gradient of the generating function is expressed by[38]

$$\text{grad } G^e_{Mn}(x,y) = [\, B^e \,] \; [\, G^e \,] \tag{3.8}$$

where

$$[\, B^e \,] = \begin{bmatrix} \frac{\delta}{\delta x} N^e_i(x,y) & \frac{\delta}{\delta x} N^e_j(x,y) & \frac{\delta}{\delta x} N^e_k(x,y) \\ & & \\ \frac{\delta}{\delta y} N^e_i(x,y) & \frac{\delta}{\delta y} N^e_j(x,y) & \frac{\delta}{\delta y} N^e_k(x,y) \end{bmatrix} \tag{3.9}$$

Substitution of eq.(3.8) and eq.(3.5) into eq.(3.1) with the integration performed over the element area and comparison with eq.(3.3) gives:

$$H(G_i,G_j,G_k) = \iint_{\text{element}} ([B^e]\,[G^e])^2 dS - k^2_{cn} \iint_{\text{element}} ([N^e]\,[G^e])^2 dS \tag{3.10}$$

Application of eq.(3.4) to eq.(3.10) leads to:

$$[\, S^e \,] \; [\, G^e \,] = k^2_{cn} \; [\, T^e \,] \; [\, G^e \,] \tag{3.11}$$

where $[S^e]$ and $[T^e]$ are square (3x3) matrices with generic components given respectively by[8]:

$$S^e_{ij} = \iint_{\text{element}} \left( \frac{\delta}{\delta x} N^e_i(x,y) \frac{\delta}{\delta x} N^e_j(x,y) + \frac{\delta}{\delta y} N^e_i(x,y) \frac{\delta}{\delta y} N^e_j(x,y) \right) dS \tag{3.11}$$

$$T^e_{ij} = \iint_{\text{element}} N^e_i(x,y) \; N^e_j(x,y) \, dS \tag{3.13}$$

As the permutation of the subscripts i and j in eq.(3.12) and eq.(3.13) does not change the integrands, the matrices $[\, S^e \,]$ and $[\, T^e \,]$ are symmetric. Therefore, the minimization of the functional F(G) over the cross-section is equivalent to solving the algebraic eigenvalue problem[39][40] expressed by:

$$[\, S \,][\, G \,] = k^2_{cn}[\, T \,][\, G \,] \tag{3.14}$$

where the matrices $[\, S \,]$ and $[\, T \,]$ are obtained by adding the contributions of all elements in the cross-section.

Each element contains three values of $G_\ell$ and each $G_\ell$ is common to those elements having the vertex $\ell$ in common. The matrices [S] and $[\, T \,]$ are then sparse since the number of elements having vertices in common is much less than the total number of elements.

### 3.3.2 COMPARISON WITH THE FINITE DIFFERENCE METHOD

The finite element method shows, when compared with the finite difference method (which again leads to the same algebraic formalism) the advantages of being able to tackle the boundaries directly (the nodes are defined over the boundary within the modeling process) and of being easily extendable to higher order approximations.

## 3.4 HIGHER ORDER APPROXIMATIONS AND OTHER APPLICATIONS

The extension of the method to higher order approximation can be done without considerable expense in computing time[41] and is accomplished by resorting to triangle area co-ordinates[42] as will be shown later. The method can be applied to dissipative propagation[43][44]. Also, the finite element technique can be transposed to 3-D scalar problems[45][46] by replacing the triangle area co-ordinates by tetrahedron volume co-ordinates (under strictly the same formalism). Further, the method can be adapted to problems defined using polar co-ordinates[47] or even general orthogonal curvilinear co-ordinates[48]. Three-dimensional vector finite element formulations have also been applied to waveguide propagation problems and as long as a large computer is available , results can be produced[36][49][50][51][52].

## 3.5 CALCULATION OF THE FIRST-ORDER FINITE ELEMENT MATRIX COMPONENTS

The calculation of the first-order finite element matrix components is presented here to illustrate the application of the general equation for the system given by eq.(3.3).

Consider one among the m elements adjacent to the node $N_0$ having vertices and associated angles as shown in Fig.(3.3). When $G_{0j}$ is perturbed and all the other nodal values of the function $G_{Mn}(x,y)$ are kept constant, the functional given by eq.(3.3) changes only in the m triangles adjoining the node $N_0$.

Denote the part of the funcional associated with the m triangles adjoining the node $N_0$ by $H_0$ and make, according to eq.(3.1),

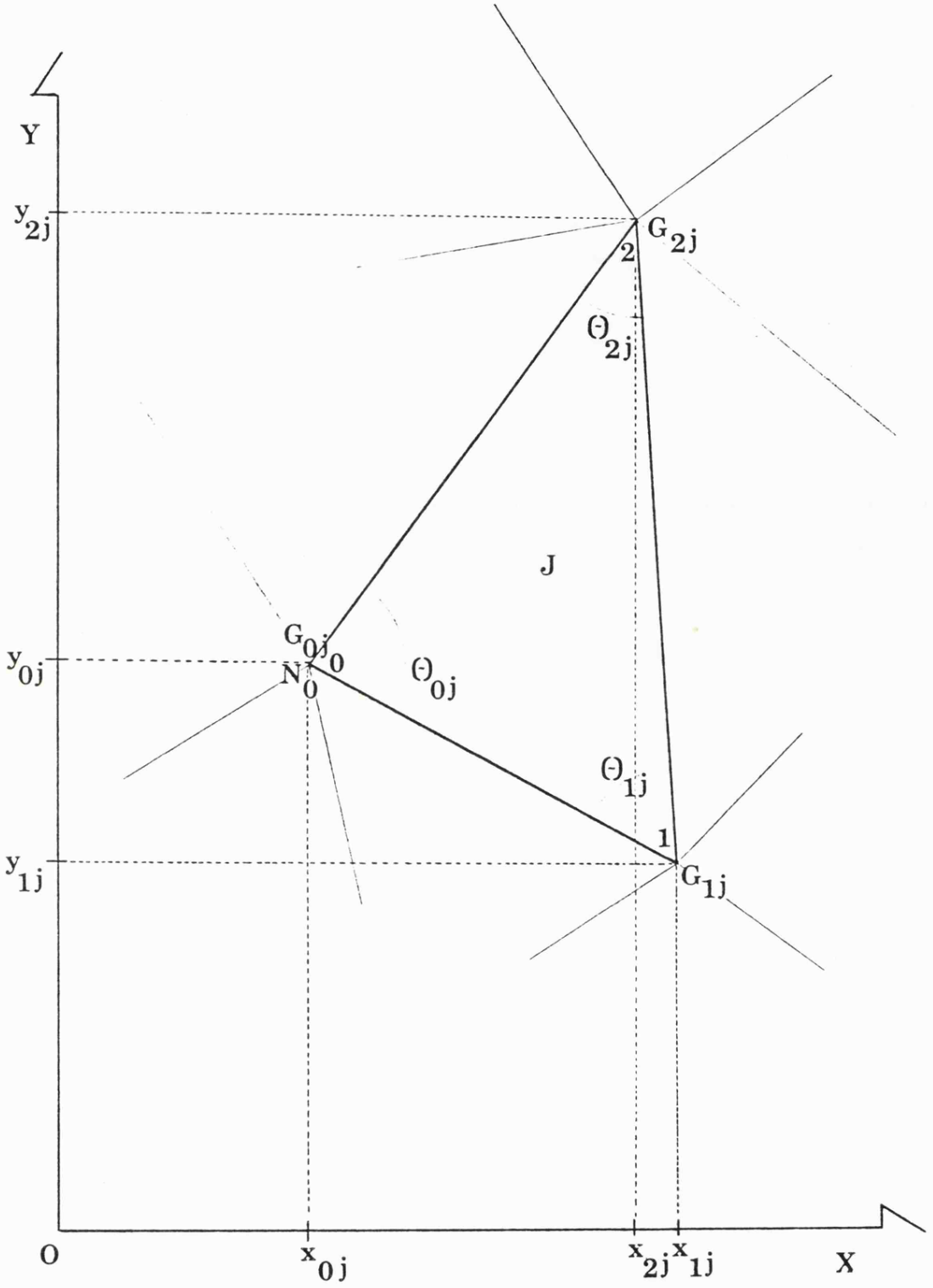


FIG. 3.3 THE ELEMENT J ADJOINING NODE $N_0$

The local numbering system, angles, nodal values and node co-ordinates of a typical first-order element are shown.

$$H_0 = H_{01} - H_{02} \tag{3.15}$$

where

$$H_{01} = \sum_{j=1}^{m} \iint_{ej} (\text{grad } (G_{Mn}^{ej}(x,y))^2 \, dS \tag{3.16}$$

$$H_{02} = k_{cn}^2 \sum_{j=1}^{m} \iint_{ej} (G_{Mn}^{ej}(x,y))^2 \, dS \tag{3.17}$$

and ej denotes the $j^{th}$ element adjoining $N_0$.

Further, assume that the function $G_{Mn}^{ej}(x,y)$ is described within the element by the first order complete polynomial:

$$G_{Mn}^{ej}(x,y) = a_1 + a_2 x + a_3 y \tag{3.18}$$

where $a_1$, $a_2$ and $a_3$ are coefficients to be determined and x and y the cartesian co-ordinates.

The gradient of $G_{Mn}^{ej}(x,y)$ is then written in the form

$$\text{grad } G_{Mn}^{ej}(x,y) = \underline{u}_x \, a_2 + \underline{u}_y \, a_3 \tag{3.19}$$

Therefore, $H_{01}$ in eq.(3.16) reduces to

$$H_{01} = \sum_{j=1}^{m} \iint_{ej} (a_2^2 + a_3^2) dxdy = \sum_{j=1}^{m} A_j (\text{grad } G_{Mn}^{ej}(x,y))^2 \tag{3.20}$$

where $A_j$ is the area of the element $e_j$.

Define $H_{01}^0$ and $H_{02}^0$ respectively as the parts of $H_{01}$ and $H_{02}$ depending on the nodal value $G_{0j}$. Differentiating F(G) (eq.(3.15)) with respect to $G_{0j}$ and equating the result to zero (eq.(3.3)) we get:

$$\frac{\delta H_{01}^0}{\delta G_{0j}} = \frac{\delta H_{02}^0}{\delta G_{0j}} \tag{3.21}$$

To calculate the derivatives in eq.(3.21), we write, making use of eq.(3.18):

$$\begin{bmatrix} G_{0j} \\ G_{1j} \\ G_{2j} \end{bmatrix} = \begin{bmatrix} 1 & x_{0j} & y_{0j} \\ 1 & x_{1j} & y_{1j} \\ 1 & x_{2j} & y_{2j} \end{bmatrix} \begin{bmatrix} a_1 \\ a_2 \\ a_3 \end{bmatrix} \tag{3.22}$$

Solving eq.(3.22) for $a_1$, $a_2$ and $a_3$ we get

$$a_1 = \frac{1}{2A_j}\big(G_{0j}(x_{1j}y_{2j} - x_{2j}y_{1j}) + G_{1j}(x_{2j}y_{0j} - x_{0j}y_{2j}) + G_{2j}(x_{0j}y_{1j} - x_{1j}y_{0j})\big) \tag{3.23}$$

$$a_2 = \frac{1}{2A_j}\big(G_{0j}(y_{1j} - y_{2j}) + G_{1j}(y_{2j} - y_{0j}) + G_{2j}(y_{0j} - y_{1j})\big) \tag{3.24}$$

$$a_3 = \frac{1}{2A_j}(G_{0j}(x_{2j} - x_{1j}) + G_{1j}(x_{0j} - x_{2j}) + G_{2j}(x_{1j} - x_{0j})) \qquad (3.25)$$

where[53]

$$2A_j = \begin{bmatrix} 1 & x_{0j} & y_{0j} \\ 1 & x_{1j} & y_{1j} \\ 1 & x_{2j} & y_{2j} \end{bmatrix} \qquad (3.26)$$

In order to calculate the derivative on the left hand side of eq.(3.21) we first consider the expression:

$$\frac{\delta}{\delta G_{0j}} (\text{grad } G^{ej}(x,y))^2 = 2 [ (\text{grad } G^{ej}_{Mn}(x,y)) . \frac{\delta}{\delta G_{0j}} (\text{grad } G^{ej}_{Mn}(x,y))]$$

$$= 2 [ \frac{\delta}{\delta G_{0j}} ( \frac{\delta}{\delta x} G^{ej}_{Mn}(x,y)) \frac{\delta}{\delta x} G^{ej}_{Mn}(x,y)$$

$$+ \frac{\delta}{\delta G_{0j}} ( \frac{\delta}{\delta y} G^{ej}_{Mn}(x,y)) \frac{\delta}{\delta y} G^{ej}_{Mn}(x,y)] \qquad (3.27)$$

Taking into account eq.(3.23) to eq.(3.25), the terms of eq.(3.27) are calculated:

$$\frac{\delta}{\delta G_{0j}} ( \frac{\delta}{\delta x} G^{ej}_{Mn}(x,y))^2 = \frac{1}{2A_j^2} [(y_{1j} - y_{2j})^2 G_{0j} + (y_{2j} - y_{0j})(y_{1j} - y_{2j}) G_{1j}$$

$$+ (y_{0j} - y_{1j})(y_{1j} - y_{2j}) G_{2j} ] \qquad (3.28)$$

$$\frac{\delta}{\delta G_{0j}} \left( \frac{\delta}{\delta y} G_{Mn}^{ej}(x,y)\right)^2 = \frac{1}{2A_j^2} [(x_{1j} - x_{2j})^2 G_{0j} + (x_{2j} - x_{1j})(x_{0j} - x_{2j}) G_{1j}$$

$$+ (x_{2j} - x_{1j})(x_{1j} - x_{0j}) G_{2j}] \qquad (3.29)$$

Addition of eq.(3.28) and eq.(3.29) and the use of eq.(3.20) and eq.(3.16) gives the derivative on the left hand side of eq.(3.21) in the form:

$$\frac{\delta H_{01}^{0}}{\delta G_{0j}} = \sum_{j=1}^{m} \sum_{i=0}^{2} k_{ij} G_{ij}. \qquad (3.30)$$

with the coefficients $k_{ij}$ given by:

$$k_{0j} = \frac{1}{2A_j} [(y_{1j} - y_{2j})^2 + (x_{2j} - x_{1j})^2] \qquad (3.31)$$

$$k_{1j} = \frac{1}{2A_j} [(y_{2j} - y_{0j})(y_{1j} - y_{2j}) + (x_{2j} - x_{1j})(x_{0j} - x_{2j})] \qquad (3.32)$$

$$k_{2j} = \frac{1}{2A_j} [(y_{0j} - y_{1j})(y_{1j} - y_{2j}) + (x_{2j} - x_{1j})(x_{1j} - x_{0j})] \qquad (3.33)$$

The right hand side of eq.(3.19) will now be calculated. The substitution of the result (together with eq.(3.20)) back into eq.(3.19) gives an equation relating the nodal value $G_{0j}$ to the nodal values of all the m triangles adjoining node $N_0$, called the nodal equation.

Differentiation of the second term in eq.(3.15) with respect to $G_{0j}$ gives:

$$\frac{\delta H_{02}^{0}}{\delta G_{0j}} = k_{cn}^{2} \sum_{j=1}^{m} 2 \iint_{ej} G_{Mn}^{ej}(x,y) \frac{\delta}{\delta G_{0j}} G_{Mn}^{ej}(x,y)\, dS \qquad (3.34)$$

Substitution of eq.(3.23) to eq.(3.25) into eq.(3.18) gives:

$$\begin{aligned} G_{Mn}^{ej} = \frac{1}{2A_j} & [(x_{1j}y_{2j} - x_{2j}y_{1j}) + (y_{1j} - y_{2j})x + (x_{2j} - x_{1j})y]\, G_{0j} \\ & + [(x_{2j}y_{0j} - x_{0j}y_{2j}) + (y_{2j} - y_{0j})x + (x_{0j} - x_{2j})y]\, G_{1j} \\ & + [(x_{0j}y_{1j} - x_{1j}y_{0j}) + (y_{0j} - y_{1j})x + (x_{1j} - x_{0j})y]\, G_{2j} \end{aligned} \qquad (3.35)$$

Defining the coefficients[41]

$$d_{i0} = \begin{bmatrix} x_{i+1} & y_{i+1} \\ x_{i+2} & y_{i+2} \end{bmatrix} \qquad (i = 0,1,2) \qquad (3.36)$$

$$d_{i1} = y_{i+1} - y_{i+2} \qquad (i = 0,1,2) \qquad (3.37)$$

$$d_{i2} = x_{i+2} - x_{i+1} \qquad (i = 0,1,2) \qquad (3.38)$$

where the subscripts (i+1) and (i+2) are cyclic with modulo 3,

the integrand in eq.(3.34) can be written in the form:

$$G_{Mn}^{ej}(x,y)\ \frac{\delta}{\delta G_{0j}}\ G_{Mn}^{ej}(x,y) = \frac{1}{4A_j^2}\ (d_{00} + d_{01}x + d_{02}y) \sum_{i=0}^{2} (d_{i0} + d_{i1}x + d_{i2}y)G_{ij} \tag{3.39}$$

Integration over the element area (see Appendix 1) gives:

$$\frac{\delta H_{02}^{0}}{\delta G_{0j}} = \sum_{j=1}^{m} A_j \left[ \frac{1}{3}\ G_{0j} + \frac{1}{6}\ (G_{1j} + G_{2j}) \right] \tag{3.40}$$

Defining the coefficients:

$$k_{3j} = \frac{1}{3}\ A_j \tag{3.41}$$

$$k_{12j} = \frac{1}{6}\ A_j \tag{3.42}$$

and combining eq.(3.40); eq.(3.30) and eq.(3.21) the nodal equation is finally obtained in the form:

$$G_{0j} = - \frac{1}{\sum_{j=1}^{m} (k_{0j} - k_{cn}^2 k_{3j})} \cdot \sum_{j=1}^{m} \left[k_{1j}G_{1j} + k_{2j}G_{2j} - k_{cn}^2 k_{12j}(G_{1j} + G_{2j})\right] \tag{3.43}$$

Once the nodal equation has been obtained, the matrices [ S ] and [ T ] in eq.(3.14) are assembled by considering each of the N nodes defined over the model region.

## 3.6 ALGEBRAIC FORM OF THE COEFFICIENTS $k_{ij}$

In the literature, the coefficients $k_{ij}$ are usually taken as one half of the coefficients given by eq.(3.31), eq.(3.32),eq(3.33) eq.(3.41) and eq.(3.42). This occurs because the functional F(G)is usually defined as one half of the functional presented here. It has been shown in Chapter 2, however, that the constant multiplier ($\frac{1}{2}$) does not appear naturally from the principle of least action governing the electromagnetic fields inside the waveguide. The introduction of any constant multiplier, although neither changing the minimum requirements over the functional F(G) nor alterating the result expressed by eq.(3.43), would lack consistency in the context of this thesis.

## 3.7 TEM PROPAGATION AND THE ANGULAR FORM OF THE COEFFICIENTS $k_{ij}$

In the case of TEM propagation, $H^0_{02} = 0$ since $k^2_{cn} = 0$. Therefore, the nodal equation simplifies, being given (eq.(3.43)) by:

$$G_{0j} = \frac{1}{k_{0j}} \sum_{j=1}^{m} \sum_{i=1}^{2} k_{ij} G_{ij} \tag{3.44}$$

The coefficients in eq.(3.44) are those given by eq.(3.31) to eq.(3.33). They can alternatively be calculated through the following relationships (Appendix 1) :

$$k_{0j} = \sum_{i=1}^{2} \operatorname{cotg} \theta_{ij} \tag{3.45}$$

$$k_{ij} = \text{cotg}\ \theta_{ij} \tag{3.46}$$

where $\theta_{ij}$ is the angle subscribed by the triangle sides joining at vertex $N_{ij}$ as shown in Fig.(3.3).

When a regular mesh is being used, all $\theta_{ij}$ are equal. In this particular case, the nodal value $G_0$ becomes , by using eq.(3.44), equal to the arithmetic average of the neighbouring nodal values,in the form:

$$G_0 = \frac{1}{m} \sum_{j=1}^{m} G_j \tag{3.47}$$

The result expressed in eq.(3.47) is identical to the finite difference formula used to solve Laplace's equation with an equilateral polygonal mesh[54][55]. The averaging property of this type of solution may be employed to generate the mesh[56] where to solve the general equation with $(\delta H^0_{02} \ / \ \delta G_{0j}) \neq 0$ .

Further illustrative comparisons between the firs-order finite element approximation and the finite difference operator for Helmholtz equation will be considered later.

## 3.8 COMPACT FORM OF THE NODAL EQUATION

Defining the coefficients[16]

$$k_1 = \sum_{j=1}^{m} k_{0j} \tag{3.48}$$

$$k_0 = \sum_{j=1}^{m} k_{3j} \tag{3.49}$$

$$k_2 = \sum_{j=1}^{m} (k_{1j}G_{1j} + k_{2j}G_{2j}) \tag{3.50}$$

$$k_3 = \sum_{j=1}^{m} k_{12j}(G_{1j} + G_{2j}) \tag{3.51}$$

it is possible to write eq.(3.43) in the compact form:

$$G_{0j} = \frac{k_{cn}^2 k_3 - k_2}{k_1 - k_{cn}^2 k_0} \tag{3.52}$$

The compact form of the first-order finite element nodal equation is particularly useful for establishing comparisons with the result obtainable by the finite difference method.

## 3.9 APPROXIMATIONS TO THE FIRST-ORDER FINITE ELEMENT NODAL EQUATION AND THE FIVE POINT DIFFERENCE OPERATOR

Consider the regular mesh of Fig.(3.4) and the elements adjoining node $N_0$. The elements and their nodes are labelled as shown. Applying eq.(3.48) to eq.(3.51), taking into account eq.(3.31) to eq.(3.33) and eq.(3.41) and eq.(3.42), the coefficients in eq.(3.52) are calculated:

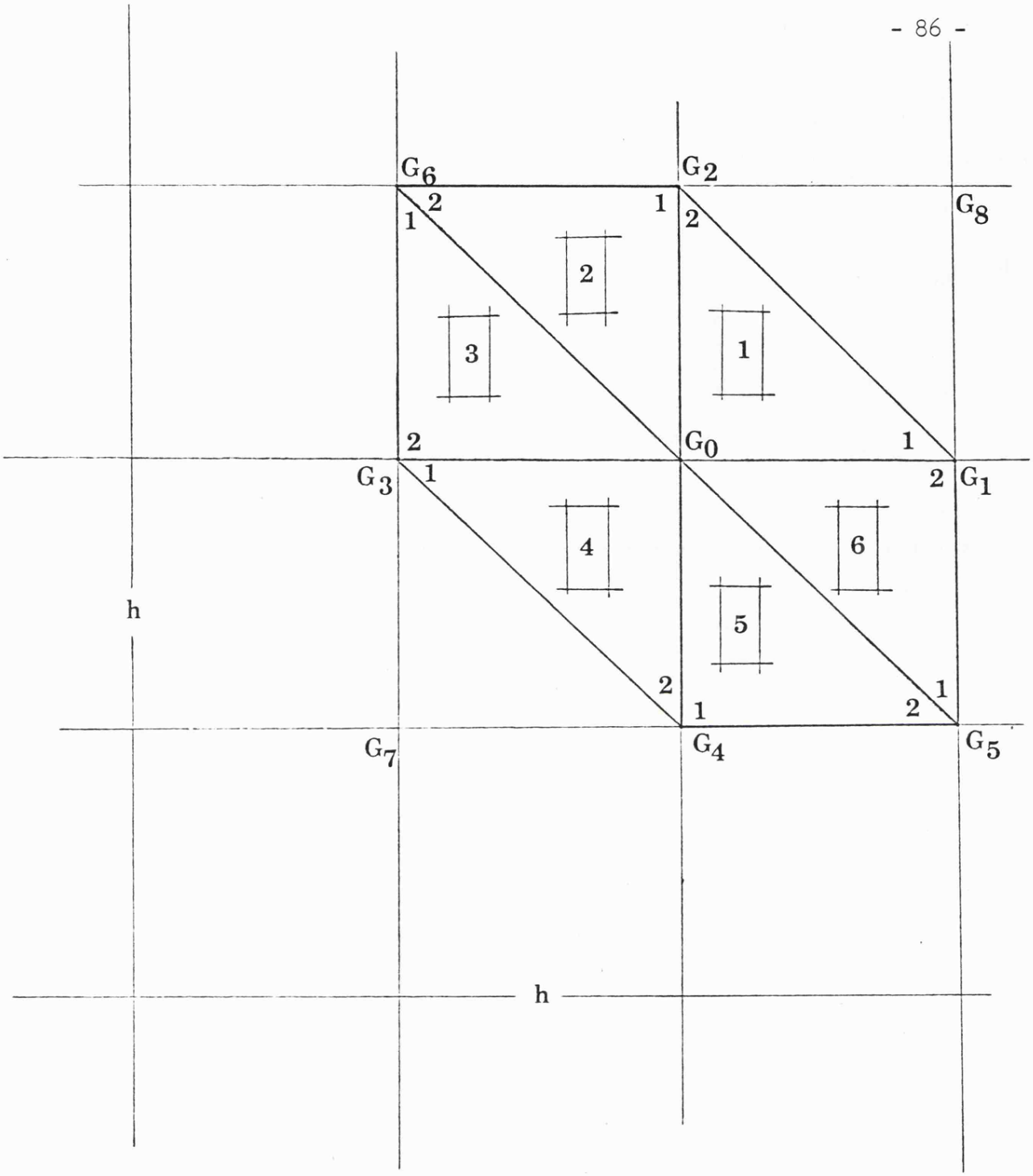


FIG.3.4 FINITE ELEMENT DIVISION OF A REGULAR MESH

The triangulation of a regularly spaced mesh for the application of the finite element nodal equation to node $G_0$.

$$k_0 = h^2 \tag{3.53}$$

$$k_1 = 8 \tag{3.54}$$

$$k_2 = -2\,(G_1 + G_2 + G_3 + G_4) \tag{3.55}$$

$$k_3 = \frac{h^2}{12}\,(G_1 + G_2 + G_3 + G_4 + G_5 + G_6) \tag{3.56}$$

Once the coefficients for the regular mesh have been calculated, eq.(3.52) can be written in the form:

$$G_0 = \frac{k_{cn}^2 \frac{h^2}{6}\,(G_1 + G_2 + G_3 + G_4 + G_5 + G_6) + 2\,(G_1 + G_2 + G_3 + G_4)}{8 - k_{cn}^2\ h^2} \tag{3.57}$$

If we assume that the nodal values are distributed in such way that eq.(3.47) can be regarded as a valid approximation to the central node value ; that is, if we assume that the solutions of Helmholtz equation also have the averaging property exhibited by the solution of Laplace's equation, then eq.(3.57) can be written in the form:

$$G_0 = \frac{1}{4 - k_{cn}^2\ h^2}\,[\,G_1 + G_2 + G_3 + G_4\,] \tag{3.58}$$

where

$$\frac{1}{6}\sum_{j=1}^{6} G_j \approx G_0 \tag{3.59}$$

Because eq.(3.58) is identical to the five-point finite difference operator for Helmholtz equation, it appears from the foregoing analysis that the five-point finite difference operator corresponds to an approximation of the first-order finite element nodal equation implying that the nodal value at any point can be calculated, as in the TEM case, by arithmetically averaging the neighbouring values.

On the other hand, assuming the validity of eq.(3.59),eq.(3.56) can be written in the form:

$$k_3 = \frac{h^2}{2} G_0 \tag{3.60}$$

Substitution of eq.(3.60) into eq.(3.57), taking into account eq.(3.53), eq.(3.54) and eq.(3.55) gives:

$$G_0 = - \frac{k_2}{k_1 - 2 k_{cn}^2 k_0} \tag{3.61}$$

Because the assumption of validity of eq.(3.59) when approximating the central node value gives the five-point finite difference operator for Helmholtz equation, eq.(3.61) can be interpreted as the expression of that operator in terms of the first-order finite element coefficients $k_0$, $k_1$ and $k_2$.

Referring to the first-order finite element nodal equation (eq.(3.43)) we write:

$$G_0 \sum_{j=1}^{6} k_{0j} = k_{cn}^2 \sum_{j=1}^{6} G_0 k_{3j} + (G_{1j} + G_{2j}) k_{2j}$$

$$- \sum_{j=1}^{6} (G_{1j} k_{1j} + G_{2j} k_{2j}) \qquad (3.62)$$

Now making,

$$(G_{1j} + G_{2j}) k_{2j} \approx k_{3j} G_0 \qquad (3.63)$$

we have

$$G_0 = - \frac{\sum_{j=1}^{6} (G_{1j} k_{1j} + G_{2j} k_{2j})}{\sum_{j=1}^{6} k_{0j} - 2k_{cn}^2 \sum_{j=1}^{6} k_{j3}} \qquad (3.64)$$

Taking account eq.(3.48) to eq.(3.51) we get

$$G_0 = - \frac{k_2}{k_1 - 2k_{cn}^2 k_0} \qquad (3.65)$$

Comparison of eq.(3.65) and eq.(3.61) shows that the approximation given respectively by eq.(3.59) and eq.(3.63) are equivalent. In fact it can be shown by substituting for $k_{12j}$ and $k_{3j}$ in eq.(3.63) that its use implies eq.(3.59).

Finally, by considering Fig.(3.4), it appears that eq.(3.57) is not a symmetric equation since it involves all the first but only

two of the second neighbours of the node $N_0$. A symmetric finite element nodal equation can be obtained, however, by considering the other possibility of dividing the regular mesh around $N_0$ into triangles including the generating function values $G_7$ and $G_8$ instead of $G_5$ and $G_6$.

Adding the nodal equations for both possibilities and solving for $G_0$, we get

$$G_0 = \frac{1}{8 - k_{cn}^2 h^2} \left[ \left(2 + \frac{h^2 k_{cn}^2}{6}\right) (G_1 + G_2 + G_3 + G_4) + \frac{h^2 k_{cn}^2}{6} (G_5 + G_6 + G_7 + G_8) \right] \tag{3.66}$$

which is the symmetric first-order finite element nodal equation.

## 3.10 A SIMPLE NUMERICAL EXPERIMENT IN RECTANGULAR WAVEGUIDE

A simple numerical experiment using the finite difference five-point operator, the first-order finite element nodal equation and the symmetric first-order finite element nodal equation to approximate the generating functions in a rectangular waveguide has been performed in order to establish a comparison between those expressions.

The rectangular waveguide has been chosen since its geometry is easily divided into a regular square mesh and the analytical expression for the generating functions are well known.

The experiment is presented here to illustrate the inherent li-

mitations of the first-order finite element model and the dependence of the finite difference results on the mesh length.

### 3.10.1 METHOD

In the experiment a rectangular waveguide cross-section having ratio of the narrower to the broader sides equal to $\frac{1}{2}$ is firstly divided into a regular square mesh as shown in Fig.(3.5). The values of the generating function for $TE_{m,n}$ modes and $TM_{m,n}$ modes are calculated at each nodal point using the analytical solutions[57].They are given respectively by:

$$G^{(2)}_{m,n} = K^{(2)}_{m,n} \cos\left(\frac{m\pi}{A} x\right) \cos\left(\frac{n\pi}{B} y\right) \tag{3.67}$$

$$G^{(3)}_{m,n} = K^{(3)}_{m,n} \sin\left(\frac{m\pi}{A} x\right) \sin\left(\frac{n\pi}{B} y\right) \tag{3.68}$$

where $K^{(i)}_{m,n}$ are amplitude constants, assumed by convenience to be unity and A and B the cross-section sides as shown in Fig.(3.5).

The results of the calculation are printed out and stored.Each internal node is then calculated based on the analytical values of the neighbourhood by

i) Five-point finite difference operator

ii) First-order finite element nodal equation

iii) Symmetric first-order finite element nodal equation.

A map of the foregoing calculation is printed out. Also a nod-

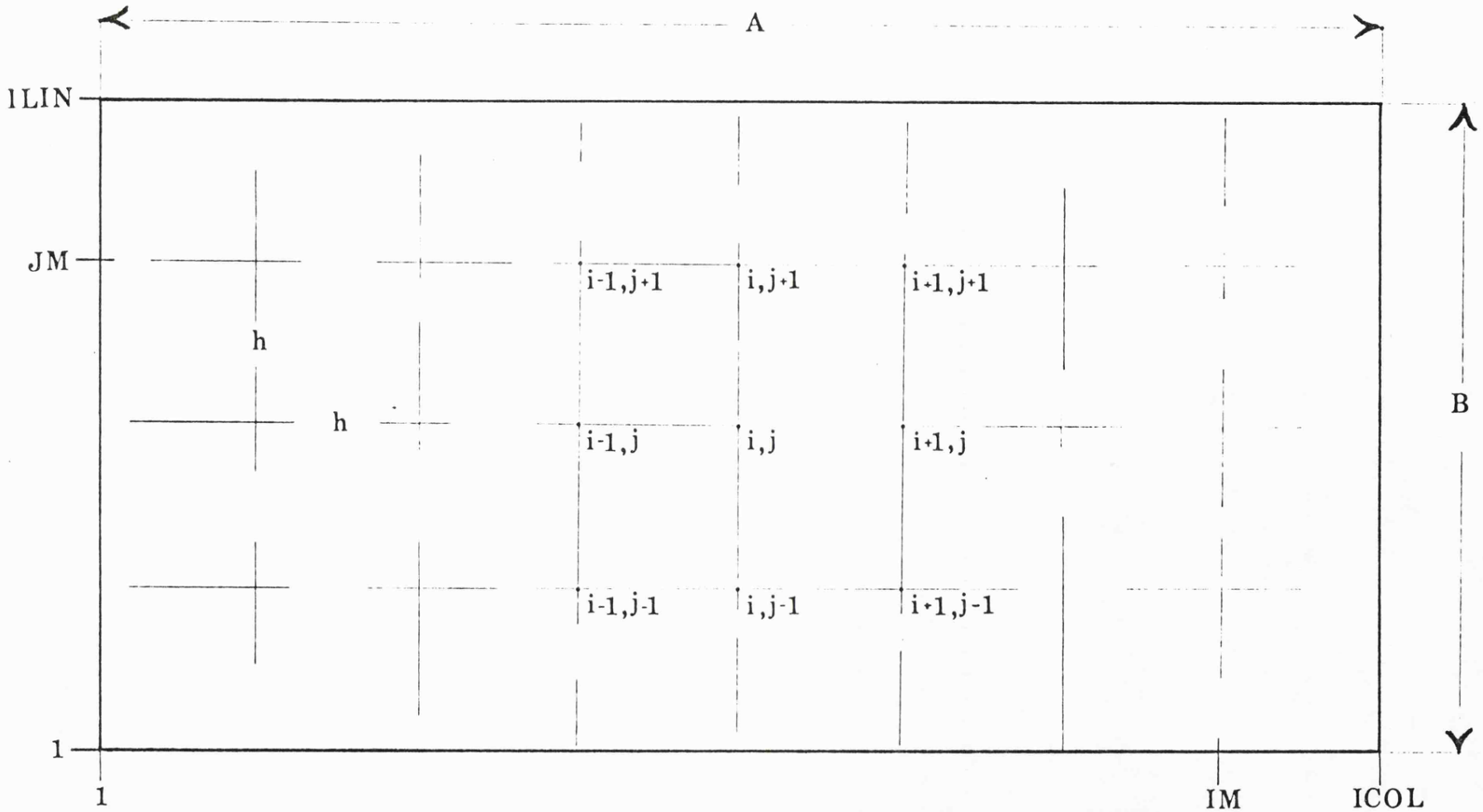


FIG.3.5 RECTANGULAR WAVEGUIDE CROSS-SECTION FOR NUMERICAL EXPERIMENTATION

The variables IM, JM, ICOL and ILIN are defined in Appendix 2 .

al percentual error map, resulting from the comparison between the analytical value at a node and its approximation, given by

$$\% E^{(i)} = 100 \frac{(G_0^{(i)} - G_0)}{G_0} \qquad (G_0 \neq 0) \qquad (3.69)$$

is generated.

In eq.(3.69) $G_0$ is the analytical nodal value and $G_0^{(i)}$ represents one of the three approximated results obtained by substituting the analytical values for the neighbouring points for $G_1, G_2 \ldots\ldots$ etc., into the pertinent expression (see paragraph 3.10.3).

Calculations using mesh length corresponding to a total of 36, and 78 internal nodes (9 and 14 divisions on the cross-section sides) have been carried out. Only internal node approximated values are compared with the analytical values and at boundary the nodal values are assumed to be calculated exactly. The reasons for assuming exact values on the waveguide boundary during the experiment are presented in the next paragraph.

### 3.10.2 BOUNDARY VALUES AND NATURAL BOUNDARY CONDITIONS

In the experiment the central node values are calculated by substituting the analytical values of the neighbouring nodes into the pertinent algebraic expression. This can be precisely done for all internal nodes but cannot for nodes lying on the boundary since, in this case, the neighbourhood is not complete.

To overcome this difficulty, the boundary values are, in the experiment, set equal to their analytical values. In fact, for all

$TM_{m,n}$ nodes the boundary values are known to be zero through the boundary conditions and the setting of the boundary nodes to their analytical values would be accurate even when they are numerically determined by either finite difference or finite element methods.

On the other hand , considering that , in the functional of eq.(3.1), a TE generating function, $G_E^{(2)}$ , composed by associating to the exact solution an error $\alpha$ E , in the form[20]

$$G_E^{(2)} = G_n^{(2)} + \alpha E \tag{3.70}$$

where $\alpha$ is an error distribution variable and E is a given error defined over the cross-section , replaces the exact solution , we have:

$$F(G_E^{(2)}) = \iint (\text{grad } G_E^{(2)})^2 \, dS - k_{cn}^2 \iint (G_E^{(2)})^2 \, dS \cdot$$

$$= \iint [\text{grad}(G_n^{(2)} + \alpha E)]^2 dS - k_{cn}^2 \iint [G_n^{(2)} + \alpha E]^2 dS \tag{3.71}$$

Differentiation of eq.(3.71) with respect to $\alpha$ , gives:

$$\frac{\delta}{\delta\alpha} F(G_E^{(2)}) = 2 \iint (\text{grad } E \cdot \text{grad } \alpha E + \text{grad } G^{(2)} \cdot \text{grad } E) \, dS$$

$$- 2 k_{cn}^2 \iint E \, G^{(2)} \, dS \tag{3.72}$$

The functional has a minimum for $\alpha = 0$, therefore,making $\alpha = 0$ in eq.(3.72) and equating the result to zero, we have:

$$\iint \text{grad } G_n^{(2)} \cdot \text{grad } E \, dS - k_{cn}^2 \iint E \, G_n^{(2)} \, dS = 0 \qquad (3.73)$$

Application of Green's first identity to eq.(3.73) gives:

$$\iint \left( \nabla_T^2 G_n^{(2)} + k_{cn}^2 G_n^{(2)} \right) E \, dS = \int_C E \frac{\delta}{\delta n} G_n^{(2)} \, dL \qquad (3.74)$$

As E is an arbitrary function, eq.(3.74) can hold only if the exact solution is obtained and also if the derivative calculated along the normal direction to the boundary curve $\frac{\delta}{\delta n} G_n^{(2)}$ vanishes. Therefore, the boundary condition $\frac{\delta}{\delta n} G_n^{(2)}(x,y) = 0$ constitutes . a natural boundary condition of the functional F(G).

Considering that, for TM modes, $G_n^{(3)}(x,y)$ is made equal to zero on the boundary points when the problem is specified, the functional F(G) satisfies the general natural boundary conditions given by:

$$G \frac{\delta}{\delta n} [ G ] = 0 \qquad (3.75)$$

(on the boundary)

In other words, the solution obtained by the minimization of the waveguide scalar functional (finite element method) satisfy the waveguide boundary conditions.

When the finite difference method is used to obtain the nodal values corresponding to a TE mode in the waveguide, the boundary conditions are met by introducing image points outside the boundary having the same value of the first internal nodes such that, for the boundary points, the five-points operator becomes[6]

$$G_0 = \frac{1}{4 - k_{cn}^2 h^2} (G_1 + G_2 + 2G_i) \qquad (3.76)$$

where $G_0$, $G_1$ and $G_2$ are nodes on the boundary curve and $G_i$ is the first internal node.

Having the boundary conditions satisfied for all cases and knowing that for TM modes the boundary percentual error is zero,for the sake of homogeneity and simplicity of the presentation, the percentual error over the waveguide boundary is assumed to be zero also for TE modes.

It should be stressed, however, that the assumption of no error on the boundary for nodal values corresponding to a TE generating function is only a matter of convenience in this experiment and may not always be justified.

### 3.10.3 RESULTS

The results are presented in matrix form. Each element $a_{ij}^{(r)}$ $(r = 1,2,3)$ of a matrix of results corresponds to the numerical value calculated at the node $(x_i, y_j)$ and its neighbourhood as shown in Fig.(3.5).

i) Finite Difference Formula:

$$a_{ij}^{(1)} = \frac{1}{4 - k_{cn}^2 h^2} (G_{i+1,j} + G_{i,j+1} + G_{i-1,j} + G_{i,j-1}) \qquad (3.77)$$

In eq.(3.77) h and $k_{cn}$ are respectively the mesh length

(Fig.(3.5)) and the cut-off wavenumber of the mode considered. The value $G_{i,j}$ in eq.(3.77) is the value of the generating function calculated by substituting into eq.(3.77) or eq.(3.68) (depending on the mode concerned) for x and y the co-ordinates of the point $(x_i, y_j)$

ii) Finite Element Formula:

$$a_{ij}^{(2)} = \frac{1}{8 - k_{cn}^2 h^2} \left[ \left(2 + \frac{k_{cn}^2 h^2}{6}\right) (G_{i+1,j} + G_{i,j+1} + G_{i-1,j} + G_{i,j-1}) + \frac{k_{cn}^2 h^2}{6} (G_{i+1,j-1} + G_{i-1,j+1}) \right] \tag{3.78}$$

The formula given by eq.(3.78) is obtained from eq.(3.77) by algebraic manipulation. The quantities $k_{cn}$, h and $G_{ij}$ in eq.(3.78) are the same defined for the finite difference formula.

iii) Symmetric Finite Element Formula

$$a_{ij}^{(3)} = \frac{1}{8 - k_{cn}^2 h^2} \left[ \left(2 + \frac{k_{cn}^2 h^2}{6}\right) (G_{i+1,j} + G_{i,j+1} + G_{i,j+1} + G_{i,j-1}) + \left(\frac{k_{cn}^2 h^2}{12}\right) (G_{i+1,j-1} + G_{i-1,j+1} + G_{i+1,j+1} + G_{i-1,j-1}) \right] \tag{3.79}$$

The quantities $k_{cn}$, h and $G_{ij}$ are defined as in the previous cases.

iv) Percentual Errors and Analytical Values:

Once the matrices corresponding to the finite difference, finite element and symmetric finite element formulae have been generated, a percentual error at each point is calculated and printed.

The percentual error print-outs are in matrix form and follow the arrangement mentioned in the previous cases. The percentual errors are calculated by eq.(3.69). The analytical values used in these calculations are also printed in matrix form. A description of the program used is presented in Appendix 2.

v) Matrices

The following matrices are the ones which have been considered to represent well the collection of results obtained during the experiment.

Each matrix is identified by a map number. Matrices with coincident elements are not repeated. Instead , the superposition of results is, where applicable, indicated in the caption.

| | | | | | | | | | | |
|---|---|---|---|---|---|---|---|---|---|---|
| 1.000 | .951 | .809 | .588 | .309 | -.000 | -.309 | -.588 | -.809 | -.951 | -1.000 |
| 1.000 | .951 | .809 | .588 | .309 | -.000 | -.309 | -.588 | -.809 | -.951 | -1.000 |
| 1.000 | .951 | .809 | .588 | .309 | -.000 | -.309 | -.588 | -.809 | -.951 | -1.000 |
| 1.000 | .951 | .809 | .588 | .309 | -.000 | -.309 | -.588 | -.809 | -.951 | -1.000 |
| 1.000 | .951 | .809 | .588 | .309 | -.000 | -.309 | -.588 | -.809 | -.951 | -1.000 |
| 1.000 | .951 | .809 | .588 | .309 | -.000 | -.309 | -.588 | -.809 | -.951 | -1.000 |

MAP 3.1 : Results obtained when estimating the central node values of the generating function by the analytical expression, the finite difference, the finite element and the symmetric finite element formulae for the $TE_{10}$ mode over 36 internal points. Discrepancies are not shown due to insufficient number of printed digits.

| | | | | | | | | | | |
|---|---|---|---|---|---|---|---|---|---|---|
| 0.000 | 0.000 | 0.000 | 0.000 | 0.000 | 0.000 | 0.000 | 0.000 | 0.000 | 0.000 | 0.000 |
| 0.000 | .021 | .021 | .021 | .021 | xxx | .021 | .021 | .021 | .021 | 0.000 |
| 0.000 | .021 | .021 | .021 | .021 | xxx | .021 | .021 | .021 | .021 | 0.000 |
| 0.000 | .021 | .021 | .021 | .021 | xxx | .021 | .021 | .021 | .021 | 0.000 |
| 0.000 | .021 | .021 | .021 | .021 | xxx | .021 | .021 | .021 | .021 | 0.000 |
| 0.000 | 0.000 | 0.000 | 0.000 | 0.000 | 0.000 | 0.000 | 0.000 | 0.000 | 0.000 | 0.000 |

MAP 3.2 : Percentual error when estimating the central node values using the finite difference formula for the $TE_{10}$ mode over 36 internal points. Percentual errors represented by xxx cannot be calculated ($G_0 = 0$)

| | | | | | | | | | | |
|---|---|---|---|---|---|---|---|---|---|---|
| 0.000 | 0.000 | 0.000 | 0.000 | 0.000 | 0.000 | 0.000 | 0.000 | 0.000 | 0.000 | 0.000 |
| 0.000 | -.020 | -.020 | -.020 | -.020 | xxx | -.020 | -.020 | -.020 | -.020 | 0.000 |
| 0.000 | -.020 | -.020 | -.020 | -.020 | xxx | -.020 | -.020 | -.020 | -.020 | 0.000 |
| 0.000 | -.020 | -.020 | -.020 | -.020 | xxx | -.020 | -.020 | -.020 | -.020 | 0.000 |
| 0.000 | -.020 | -.020 | -.020 | -.020 | xxx | -.020 | -.020 | -.020 | -.020 | 0.000 |
| 0.000 | 0.000 | 0.000 | 0.000 | 0.000 | 0.000 | 0.000 | 0.000 | 0.000 | 0.000 | 0.000 |

MAP 3.3 : Coincident percentual errors when estimating the central node value using the finite element and the symmetric finite element formulae for the $TE_{10}$ mode over 36 internal points. Percentual errors represented by xxx cannot be calculated ($G_0 = 0$)

| | | | | | | | | | | |
|---|---|---|---|---|---|---|---|---|---|---|
| 0.000 | 0.000 | 0.000 | 0.000 | 0.000 | 0.000 | 0.000 | 0.000 | 0.000 | 0.000 | 0.000 |
| 0.000 | .182 | .345 | .476 | .559 | .588 | .559 | .476 | .345 | .182 | 0.000 |
| 0.000 | .294 | .559 | .769 | .905 | .951 | .905 | .769 | .559 | .294 | 0.000 |
| 0.000 | .294 | .559 | .769 | .905 | .951 | .905 | .769 | .559 | .294 | 0.000 |
| 0.000 | .182 | .345 | .476 | .559 | .588 | .559 | .476 | .345 | .182 | 0.000 |
| 0.000 | 0.000 | 0.000 | 0.000 | 0.000 | 0.000 | 0.000 | 0.000 | 0.000 | 0.000 | 0.000 |

MAP 3.4 : Analytical node values of the generating function for the $TM_{11}$ mode over 36 internal points.

| | | | | | | | | | | |
|---|---|---|---|---|---|---|---|---|---|---|
| 0.000 | 0.000 | 0.000 | 0.000 | 0.000 | 0.000 | 0.000 | 0.000 | 0.000 | 0.000 | 0.000 |
| 0.000 | .182 | .347 | .477 | .561 | .590 | .561 | .477 | .347 | .182 | 0.000 |
| 0.000 | .295 | .561 | .772 | .908 | .955 | .908 | .772 | .561 | .295 | 0.000 |
| 0.000 | .295 | .561 | .772 | .908 | .955 | .908 | .772 | .561 | .295 | 0.000 |
| 0.000 | .182 | .347 | .477 | .561 | .590 | .561 | .477 | .347 | .182 | 0.000 |
| 0.000 | 0.000 | 0.000 | 0.000 | 0.000 | 0.000 | 0.000 | 0.000 | 0.000 | 0.000 | 0.000 |

MAP 3.5 : Central node values estimated by the finite difference formula for the $TM_{11}$ mode over 36 internal points.

| | | | | | | | | | | |
|---|---|---|---|---|---|---|---|---|---|---|
| 0.000 | 0.000 | 0.000 | 0.000 | 0.000 | 0.000 | 0.000 | 0.000 | 0.000 | 0.000 | 0.000 |
| 0.000 | .183 | .346 | .474 | .556 | .584 | .554 | .470 | .341 | .177 | 0.000 |
| 0.000 | .293 | .556 | .765 | .899 | .945 | .898 | .764 | .554 | .291 | 0.000 |
| 0.000 | .291 | .554 | .764 | .898 | .945 | .899 | .765 | .556 | .293 | 0.000 |
| 0.000 | .177 | .341 | .470 | .554 | .584 | .556 | .474 | .346 | .183 | 0.000 |
| 0.000 | 0.000 | 0.000 | 0.000 | 0.000 | 0.000 | 0.000 | 0.000 | 0.000 | 0.000 | 0.000 |

MAP 3.6 : Central node values estimated by the finite element formula for the $TM_{11}$ mode over 36 internal points.

| | | | | | | | | | | |
|---|---|---|---|---|---|---|---|---|---|---|
| 0.000 | 0.000 | 0.000 | 0.000 | 0.000 | 0.000 | 0.000 | 0.000 | 0.000 | 0.000 | 0.000 |
| 0.000 | .180 | .343 | .472 | .555 | .584 | .555 | .472 | .343 | .180 | 0.000 |
| 0.000 | .292 | .555 | .764 | .898 | .945 | .898 | .764 | .555 | .292 | 0.000 |
| 0.000 | .292 | .555 | .764 | .898 | .945 | .898 | .764 | .555 | .292 | 0.000 |
| 0.000 | .180 | .343 | .472 | .555 | .584 | .555 | .472 | .343 | .180 | 0.000 |
| 0.000 | 0.000 | 0.000 | 0.000 | 0.000 | 0.000 | 0.000 | 0.000 | 0.000 | 0.000 | 0.000 |

MAP 3.7 : Central node values estimated by the symmetric finite element formula for the $TM_{11}$ mode over 36 internal points.

| | | | | | | | | | | |
|---|---|---|---|---|---|---|---|---|---|---|
| 0.000 | 0.000 | 0.000 | 0.000 | 0.000 | 0.000 | 0.000 | 0.000 | 0.000 | 0.000 | 0.000 |
| 0.000 | .389 | .389 | .389 | .389 | .389 | .389 | .389 | .389 | .389 | 0.000 |
| 0.000 | .389 | .389 | .389 | .389 | .389 | .389 | .389 | .389 | .389 | 0.000 |
| 0.000 | .389 | .389 | .389 | .389 | .389 | .389 | .389 | .389 | .389 | 0.000 |
| 0.000 | .389 | .389 | .389 | .389 | .389 | .389 | .389 | .389 | .389 | 0.000 |
| 0.000 | 0.000 | 0.000 | 0.000 | 0.000 | 0.000 | 0.000 | 0.000 | 0.000 | 0.000 | 0.000 |

MAP 3.8 : Percentual error when estimating the central node values by the finite difference formula for the $TM_{11}$ mode over 36 internal points.

| | | | | | | | | | | |
|---|---|---|---|---|---|---|---|---|---|---|
| 0.000 | 0.000 | 0.000 | 0.000 | 0.000 | 0.000 | 0.000 | 0.000 | 0.000 | 0.000 | 0.000 |
| 0.000 | 1.018 | .086 | -.270 | -.490 | -.668 | -.846 | -1.066 | -1.422 | -2.354 | 0.000 |
| 0.000 | -.270 | -.490 | -.574 | -.626 | -.668 | -.710 | -.762 | -.846 | -1.066 | 0.000 |
| 0.000 | -1.066 | -.846 | -.762 | -.710 | -.668 | -.626 | -.574 | -.490 | -.270 | 0.000 |
| 0.000 | -2.354 | -1.422 | -1.066 | -.846 | -.668 | -.490 | -.270 | .086 | 1.018 | 0.000 |
| 0.000 | 0.000 | 0.000 | 0.000 | 0.000 | 0.000 | 0.000 | 0.000 | 0.000 | 0.000 | 0.000 |

MAP 3.9 : Percentual errors when estimating the central node values by the finite element formula for the $TM_{11}$ mode over 36 internal points.

| | | | | | | | | | | |
|---|---|---|---|---|---|---|---|---|---|---|
| 0.000 | 0.000 | 0.000 | 0.000 | 0.000 | 0.000 | 0.000 | 0.000 | 0.000 | 0.000 | 0.000 |
| 0.000 | -.668 | -.668 | -.668 | -.668 | -.668 | -.668 | -.668 | -.668 | -.668 | 0.000 |
| 0.000 | -.668 | -.668 | -.668 | -.668 | -.668 | -.668 | -.668 | -.668 | -.668 | 0.000 |
| 0.000 | -.668 | -.668 | -.668 | -.668 | -.668 | -.668 | -.668 | -.668 | -.668 | 0.000 |
| 0.000 | -.668 | -.668 | -.668 | -.668 | -.668 | -.668 | -.668 | -.668 | -.668 | 0.000 |
| 0.000 | 0.000 | 0.000 | 0.000 | 0.000 | 0.000 | 0.000 | 0.000 | 0.000 | 0.000 | 0.000 |

MAP 3.10 : Percentual error when estimating the central node values by the symmetric finite element formula for the $TM_{11}$ mode over 36 internal points.

| | | | | | | | | | | | | | | |
|---|---|---|---|---|---|---|---|---|---|---|---|---|---|---|
| 1.000 | .975 | .901 | .782 | .623 | .434 | .223 | -.000 | -.223 | -.434 | -.623 | -.782 | -.901 | -.975 | -1.000 |
| 1.000 | .975 | .901 | .782 | .623 | .434 | .223 | -.000 | -.223 | -.434 | -.623 | -.782 | -.901 | -.975 | -1.000 |
| 1.000 | .975 | .901 | .782 | .623 | .434 | .223 | -.000 | -.223 | -.434 | -.623 | -.782 | -.901 | -.975 | -1.000 |
| 1.000 | .975 | .901 | .782 | .623 | .434 | .223 | -.000 | -.223 | -.434 | -.623 | -.782 | -.901 | -.975 | -1.000 |
| 1.000 | .975 | .901 | .782 | .623 | .434 | .223 | -.000 | -.223 | -.434 | -.623 | -.782 | -.901 | -.975 | -1.000 |
| 1.000 | .975 | .901 | .782 | .623 | .434 | .223 | -.000 | -.223 | -.434 | -.623 | -.782 | -.901 | -.975 | -1.000 |
| 1.000 | .975 | .901 | .782 | .623 | .434 | .223 | -.000 | -.223 | -.434 | -.623 | -.782 | -.901 | -.975 | -1.000 |
| 1.000 | .975 | .901 | .782 | .623 | .434 | .223 | -.000 | -.223 | -.434 | -.623 | -.782 | -.901 | -.975 | -1.000 |

MAP 3.11 : Results obtained when estimating the central node values by the analytical, the finite difference, the finite element and the symmetric finite element formulae for the $TE_{10}$ mode over 78 internal points. Discrepancies are not shown due to insufficient number of printed digits.

| | | | | | | | | | | | | | | |
|---|---|---|---|---|---|---|---|---|---|---|---|---|---|---|
| 0.000 | 0.000 | 0.000 | 0.000 | 0.000 | 0.000 | 0.000 | 0.000 | 0.000 | 0.000 | 0.000 | 0.000 | 0.000 | 0.000 | 0.000 |
| 0.000 | .005 | .005 | .005 | .005 | .005 | .005 | xxx | .005 | .005 | .005 | .005 | .005 | .005 | 0.000 |
| 0.000 | .005 | .005 | .005 | .005 | .005 | .005 | xxx | .005 | .005 | .005 | .005 | .005 | .005 | 0.000 |
| 0.000 | .005 | .005 | .005 | .005 | .005 | .005 | xxx | .005 | .005 | .005 | .005 | .005 | .005 | 0.000 |
| 0.000 | .005 | .005 | .005 | .005 | .005 | .005 | xxx | .005 | .005 | .005 | .005 | .005 | .005 | 0.000 |
| 0.000 | .005 | .005 | .005 | .005 | .005 | .005 | xxx | .005 | .005 | .005 | .005 | .005 | .005 | 0.000 |
| 0.000 | .005 | .005 | .005 | .005 | .005 | .005 | xxx | .005 | .005 | .005 | .005 | .005 | .005 | 0.000 |
| 0.000 | 0.000 | 0.000 | 0.000 | 0.000 | 0.000 | 0.000 | 0.000 | 0.000 | 0.000 | 0.000 | 0.000 | 0.000 | 0.000 | 0.000 |

MAP 3.12 : Percentual errors when estimating the central node values by the finite difference formula for the $TE_{10}$ mode over 78 internal points.

| | | | | | | | | | | | | | | |
|---|---|---|---|---|---|---|---|---|---|---|---|---|---|---|
| 0.000 | 0.000 | 0.000 | 0.000 | 0.000 | 0.000 | 0.000 | 0.000 | 0.000 | 0.000 | 0.000 | 0.000 | 0.000 | 0.000 | 0.000 |
| 0.000 | -.005 | -.005 | -.005 | -.005 | -.005 | -.005 | xxx | -.005 | -.005 | -.005 | -.005 | -.005 | -.005 | 0.000 |
| 0.000 | -.005 | -.005 | -.005 | -.005 | -.005 | -.005 | xxx | -.005 | -.005 | -.005 | -.005 | -.005 | -.005 | 0.000 |
| 0.000 | -.005 | -.005 | -.005 | -.005 | -.005 | -.005 | xxx | -.005 | -.005 | -.005 | -.005 | -.005 | -.005 | 0.000 |
| 0.000 | -.005 | -.005 | -.005 | -.005 | -.005 | -.005 | xxx | -.005 | -.005 | -.005 | -.005 | -.005 | -.005 | 0.000 |
| 0.000 | -.005 | -.005 | -.005 | -.005 | -.005 | -.005 | xxx | -.005 | -.005 | -.005 | -.005 | -.005 | -.005 | 0.000 |
| 0.000 | -.005 | -.005 | -.005 | -.005 | -.005 | -.005 | xxx | -.005 | -.005 | -.005 | -.005 | -.005 | -.005 | 0.000 |
| 0.000 | 0.000 | 0.000 | 0.000 | 0.000 | 0.000 | 0.000 | 0.000 | 0.000 | 0.000 | 0.000 | 0.000 | 0.000 | 0.000 | 0.000 |

MAP 3.13 : Percentual errors when estimating the central node values by the finite element formula for the $TE_{10}$ mode over 78 internal points.

| | | | | | | | | | | | | | | |
|---|---|---|---|---|---|---|---|---|---|---|---|---|---|---|
| 0.000 | 0.000 | 0.000 | 0.000 | 0.000 | 0.000 | 0.000 | 0.000 | 0.000 | 0.000 | 0.000 | 0.000 | 0.000 | 0.000 | 0.000 |
| 0.000 | .097 | .188 | .271 | .339 | .391 | .423 | .434 | .423 | .391 | .339 | .271 | .188 | .097 | 0.000 |
| 0.000 | .174 | .339 | .487 | .611 | .704 | .762 | .782 | .762 | .704 | .611 | .487 | .339 | .174 | 0.000 |
| 0.000 | .217 | .423 | .608 | .762 | .878 | .950 | .975 | .950 | .878 | .762 | .608 | .423 | .217 | 0.000 |
| 0.000 | .217 | .423 | .608 | .762 | .878 | .950 | .975 | .950 | .878 | .762 | .608 | .423 | .217 | 0.000 |
| 0.000 | .174 | .339 | .487 | .611 | .704 | .762 | .782 | .762 | .704 | .611 | .487 | .339 | .174 | 0.000 |
| 0.000 | .097 | .188 | .271 | .339 | .391 | .423 | .434 | .423 | .391 | .339 | .271 | .188 | .097 | 0.000 |
| 0.000 | 0.000 | 0.000 | 0.000 | 0.000 | 0.000 | 0.000 | 0.000 | 0.000 | 0.000 | 0.000 | 0.000 | 0.000 | 0.000 | 0.000 |

MAP 3.14 : Analytical node values of the generating function for the $TM_{11}$ mode over 78 internal points.

| | | | | | | | | | | | | | | |
|---|---|---|---|---|---|---|---|---|---|---|---|---|---|---|
| 0.000 | 0.000 | 0.000 | 0.000 | 0.000 | 0.000 | 0.000 | 0.000 | 0.000 | 0.000 | 0.000 | 0.000 | 0.000 | 0.000 | 0.000 |
| 0.000 | .097 | .188 | .271 | .340 | .391 | .423 | .434 | .423 | .391 | .340 | .271 | .188 | .097 | 0.000 |
| 0.000 | .174 | .340 | .488 | .612 | .705 | .763 | .783 | .763 | .705 | .612 | .488 | .340 | .174 | 0.000 |
| 0.000 | .217 | .423 | .608 | .763 | .879 | .951 | .976 | .951 | .879 | .763 | .608 | .423 | .217 | 0.000 |
| 0.000 | .217 | .423 | .608 | .763 | .879 | .951 | .976 | .951 | .879 | .763 | .608 | .423 | .217 | 0.000 |
| 0.000 | .174 | .340 | .488 | .612 | .705 | .763 | .783 | .763 | .705 | .612 | .488 | .340 | .174 | 0.000 |
| 0.000 | .097 | .188 | .271 | .340 | .391 | .423 | .434 | .423 | .391 | .340 | .271 | .188 | .097 | 0.000 |
| 0.000 | 0.000 | 0.000 | 0.000 | 0.000 | 0.000 | 0.000 | 0.000 | 0.000 | 0.000 | 0.000 | 0.000 | 0.000 | 0.000 | 0.000 |

MAP 3.15 : Central node values estimated by the finite difference formula for the $TM_{11}$ over 78 internal points.

| | | | | | | | | | | | | | | |
|---|---|---|---|---|---|---|---|---|---|---|---|---|---|---|
| 0.000 | 0.000 | 0.000 | 0.000 | 0.000 | 0.000 | 0.000 | 0.000 | 0.000 | 0.000 | 0.000 | 0.000 | 0.000 | 0.000 | 0.000 |
| 0.000 | .097 | .189 | .271 | .339 | .391 | .422 | .433 | .422 | .390 | .338 | .269 | .187 | .095 | 0.000 |
| 0.000 | .174 | .339 | .487 | .611 | .703 | .761 | .780 | .761 | .703 | .610 | .486 | .338 | .173 | 0.000 |
| 0.000 | .217 | .422 | .607 | .761 | .877 | .949 | .973 | .949 | .877 | .761 | .607 | .422 | .216 | 0.000 |
| 0.000 | .216 | .422 | .607 | .761 | .877 | .949 | .973 | .949 | .877 | .761 | .607 | .422 | .217 | 0.000 |
| 0.000 | .173 | .338 | .486 | .610 | .703 | .761 | .780 | .761 | .703 | .611 | .487 | .339 | .174 | 0.000 |
| 0.000 | .095 | .187 | .269 | .338 | .390 | .422 | .433 | .422 | .391 | .339 | .271 | .189 | .097 | 0.000 |
| 0.000 | 0.000 | 0.000 | 0.000 | 0.000 | 0.000 | 0.000 | 0.000 | 0.000 | 0.000 | 0.000 | 0.000 | 0.000 | 0.000 | 0.000 |

MAP 3.16 : Central node values estimated by the finite element formula for the $TM_{11}$ mode over 78 internal points.

| | | | | | | | | | | | | | | |
|---|---|---|---|---|---|---|---|---|---|---|---|---|---|---|
| 0.000 | 0.000 | 0.000 | 0.000 | 0.000 | 0.000 | 0.000 | 0.000 | 0.000 | 0.000 | 0.000 | 0.000 | 0.000 | 0.000 | 0.000 |
| 0.000 | .096 | .188 | .270 | .339 | .390 | .422 | .433 | .422 | .390 | .339 | .270 | .188 | .096 | 0.000 |
| 0.000 | .174 | .339 | .487 | .610 | .703 | .761 | .780 | .761 | .703 | .610 | .487 | .339 | .174 | 0.000 |
| 0.000 | .217 | .422 | .607 | .761 | .877 | .949 | .973 | .949 | .877 | .761 | .607 | .422 | .217 | 0.000 |
| 0.000 | .217 | .422 | .607 | .761 | .877 | .949 | .973 | .949 | .877 | .761 | .607 | .422 | .217 | 0.000 |
| 0.000 | .174 | .339 | .487 | .610 | .703 | .761 | .780 | .761 | .703 | .610 | .487 | .339 | .174 | 0.000 |
| 0.000 | .096 | .188 | .270 | .339 | .390 | .422 | .433 | .422 | .390 | .339 | .270 | .188 | .096 | 0.000 |
| 0.000 | 0.000 | 0.000 | 0.000 | 0.000 | 0.000 | 0.000 | 0.000 | 0.000 | 0.000 | 0.000 | 0.000 | 0.000 | 0.000 | 0.000 |

MAP 3.17 : Central node values estimated by the symmetric finite element formula for the $TM_{11}$ mode over 78 internal points.

| | | | | | | | | | | | | | | |
|---|---|---|---|---|---|---|---|---|---|---|---|---|---|---|
| 0.000 | 0.000 | 0.000 | 0.000 | 0.000 | 0.000 | 0.000 | 0.000 | 0.000 | 0.000 | 0.000 | 0.000 | 0.000 | 0.000 | 0.000 |
| 0.000 | .095 | .095 | .095 | .095 | .095 | .095 | .095 | .095 | .095 | .095 | .095 | .095 | .095 | 0.000 |
| 0.000 | .095 | .095 | .095 | .095 | .095 | .095 | .095 | .095 | .095 | .095 | .095 | .095 | .095 | 0.000 |
| 0.000 | .095 | .095 | .095 | .095 | .095 | .095 | .095 | .095 | .095 | .095 | .095 | .095 | .095 | 0.000 |
| 0.000 | .095 | .095 | .095 | .095 | .095 | .095 | .095 | .095 | .095 | .095 | .095 | .095 | .095 | 0.000 |
| 0.000 | .095 | .095 | .095 | .095 | .095 | .095 | .095 | .095 | .095 | .095 | .095 | .095 | .095 | 0.000 |
| 0.000 | .095 | .095 | .095 | .095 | .095 | .095 | .095 | .095 | .095 | .095 | .095 | .095 | .095 | 0.000 |
| 0.000 | 0.000 | 0.000 | 0.000 | 0.000 | 0.000 | 0.000 | 0.000 | 0.000 | 0.000 | 0.000 | 0.000 | 0.000 | 0.000 | 0.000 |

MAP 3.18 : Percentual errors when estimating central node values by the finite difference formula for the $TM_{11}$ mode over 78 internal points.

| | | | | | | | | | | | | | | |
|---|---|---|---|---|---|---|---|---|---|---|---|---|---|---|
| 0.000 | 0.000 | 0.000 | 0.000 | 0.000 | 0.000 | 0.000 | 0.000 | 0.000 | 0.000 | 0.000 | 0.000 | 0.000 | 0.000 | 0.000 |
| 0.000 | .777 | .277 | .098 | -.001 | -.069 | -.124 | -.174 | -.224 | -.279 | -.347 | -.446 | -.625 | -1.125 | 0.000 |
| 0.000 | .191 | -.001 | -.069 | -.108 | -.134 | -.155 | -.174 | -.193 | -.214 | -.241 | -.279 | -.347 | -.539 | 0.000 |
| 0.000 | -.069 | -.124 | -.144 | -.155 | -.163 | -.169 | -.174 | -.179 | -.186 | -.193 | -.204 | -.224 | -.279 | 0.000 |
| 0.000 | -.279 | -.224 | -.204 | -.193 | -.186 | -.179 | -.174 | -.169 | -.163 | -.155 | -.144 | -.124 | -.069 | 0.000 |
| 0.000 | -.539 | -.347 | -.279 | -.241 | -.214 | -.193 | -.174 | -.155 | -.134 | -.108 | -.069 | -.001 | .191 | 0.000 |
| 0.000 | -1.125 | -.625 | -.446 | -.347 | -.279 | -.224 | -.174 | -.124 | -.069 | -.001 | .098 | .277 | .777 | 0.000 |
| 0.000 | 0.000 | 0.000 | 0.000 | 0.000 | 0.000 | 0.000 | 0.000 | 0.000 | 0.000 | 0.000 | 0.000 | 0.000 | 0.000 | 0.000 |

MAP 3.19 : Percentual errors when estimating the central node values by the finite element formula for the $TM_{11}$ mode over 78 internal points.

| | | | | | | | | | | | | | | |
|---|---|---|---|---|---|---|---|---|---|---|---|---|---|---|
| 0.000 | 0.000 | 0.000 | 0.000 | 0.000 | 0.000 | 0.000 | 0.000 | 0.000 | 0.000 | 0.000 | 0.000 | 0.000 | 0.000 | 0.000 |
| 0.000 | -.174 | -.174 | -.174 | -.174 | -.174 | -.174 | -.174 | -.174 | -.174 | -.174 | -.174 | -.174 | -.174 | 0.000 |
| 0.000 | -.174 | -.174 | -.174 | -.174 | -.174 | -.174 | -.174 | -.174 | -.174 | -.174 | -.174 | -.174 | -.174 | 0.000 |
| 0.000 | -.174 | -.174 | -.174 | -.174 | -.174 | -.174 | -.174 | -.174 | -.174 | -.174 | -.174 | -.174 | -.174 | 0.000 |
| 0.000 | -.174 | -.174 | -.174 | -.174 | -.174 | -.174 | -.174 | -.174 | -.174 | -.174 | -.174 | -.174 | -.174 | 0.000 |
| 0.000 | -.174 | -.174 | -.174 | -.174 | -.174 | -.174 | -.174 | -.174 | -.174 | -.174 | -.174 | -.174 | -.174 | 0.000 |
| 0.000 | -.174 | -.174 | -.174 | -.174 | -.174 | -.174 | -.174 | -.174 | -.174 | -.174 | -.174 | -.174 | -.174 | 0.000 |
| 0.000 | 0.000 | 0.000 | 0.000 | 0.000 | 0.000 | 0.000 | 0.000 | 0.000 | 0.000 | 0.000 | 0.000 | 0.000 | 0.000 | 0.000 |

MAP 3.20 : Percentual errors when estimating the central node values by the symmetric finite element formula for the $TM_{11}$ mode over 78 internal points.

### 3.10.4 CONCLUSIONS

The matrix in Map(3.1) shows that the results of calculations by any of the three expressions (eq.(3.77) to eq.(3.79)) agree at least up to the third decimal place with the analytical (correct) values. So, for the dominant mode, the algebraic distributions of values given by the nodal equations and the five-point finite difference operator and the actual nodal value distribution are very close when a regular mesh having (10x5) divisions is used.

In fact, Map(3.2) and Map(3.3) show that the percentual error is approximately equal to 0,02% (no attempt was made to estimate the influence of round-off errors) and also that the finite difference formula corresponds to an over-estimation while the finite element formulae correspond to an under-estimation by almost the same amount. In this particular case, the exact value appears to be very close to the arithmetic average of the two algebraic distributions.

For the $TE_{10}$ mode either the symmetric or non-symmetric finite element formulae show the same percentual errors due to the cosinoidal distribution within the regular mesh.

The situation is different when the first TM mode is considered. In this case, the central node values do not agree but to the second decimal place as shown in Map(3.4) to Map(3.7). In this case the best results are obtained by using the finite difference formula which gives an error less than 0.4% (Map(3.8)). The finite element formula shows errors greater than 2.0% (Map(3.9)) while the symmetric finite element formula, in this case, gives results with errors around 0.7% (Map(3.10)).

The situation for the dominant mode is improved in general by shortening the mesh length as shown in Map(3.11) to Map(3.13). With a shorter mesh length giving 78 internal points, the percentual error for the dominant mode appeared reduced to $\frac{1}{4}$ of its original value.

The $TM_{11}$ mode calculations (Map(3.14) to Map(3.20)) also show an improvement with the shorter mesh length. Here, again the error of the five-point finite difference formula reduces to $\frac{1}{4}$ of its previous value. It is seen, however, that the finite element expressions are poorer than the finite difference expressions. This happens because, when the generating function varies more quickly over the surface, the linear dependence imposed to obtain the finite element expressions becomes irrealistic. In fact, even for a mesh having 119 internal points (not included here) the first order finite element formulae have shown poorer agreement with the analytical nodal distribution than the finite difference formula.

Finally, it is reasonable to expect greater discrepancies between the analytical and the computed nodal values when those values are determined numerically. Here, no error was assumed to exist in the central node neighbourhood and therefore the only cumulative error process which has interfered with the experiment was the rounding of results.

## 3.11 INTERPRETATION OF THE FIRST-ORDER FINITE ELEMENT APPROXIMATION IN TERMS OF TRIANGLE AREA CO-ORDINATES

Before extending the finite element model to higher-order approximations, it is convenient to interpret eq.(3.43) in terms of

triangle area co-ordinates. This interpretation is used later to generalize the finite element modeling process; bringing high-order and 3-dimensional models together under the same formalism.

Consider the triangle $P_1P_2P_3$ having vertices on points $P_1(x_1,y_1)$ $P_2(x_2,y_2)$ and $P_3(x_3,y_3)$ as shown in Fig.(3.26). The area of the triangle $P_1P_2P_3$, denoted by A can be calculated by eq.(3.26); that is:

$$A = \frac{1}{2} \begin{bmatrix} 1 & x_1 & y_1 \\ 1 & x_2 & y_2 \\ 1 & x_3 & y_3 \end{bmatrix} \tag{3.80}$$

Any interior point (including those on the sides), P(x,y), can be uniquely defined by 3 linearly dependent homogeneous area co-ordinates, $s_1$, $s_2$ and $s_3$ which are the ratio of the areas $A_i(i=1,2,3)$ defined by the triangles formed by joining P to the vertices $P_1$, $P_2$ and $P_3$ (as shown in Fig.(3.6)) and the total area A, in the form:

$$P\,(s_1\,,\,s_2\,,\,s_3\,) \tag{3.81}$$

where

$$s_i = \frac{A_i}{A} \tag{3.82}$$

Calculation of the areas $A_i$ in eq.(3.82) making use of the expanded form of eq.(3.80) gives:

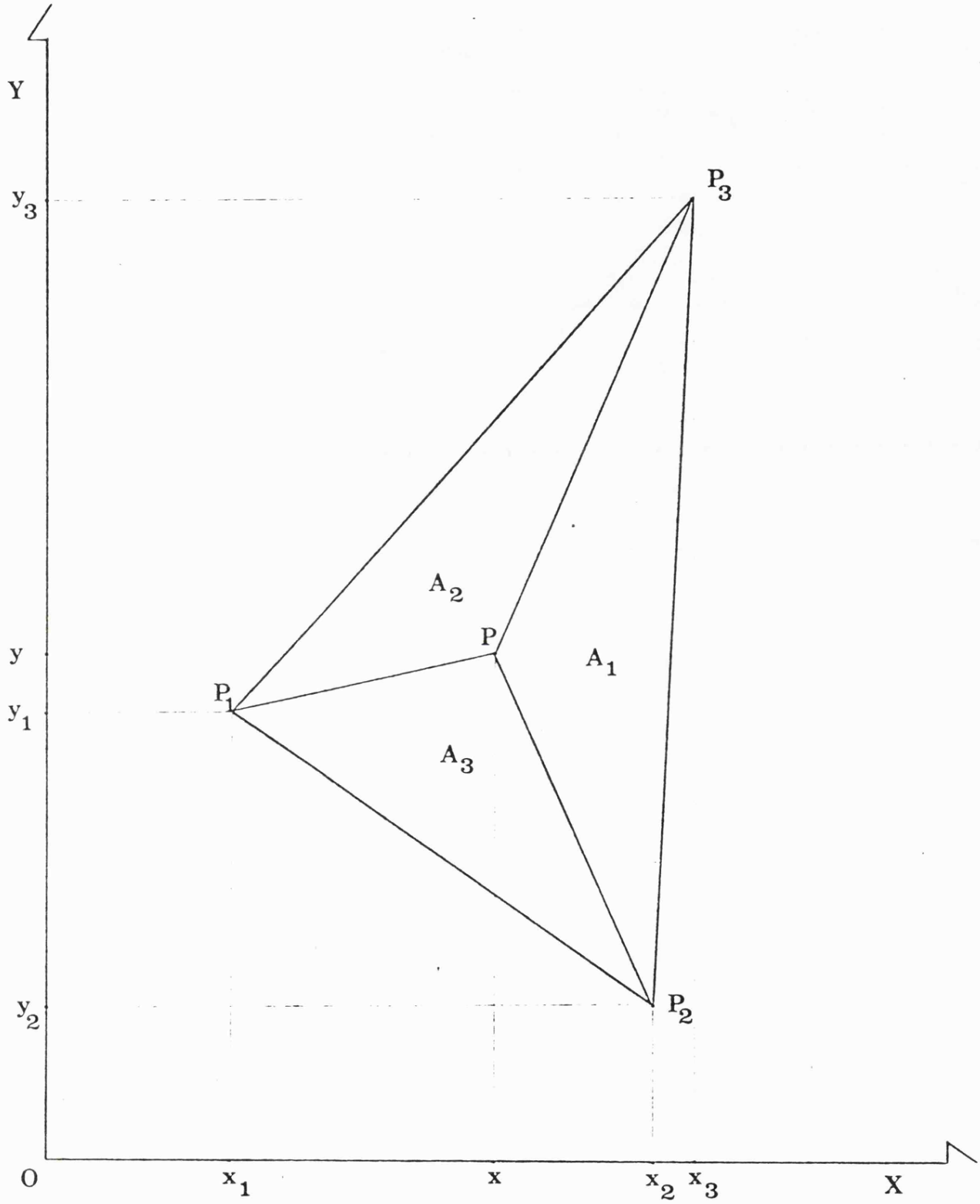


FIG. 3.6 AREA CO-ORDINATES

The interior point P(x,y) can be described by the area co-ordinates $s_1$ , $s_2$ and $s_3$ .

$$s_1 = \frac{1}{2A} [ x_2y_3 - x_3y_2 + (y_2 - y_3)x + (x_3 - x_2)y ] \tag{3.83}$$

$$s_2 = \frac{1}{2A} [ x_3y_1 - x_1y_3 + (y_3 - y_1)x + (x_1 - x_3)y ] \tag{3.84}$$

$$s_3 = \frac{1}{2A} [ x_1y_2 - x_2y_1 + (y_1 - y_2)x + (x_2 - x_1)y ] \tag{3.85}$$

Comparison of eq.(3.83) to eq.(3.85) with eq.(3.36) to eq.(3.38) shows that a general equation relating cartesian co-ordinates to triangle area co-ordinates can be written as:

$$s_i = \frac{1}{2A} (d_{i0} + d_{i1}x + d_{i2}y) \tag{3.86}$$

Also considering eq.(3.35) it is possible to show that the generating function inside an element of the first-order model can be written in terms of triangle area co-ordinates in the form:

$$G_{Mn}^{ej} = \sum_{i=1}^{3} s_i G_i \tag{3.87}$$

Consequently, it is possible to interpret eq.(3.43) as being the nodal equation obtained when the simplest approximation to the dependence of the generating function on the area co-ordinates (first-order) and its values at specific triangle points (vertices) is assumed.

Higher-order finite element models of the waveguide cross-section can be developed by assuming a higher-order dependence of the generating function on the area co-ordinates and values at specific

triangle points. This corresponds to generalizing eq.(3.2) in order to accomodate a N-order complete polynomial description of the generating function inside the element.

## 3.12 HIGHER-ORDER ELEMENTS

Consider that, instead of approximating the generating function inside an element of the cross-section model through eq.(3.2), a general N-order complete polynomial in triangle area co-ordinates, $P_N^e(s_1,s_2,s_3)$ is used, in the form:

$$G_{Mn}^e = P_N^e(s_1, s_2, s_3) \tag{3.88}$$

Since $G_{Mn}^e$ is a complete polynomial of order N, the number of terms of the expression for $P_N^e(s_1,s_2,s_3)$ is given by

$$n = \frac{1}{2}(N+1)(N+2) \tag{3.89}$$

Consequently n nodal values $G_\ell$ must be specified for each element. Furthermore, to assure continuity of $G_{Mn}^e$ between adjacent elements, N+1 coefficients of $P_N^e(s_1,s_2,s_3)$ must depend only on nodal values along each triangle side. This means that the nodes to be considered along each triangle edge include not only the vertices but N-1 points on each triangle side. The remaining nodal values must be defined elsewhere over the element.

A convenient systematic way of chosing a set of nodal values for the higher-order elements satisfying the foregoing requirements is to place the nodes on the regularly spaced set of points $P_{i,j,k}$

defined over an element by the area co-ordinates[41]

$$\left( \frac{i}{N} , \frac{j}{N} , \frac{k}{N} \right); \; 0 \leqslant i , j , k \leqslant N \tag{3.90}$$

where i, j and k are integers which add up to N; that is

$$i + j + k = N \tag{3.91}$$

The points $P_{i,j,k}$ are on the intersections of the lines $s_i$ = constant ; with $s_i$ being defined by eq.(3.90) and eq.(3.91). It can be shown[46] that the number of intersections is equal to the number of polynomial terms and, that, among those, N+1 equi-spaced points are on each triangle side (including the vertices).An illustration of a $4^{th}$-order element with node distribution obtained by the method above is shown in Fig.(3.7).

## 3.13 FORMALISM OF THE HIGHER-ORDER FINITE ELEMENT MODELS

In order to develop the formalism of the higher-order finite elements models, it is convenient to adopt a numbering system for the identification of the nodal values $G_\ell$ simpler than the one used to identify the equispaced nodal points $P_{i,j,k}$.

A single subscript numbering system avoids the manipulation of 3 subscripts during the calculations and can be accomplished by numbering the element nodal values in descending order of the numbers formed by the subscripts i,j,k at each point[41]; as shown in Fig.(3.8).

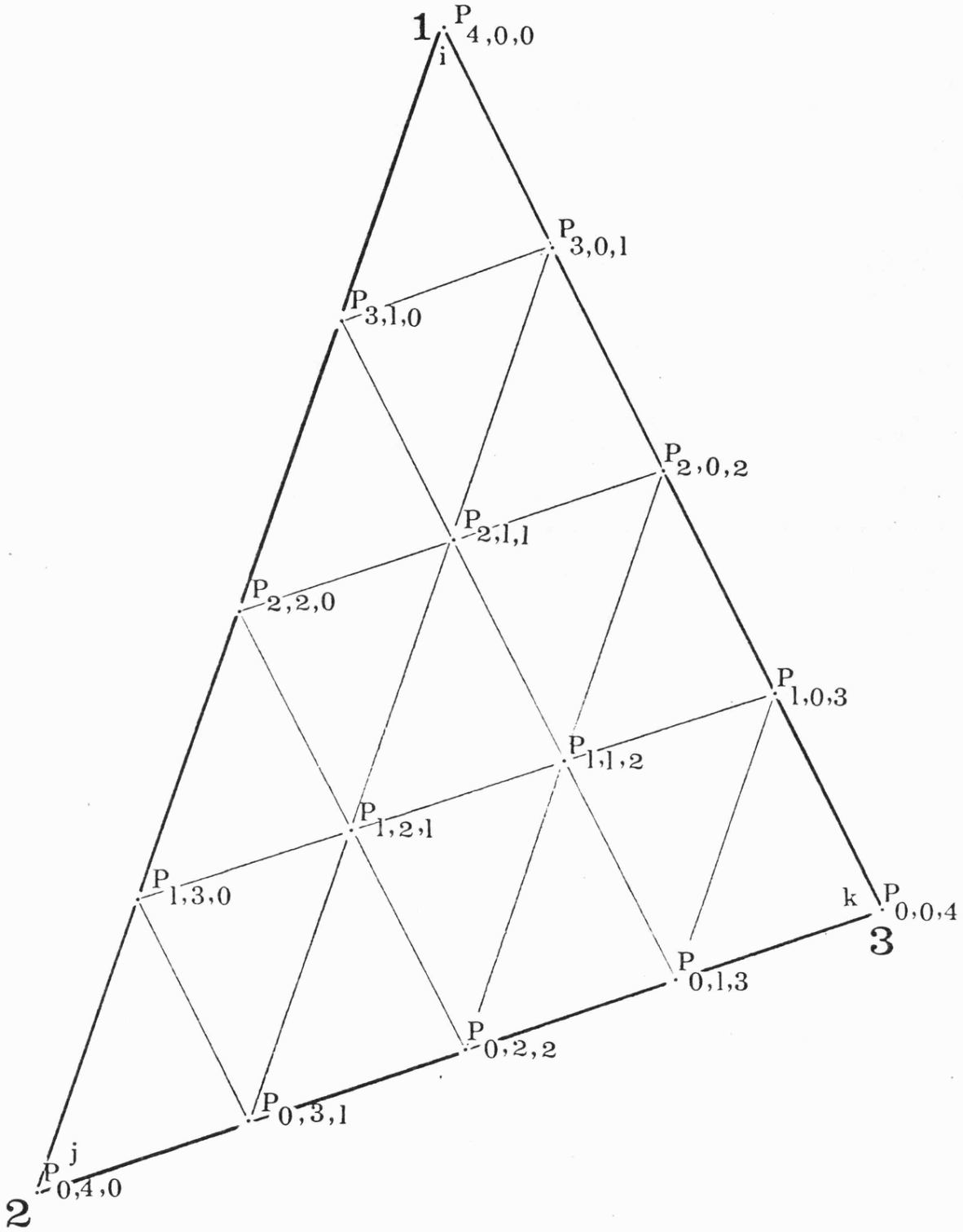


FIG. 3.7 $4^{th}$ ORDER ELEMENT

The equispaced nodal distribution in a $4^{th}$ order element obtained by application of eq.(3.90).

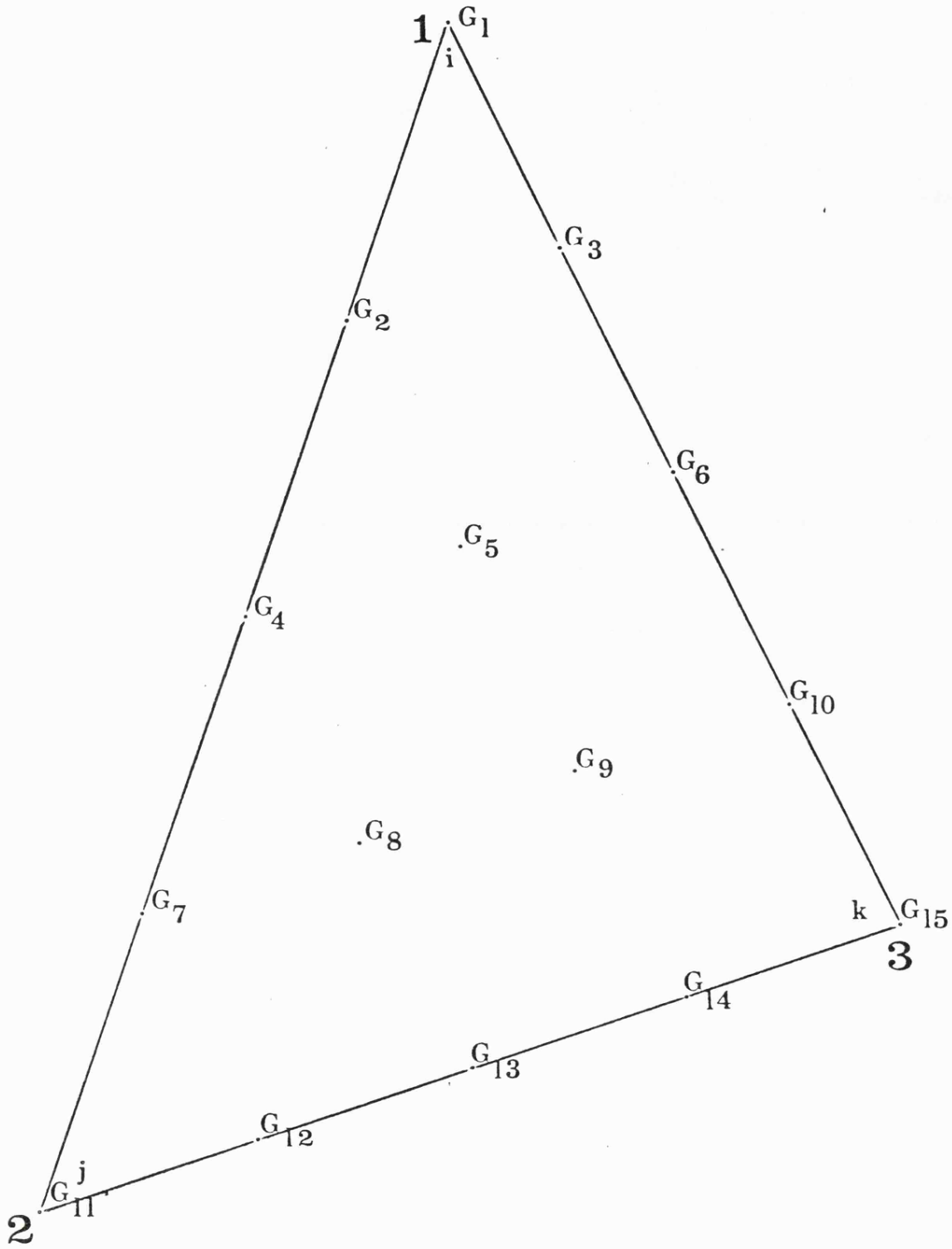


FIG. 3.8 SINGLE SUBSCRIPT NUMBERING SYSTEM

Numbering of the nodal values of a $4^{th}$ order element in descending order of the numbers formed by the subscripts i, j and k.

The generalization of eq.(3.87) to represent a n-order polynomial approximation to the generating function inside the element can be written in the form:

$$G_{Mn}^{ej} = \sum_{q=1}^{n} c_q (s_1, s_2, s_3) G_q \tag{3.92}$$

where $c_q (s_1, s_2, s_3)$ are now polynomials of the $n^{th}$-order in area co-ordinates and $G_q$ are nodal values defined over the $n^{th}$-order element.

Within an element, the minimization of the functional given by eq.(3.1) corresponds to satisfying

$$\frac{\delta}{\delta G_\ell} F(G) = 0 \tag{3.93}$$

$$(\ell = 1,2,\ldots,n)$$

where G is now a function of the area co-ordinates in the form given by eq.(3.92) and the integrals in F are carried out in the area co-ordinates space[58].

Similarly to the calculations performed for the first-order finite element model the derivatives involved in eq.(3.93) will be calculated separately. The derivatives in the first term of the functional F(G) are calculated by substituting eq.(3.92) into eq.(3.27). This gives:

$$\frac{\delta}{\delta G_\ell}\left[(\text{grad } G_{Mn}^{ej})\right]^2 = 2\,\frac{\delta}{\delta G_\ell}\left[\left(\frac{\delta}{\delta x}\,G_{Mn}^{ej}\right)\right]\frac{\delta}{\delta x}\,G_{Mn}^{ej} + \frac{\delta}{\delta G_\ell}\left[\left(\frac{\delta}{\delta y}\,G_{Mn}^{ej}\right)\right]\frac{\delta}{\delta y}\,G_{Mn}^{ej}$$

$$= 2\,\frac{\delta}{\delta G_\ell}\left[\frac{\delta}{\delta x}\left(\sum_{q=1}^{n} c_q(s_1,s_2,s_3)G_q\right)\right]\frac{\delta}{\delta x}\sum_{q=1}^{n} c_q(s_1,s_2,s_3)G_q$$

$$+ \frac{\delta}{\delta G_\ell}\left[\frac{\delta}{\delta y}\left(\sum_{q=1}^{n} c_q(s_1,s_2,s_3)G_q\right)\right]\frac{\delta}{\delta y}\sum_{q=1}^{n} c_q(s_1,s_2,s_3)\,G_q \tag{3.94}$$

Carrying out the operations in eq.(3.94) we get:

$$\frac{\delta}{\delta G_\ell}\left[(\text{grad } G_{Mn}^{ej})^2\right] = 2\sum_{q=1}^{n}\left(\frac{\delta c_\ell}{\delta x}\,\frac{\delta c_q}{\delta x} + \frac{\delta c_\ell}{\delta y}\,\frac{\delta c_q}{\delta y}\right)G_q \tag{3.95}$$

where, for conciseness, the parenthesis showing the dependence of the polynomials $c_\ell$ and $c_q$ on the area co-ordinates have been supressed.

Application of the chain rule for derivatives into eq.(3.95) gives:

$$\frac{\delta}{\delta G_\ell}\left[(\text{grad } G_{Mn}^{ej})^2\right] = 2\sum_{q=1}^{n}\left[\sum_{i=1}^{3}\sum_{j=1}^{3}\left(\frac{\delta s_i}{\delta x}\,\frac{\delta s_j}{\delta x} + \frac{\delta s_i}{\delta y}\,\frac{\delta s_j}{\delta y}\right)\frac{\delta c_\ell}{\delta s_i}\,\frac{\delta c_q}{\delta s_j}\right]G_q \tag{3.96}$$

The derivatives of the area co-ordinates $s_i$ , $s_j$ , etc., are calculated making use of eq.(3.86) and then substituted into eq.(3.96) , leading finally to:

$$\frac{\delta}{\delta G_\ell}\left[(\text{grad } G_{Mn}^{ej})^2\right] = \frac{1}{2A^2}\sum_{q=1}^{n}\left[\sum_{i=1}^{3}\sum_{j=1}^{3}(d_{i1}d_{j1} + d_{i2}d_{j2})\frac{\delta c_\ell}{\delta s_i}\frac{\delta c_q}{\delta s_j}\right]G_q \tag{3.97}$$

The derivative of the second term of the functional is much simpler to evaluate. Substituting eq.(3.92) into the integral and calculating the derivative we have:

$$\frac{\delta}{\delta G_\ell}\left[(G_{Mn}^{ej})^2\right] = 2\sum_{q=1}^{n} c_\ell c_q G_q \tag{3.98}$$

Now defining the element matrices $[S^e]$ and $[T^e]$ for which typical components are given respectively by[46]:

$$S_{\ell q}^e = \frac{1}{4A^2}\sum_{k=1}^{2}\sum_{i=1}^{3}\sum_{j=1}^{3} d_{ik}\, d_{jk} \iint \frac{\delta c_\ell}{\delta s_i}\frac{\delta c_q}{\delta s_j}\, dS \tag{3.99}$$

$$T_{\ell q}^e = \iint c_\ell\, c_q\, dS \tag{3.100}$$

the waveguide functional minimization problem becomes the algebraic eigenvalue problem, in the form:

$$[S]\,[G] = k_{cn}^2\,[T]\,[G] \tag{3.101}$$

where the global matrices [S], [G] and [T] are obtained by considering all the individual contributions of all elements in the cross-section as in the first-order model.

## 3.14 CALCULATION OF THE MATRICES $[S^e]$ AND $[T^e]$

Defining the polynomials

$$c_q = \sigma_{ijk} = P_i(s_1)\, P_j(s_2)\, P_k(s_3) \tag{3.102}$$

where

$$i + j + k = N \tag{3.103}$$

$$P_m(z) = \prod_{i=1}^{m} \left( \frac{Nz - i + 1}{i} \right) \qquad (m \geqslant 1) \tag{3.104}$$

$$P_m(z) = 1 \qquad (m = 0) \tag{3.105}$$

and making use of the geometric properties of a triangle,from which

$$d_{1i}d_{1j} + d_{2i}d_{2j} = -\, 2A \cot g\, \theta_k \qquad (i \neq j) \tag{3.106}$$

$$d_{1i}^{\,2} + d_{2i}^{\,2} = 2A\, (\cot g\, \theta_j + \cot g\, \theta_k) \tag{3.107}$$

($\theta_i$ = angle at vertex i)

Silvester[41] has shown that the matrix $[S^e]$ can be written in the form

$$[\, S^e \,] = \sum_{i=1}^{3} [\, Q_i^e \,] \cot g\, \theta_i \tag{3.108}$$

The matrices $[Q^e]$ in eq.(3.108) do not depend on triangle shape and moreover it is verified that the three matrices $[Q_i^e]$ are permutations of each other in such way that the matrix $[S^e]$ for a given element can be constructed if one of the matrices, say $[Q_1^e]$, is known.

In order to evaluate the components of matrices $[T^e]$ and $[Q_1^e]$ the polynomials in eq.(3.102) must be differentiated and the integration in the area co-ordinates space performed.

The polynomials in eq.(3.102) may be differentiated and multiplied in a straightforward manner. For the integration, the number of independent variables are reduced to two using the relationship

$$\sum_{i=1}^{3} s_i = 1 \tag{3.109}$$

and a formula for the integration of the typical term[59]

$$I_{mn} = \iint s_1^m \; s_2^n \; dS \tag{3.110}$$

may be used.

The calculation of the higher-order element matrices is, therefore, uncomplicated. However, as pointed out by Silvester[41], "the manipulative labour involved in finding any but the lowest order elements is formidable."

To overcome this difficulty, Silvester and associates devised individual sub-programs which produce the matrices $[Q^e]$ and $[T^e]$ up to the $6^{th}$-order and generate automatically the matrix $[S^e]$ for a

given element. These numerical arrays became available in Leicester during this research work as part of a more general package to solve Laplace's , Poisson's and Helmholtz's equations, to be considered below*.

## 3.15 PROGRAM PACKAGE FOR 2-D FIELD PROBLEMS

A program package for solving two dimensional field problems involving either Laplace's, Poisson's or Helmholtz equations was developed at McGill University, Montreal, by P.Silvester and A.Konrad.

The source is written in Fortran IV having a deck length of approximately 3.000 cards including comment cards and general documentation. The program deck also includes instructions on how to use the program , to set-up the input data, details of the defaults used by the program and sample data sets and results.

The complete program listing and documentation is available from ASIS NATIONAL AUXILIARY PUBLICATIONS SERVICES, New York, document No. NAPS 01604 (see reference (11)).

### 3.15.1 DESCRIPTION

The program provides elements up to $6^{th}$-order and consists of routines for reading in the data, assembling the finite element matrices, matrix manipulation, data handling and solving linear equations.

---

* See references (11), (35) and (41) for the details of the calculations.

All the input and generated data are printed out together with a set of program statistics and a node assembling map to allow a quick check of the output.

After reading the input data the program assembles the finite element matrices according to the specified element order. These are solved by Gaussian elimination or by an eigenvalue problem package, depending on the field equation under consideration.

The solutions to the field problem are then printed out in the form of numbered nodal values which correspond to numbered points on a map generated in the line-printer. In the case of solving Helmholtz's equation, the nodal values print out is preceeded by the print out of the cut-off wave-number.

Several problems may be dealt with a single run of the program and any data set containing errors is skiped without provoking abortive stoppage. For a detailed description including structural and operational characteristics of the program, see references (11) and (35). For access and use of the program from Leicester see also Appendix 3.

### 3.15.2 IMPLEMENTATION

The implementation of the program package as originally developed by Silvester and Konrad requires about 200K bytes of main storage and is able to deal with finite element matrices up to an order of 100. Cambridge University Engineering Department has produced a modified version of the same package reducing the matrix handling capability to an order of 55 and consequently reducing the main

storage requirements to approximately 120K bytes. The reduced core version also includes a data formating procedure which enables the user to feed in data via terminal or card reader by means of concise arrays.

Unfortunately, no implementation of either version could take place at Leicester University Computer Laboratory since the core requirements could not be met by the present computer. The calculations using the package during this research were carried out through a telephone link with Cambridge and only the 120K bytes version has been used.

### 3.15.3 EXAMPLES OF NODAL VALUE DISTRIBUTIONS

The generating function nodal value distributions presented in Map(3.21) to Map(3.23) are in matrix form, following the method of presentation described in paragraph (3.10.3). These matrices have been constructed from the program outputs (Appendix 3). Nodal value distributions corresponding to the first propagating TE mode (dominant) – $TE_{10}$ – and first TM mode – $TM_{11}$ – are presented. Also the nodal value distribution corresponding to the $TE_{11}$ mode which has the same cut-off wave-number of the $TM_{11}$ (degenerate) is shown. A detailed description of the data generation, job submission and output samples are presented in Appendix 3.

In all maps, the rectangular waveguide considered has a narrower to broader cross-section sides ratio equal to $\frac{1}{2}$, relative dielectric constant equal to 1.0 and has been split diagonally into two $6^{th}$-order elements during the finite element calculations. (Appendix 3).

| | | | | | | |
|---|---|---|---|---|---|---|
| -7.004 | -6.066 | -3.502 | -0.001 | 3.498 | 6.060 | 6.997 |
| -7.003 | -6.065 | -3.502 | -0.002 | 3.497 | 6.060 | 6.998 |
| -7.003 | -6.065 | -3.503 | -0.003 | 3.497 | 6.060 | 6.998 |
| -7.003 | -6.065 | -3.503 | -0.004 | 3.496 | 6.060 | 6.998 |
| -7.003 | -6.065 | -3.503 | -0.005 | 3.496 | 6.060 | 6.998 |
| -7.002 | -6.065 | -3.504 | -0.006 | 3.495 | 6.059 | 6.997 |
| -7.002 | -6.065 | -3.504 | -0.006 | 3.495 | 6.060 | 6.999 |

MAP 3.21 : Nodal values of the generating function for the $TE_{10}$ mode in a rectangular waveguide obtained by using the finite element program package.

| | | | | | | |
|---|---|---|---|---|---|---|
| 0.000 | 0.000 | 0.000 | 0.000 | 0.000 | 0.000 | 0.000 |
| 0.000 | 1.762 | 3.066 | 3.538 | 3.061 | 1.769 | 0.000 |
| 0.000 | 3.066 | 5.308 | 6.121 | 5.299 | 3.063 | 0.000 |
| 0.000 | 3.539 | 6.123 | 7.067 | 6.123 | 3.540 | 0.000 |
| 0.000 | 3.063 | 5.298 | 6.121 | 5.309 | 3.066 | 0.000 |
| 0.000 | 1.768 | 3.061 | 3.538 | 3.066 | 1.762 | 0.000 |
| 0.000 | 0.000 | 0.000 | 0.000 | 0.000 | 0.000 | 0.000 |

MAP 3.22 : Nodal values of the generating function for the $TM_{11}$ mode in a rectangular waveguide obtained by using the finite element program package.

| | | | | | | |
|---|---|---|---|---|---|---|
| -9.919 | -8.575 | -4.957 | -0.002 | 4.947 | 8.568 | 9.898 |
| -8.573 | -7.434 | -4.288 | 0.002 | 4.283 | 7.420 | 8.571 |
| -4.954 | -4.286 | -2.471 | -0.003 | 2.470 | 4.285 | 4.948 |
| -0.003 | 0.004 | 0.000 | -0.005 | 0.000 | 0.004 | -0.002 |
| 4.950 | 4.287 | 2.473 | 0.001 | -2.467 | -4.283 | -4.952 |
| 8.575 | 7.425 | 4.290 | 0.010 | -4.281 | -7.428 | -8.569 |
| 9.903 | 8.574 | 4.955 | 0.007 | -4.948 | -8.569 | -9.914 |

MAP 3.23 : Nodal values of the generating function for the $TE_{11}$ mode in a rectangular waveguide obtained by using the finite element program package.

### 3.15.4 COMPARATIVE RESULTS

It is instructive to compare the $TE_{10}$ and $TM_{11}$ results obtained by using $6^{th}$-order finite elements – Map(3.21) and Map(3.22) – with the corresponding analytical nodal values – Map(3.24) and Map(3.25) – obtained through eq.(3.67) and eq.(3.68). For clarity, the arbitrary amplitude constants used in the latter calculations are taken as $\mp$ 7.000. Comparison between Map(3.21) and Map(3.24) and Map(3.22) and Map(3.25) respectively, shows that the $6^{th}$-order finite element results are very accurate. The percentual errors calculated by using eq.(3.69) are shown in Map(3.26) and Map(3.27) respectively. It is noted that the corresponding absolute percentual errors in the nodal value distributions are less than 0.15% and 1.16%.

The results for the $TE_{11}$ mode are shown in Map(3.28) and Map(3.29). The arbitrary constant in this case has been assumed to be 10.000. It must be pointed out that when the finite element nodal value distribution is normalized with respect to its maximum valued component, the percentual errors are different from the ones shown. The value chosen for the arbitrary constant in the analytical distribution has certainly influenced the percentual error map. The comment applies to the other nodal value distributions as well.

| | | | | | | |
|---|---|---|---|---|---|---|
| -7.000 | -6.062 | -3.500 | 0.000 | 3.500 | 6.062 | 7.000 |
| -7.000 | -6.062 | -3.500 | 0.000 | 3.500 | 6.062 | 7.000 |
| -7.000 | -6.062 | -3.500 | 0.000 | 3.500 | 6.062 | 7.000 |
| -7.000 | -6.062 | -3.500 | 0.000 | 3.500 | 6.062 | 7.000 |
| -7.000 | -6.062 | -3.500 | 0.000 | 3.500 | 6.062 | 7.000 |
| -7.000 | -6.062 | -3.500 | 0.000 | 3.500 | 6.062 | 7.000 |
| -7.000 | -6.062 | -3.500 | 0.000 | 3.500 | 6.062 | 7.000 |

MAP 3.24 : Nodal values of the generating function for the $TE_{10}$ mode in a rectangular waveguide obtained by using the analytical expression.

| | | | | | | |
|---|---|---|---|---|---|---|
| 0.000 | 0.000 | 0.000 | 0.000 | 0.000 | 0.000 | 0.000 |
| 0.000 | 1.750 | 3.031 | 3.500 | 3.031 | 1.750 | 0.000 |
| 0.000 | 3.031 | 5.250 | 6.062 | 5.250 | 3.031 | 0.000 |
| 0.000 | 3.500 | 6.062 | 7.000 | 6.062 | 3.500 | 0.000 |
| 0.000 | 3.031 | 5.250 | 6.062 | 5.250 | 3.031 | 0.000 |
| 0.000 | 1.750 | 3.031 | 3.500 | 3.031 | 1.750 | 0.000 |
| 0.000 | 0.000 | 0.000 | 0.000 | 0.000 | 0.000 | 0.000 |

MAP 3.25 : Nodal values of the generating function for the $TM_{11}$ mode in a rectangular waveguide obtained by using the analytical expression.

| | | | | | | |
|---|---|---|---|---|---|---|
| -0.057 | -0.066 | -0.057 | xxx | -0.057 | -0.033 | -0.043 |
| -0.043 | -0.049 | -0.057 | xxx | -0.086 | -0.033 | -0.029 |
| -0.043 | -0.049 | -0.086 | xxx | -0.086 | -0.033 | -0.029 |
| -0.043 | -0.049 | -0.086 | xxx | -0.086 | -0.033 | -0.029 |
| -0.043 | -0.049 | -0.086 | xxx | -0.114 | -0.033 | -0.029 |
| -0.043 | -0.049 | -0.086 | xxx | -0.114 | -0.033 | -0.029 |
| -0.029 | -0.049 | -0.114 | xxx | -0.143 | -0.049 | -0.043 |
| -0.029 | -0.049 | -0.114 | xxx | -0.143 | -0.033 | -0.014 |

MAP 3.26 : Percentual errors in the nodal value distribution for the $TE_{10}$ mode in a rectangular waveguide obtained by using the finite element program package.

| | | | | | | |
|---|---|---|---|---|---|---|
| 0.000 | 0.000 | 0.000 | 0.000 | 0.000 | 0.000 | 0.000 |
| 0.000 | 0.686 | 1.155 | 1.086 | 0.990 | 1.086 | 0.000 |
| 0.000 | 1.155 | 1.105 | 0.973 | 0.933 | 1.056 | 0.000 |
| 0.000 | 1.114 | 1.006 | 0.957 | 1.006 | 1.143 | 0.000 |
| 0.000 | 1.056 | 0.914 | 0.973 | 1.124 | 1.155 | 0.000 |
| 0.000 | 1.029 | 0.990 | 1.086 | 1.155 | 0.686 | 0.000 |
| 0.000 | 0.000 | 0.000 | 0.000 | 0.000 | 0.000 | 0.000 |

MAP 3.27 : Percentual errors in the nodal value distribution for the $TM_{11}$ mode in a rectangular waveguide obtained by using the finite element program package.

| | | | | | | |
|---|---|---|---|---|---|---|
| -10.000 | -8.660 | -5.000 | 0.000 | 5.000 | 8.660 | 10.000 |
| -8.660 | -7.500 | -4.330 | 0.000 | 4.330 | 7.500 | 8.660 |
| -5.000 | -4.330 | -2.500 | 0.000 | 2.500 | 4.330 | 5.000 |
| 0.000 | 0.000 | 0.000 | 0.000 | 0.000 | 0.000 | 0.000 |
| 5.000 | 4.330 | 2.500 | 0.000 | -2.500 | -4.330 | -5.000 |
| 8.660 | 7.500 | 4.330 | 0.000 | -4.330 | -7.500 | -8.660 |
| 10.000 | 8.660 | 5.000 | 0.000 | -5.000 | -8.660 | -10.000 |

MAP 3.28 : Nodal values of the generating function for the $TE_{11}$ mode in a rectangular waveguide obtained by using the analytical expression.

| | | | | | | |
|---|---|---|---|---|---|---|
| 0.810 | 0.982 | 0.860 | xxx | -1.060 | -1.062 | -1.020 |
| 1.005 | 0.880 | 0.970 | xxx | -1.085 | -1.067 | -1.028 |
| 0.920 | 1.016 | 1.160 | xxx | -1.200 | -1.039 | -1.040 |
| xxx | xxx | xxx | xxx | xxx | xxx | xxx |
| -1.000 | -0.993 | -1.080 | xxx | 1.320 | 1.085 | 0.960 |
| -0.982 | -1.000 | -0.924 | xxx | 1.132 | 0.960 | 1.051 |
| -0.970 | -0.993 | -0.900 | xxx | 1.040 | 1.051 | 0.860 |

MAP 3.29 : Percentual errors in the nodal value distribution for the $TE_{11}$ mode in a rectangular waveguide obtained by using the finite element program package.

## 3.16 EXTENSION OF THE HIGHER-ORDER FINITE ELEMENT MODEL TO SOLVE d-DIMENSIONAL HELMHOLTZ'S EQUATIONS

The higher-order finite element method can be extended to solve the d-dimensional Helmholtz's equation[46]

$$( \nabla_d^2 + k_c^2 ) G = 0 \tag{3.111}$$

where G is a scalar function of d variables, that is

$$G = G (x^{(1)}, x^{(2)}, \ldots x^{(d)}) \tag{3.112}$$

with the d-dimensional Laplacian operator $\nabla_d^2$ being defined in the form

$$\nabla_d^2 = \frac{\delta}{\delta x^{(1)}} ( \frac{\delta}{\delta x^{(1)}} ) + \cdots \frac{\delta}{\delta x^{(d)}} ( \frac{\delta}{\delta x^{(d)}} ) \tag{3.113}$$

and the associated functional given by:

$$F(G) = \iint \ldots \int (\text{grad } G)^2 \, dx^{(1)} \, dx^{(2)} \ldots dx^{(d)}$$

$$- k_c^2 \iint \ldots \int G^2 \, dx^{(1)} \, dx^{(2)} \ldots dx^{(d)} \tag{3.114}$$

The extension of the method is accomplished by generalizing the equations developed for solving the 2D-Helmholtz equation. Following procedure similar to the two-dimensional analysis a system of (d+1) linearly dependent generalized volume co-ordinates $v_i (i=1,2,\ldots,d+1)$ such that

$$\sum_{i=1}^{d+1} v_i = 1 \tag{3.115}$$

defined in the form:

$$v_i = \frac{1}{\Delta} (a_i^{(0)} + a_i^{(1)} x^{(1)} + \cdots a_i^{(d)} x^{(d)} \tag{3.116}$$

where

$$\Delta = \left[\!\!\left[ \begin{array}{ccccc} 1 & x_1^{(1)} & x_1^{(2)} & \cdots & x_1^{(d)} \\ 1 & x_2^{(1)} & x_2^{(2)} & \cdots & x_2^{(d)} \\ \vdots & & & & \\ 1 & x_{d+1}^{(1)} & x_{d+1}^{(2)} & \cdots & x_{d+1}^{(d)} \end{array} \right]\!\!\right] , \tag{3.117}$$

the coefficients $a_i^{(r)}$ $(i=1,\ldots d+1 \; ; \; r=1,\ldots d)$ are the minors of the $r^{th}$ row of and $x_1^{(1)}$, $x_1^{(2)}$, $x_2^{(1)}$, $x_2^{(2)}$, ... etc., are the d-dimensional co-ordinate of the (d+1) vertices of the element in the d-dimensional space.

Defining the generating function inside the element as a complete N-order polynomial in the generalized volume co-ordinates, in the form

$$G^e = \sum_{q=1}^{n} c_q G_q$$

$$= \sum_{j_1,\ldots j_{d+1}} \left( \sigma (j_1, j_2 \ldots, j_{d+1}) \, G (j_1, j_2 \ldots j_{d+1}) \right) \tag{3.118}$$

where

$$j_1 + j_2 + \cdots j_{d+1} = N , \tag{3.119}$$

n is the total number of nodal points defined inside the element , given by

$$n = ( N + d) ! \ / \ n! \ d! \tag{3.120}$$

and

$$\mathcal{T}(j_1 , j_2 , \cdots j_{d+1}) = P_{j1}(v_1) \ P_{j2}(v_2) \ \cdots \ P_{jd+1}(v_{d+1}) \tag{3.121}$$

$$P_m(v_i) = \prod_{i=1}^{m} \left( \frac{Nv_i - i + 1}{i} \right) \qquad (m \geqslant 1) \tag{3.122}$$

$$P_m(v_i) = 1 \qquad (m = 0) \tag{3.123}$$

the integro-differential problem of minimizing the functional in eq.(3.114) is transformed into the algebraic eigenvalue problem

$$[ S ] [ G ] = k_c^2 \ [ T ] [ G ] \tag{3.124}$$

where the global matrices [S], [T] and [G] are obtained by considering the contributions of all elements in the region of definition of

eq.(3.114). The individual components of the matrices [S] and [T] are calculated respectively by

$$S_{\ell q} = \frac{1}{\Delta^2} \sum_{k=1}^{d} \sum_{i=1}^{d+1} \sum_{j=1}^{d+1} a_i^{(k)} a_j^{(k)} \iint_{\text{element}} \cdots \int \frac{\delta c_\ell}{\delta v_i} \frac{\delta c_q}{\delta v_j} \, d\Omega \tag{3.125}$$

$$T_{\ell q} = \iint_{\text{element}} \cdots \int c_\ell c_q \, d\Omega \tag{3.126}$$

where $d\Omega$ is the generalized volume differential.

In the three-dimensional case the elements are tetrahedra and the generalized volume co-ordinates become the tetrahedral volume co-ordinates

$$v_i = V_i / V_e \tag{3.127}$$

$$\sum_{i=1}^{4} v_i = 1 \tag{3.128}$$

describing any interior point $P(x,y,z)$ of the element in the form $P(v_1,v_2,v_3,v_4)$.

In eq.(3.127) $V_i$ is the volume of one amongst the four tetrahedra dividing the element and having vertex on point P and $V_e$ is the element volume. As in the two-dimensional case, element matrices $[T^e]$ and $[Q^{12}]$ (the matrix $[S^e]$ is again decomposed and matrices $[Q^{ij}]$ which do not depend on the element geometric properties and

are row and column permutations of each other are defined)have been calculated (up to the $3^{rd}$-order)[45].

## 3.17 APPLICATION OF THE FINITE ELEMENT MINIMIZATION TECHNIQUE TO 3-D VECTOR WAVE PROBLEMS

Research effort is being made for calculating the scattering parameters of an arbitrary shaped waveguide discontinuity at Cambridge Engineering Department by means of tetrahedral elements[36]. Because no scalar functional has been found to describe the problem, vector functionals involving the electric field intensity or the magnetic field intensity vector components at each one of the tetrahedral element vertices are used in conjunction with the finite element minimization technique.

The computer solution of a waveguide discontinuity problem is then obtained as arrays of numbers corresponding to the three vector components at each element vertex since numerical calculations are performed in an essentially vector described problem.

If the nodal points inside the microwave junction are placed on planes cutting the junction into sections, the scalar functions describing the solution through their nodal values are in a number of three (one for each vector component) per cutting plane. Consequently the storage requirements for vector problems are necessarily high (approximately 500K bytes have been used in Cambridge) and the interpretation of the results from standard computer print-outs very difficult.

# CHAPTER 4

# WAVEGUIDE FIELD PATTERNS

## 4.1 INTRODUCTION

It has been shown in the previous chapter that discrete values of the generating function of propagating modes inside general cross-section waveguides can be obtained by the finite element method. Because the finite element method is a discretizing procedure it does not lead to the generating functions themselves but to a set of approximate scalar values distributed over the waveguide cross-section. A set of scalar values is not, however , a convenient form of presenting the answer to a microwave field problem. What is required is a method of visualizing the field configuration in the waveguide. Consequently , once the finite element solution has been obtained, an adequate interpolation method must be applied to the nodal value distributions in order to generate interpretable field information. The interpolation process should produce field results within a given tolerance depending on the problem in hand. No interpolation is necessary when vector finite element techniques are being considered. In this case,the field information is readily available. Only the visualization of the field behaviour remains to be cared for. It involves the man-machine interface for adequate presentation of the results. This is particularly

important since analytical descriptions of the field functions are not available. In addition, it must be kept in mind that computer solutions may contain spurious results[50][60][61]. The use of an inadequate interface not allowing quick identification of undesired outputs may correspond to wasting a considerable amount of time and effort.

This chapter proposes an original graphic method, capable of describing numerically obtained vector field distributions, very accurately. The technique to be discussed here gives a complete representation of the electromagnetic vectors in the waveguide. All the characteristics of a propagating vector field at a point (direction, relative magnitude and phase) are explicitly present in the output. Particular attention has been given to the user-machine interface such that a minimum of conventions has to be assimilated to interprete the results. The geometric image of a vector field has been chosen to consist of a representative assembly of arrows. The uniqueness of vector representation is obtained by imposing on this classical image specific geometric rules and fixed proportions.This speeds up the interpretation of the output making it easy to detect spurious results. The inherent ability of the method to generate readily interpretable outputs containing all the field information also makes it attractive to interactive applications. The method is general, and so, its extension to other situations in engineering can probably be carried out without difficulty. In this sense, the graphic technique developed during this research work complements the existing graphic software devoted to scalar representation. It opens the possibility of representing 3-dimensional and other

fields for which conventional field line diagrams and contour maps are not adequate.

The chapter starts by describing the usual field line representation of waveguide modes and its limitations. This is followed by a discussion of the contour map technique. Then it proceeds to explain the general concepts used in the development of the graphic image for vector quantities. Examples of application to waveguide propagation are given. The calculation and display of waveguide vector fields from the nodal value distributions is exemplified. Applications of the proposed vector imaging process to essentially 3-dimensional waveguide discontinuity problems are also shown in the chapter.

## 4.2 BASIC LIMITATION OF WAVEGUIDE MODE PATTERNS

The use of mode patterns describing the normal mode field configurations of conventional waveguides, that is, waveguides for which a closed analytical form of the field distributions can be obtained, is a well established practice in microwave engineering. The waveguide mode patterns are usually constructed from the analytical expressions for the electromagnetic fields using field lines[62] also called lines of force[63] as for static fields and appear in most books dealing with the fundamentals of microwave techniques[25][64].

In general, however, the electromagnetic field $\underline{V}$ ($\underline{V}$ = $\underline{E}$ or $\underline{H}$ ) on the displaying or plotting plane, that is, on a plane of constant phase along the direction of power flow in the waveguide for which the diagrams are constructed, does not satisfy

$$\text{div. } \underline{V} = 0 \tag{4.1}$$

and therefore the resulting patterns cannot be interpreted in the same way.

This difficulty in the interpretation of the classical mode patterns has been realized by Marcuvitz[57] nearly 30 years ago, pointing out that his diagrams are not true flux plots and therefore do not indicate the field intensity everywhere. The reason of inadequacy of the field line diagrams in electrodynamical situations presented by Marcuvitz, is essential. It produces some interpretation difficulties which have been analysed by the author and are discussed in the following paragraphs.

## 4.3 DIFFICULTIES IN THE INTERPRETATION OF FIELD INTENSITY VARIATIONS BY MEANS OF FIELD LINES

### 4.3.1 CONVENTIONAL DIAGRAMS

Before analysing the difficulties of interpretation of the behaviour over the cross-section for fields which cannot be graphically represented through an accurate field line diagram, let us consider the pictorial arrangement by which the field information is conveyed to the observer by means of those diagrams.

Consider the simplest of the waveguide mode patterns, namely the mode pattern of the $TE_{10}$ mode of a typical rectangular waveguide. According to the field line diagrams graphic technique, the transverse electric field is represented, in this case, by a certain number of straight lines which are parallel to the narrower cross-

section sides. This indicates that the field has that direction everywhere on the cross-section. The straight lines are distributed over the cross-section in such way that the number of lines per unity length along the broader cross-section sides indicates the sinusoidal variation of the relative magnitude of the field along that direction in the waveguide. The magnetic field is also represented by straight lines which are, now, parallel to the broader cross-section sides and equispaced. Because, for this particular mode(and all TE modes) the magnetic field has, in general, non-vanishing longitudinal components at cross-section points, it is impossible to give an accurate description of its relative magnitude variations or direction. The field line diagrams actually collapse for such vector fields. Therefore, the magnetic field representation can only be interpreted as a vague indication of the magnetic field behaviour for this mode.

Two conventional $TE_{10}$ mode patterns are presented in Fig.(4.1) and Fig.(4.2). The diagram depicted in Fig.(4.1) shows a total of 5 field lines per displayed field while Fig.(4.2) shows a total of 19 field lines per displayed field. Both pictures will be referenced at a later paragraph in the chapter. For clarity, the magnetic field lines have been ommitted in the diagrams. It appears , from the observation of both diagrams that, if they are used without the previous knowledge of the functional form of the field expressions (which is a natural condition for numerically evaluated fields) the comprehension of the sinusoidal variation of the relative magnitude of the transverse electric field along the broader cross-section sides direction,

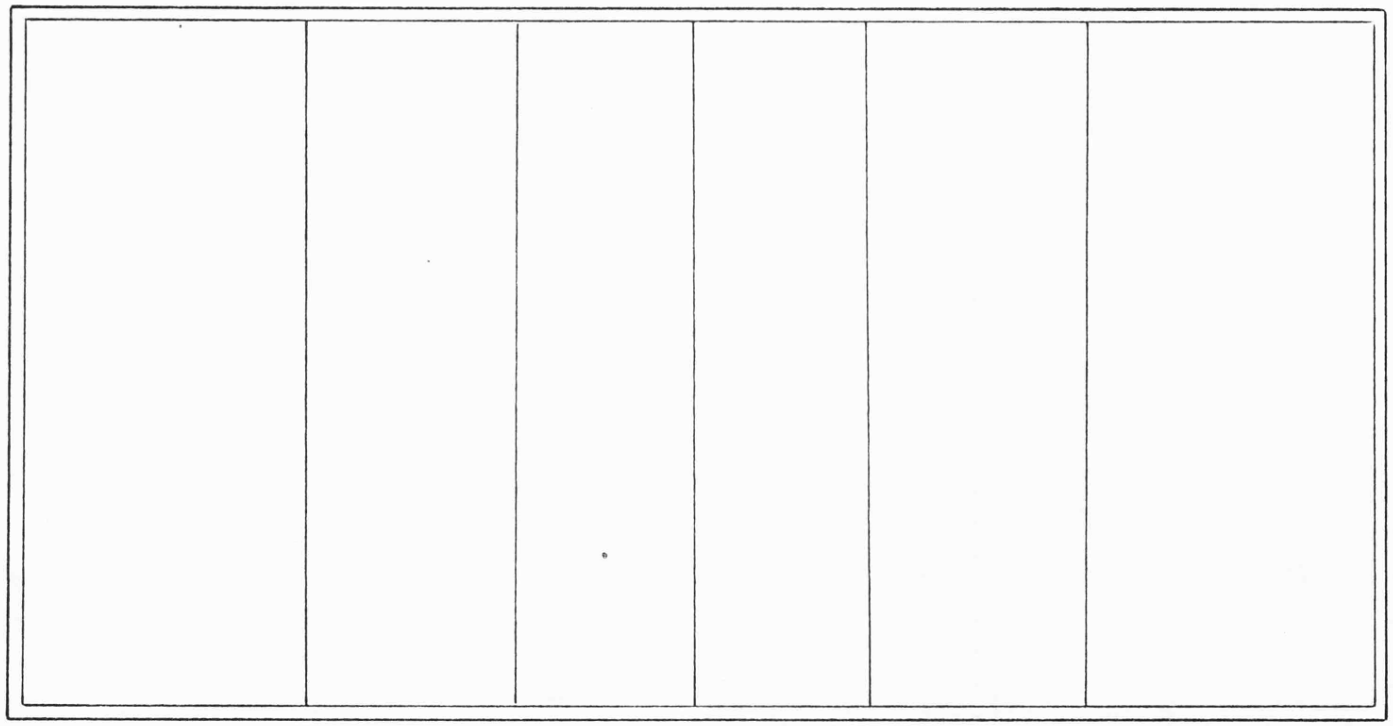

FIG. 4.1 $TE_{10}$ ELECTRIC FIELD LINES

Field line diagram of the $TE_{10}$ mode in a typical rectangular waveguide.

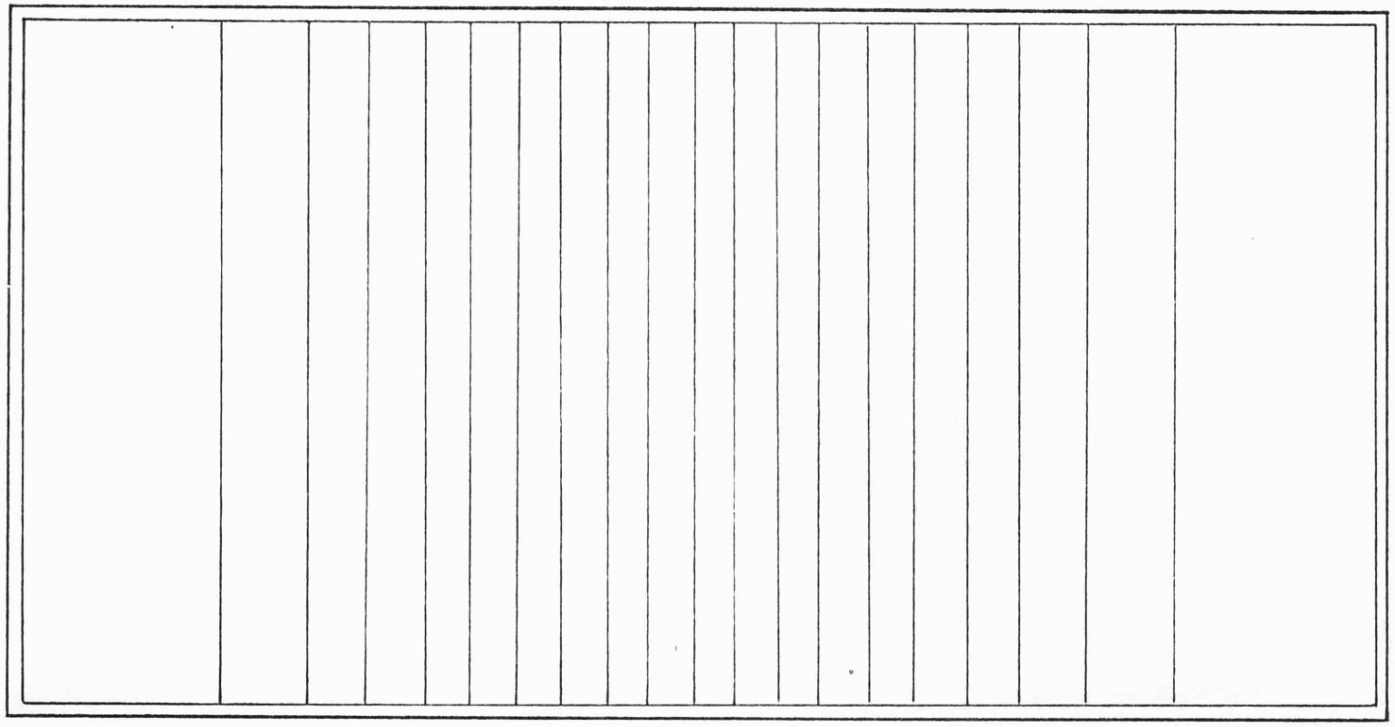

FIG. 4.2 $TE_{10}$ ELECTRIC FIELD LINES

Field line diagram of the $TE_{10}$ mode in a typical rectangular waveguide.

The picture shows 19 electric field lines.

$$E = E_0 \sin\left(\frac{\pi x}{A}\right) \tag{4.2}$$

where $E_0$ is an arbitrary amplitude constant and A is the broader cross-section side length, cannot be easily accomplished.

In other words, the information about the field intensity variations over the waveguide cross-section, although precisely present in both pictures (with obvious emphasis in the second picture) is hard to assimilate.

### 4.3.2 AUTOMATICALLY GENERATED CONTOUR DIAGRAMS

The difficulty of interpreting the field distribution is increased when contour diagrams are used for representing the field behaviour in the guiding structure. It can be shown that the field lines of transverse fields in a general cross-section waveguide follow the contour maps of the generating function nodal value distributions. For this purpose, consider the general equation for the transverse electromagnetic field vector, $\underline{V}_{Tn}$, of a propagating mode in a general cross-section waveguide, obtained by combining the mode field equations, eq.(2.138) to eq.(2.147):

$$\underline{V}_{Tn} = p\, \underline{u}_z \times \text{grad}\, G_n \tag{4.3}$$

where p is a proportionality factor and $G_n$ is the generating function for the mode under consideration.

As the vector (grad $G_n$) has a direction which is perpendicular to the curves obtained by joining the points for which

$$G_n = \text{constant} \tag{4.4}$$

in a contouring sense, and because the cross-product of the unity vector $\underline{u}_z$ times (grad $G_n$) actually rotates the latter through an angle equal to $(\pi/2)$ radians; it is concluded that the direction of $\underline{V}_{Tn}$ at any point of the curve described by eq.(4.4) is the direction of the tangent to the curve at that point. Comsequently, field lines of the transverse fields can be obtained by applying contouring routines to the generating function nodal value distributions.

It must be said here, however, that although standard contouring routines are available in most computer laboratories, the structure of the finite element evaluated nodal point distribution is such that, very rarely, they are located on a regularly spaced mesh required for the vast majority of contouring algorithms. In general, the generating function nodal values distributions can be regarded as "scattered data" for contouring purposes.

If the nodal values are arranged in such way that their displacement from an hypothetical regular mesh dividing the cross-section is reasonably small, interpolation techniques can be used to evaluated the nodal values on the mesh points based on the actually known nodal points(65)(66). This procedure is in general, however , incovenient since it not only limits the inherent ability of the finite element method which is to allow an arbitrary definition of the nodal points, but also introduces an interpolation process before any field information can be obtained. This magnifies the cumulative error of the overall process. Even in a particular situation where no substantial error would be introduced by re-interpolating

the nodal values distribution, the actual process of contouring over a regularly spaced mesh may present difficulties[67][68].

The difficulties of automatically generated field lines are not confined, however, to algorithm difficulties. In fact, by using such technique the observation of relative field intensity variations may become particularly difficult. The difficulty in the interpretation of those diagrams occurs because the field lines are to be drawn over nodal points which have been located over the cross-section, without, in general, bearing a geometric distribution taylored for relative field intensity description by the field line diagrams technique. Evidence of the above comment can be obtained by comparing Fig.(4.1) with the application of a contouring technique to the $TE_{10}$ nodal value distribution given in Map(3.21) in order to obtain the corresponding field lines, shown in Fig.(4.3).

The diagrams depicted in Fig.(4.4) and Fig.(4.5) show the contour obtained for the $TM_{11}$ and the $TE_{11}$ modes from the nodal value distributions in Map(3.22) and Map(3.23), respectively. The numbers which appear in the disgrams represent the constant nodal value along the field lines and are shown for illustrative purpose only. They are not usually shown in pictures drawn according to this graphic technique. Also the field lines of the non-transverse fields (which are depicted in the classical field line diagrams for waveguide modes) are not produced by this method.

Finally, it must be pointed out that, in the category of automatic generation of field lines, a computer program for contouring over a triangular grid based on 2-dimensional Newton-Cotes interpolation polynomials[69][70] has been developed[17] and applied to finite element results of electromagnetic problems[71][72][73][74][75][76][77].

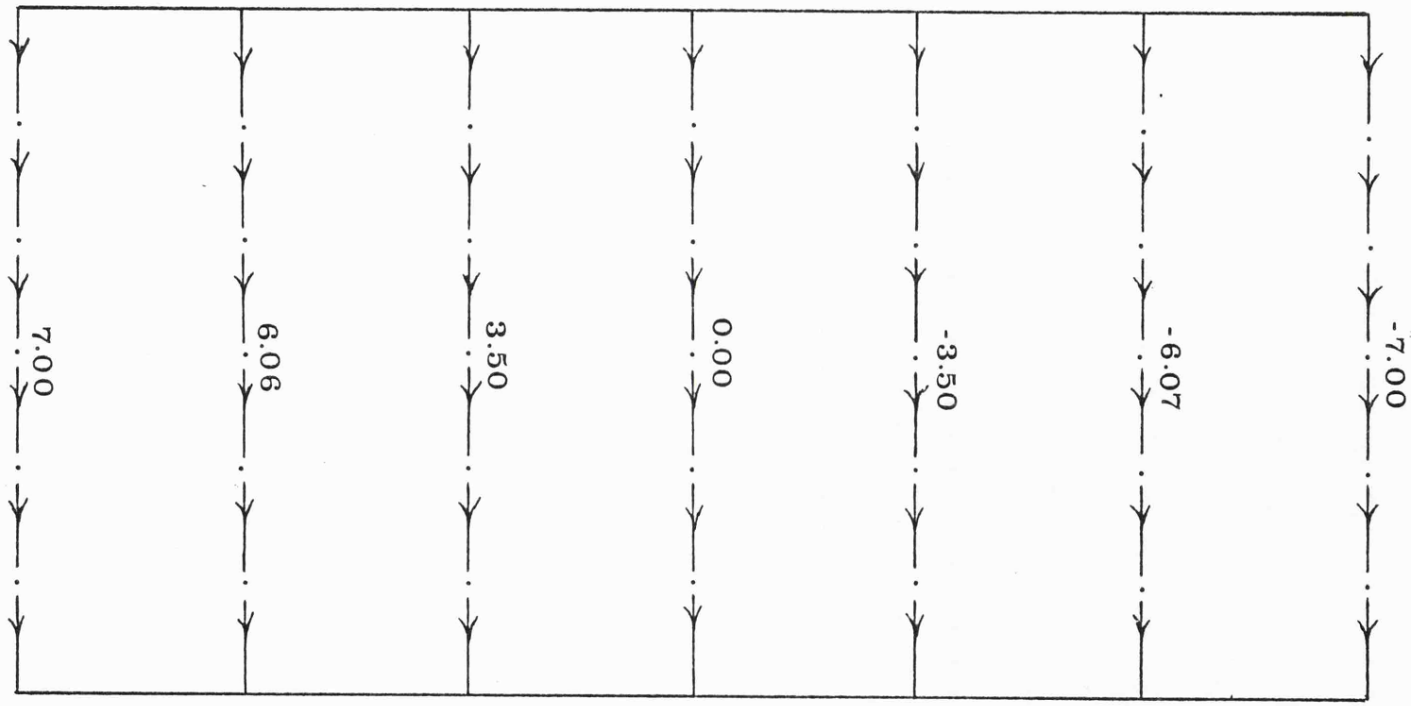


FIG. 4.3 $TE_{10}$ CONTOUR MAP

Contours of the nodal value distribution (Map(3.21)) for the $TE_{10}$ mode.

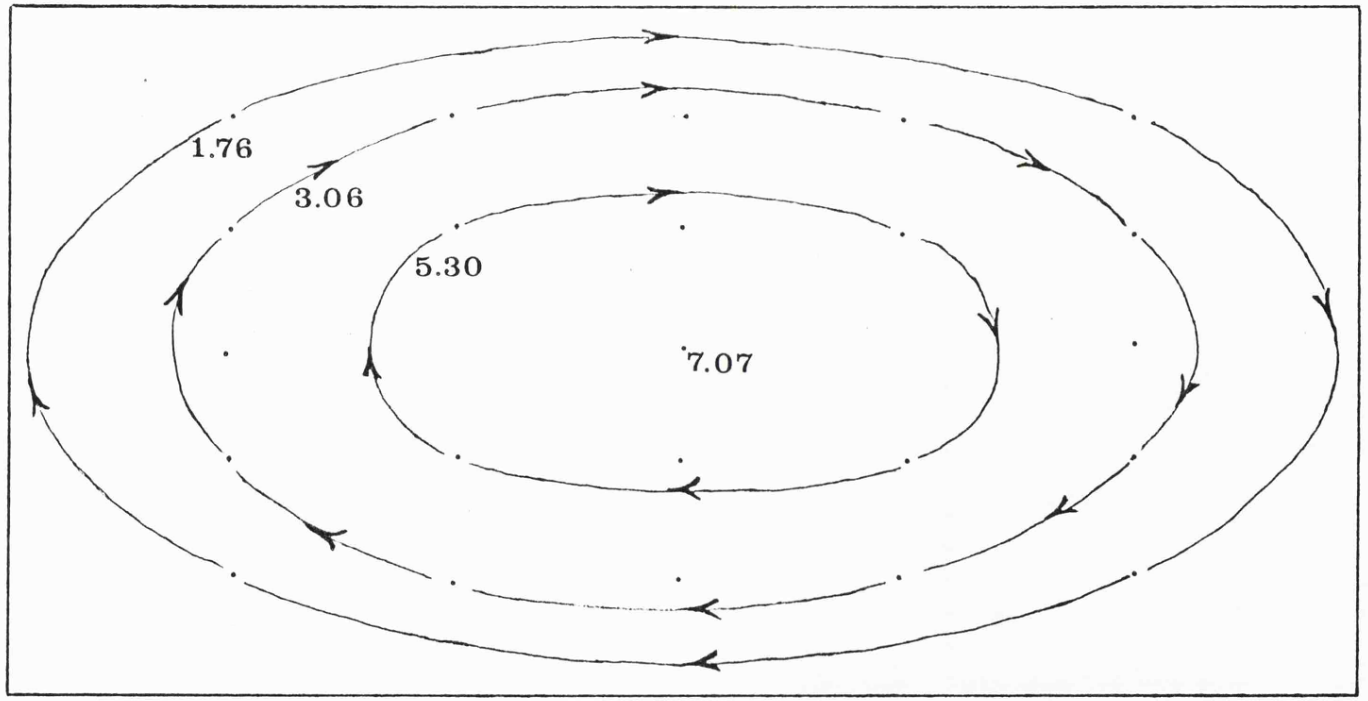


FIG. 4.4 $TM_{11}$ CONTOUR MAP

Contours of the nodal value distribution (Map(3.22)) for the $TM_{11}$ mode.

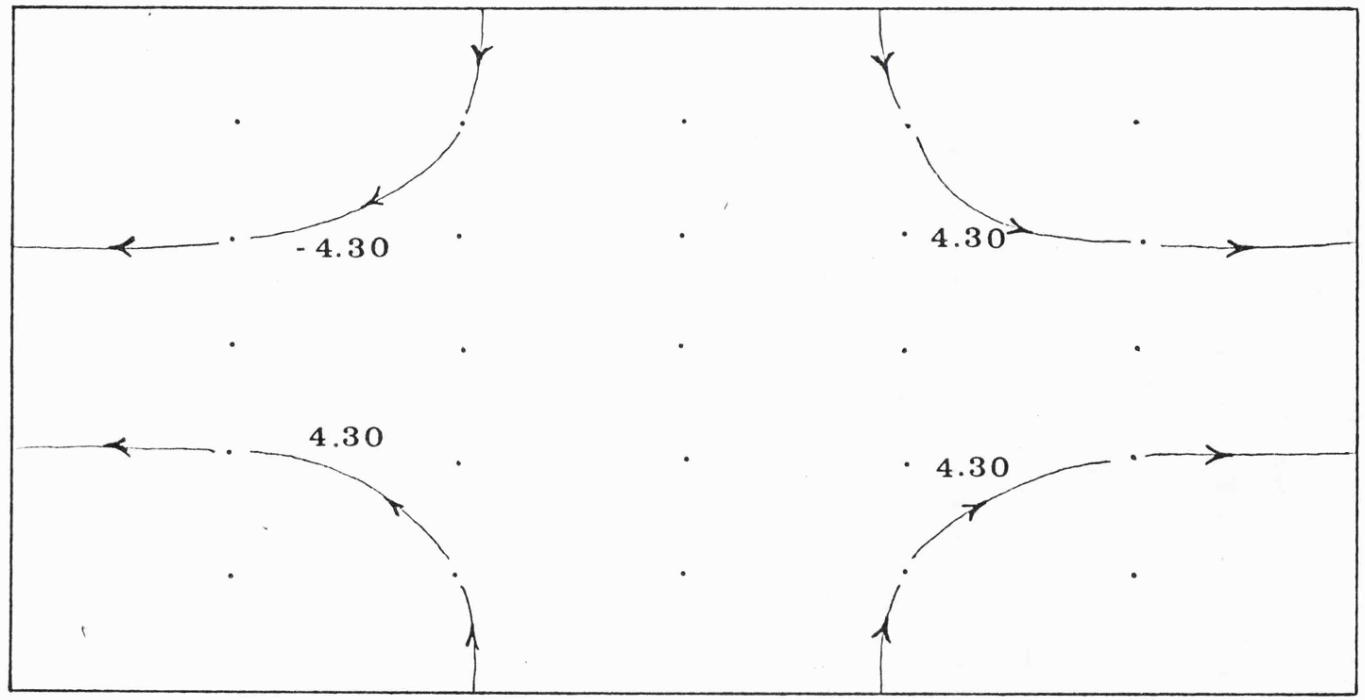


FIG. 4.5 $TE_{11}$ CONTOUR MAP

Contours of the nodal value distribution (Map(3.23)) for the $TE_{11}$ mode.

## 4.4 REGIONS OF PSEUDO INTENSE FIELD

Another kind of interpretation difficulty which does not involve the transverse field but affects the consistency of the field line diagrams, regarded as a whole, is raised by observing for instance, the curvature of the field lines displayed in Fig.(4.4) and Fig.(4.5). It is noticeable in Fig.(4.4) that the magnetic field lines are concave when observed from the waveguide centre region. This means that, when the electric field lines are drawn to approximately represent the electric field behaviour on the displaying plane, they will converge in the centre region and diverge in the corner regions since, according to eq.(2.148), they must intercept the magnetic field lines at right angles.

The convergence of the electric field lines in the centre region suggests the existence of a highly intense field at the waveguide axis while their divergence at the corners suggests a weak field there. The field line density is high in the centre region and low in the corners. In fact, although the electric field is relatively weak at the waveguide corners, the increase in the field line density in the centre region creates pseudo intense fields because the increase in the field line density is not motivated by higher non-transverse fields in the region but happens as an unavoidable graphic consequence of the curvature of the transverse field lines. This region of pseudo intense field may wrongly suggest the existence of an electric field showing an unaccountable high relative intensity at the waveguide axis for every phase along the wavelength because the same diagram truely suggests weak fields at corners for every phase in the propagation. A sketch showing the for-

mation of the pseudo intense field region for the $TM_{11}$ mode is presented in Fig.(4.6).

Similarly, the convexity of the electric field lines of the $TE_{11}$ mode (Fig.(4.5)) with respect to the waveguide centre could misleadingly suggest a magnetic field showing low intensity on the waveguide axis and high intensity at the cross-section corners for every phase in the propagation. Here, the pseudo intense field regions are the waveguide corners and the effect for this particular mode is depicted in Fig.(4.7).

The formation of those pseudo intense field regions occurs for every transverse displaying plane and cannot be corrected by observing field line diagrams obtained at different phases along the propagation direction.

## 4.5 PERSPECTIVE VIEW OF WAVEGUIDE FIELDS

The difficulty of interpreting the field distribution described in the previous paragraph arises more from the inherent properties of the waveguide fields and from the graphic technique of vector representation used in the field diagrams than from the 2-dimensional structure of the field plots.

In fact, an attempt, made by Glazier and Lamont[78], to show a perspective representation of the electromagnetic fields inside a square waveguide still carry the effect of pseudo increase in field intensity in certain regions of the cross-section. However, in those diagrams, a technique of reducing the drawing intensity* (eventually no lines are drawn at weak field regions) in a darkness control

---

* Colour is used to identify the fields in the original diagrams.

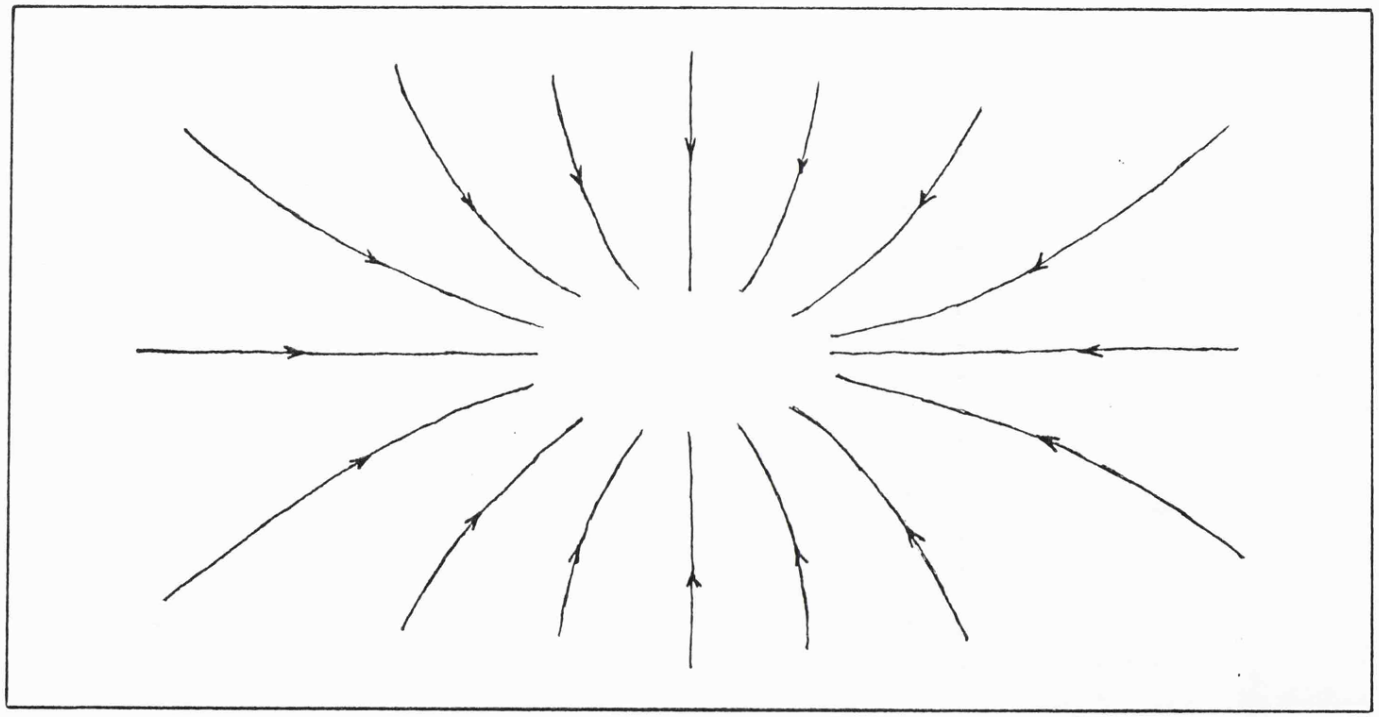

FIG. 4.6 $TM_{11}$ PSEUDO INTENSE FIELD REGION

The effect of pseudo intense electric field on waveguide axis for the $TM_{11}$ mode

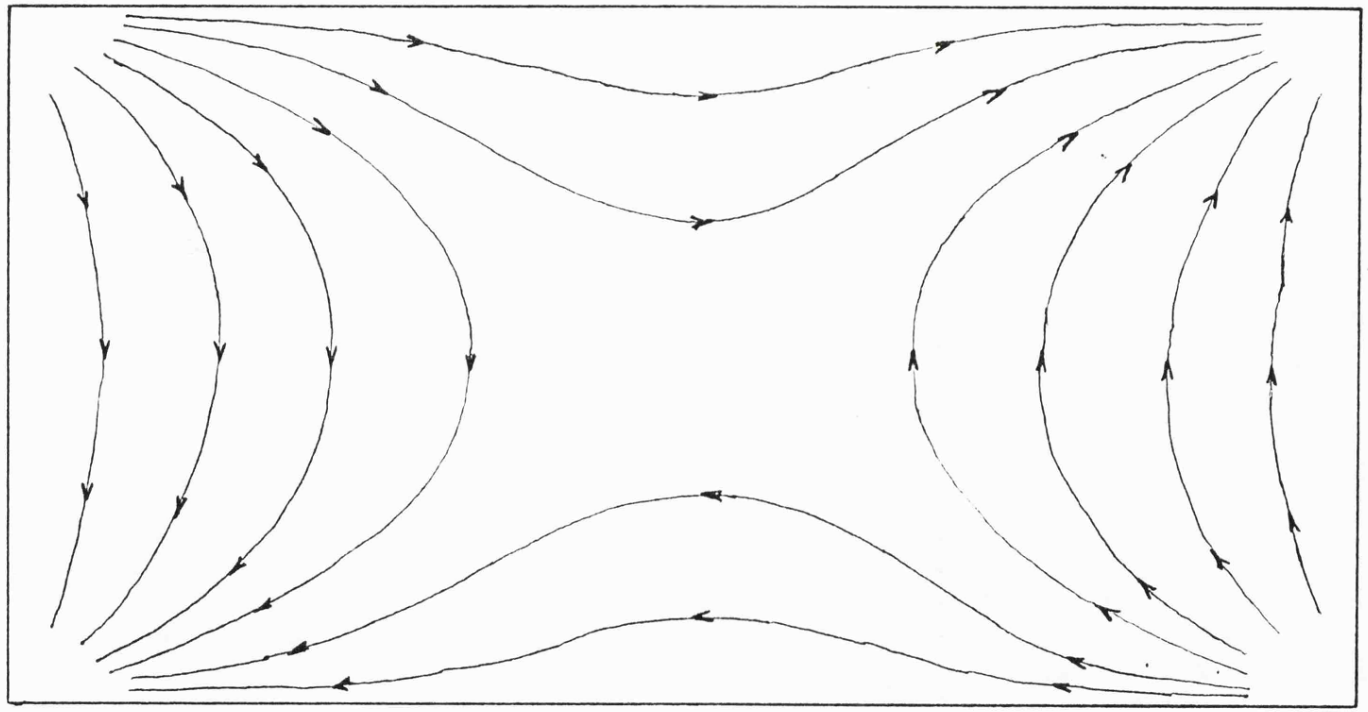

FIG. 4.7 $TE_{11}$ PSEUDO INTENSE FIELD REGIONS

The effect of pseudo intense magnetic field at waveguide corners for the $TE_{11}$ mode.

fashion has been used to avoid the misleading interpretation in the relative magnitude of the field due to the pseudo increase in the field line density. The diagrams are reproduced in Fig.(4.8).

Because the relative field intensity of the non-transverse electromagnetic field is not always high nor always low but depends in a somewhat more complicated way upon the phase plane along the wavelength, 3-dimensional diagrams as shown in Fig.(4.8) are yet not able to represent the non-transverse fields, accurately.

## 4.6 PHASE AND POLARIZATION

It is not possible to display phase relationships between the electromagnetic vectors by utilizing graphic techniques based on field lines. The amount of information which can be conveyed by that technique is restricted to the presentation of direction and intensity of 2-dimensional fields.

Also, the important aspect of polarization of the electromagnetic field vectors, as for instance the circular polarization of the magnetic field vector of the $TE_{10}$ mode on planes parallel and near to the narrower waveguide walls in a typical rectangular waveguide[79][80] (the effect is used in ferrite devices) cannot be made pictorially evident in diagrams based on field line techniques.

## 4.7 ALTERNATIVE GRAPHIC TECHNIQUES FOR VECTOR FIELD REPRESENTATION

In spite of the clear vectorial nature of the waveguide propagation problem, the inadequacy of the classical field line diagrams, the limitations of the contour diagrams and although vector variational techniques enabling the direct calculation of the vector com-

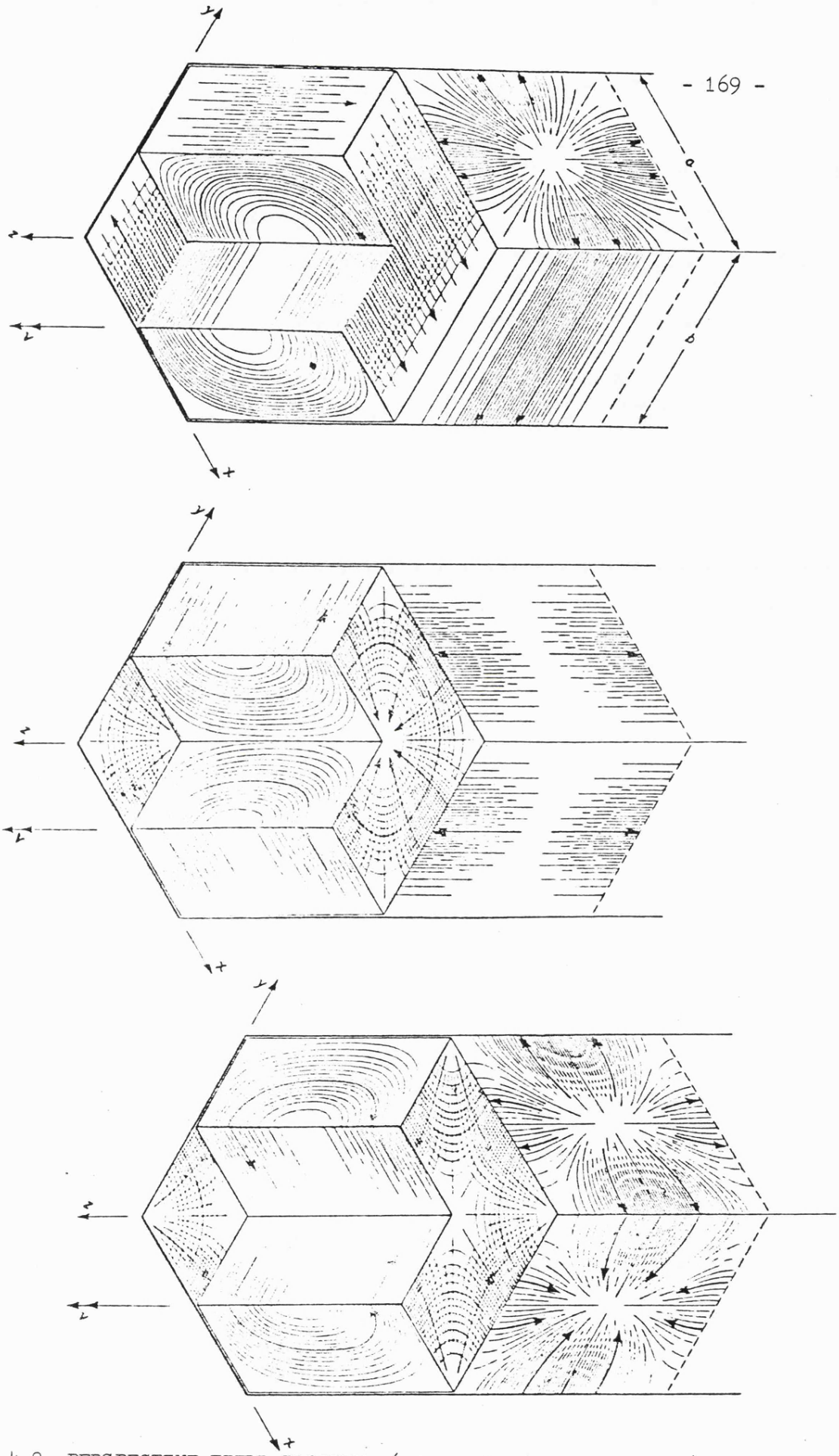

FIG. 4.8 PERSPECTIVE FIELD PLOTTING (after Glazier and Lamont)

ponents inside waveguides have been published [21][49][50][51][52][81][82], no alternative graphic technique for vector field representation is available. The state of the art is such that 3-dimensional fields are represented by contouring (independently) the 3 scalar components to produce a set of 3 pictures which must be interpreted concomitantly[81] and 2-dimensional fields are either represented by automatically generated contour diagrams[17] or by means of assembling classical 1-dimensional arrows having the length proportional to the vector intensity at a point[60][83].

Also, there are no provisions in the commercial computer graphic packages to enable the representation of vector fields. Those packages are powerful tools for dealing with graphic representation of scalar quantities and for assisting scalar engineering problems but offer very little help for the essentially vector microwave problems. The built-in graphic facilities of commercial packages can, however, be applied to generate diagrams for vector representation, as for instance to produce a set of component contour pictures. An ingeneous example of such applications can be found in the recently available program[84] where 3-dimensional field lines are constructed for the lowest modes of a typical rectangular waveguide. The program utilizes the 3 components of the electromagnetic vectors at a specific point on a set of planes along the wavelength (or half wavelength ) to integrate the field line in space by means of a predictor-corrector method. The resulting curves are then output via display terminal. Unfortunately, because the field line technique has been employed in the program, it is not possible to avoid the pseudo increase in field intensity effect for the non-transverse field and po-

larization and phase relationships cannot be shown. Moreover, even when only the non-transverse field is represented by 3-dimensional continuous field lines (the transverse electric field cannot be represented by continuous 3-dimensional lines) the expected incomprehensibility of the resulting diagrams[84] does not recommend any attempt to display general cross-section waveguide field distributions by that technique. Two typical field distribution displays generated by the program are shown in Fig.(4.9) and Fig.(4.10).

## 4.8 3-DIMENSIONAL REPRESENTATION OF VECTORS

It has been shown in the foregoing paragraphs that the available techniques of field line diagrams, contouring and 3-dimensional field line representation do not constitute an adequate graphic approach for the display of the electromagnetic fields in general cross-section waveguides. All those techniques have the common property of utilizing a set of continuous curves in order to convey the field information.

Although the method is shown to be adequate for static 2-dimensional fields where flux functions can be defined[85] ,it collapses for 3-dimensional and electrodynamic fields, in general. The failure of the conventional techniques in 3-dimensional problems may be regarded as a consequence of the use of an oversimplified graphical image (continuous lines and their relative position) which is incapable of accommodating the necessary field information present in a 3-dimensional situation.

It will be shown in the next sections that by adopting a convenient 3-dimensional image for the vector quantity at a point in

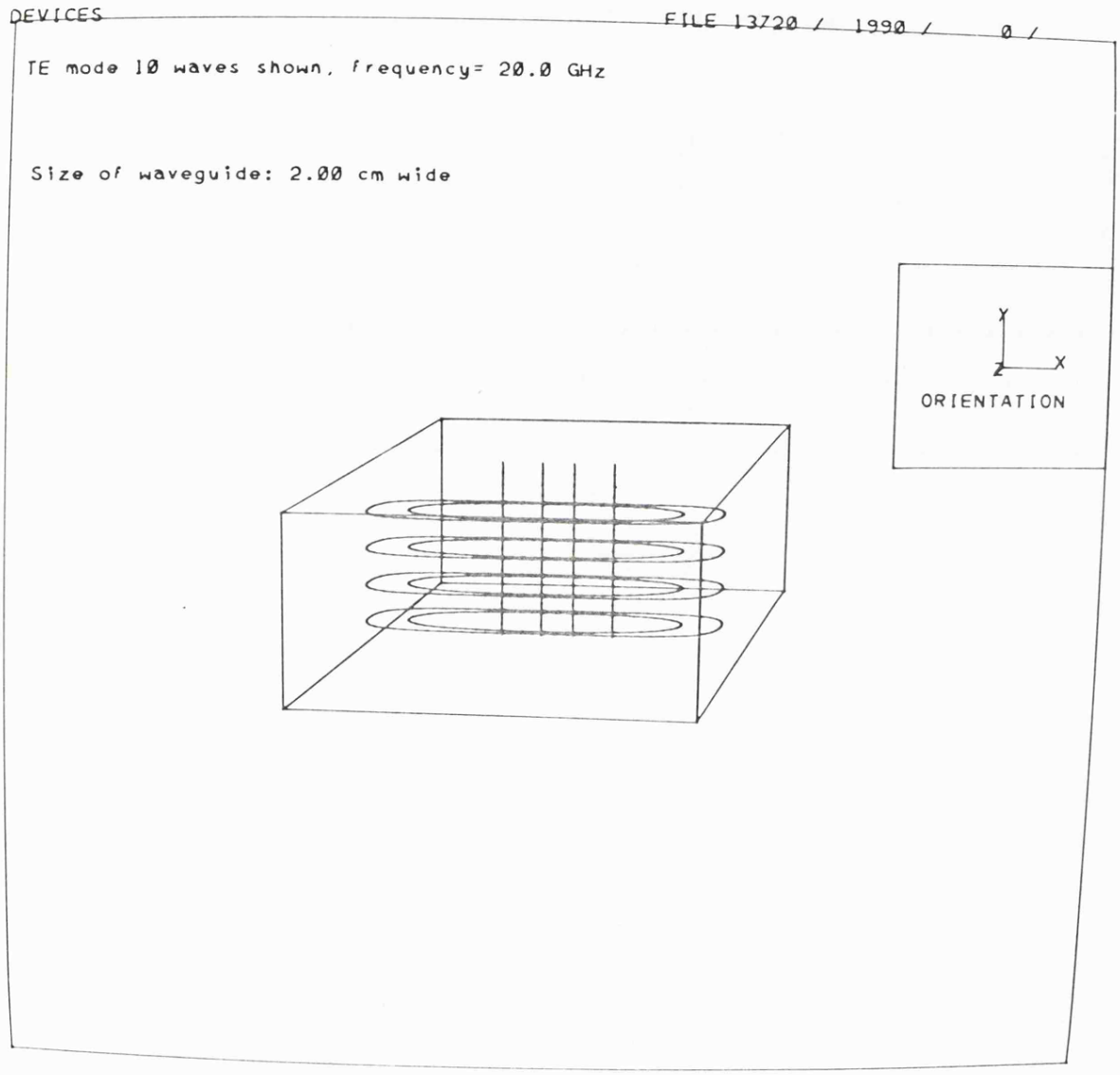


FIG. 4.9 $TE_{10}$ 3-D FIELD LINE DISPLAY

Field lines of the electric and magnetic field intensities of the $TE_{10}$ mode in a typical rectangular waveguide. (Program WAVGDS).

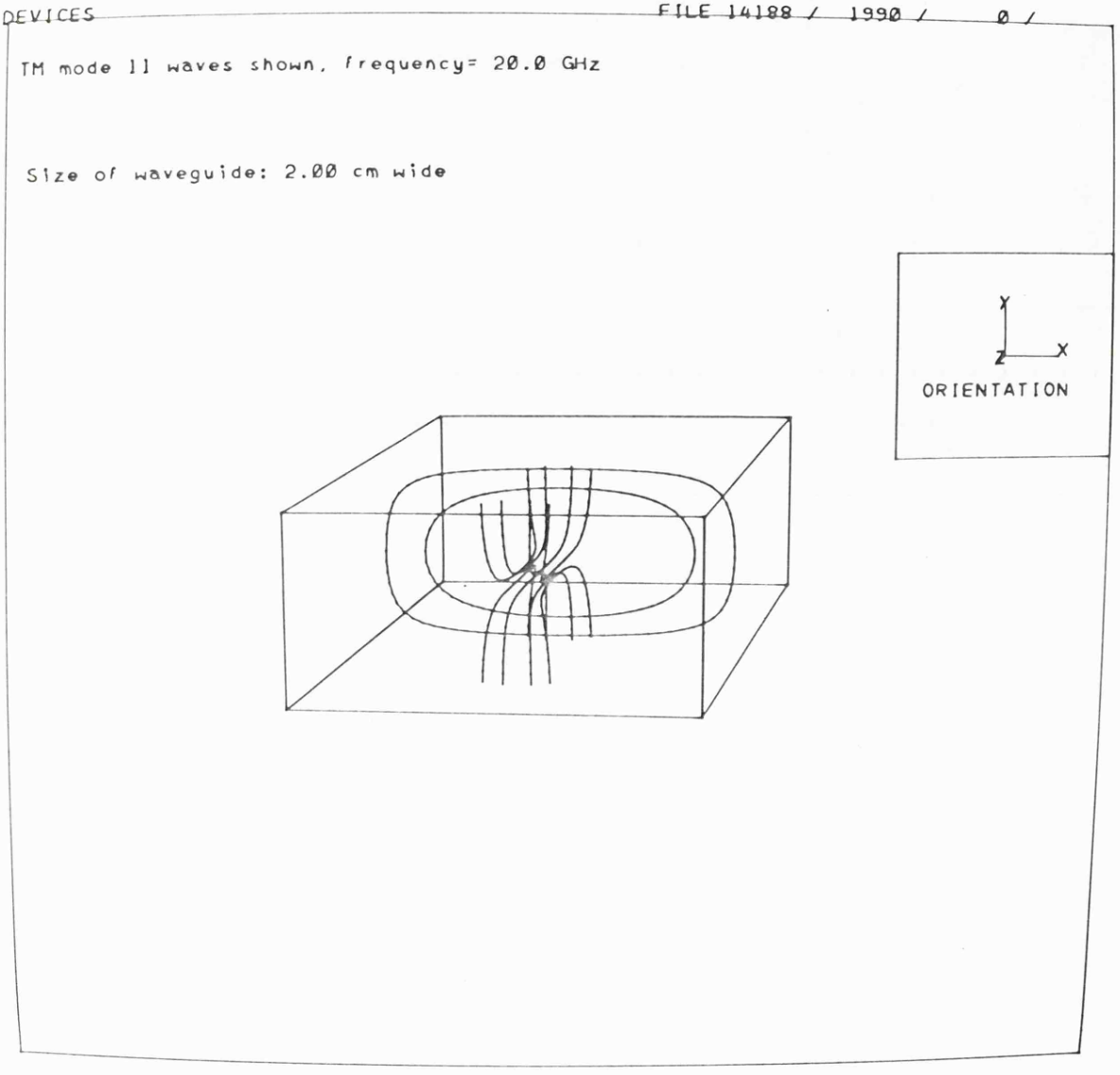


FIG. 4.10 $TM_{11}$ 3-D FIELD LINE DISPLAY

Field lines of the electric and magnetic field intensities of the $TM_{11}$ mode in a typical rectangular waveguide. (Program WAVGDS).

the 3-dimensional space, it is possible to accommodate all the pertinent field information accurately and produce a satisfactory field pattern to represent the general cross-section waveguide field distribution. Because the plots generated by this technique are phase dependent, polarization and phase relationships of the electromagnetic vectors can be shown and the pseudo increase in field intensity effect overcome.

### 4.8.1 PLANE SAMPLE OF A VECTOR FIELD

Consider either a simply or multiply-connected bounded region R in the 3-dimensional cartesian space with boundary surface S as illustrated in Fig.(4.11). The boundary surface S may consist of a finite number N of closed non self-intersecting surfaces $S_j (j = 1,2,...N)$ which are assumed to be included in R. Assume that associated with every point on R there exists a vector quantity $\underline{V}$ which can be described by means of a well behaved vector function of the 3 co-ordinates, $\underline{f}(x,y,z)$, in the form:

$$\underline{V} = \underline{f}(x,y,z) = M(x,y,z) \angle A(x,y,z) \qquad (4.5)$$

where M and A are scalar functions which give the magnitude or intensity of $\underline{V}$ and the direction of $\underline{V}$, at every point of $\underline{R}$, respectively. Further, assume that M(x,y,z) is bounded in R, that is

$$M(x,y,z) \leqslant Q \qquad (4.6)$$

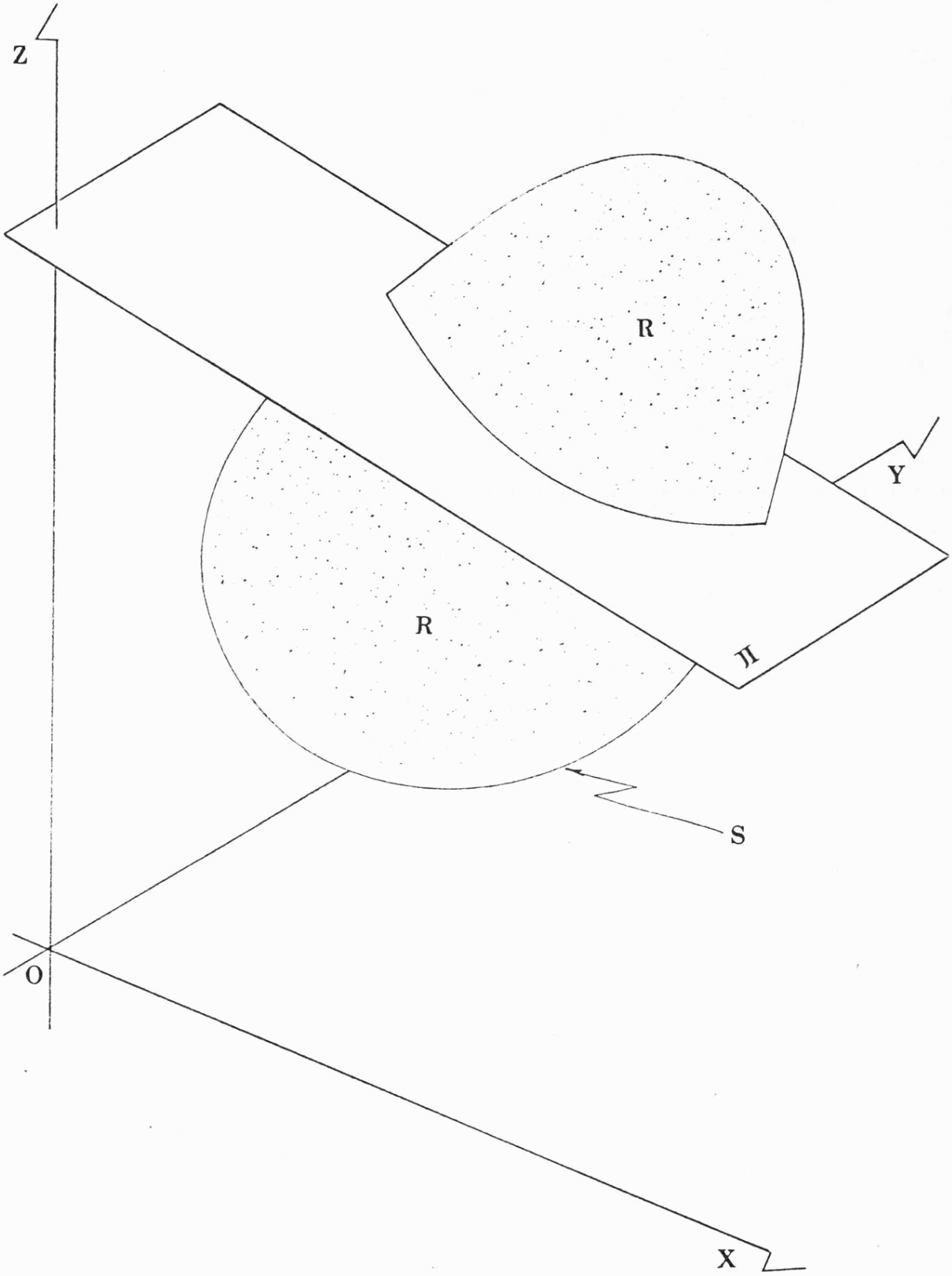


FIG. 4.11 BOUNDED REGION AND PLANE SAMPLE

The region R where a vector field $\underline{V}$ is defined and the sampling plane $\pi$.

where Q is a finite number. The function $A(x,y,z)$ is bounded by definition.

Let the function $\underline{f}(x,y,z)$ although in general unknown, have a behaviour which makes it possible to obtain a good approximation to its form and values in the entire region by performing a set of discrete measurements inside R. The measurements are carried out by sampling R into representative plane slices and measuring the visible projection of a suitable 3-D representation of the vector $\underline{V}_c$ associated with each point $P_c(x,y,z)$ of a finite set chosen on the surface of each slice.

The situation is illustrated in Fig.(4.12) where to each chosen point $P_c$ of the slice there corresponds the measured values $M_c$ and $A_c$ which determine the value of $\underline{f}$ at that point. Those values are assumed to be obtained by measuring the projection of an image (not shown in the figure) of $\underline{V}_c$ at $P_c$.

### 4.8.2 GEOMETRIC DEFINITIONS

The geometry used in the development of the method by which the vector quantity at a sampling point on the slice surface can be graphically displayed is defined as follows. Consider a slice of R consisting of all the points enclosed by a closed curve C (including all points on C), obtained by cutting R with an arbitrary plane $\pi$ . Associate with the slice an orthogonal right-hand system $(x_p, y_p, z_p)$ such that a projection or image plane $(x_p, y_p)$ is defined on the slice surface ($z_p$ perpendicular to the slice) and the position of every point of a finite representative set chosen on the slice surface becomes defined with respect to the system $(x_p, y_p)$. Also

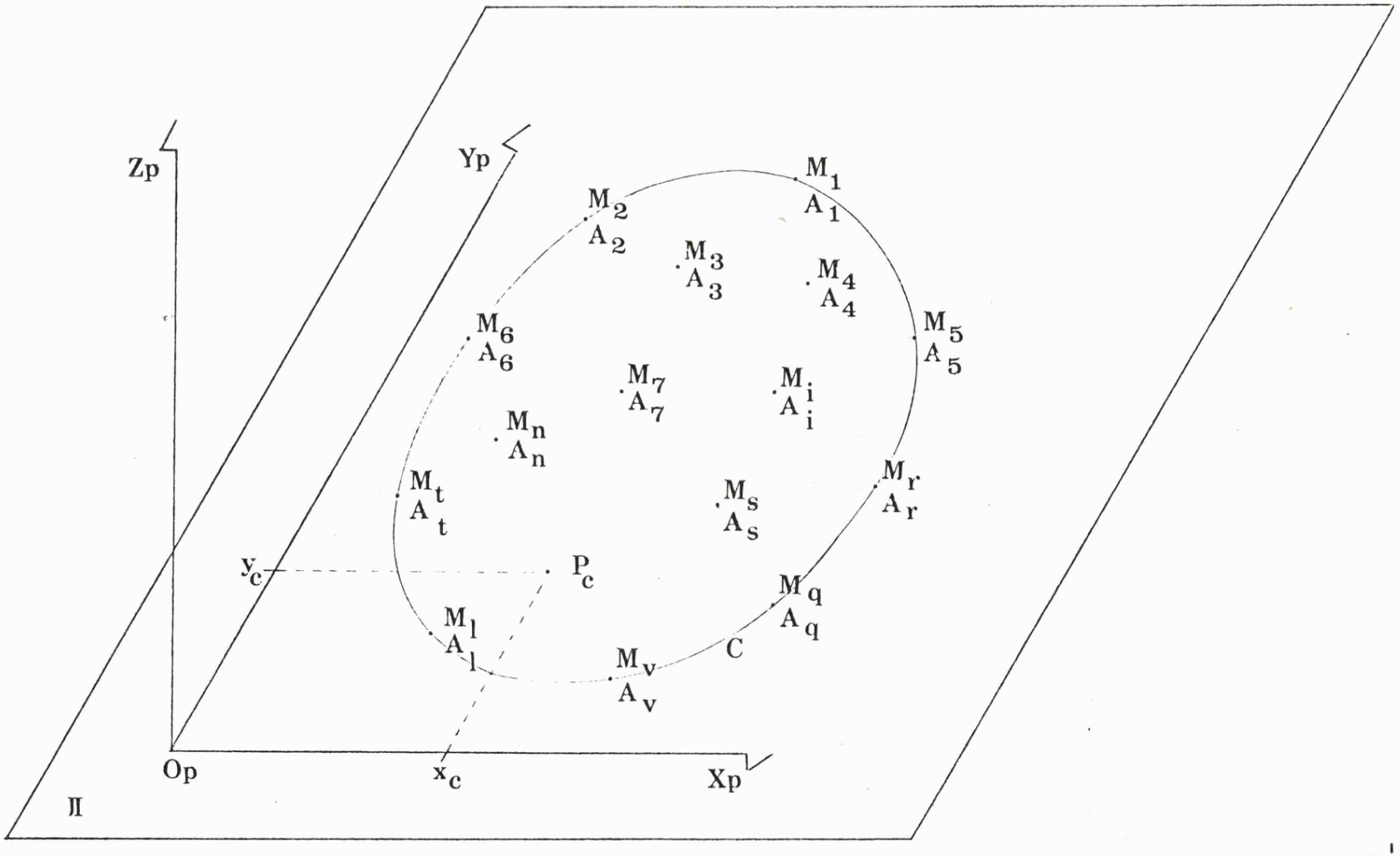


FIG. 4.12 SAMPLE POINTS

Measurements of the functions M(x,y,z) and A(x,y,z) on the surface of the sampling plane $\pi$ .

consider one of the representative points on the slice surface, $P_c$, and the vector quantity $\underline{V}_c$ associated with that point.

Let the decomposition of $\underline{V}_c$ according to a local co-ordinate system $(x_s, y_s, z_s)$, with origin on $P_c$ and parallel to the slice system $(x_p, y_p, z_p)$ be given by

$$\underline{V}_c = \sum_{i=1}^{3} V_{cis} \underline{u}_{is} \tag{4.7}$$

where, according to eq.(4.6), it is always possible to chose a scale factor such that:

$$V_{cis} \leqslant 1 \tag{4.8}$$

The co-ordinate systems are shown in Fig.(4.13). Define, as illustrated in Fig.(4.14), the advancing angle $\alpha$ and the elevating angle $\beta$ , through the expressions:

$$\alpha = \tan^{-1} (V_{c2s} / V_{c1s}) \tag{4.9}$$

$$\beta = \tan^{-1} [ V_{c3s} / (V_{c1s}^2 + V_{c2s}^2)^{\frac{1}{2}} ] \tag{4.10}$$

Associate with the vector quantity $\underline{V}_c$ another local co-ordinate system $(x_v, y_v, z_v)$ such that the $y_v$ axis is made coincident with the line joining the points $P_c(0,0,0)$ and $Q_c(V_{c1s}, V_{c2s}, V_{c3s})$. Let the origin of this local co-ordinate system be placed on the point $O_v$ ,

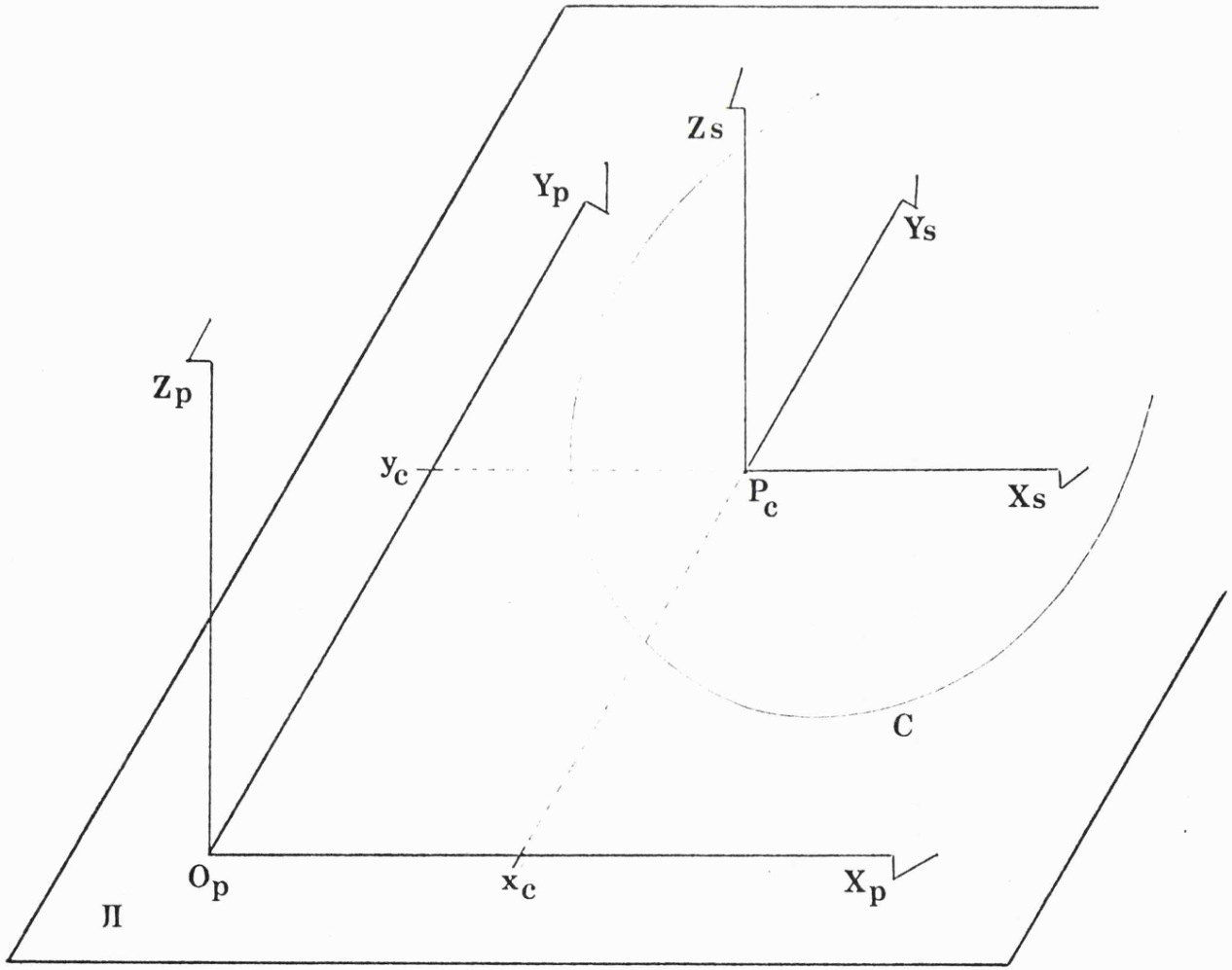


FIG. 4.13 REFERENCE SYSTEMS

The co-ordinate systems on the slice surface, as defined in section 4.8.2.

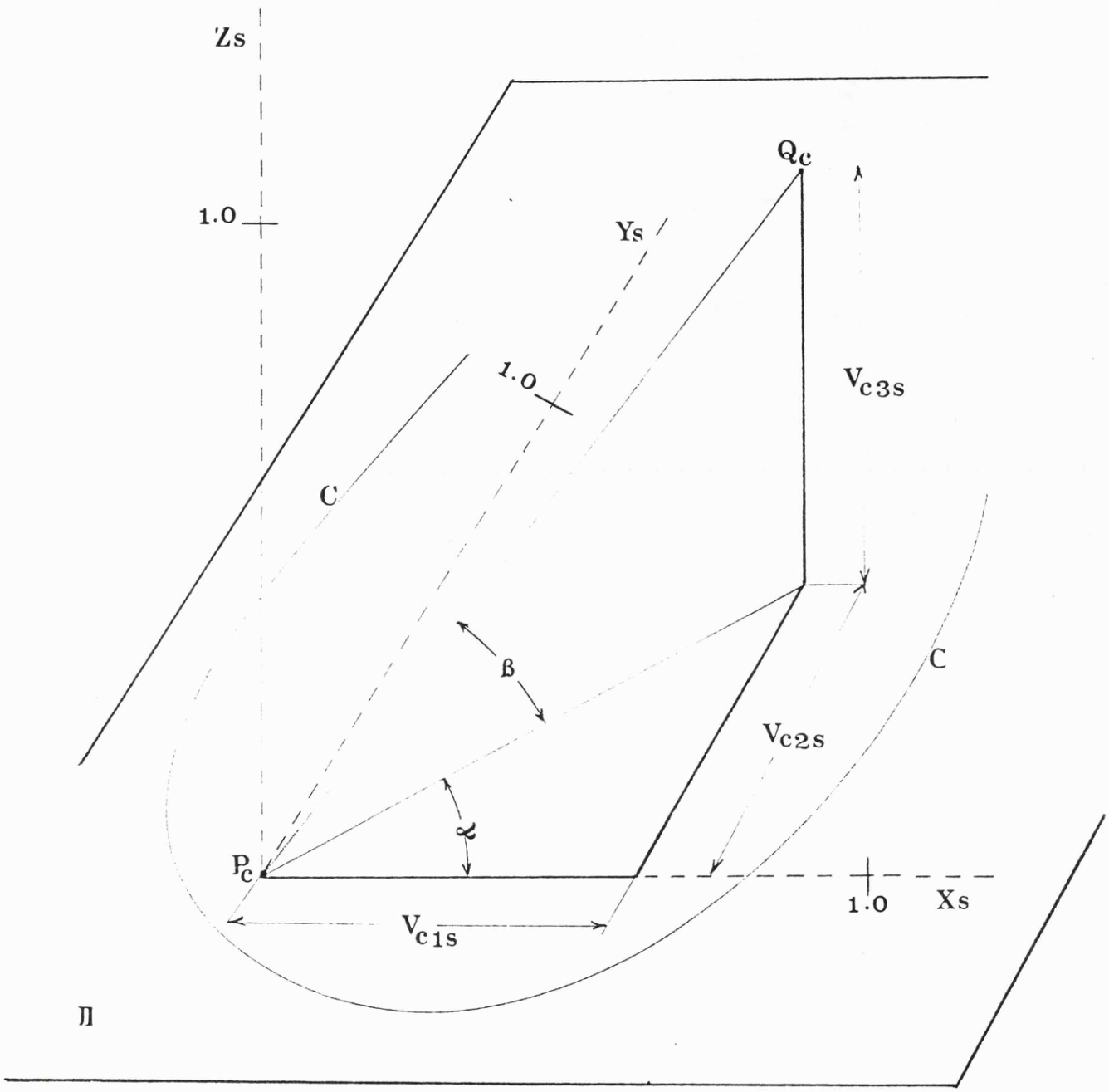


FIG. 4.14 ADVANCING AND ELEVATING ANGLES.

The angles α and β as defined in eq.(4.9) and eq.(4.10), respectively.

between the points $P_c$ and $Q_c$, at a distance $\ell$ from $P_c$.

Finally specify the orientation of this system in the space, that is, fix the positions of the $x_v$ and $z_v$ axes, by defining the rotation angle $\gamma$ , measured between the $x_v$ axis and its projection on the face of the slice. The geometric arrangement is depicted in Fig.(4.15).

### 4.8.3 IMAGE OF A POINT ON THE SLICE SURFACE

The properties of the image obtained by orthogonal projection of a 3-dimensional representation of the vector quantity $\underline{V}_c$ onto the slice surface can be established by considering the orthogonal projection of the arbitrary point $W(x_v, y_v, z_v)$ onto the image plane $(x_p, y_p)$. The method by which the arbitrary point W is projected on the slice surface in order to generate its orthogonal image is straightforward but tedious. A detailed description of the process used by the author appears in Appendix 4.

The resulting equations which establish the co-ordinates of the orthogonal image, $x_p$ and $y_p$ , of an arbitrary point W in space with co-ordinates $x_v$, $y_v$ and $z_v$, are given by:

$$x_p\,(W) = x_c + x_s\,(W) \tag{4.11}$$

$$y_p\,(W) = y_c + y_s\,(W) \tag{4.12}$$

where $x_c$ and $y_c$ are the co-ordinates of the point $P_c$ and

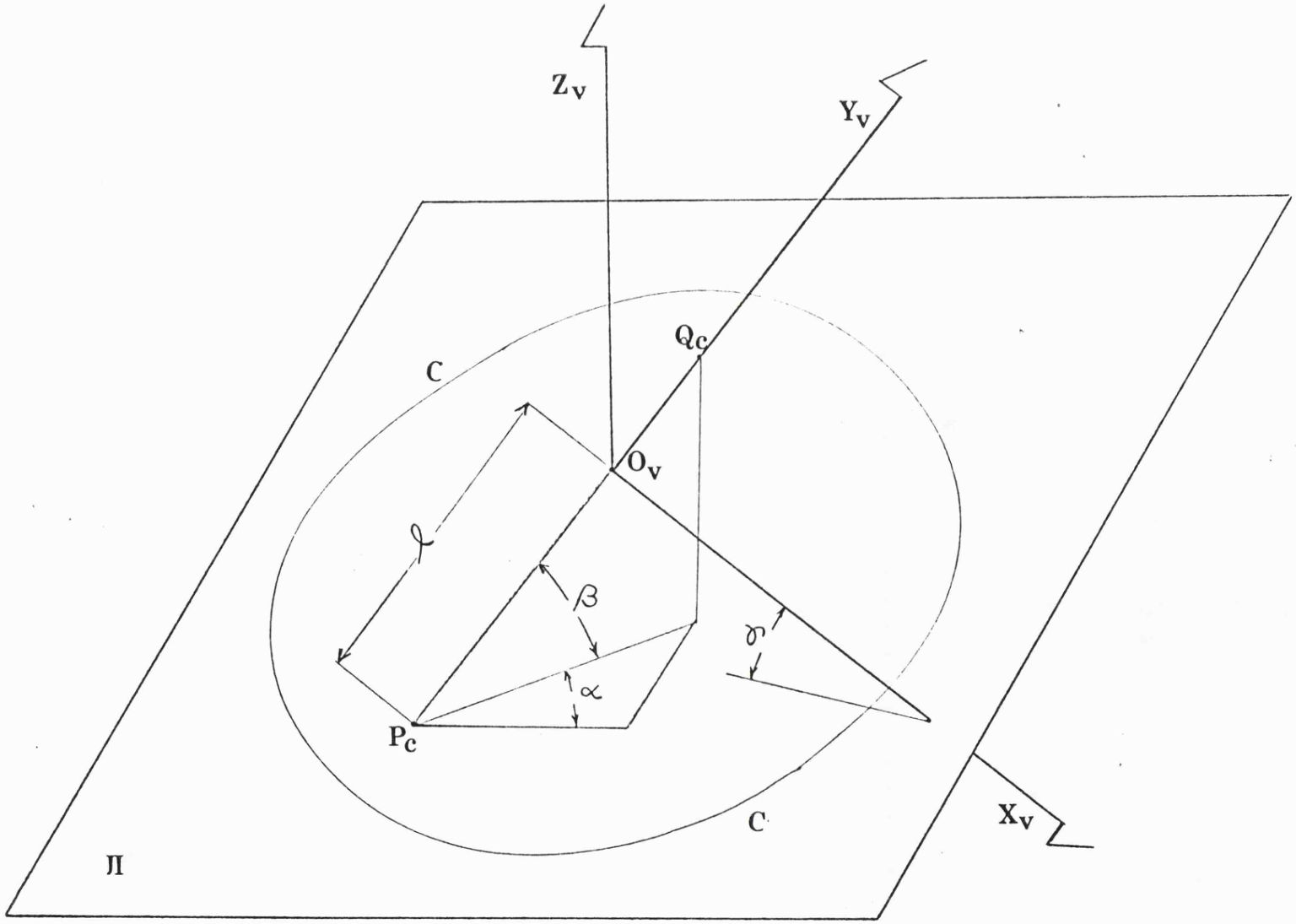


FIG. 4.15 LOCAL REFERENCE SYSTEM

The co-ordinate system $(x_v, y_v, z_v)$ associated to the vector quantity $\underline{V}_c$.

$$x_s(W) = x_v(\sin\alpha\cos\gamma - \cos\alpha\sin\beta\sin\gamma)$$
$$+ (\ell + y_v)\cos\alpha\cos\beta$$
$$- z_v(\sin\alpha\sin\gamma + \cos\alpha\sin\beta\cos\gamma) \qquad (4.13)$$

$$y_s(W) = -x_v(\cos\alpha\cos\gamma + \sin\alpha\sin\beta\sin\gamma)$$
$$+ (\ell + y_v)\sin\alpha\cos\beta$$
$$+ z_v(\cos\alpha\sin\gamma - \sin\alpha\sin\beta\cos\gamma) \qquad (4.14)$$

The application of eq.(4.11) to eq.(4.14) to points W of the 3-D representation of the vector $\underline{V}_c$, at a chosen point $P_c$ on the surface of the sampling slice, generates the orthogonal image of the vector quantity under consideration.

### 4.8.4 3-DIMENSIONAL REPRESENTATION AND FRONTAL IMAGE OF A VECTOR

Consider the solid figure generated by the line $\ell$ together with the rectangular pyramid with vertices on the points (related to the $(x_v, y_v, z_v)$ system:

$Q_c(0,h,0)$

$A_c(a/2,0,-b/2)$

$B_c(a/2,0,b/2)$

$C_c(-a/2,0,b/2)$

$D_c(-a/2,0,-b/2)$

as illustrated in Fig.(4.16). The line $\ell$ goes from the point $P_c$ to the origin of the local system $O_v$. The total length of the solid is

$$L = \ell + h \tag{4.15}$$

where h is the pyramid height.

When the pyramid rotates about the $y_v$ axis in a situation as shown in Fig.(4.17), the point (a/2,0,0) describes a circle given by the parametric equations:

$$x_v = \tfrac{1}{2}\, a \cos\theta \tag{4.16}$$

$$z_v = \tfrac{1}{2}\, a \sin\theta \tag{4.17}$$

where $\theta$ is the angle between the $x_v$ axis and the line joining the point $O_v$ to the point (a/2,0,0).

The orthogonal image of the described circle on the plane ($x'_s$, $y'_s$) (Fig.(4.17)) is an ellipse with parametric equations given by

$$x'_s = \tfrac{1}{2}\, a\, (\sin\alpha \cos\lambda - \cos\alpha \sin\beta \sin\lambda) \tag{4.18}$$

$$y'_s = -\tfrac{1}{2}\, a\, (\cos\alpha \cos\lambda + \sin\alpha \sin\beta \sin\lambda) \tag{4.19}$$

where

$$\lambda = \gamma + \theta \tag{4.20}$$

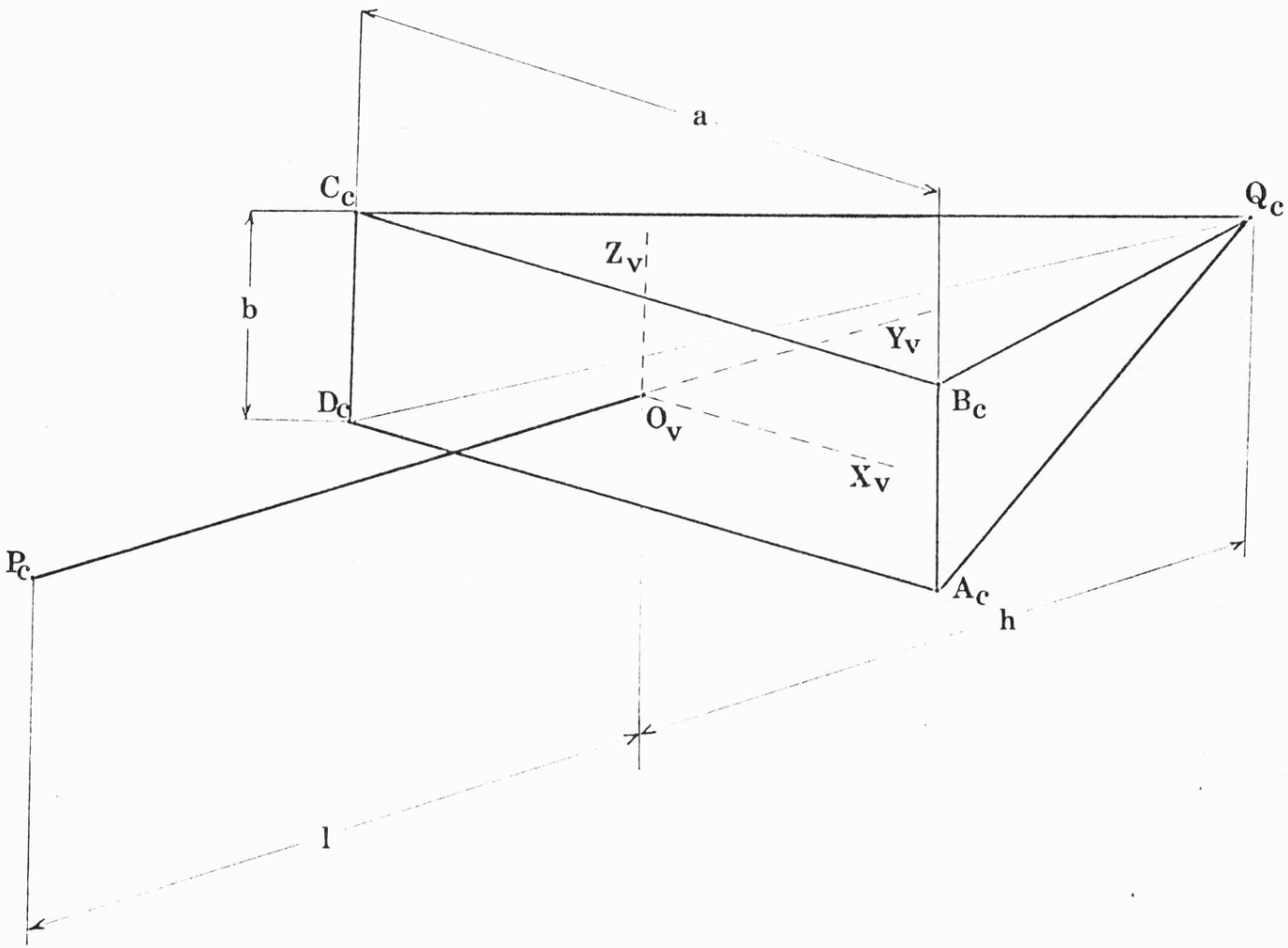


FIG. 4.16 3-DIMENSIONAL ARROW REPRESENTING THE VECTOR QUANTITY $\underline{V}_c$

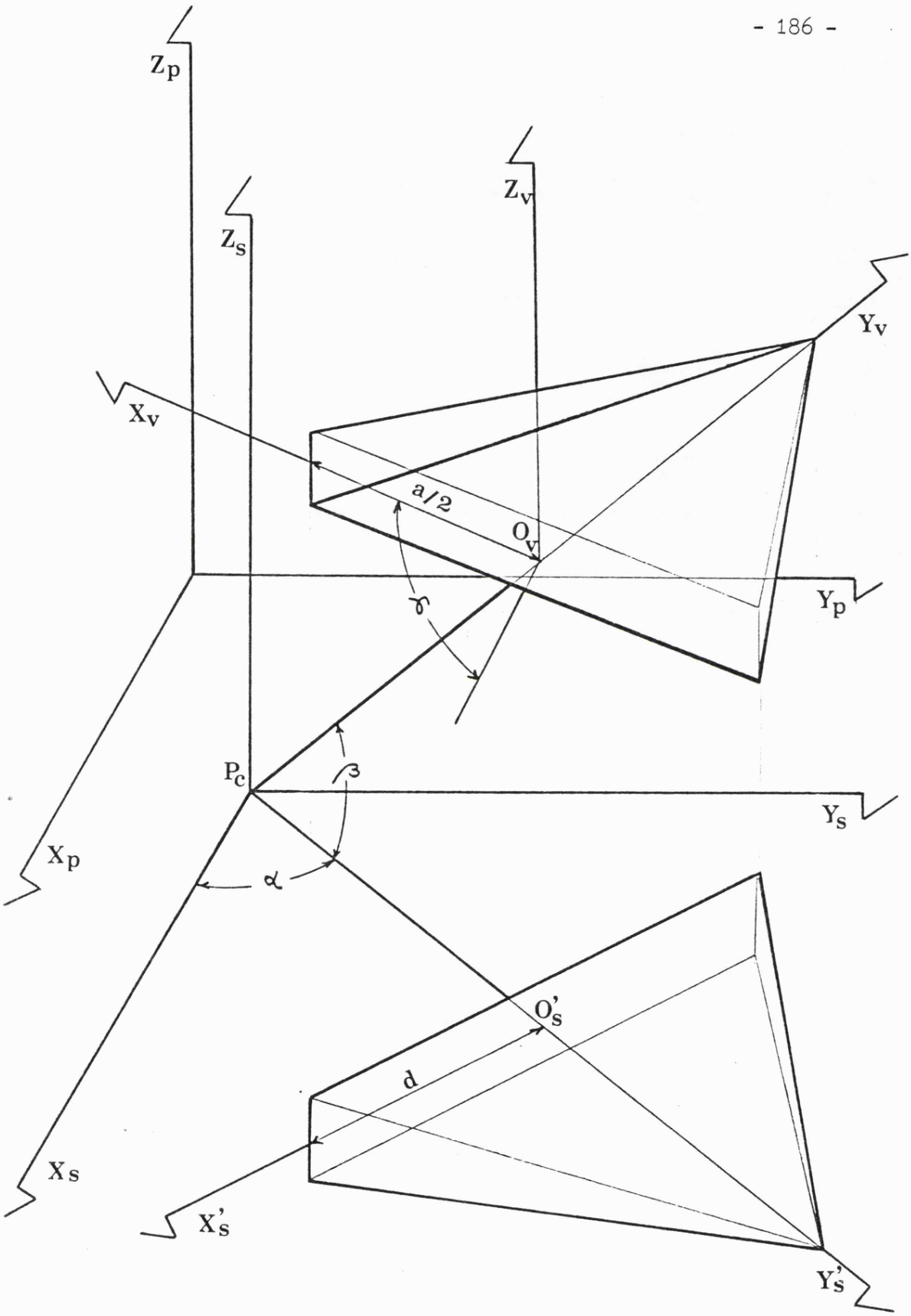


FIG. 4.17 ORTHOGONAL IMAGE OF THE 3-D ARROW ONTO THE SAMPLING PLANE

The distance d from the image of the point (a/2,0,0) to the origin of the system $(x'_s, y'_s)$ is given, for any angle $\lambda$ , by the expression:

$$d = (x_s'^2 + y_s'^2)^{\frac{1}{2}}$$

$$= \tfrac{1}{2}\, a\, (1 - \sin^2\lambda \ \cos^2\beta\ )^{\frac{1}{2}} \qquad (4.21)$$

Define for the purposes of this work that a frontal image of the solid arrow $(P_c, O_v, A_c, B_c, C_c, D_c, Q_c)$ is obtained when the distance d is equal to a/2. From eq.(4.21), it is seen that this frontal image occurs when

$$\lambda = 2n\,\pi \qquad (4.22)$$

$$(n = 0,1,2,\ldots)$$

that is, taking into account eq.(4.20) when

$$\theta = 2n\,\pi - \gamma \qquad (4.23)$$

In this case the pyramid base length a will project in true value and the pyramid base width b will have an image length $b_i$ equal to

$$b_i = b \sin\beta \qquad (4.24)$$

while the length of the images of the line $\ell$ and the pyramid heigth

h will be given respectively by

$$\ell_i = \ell \cos\beta \tag{4.25}$$

$$h_i = h \cos\beta \tag{4.26}$$

and the total length of the image, therefore, given by

$$L_i = L \cos\beta \tag{4.27}$$

The segments $b_i, \ell_i, h_i$, and $L_i$ are shown in Fig.(4.18).

Postulate now that associated with every point in a region R in which a vector field satisfying eq.(4.5) and eq.(4.6) exists, there is a solid arrow (as depicted in Fig.(4.16)), oriented by the vector field, satisfying the following properties:

i) The segments which constitute the arrow (tail and head edges) have fixed proportions throughout R, determined by the vector magnitude M(x,y,z);

ii) The solid arrow always rotates itself to reach an equilibrium position which produces a frontal image on the image plane;

iii) The solid arrow is not transparent.

The first postulated property guarantees the homogeneity of the representation. The second establishes the possibility of measuring

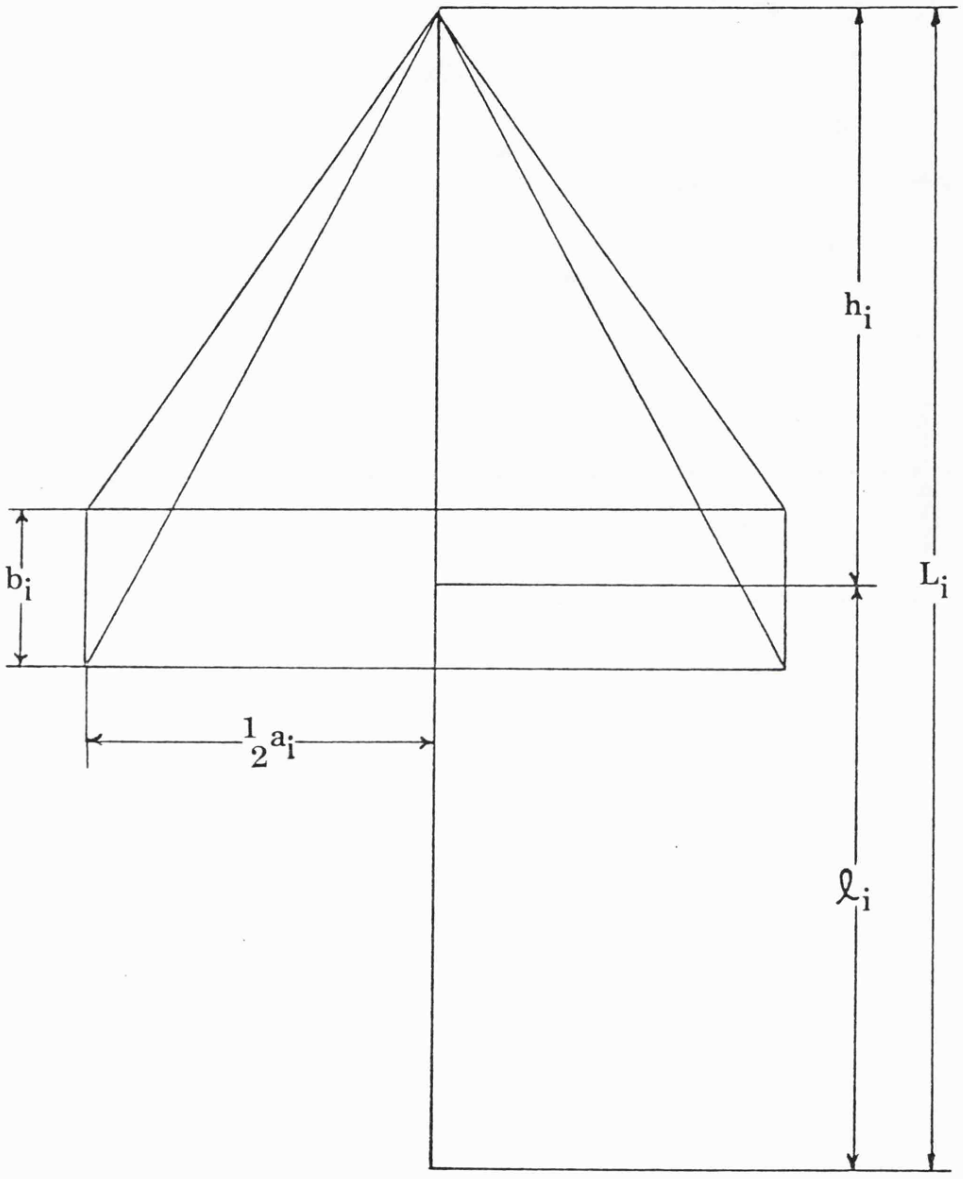


FIG. 4.18 IMAGE SEGMENTS

Segments of the orthogonal projection of the solid arrow onto the sampling plane.

accurately the vector intensity at a point when 3-dimensional fields are being displayed. The third ensures that the angle of elevation with respect to the sampling plane can be measured from the frontal image without ambiguity.

### 4.8.5 GENERAL IMAGE CO-ORDINATES

The application of the first two postulated properties to eq.(4.11) to eq.(4.14) when the arbitrary point W take the position of the points $P_c, O_v, A_c, B_c, C_c, D_c$ and $Q_c$ leads to the following general point frontal image co-ordinates:

$P_c$ :

$$x_p\ (P_c) = x_c \tag{4.28}$$

$$y_p\ (P_c) = y_c \tag{4.29}$$

$O_v$ :

$$x_p\ (O_v) = x_c + \ell\ \cos\alpha\ \cos\beta \tag{4.30}$$

$$y_p\ (O_v) = y_c + \ell\ \sin\alpha\ \cos\beta \tag{4.31}$$

$A_c$ :

$$x_p\ (A_c) = x_c + \tfrac{1}{2}\left[2\ell\ \cos\alpha\ \cos\beta\ \left(1 + \frac{b}{2\ell}\ \tan\beta\right) + a\ \sin\alpha\right] \tag{4.32}$$

$$y_p\ (A_c) = y_c + \tfrac{1}{2}\left[2\ell\ \sin\alpha\ \cos\beta\ \left(1 + \frac{b}{2\ell}\ \tan\beta\right) - a\ \cos\alpha\right] \tag{4.33}$$

$B_c$ :

$$x_p\,(B_c) = x_c + \tfrac{1}{2}\left[2\ell\,\cos\alpha\,\cos\beta\,\left(1 - \frac{b}{2\ell}\tan\beta\right) + a\,\cos\alpha\right] \quad (4.34)$$

$$y_p\,(B_c) = y_c + \tfrac{1}{2}\left[2\ell\,\sin\alpha\,\cos\beta\,\left(1 - \frac{b}{2\ell}\tan\beta\right) - a\,\cos\alpha\right] \quad (4.35)$$

$C_c$ :

$$x_p\,(C_c) = x_c + \tfrac{1}{2}\left[2\ell\,\cos\alpha\,\cos\beta\,\left(1 - \frac{b}{2\ell}\tan\beta\right) - a\,\sin\alpha\right] \quad (4.36)$$

$$y_p\,(C_c) = y_p + \tfrac{1}{2}\left[2\ell\,\sin\alpha\,\cos\beta\,\left(1 - \frac{b}{2\ell}\tan\beta\right) + a\,\cos\alpha\right] \quad (4.37)$$

$D_c$ :

$$x_p\,(D_c) = x_c + \tfrac{1}{2}\left[2\ell\,\cos\alpha\,\cos\beta\,\left(1 + \frac{b}{2\ell}\tan\beta\right) - a\,\sin\alpha\right] \quad (4.38)$$

$$y_p\,(D_c) = y_c + \tfrac{1}{2}\left[2\ell\,\sin\alpha\,\cos\beta\,\left(1 + \frac{b}{2\ell}\tan\beta\right) + a\,\cos\alpha\right] \quad (4.39)$$

$Q_c$ :

$$x_p\,(Q_c) = x_c + L\,\cos\alpha\,\cos\beta \quad (4.40)$$

$$y_p\,(Q_c) = y_c + L\,\sin\alpha\,\cos\beta \quad (4.41)$$

In eq.(4.28) to eq.(4.41) according to the first postulated property, the quantities $\ell$, a , b and L are all interdependent and proportional to the vector magnitude at the point $P_c$ where the image is constructed. This proportionality remains constant (second property) over the entire region R.

### 4.8.6 PICTURE GENERATION

The picture is generated by using eq.(4.28) to eq.(4.41) for calculating the necessary increment in $x_p$ and $y_p$ directions in order to move the pen* from one point to another. Assuming that the pen initially rests on point $P_c$ and denoting the increment from the general picture point $I_c$ to any other convenient picture point $J_c$ by $\underline{D}(I_c\ J_c)$ we have:

$$\underline{D}(I_cJ_c) = \underline{u}_{xp}\ D_x\ (I_cJ_c) + \underline{u}_{yp}\ D_y\ (I_cJ_c) \tag{4.42}$$

The directional increments $D_x(I_cJ_c)$ and $D_y(I_cJ_c)$ in eq.(4.42) are given by

$$D_x(I_cJ_c) = J_{cx} - I_{cx} \tag{4.43}$$

$$D_y(I_cJ_c) = J_{cy} - I_{cy} \tag{4.44}$$

where $J_{cx}, J_{cy}, I_{cx}$ and $I_{cy}$ are the $x_p$ and $y_p$ co-ordinates of the points $J_c$ and $I_c$ respectively.

Applying eq.(4.43) and eq.(4.44) to the sequence of movements shown in Fig.(4.19) and using eq.(4.28) to eq.(4.41); the following general direction increments are obtained:

---

* In the context of this work , pen is used to denote the automatic drawing mechanism.

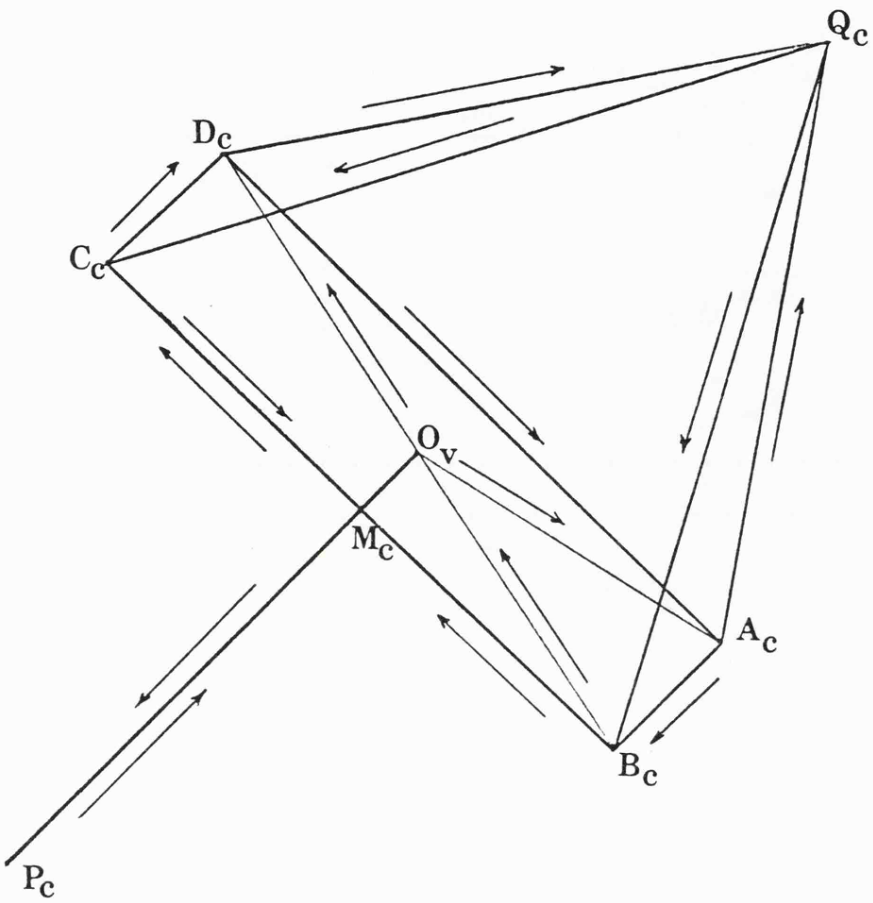


FIG. 4.19 DRAWING SEQUENCE

Sequence of movements used to draw the frontal image of the 3-D arrow.

$\underline{D}(P_cO_v)$ :

$$D_x(P_cO_v) = \ell \cos\alpha \cos\beta \tag{4.45}$$

$$D_y(P_cO_v) = \ell \sin\alpha \cos\beta \tag{4.46}$$

$\underline{D}(O_vA_c)$ :

$$D_x(O_vA_c) = \tfrac{1}{2}\,(a \sin\alpha + b \cos\alpha \sin\beta) \tag{4.47}$$

$$D_y(O_vA_c) = -\tfrac{1}{2}\,(a \cos\alpha - b \sin\alpha \sin\beta) \tag{4.48}$$

$\underline{D}(A_cB_c)$ :

$$D_x(A_cB_c) = -\,b \cos\alpha \sin\beta \tag{4.49}$$

$$D_y(A_cB_c) = -\,b \sin\alpha \sin\beta \tag{4.50}$$

$\underline{D}(B_cC_c)$ :

$$D_x(B_cC_c) = -\,a \sin\alpha \tag{4.51}$$

$$D_y(B_cC_c) = a \cos\alpha \tag{4.52}$$

$\underline{D}(C_cD_c)$ :

$$D_x(C_cD_c) = b \cos\alpha \sin\beta \tag{4.53}$$

$$D_y(C_cD_c) = b \sin\alpha \sin\beta \tag{4.54}$$

$\underline{D}(D_cA_c)$ :

$$D_x(D_cA_c) = a \sin\alpha \tag{4.55}$$

$$D_y(D_cA_c) = - a \cos\alpha \tag{4.56}$$

$\underline{D}(A_cQ_c)$ :

$$D_x(A_cQ_c) = \tfrac{1}{2} \left[2 h \cos\alpha \cos\beta \left(1 - \frac{b}{2h} \tan\beta\right) - a \sin\alpha\right] \tag{4.57}$$

$$D_y(A_cQ_c) = \tfrac{1}{2} \left[2 h \sin\alpha \cos\beta \left(1 - \frac{b}{2h} \tan\beta\right) + a \cos\alpha\right] \tag{4.58}$$

$\underline{D}(Q_cB_c)$ :

$$D_x(Q_cB_c) = - \tfrac{1}{2} \left[2 h \cos\alpha \cos\beta \left(1 + \frac{b}{2h} \tan\beta\right) - a \sin\alpha\right] \tag{4.59}$$

$$D_y(Q_cB_c) = - \tfrac{1}{2} \left[2 h \sin\alpha \cos\beta \left(1 + \frac{b}{2h} \tan\beta\right) + a \cos\alpha\right] \tag{4.60}$$

$\underline{D}(B_cD_c)$ :

$$D_x(B_cD_c) = - (a \sin\alpha - b \cos\alpha \sin\beta) \tag{4.61}$$

$$D_y(B_cD_c) = a \cos\alpha + b \sin\alpha \sin\beta \tag{4.62}$$

$\underline{D}(D_cQ_c)$ :

$$D_x(D_cQ_c) = \tfrac{1}{2} \left[2 h \cos\alpha \cos\beta \left(1 - \frac{b}{2h} \tan\beta\right) + a \sin\alpha\right] \tag{4.63}$$

$$D_y(D_cQ_c) = \tfrac{1}{2} \left[2 h \sin\alpha \cos\beta \left(1 - \frac{b}{2h} \tan\beta\right) - a \cos\alpha\right] \tag{4.64}$$

$\underline{D}(Q_cC_c)$ :

$$D_x(Q_cC_c) = -\tfrac{1}{2}\left[2\ h\ \cos\alpha\ \cos\beta\ \left(1 + \frac{b}{2h}\tan\beta\right) + a\ \sin\alpha\right] \quad (4.65)$$

$$D_y(Q_cC_c) = -\tfrac{1}{2}\left[2\ h\ \sin\alpha\ \cos\beta\ \left(1 + \frac{b}{2h}\tan\beta\right) - a\ \cos\alpha\right] \quad (4.66)$$

4.8.7 SEGMENT VISIBILITY AND IMAGE DEGENERATION

According to the third postulated property some drawing movements have to be hidden. Let us consider for this effect that the angular function $A(x,y,z)$ in eq.(4.5) defined for all $\alpha$ and $\beta$ such that

$$0 \leqslant \alpha \leqslant 2\pi \quad (4.67)$$

$$-\frac{\pi}{2} \leqslant \beta \leqslant \frac{\pi}{2} \quad (4.68)$$

The visibility of the drawing movements depends on the angle of elevation $\beta$ , only. For images obtained when the angle of elevation is positive, the segment $\ell_i$ becomes completely invisible when $\beta$ reaches a critical angle $\beta_{c+}$ , given by:

$$\beta_{c+} = \tan^{-1}\ \frac{2\ell}{b} \quad (4.69)$$

$$(b \neq 0)$$

The segment $\ell_i$ will be partially visible for every positive elevating angle $\beta$ , such that

$$0 \leqslant \beta < \beta_{c+} \tag{4.70}$$

and visible for all negative elevating angles (Fig.(4.20)).

On the other hand, as the pyramid has its height equal to h, for elevating angles $\beta$, such that

$$\beta \geqslant \beta_{c-} \tag{4.71}$$

where

$$\beta_{c-} = - \tan^{-1} \frac{2h}{b} \qquad (b \neq 0) \tag{4.72}$$

the segments $Q_c B_c$ and $Q_c C_c$ are visible. When the negative elevation reaches the critical angle $\beta_{c-}$ the point $Q_c$ will start having its image inside the base image and the segments $Q_c B_c$ and $Q_c C_c$ , otherwise visible as in Fig.(4.20) will become invisible. The range of visibility of the points $P_c$ and $Q_c$ is, therefore dependent on the ratio between the parameters $\ell$ and h .

For the purposes of the present work, images for which

$$0 \leqslant \beta < \beta_{c+} \tag{4.73}$$

will be called positive images, and those for which the reverse condition

$$0 \geqslant \beta > \beta_{c-} \tag{4.74}$$

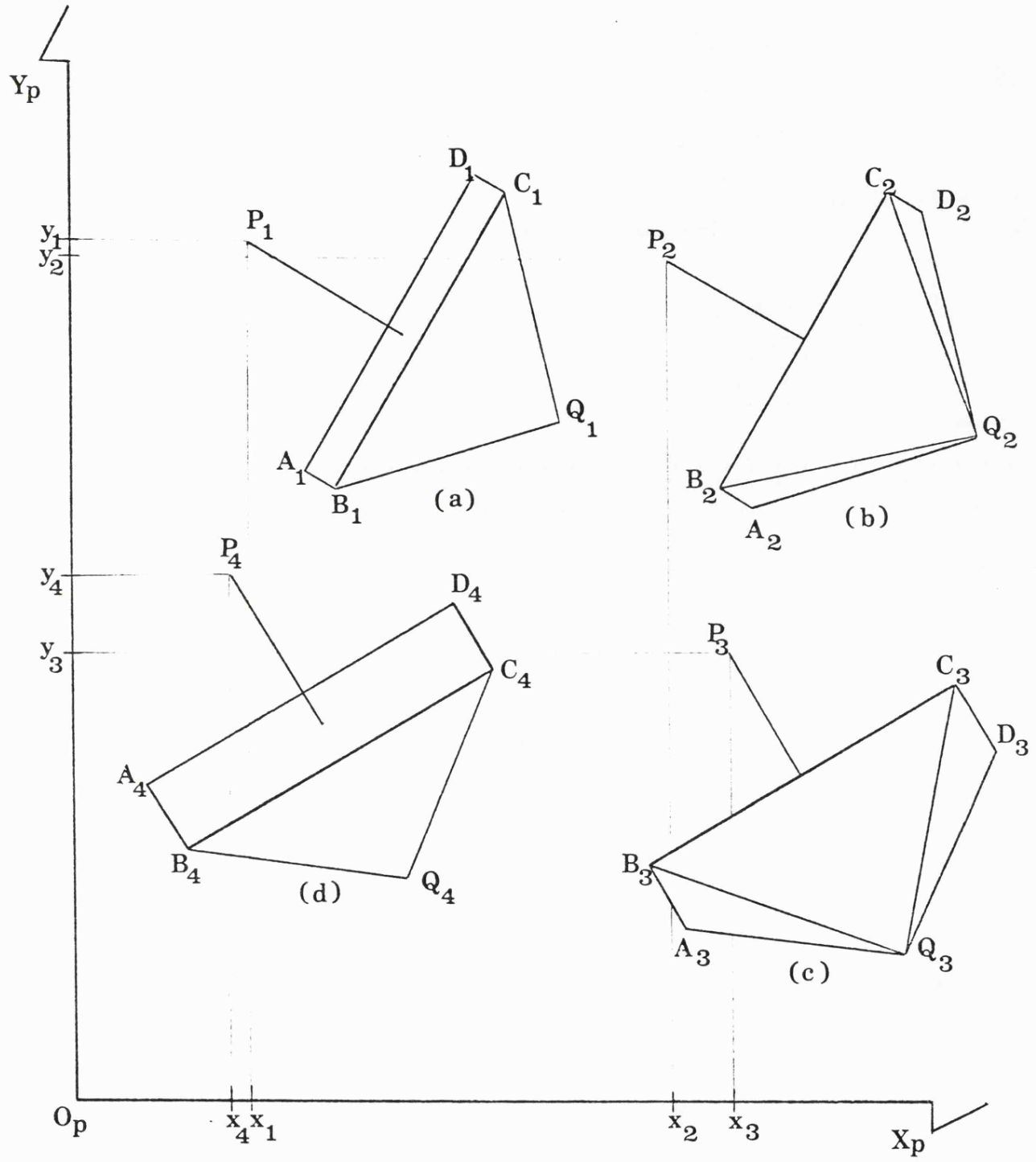


FIG. 4.20 EXAMPLES OF POSITIVE AND NEGATIVE FRONTAL IMAGES.

applies, will be called negative images. Positive and negative images have both points $P_c$ and $Q_c$ , the base length a and the base width b, displayed. When the corresponding critical angle is reached, however, either point $P_c$ or point $Q_c$ is not displayed. In each case, the images will be called respectively, positive and negative degenerated images.

A third possibility of image degeneration occurs for small angles of elevation. In this case, both points $P_c$ and $Q_c$ are displayed but the base width b is not displayed.If the elevating angle $\beta$ is comprehended inside a small angle $2\Gamma$ such that

$$-\Gamma \leqslant \beta \leqslant \Gamma \tag{4.75}$$

the segments of the arrow tend to present superimposed images on the image plane.

When the length of the image of the segment b is equal to the minimum detectable distance between two parallel lines on the displaying system, $d_m$, it becomes impossible to know wether $\beta$ is a positive or negative small angle. In this case the images will look like 2-dimensional images and will be called, in the context of this work, null degenerated images. The angles $\Gamma$ between which a null degenerated image is produced are given in terms of $d_m$ and b, approximately by

$$\Gamma = \pm \frac{d_m}{b} \tag{4.76}$$

$$(b \gg d_m)$$

It must be pointed out that this is the only degenerated image which leads to an indetermination in the measurement of the elevation angle. Positive degenerated images and negative degenerated images although not displaying the points $P_c$ or $Q_c$, respectively, are still capable of producing an estimate of the elevating angle. The magnitude of the vector quantity is always represented accurately by the imaging process.

Finally, let us consider, for positive angles of elevation, the point where the segment $\ell_i$ starts being hidden. For $\beta < \beta_c$ this point is shown in Fig.(4.19) as point $M_c$ which coincides with the middle point of the segment $B_cC_c$. The point $M_c$ is a mobile one, with $(x_v, y_v, z_v)$ co-ordinates given by

$$M_c\ (0, -b/2\ |\tan\beta|\ , 0)$$

Application of eq.(4.13) and eq.(4.14) to $M_c$ leads to:

$$x_p(M_c) = \ell - \frac{b}{2} \cos\alpha \cos\beta\ |\tan\beta| \qquad (4.77)$$

$$y_p(M_c) = \ell - \frac{b}{2} \sin\alpha \cos\beta\ |\tan\beta| \qquad (4.78)$$

Now, to reach $M_c$ from the point $C_c$, the necessary directional increments are:

$\underline{D}(C_cM_c)$ :

$$D_x(C_cM_c) = \tfrac{1}{2}\left[b \cos\alpha\ (\sin\beta - \cos\beta\ |\tan\beta|\ ) + a \sin\alpha\right] \qquad (4.79)$$

$$D_y(C_cM_c) = -\tfrac{1}{2}\left[b \sin\alpha \left(\cos\beta \,|\tan\beta| - \sin\beta\right) + a \cos\alpha\right] \quad (4.80)$$

Assuming that the computer only gives positive values of square roots, the moduli can be taken as the square root of a square.Therefore, eq.(4.79) and eq.(4.80) become:

$$D_x(C_cM_c) = \tfrac{1}{2}\left( b \cos\alpha \left[\sin\beta - (\tan^2\beta)^{\frac{1}{2}} \cos\beta\right] + a \sin\alpha\right) \quad (4.81)$$

$$D_y(C_cM_c) = \tfrac{1}{2}\left( b \sin\alpha \left[\sin\beta - (\tan^2\beta)^{\frac{1}{2}} \cos\beta\right] - a \cos\alpha\right) \quad (4.82)$$

The last increment which will mode the pen back to the point $P_c$, is given by:

$\underline{D}(M_cP_c)$ :

$$D_x(M_cP_c) = -\tfrac{1}{2}\left[ \ell - b\,(\tan^2\beta)^{\frac{1}{2}} \right] \cos\alpha \cos\beta \quad (4.83)$$

$$D_y(M_cP_c) = -\tfrac{1}{2}\left[ \ell - b\,(\tan^2\beta)^{\frac{1}{2}} \right] \sin\alpha \cos\beta \quad (4.84)$$

The segments and their visibility for each type of image are summarized in Table T(4.1).

### 4.8.8 TRANSVERSE FIELDS AND NULL DEGENERATED IMAGES

When all the elevating angles are in the range $(-\Gamma, +\Gamma)$the field is transverse, that is, there is no measurable field component perpendicular to the image plane. In this case a plane arrow, as shown in Fig.(4.21) is generated to represent the vector quantity at

| SEGMENT | POSITIVE | POS.DEG. | NEGATIVE | NEG.DEG. | NULL DEG. |
|---|---|---|---|---|---|
| $P_cO_v$ | INVIS. | INVIS. | VISIBLE | VISIBLE | VISIBLE |
| $O_vA_c$ | INVIS. | INVIS. | INVIS. | INVIS. | INVIS. |
| $A_cB_c$ | VISIBLE | VISIBLE | VISIBLE | VISIBLE | VISIBLE |
| $B_cC_c$ | VISIBLE | VISIBLE | VISIBLE | VISIBLE | VISIBLE |
| $C_cD_c$ | VISIBLE | VISIBLE | VISIBLE | VISIBLE | VISIBLE |
| $D_cA_c$ | INVIS. | VISIBLE | VISIBLE | VISIBLE | VISIBLE |
| $A_cQ_c$ | VISIBLE | VISIBLE | INVIS. | INVIS. | VISIBLE |
| $Q_cB_c$ | VISIBLE | VISIBLE | VISIBLE | INVIS. | VISIBLE |
| $B_cD_c$ | INVIS. | INVIS. | INVIS. | INVIS. | INVIS. |
| $Q_cC_c$ | VISIBLE | VISIBLE | VISIBLE | INVIS. | VISIBLE |
| $C_cM_c$ | INVIS. | INVIS. | INVIS. | INVIS. | INVIS. |
| $M_cP_c$ | VISIBLE | INVIS. | INVIS. | INVIS. | VISIBLE |

TABLE T 4.1 Image segment visibility.

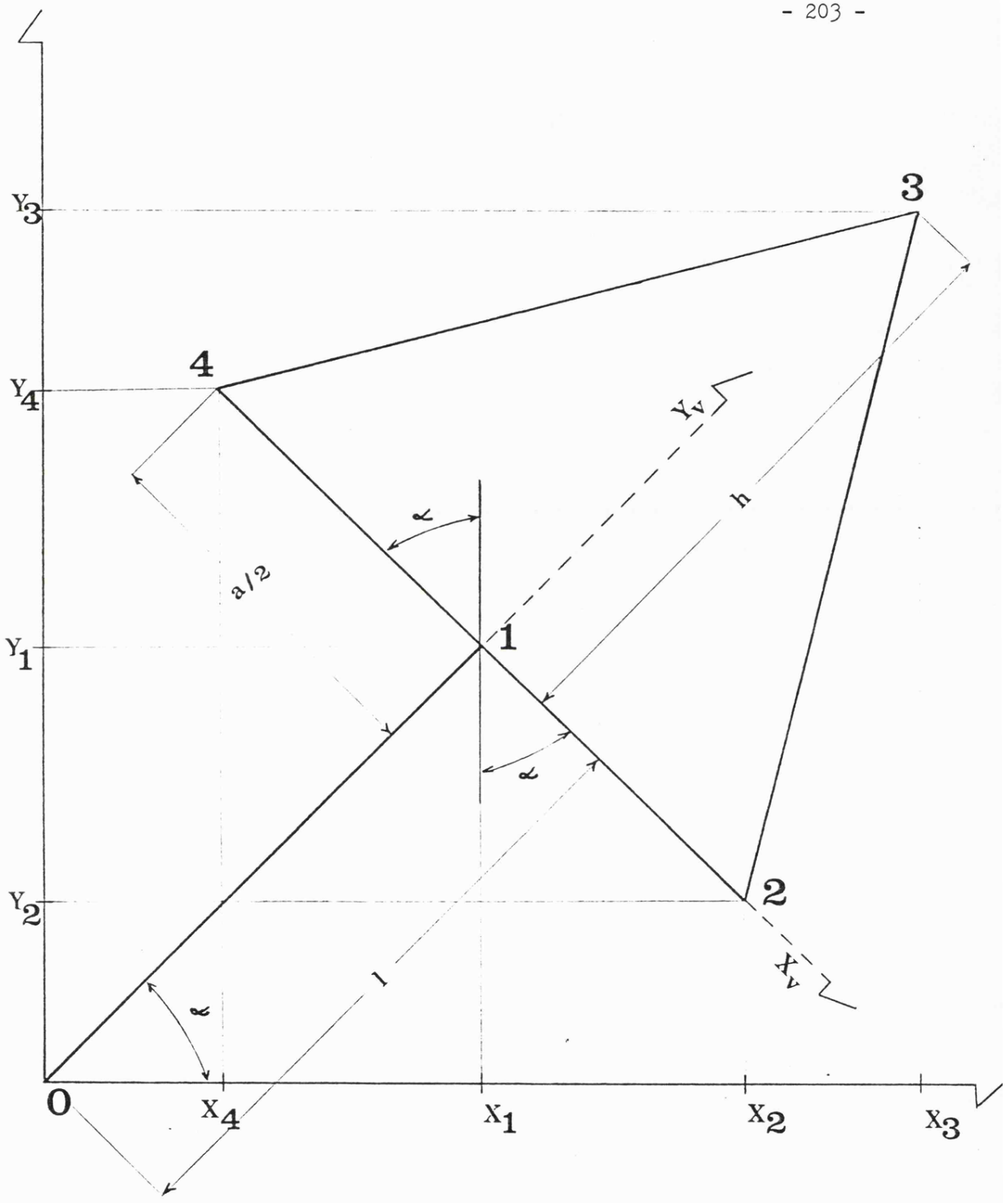


FIG. 4.21 PLANE ARROW

Sequence of movements used to draw a null degenerated frontal image. The co-ordinates $x_1, x_2, \ldots, y_1, y_2, \ldots$ etc., correspond to the co-ordinates $x_p(1), x_p(2) \ldots$, $y_p(1), y_p(2), \ldots$ etc., in eq.(4.85) to eq.(4.94).

$P_c$. Referring to the geometry of Fig.(4.21) the general image co-ordinates of the numbered points may be written as:

0 :

$$x_p(0) = x_c \tag{4.85}$$

$$y_p(0) = y_c \tag{4.86}$$

1 :

$$x_p(1) = x_c + \ell \cos\alpha \tag{4.87}$$

$$y_p(1) = y_c + \ell \sin\alpha \tag{4.88}$$

2 :

$$x_p(2) = x_p(1) + \frac{a}{2} \sin\alpha \tag{4.89}$$

$$y_p(2) = y_p(1) - \frac{a}{2} \cos\alpha \tag{4.90}$$

3 :

$$x_p(3) = x_c + L \cos\alpha \tag{4.91}$$

$$y_p(3) = y_c + L \sin\alpha \tag{4.92}$$

4 :

$$x_p(4) = x_p(1) - \frac{a}{2} \sin\alpha \tag{4.93}$$

$$y_p(4) = y_p(1) + \frac{a}{2} \cos\alpha \tag{4.94}$$

The drawing movements necessary to generate the picture may now be written, using the notation of eq.(4.42) to eq.(4.44) in the form

$\underline{D}(01)$ :

$$D_x(01) = \ell \cos\alpha \tag{4.95}$$

$$D_y(01) = \ell \sin\alpha \tag{4.96}$$

$\underline{D}(12)$ :

$$D_x(12) = \frac{a}{2} \sin\alpha \tag{4.97}$$

$$D_y(12) = -\frac{a}{2} \cos\alpha \tag{4.98}$$

$\underline{D}(23)$ :

$$D_x(23) = h \cos\alpha \left( 1 - \frac{a}{2h} \tan\alpha \right) \tag{4.99}$$

$$D_y(23) = h \sin\alpha \left( 1 + \frac{a}{2h} \cot\alpha \right) \tag{4.100}$$

$\underline{D}(34)$ :

$$D_x(34) = - h \cos\alpha \left( 1 + \frac{a}{2h} \tan\alpha \right) \tag{4.101}$$

$$D_y(34) = - h \sin\alpha \left( 1 - \frac{a}{2h} \cot\alpha \right) \tag{4.102}$$

$\underline{D}(41)$ :

$$D_x(41) = \frac{a}{2} \sin\alpha \tag{4.103}$$

$$D_y(41) = - \frac{a}{2} \cos\alpha \tag{4.104}$$

$\underline{D}(10)$ :

$$D_x(10) = - D_x(01) = - \ell \cos\alpha \tag{4.105}$$

$$D_y(10) = - D_y(01) = - \ell \sin\alpha \tag{4.106}$$

The use of eq.(4.95) to eq.(4.106) to construct the vector image for the transverse fields results in the same image which would be generated by the general equations (eq.(4.45) to eq.(4.66)) . However, if the latter are used, the number of drawing movements would double and the plotting density of the image segments may appear intensified.

4.8.9 SPECIALIZED IMAGE

During the foregoing analysis a general representation of the vector quantity has been developed in detail and general image coordinate expressions obtained. As a consequence of the third postulated property a conflicting situation has arisen in the range of visibility of the points $P_c$ and $Q_c$ . Any attempt to extend the range of visibility of one of those points corresponds to an equal reduction on the range of visibility of the other. However, because it is not reasonable to expect in a general region R to find a dominance of positive or negative elevating angles when an arbitrary plane sample of the field is taken, the specializing condition

$$\ell = h \tag{4.107}$$

may be imposed as a natural condition for the 3-dimensional arrow . Also, because the magnitude function in R has a bound value Q, it is possible to specify for the image a second specializing condition namely:

$$L = | M(x_c, y_c, z_c) | \tag{4.108}$$

Using eq.(4.15), eq.(4.69), eq.(4.72) and eq.(4.73) the moduli of the critical angles become equal when the condition stated in eq.(4.107) prevails. Therefore, for the specialized image we have:

$$\beta_{c+} = | \beta_{c-} | = \beta_c \tag{4.109}$$

Defining an image shape parameter for the specialized arrow assembly diagram, q , in the form

$$q = ( \tan\beta_c )^{-1} \tag{4.110}$$

and using eq.(4.108), the base width b is now determined through the expression:

$$b = q\,|M(x,y,z)| = qM \tag{4.111}$$

Further, the application of the conditions in eq.(4.107) and eq.(4.108) makes it possible to introduce useful simplifications in the general image co-ordinate expressions. Considering that , under the specializing conditions,

$$\begin{aligned} V_{c1s} &= 2\,\ell\ \cos\alpha\ \cos\beta \\ &= 2\,h\ \cos\alpha\ \cos\beta \\ &= L\ \cos\alpha\ \cos\beta \\ &= M\ \cos\alpha\ \cos\beta \end{aligned} \tag{4.112}$$

$$\begin{aligned} V_{c2s} &= 2\,\ell\ \sin\alpha\ \cos\beta \\ &= 2\,h\ \sin\alpha\ \cos\beta \\ &= L\ \sin\alpha\ \cos\beta \\ &= M\ \sin\alpha\ \cos\beta \end{aligned} \tag{4.113}$$

and defining another image shape parameter for the arrow assembly diagram , p , which relates the segment a to the vector magnitude M(x,y,z) at every point, in the form

$$a = p \, | M(x,y,z) | = pM \tag{4.114}$$

the directional increments for the specialized image become expressed in terms of the transverse field components, the vector magnitude and the diagram shape parameters by the following relationships

Positive and Negative Images:

$\underline{D}(P_c O_v)$ :

$$D_x(P_c O_v) = \tfrac{1}{2} \, V_{c1s} \tag{4.115}$$

$$D_y(P_c O_v) = \tfrac{1}{2} \, V_{c2s} \tag{4.116}$$

$\underline{D}(O_v A_c)$ :

$$D_x(O_v A_c) = \tfrac{1}{2} M \, (p \sin\alpha + q \cos\alpha \sin\beta) \tag{4.117}$$

$$D_y(O_v A_c) = - \tfrac{1}{2} M \, (p \cos\alpha - q \sin\alpha \sin\beta) \tag{4.118}$$

$\underline{D}(A_c B_c)$ :

$$D_x(A_c B_c) = - q \, M \cos\alpha \sin\beta \tag{4.119}$$

$$D_y(A_cB_c) = -\,q\,M\,\sin\alpha\,\sin\beta \tag{4.120}$$

$\underline{D}(B_cC_c)$ :

$$D_x(B_cC_c) = -\,p\,M\,\sin\alpha \tag{4.121}$$

$$D_y(B_cC_c) = p\,M\,\cos\alpha \tag{4.122}$$

$\underline{D}(C_cD_c)$ :

$$D_x(C_cD_c) = q\,M\,\cos\alpha\,\sin\beta \tag{4.123}$$

$$D_y(C_cD_c) = q\,M\,\sin\alpha\,\sin\beta \tag{4.124}$$

$\underline{D}(D_cA_c)$ :

$$D_x(D_cA_c) = p\,M\,\sin\alpha \tag{4.125}$$

$$D_y(D_cA_c) = -\,p\,M\,\cos\alpha \tag{4.126}$$

$\underline{D}(A_cQ_c)$ :

$$D_x(A_cQ_c) = -\,\tfrac{1}{2}\,[p\,M\,\sin\alpha - V_{c1s}\,(\,1 - q\,\tan\beta)] \tag{4.127}$$

$$D_y(A_cQ_c) = \tfrac{1}{2}\,[p\,M\,\cos\alpha + V_{c2s}(\,1 - q\,\tan\beta\,)] \tag{4.128}$$

$\underline{D}(Q_cB_c)$ :

$$D_x(Q_cB_c) = \tfrac{1}{2}\,[p\,M\,\sin\alpha - V_{c1s}\,(1 + q\,\tan\beta\,)] \qquad (4.129)$$

$$D_y(Q_cB_c) = -\,\tfrac{1}{2}\,[p\,M\,\cos\alpha + V_{c2s}\,(1 + q\,\tan\beta\,)] \qquad (4.130)$$

$\underline{D}(B_cD_c)$ :

$$D_x(B_cD_c) = -\,M\,(p\,\sin\alpha - q\,\cos\alpha\,\sin\beta\,) \qquad (4.131)$$

$$D_y(B_cD_c) = M\,(p\,\cos\alpha + q\,\sin\alpha\,\sin\beta\,) \qquad (4.132)$$

$\underline{D}(D_cQ_c)$ :

$$D_x(D_cQ_c) = \tfrac{1}{2}\,[p\,M\,\sin\alpha + V_{c1s}(1 - q\,\tan\beta\,)] \qquad (4.133)$$

$$D_y(D_cQ_c) = -\,\tfrac{1}{2}\,[p\,M\,\cos\alpha - V_{c2s}\,(1 - q\,\tan\beta\,)] \qquad (4.134)$$

$\underline{D}(Q_cC_c)$ :

$$D_x(Q_cC_c) = -\,\tfrac{1}{2}\,[p\,M\,\sin\alpha + V_{c1s}\,(1 + q\,\tan\beta\,)] \qquad (4.135)$$

$$D_y(Q_cC_c) = \tfrac{1}{2}\,[p\,M\,\cos\alpha - V_{c2s}\,(1 + q\,\tan\beta\,)] \qquad (4.136)$$

$\underline{D}(C_cM_c)$ :

$$D_x(C_cM_c) = \tfrac{1}{2}\,M\,(\,p\,\sin\alpha + q\,\cos\alpha[\sin\beta - (\tan^2\beta)^{\frac{1}{2}}\,\cos\beta])\qquad (4.137)$$

$$D_y(C_cM_c) = -\tfrac{1}{2} M\left( p \cos\alpha + q \sin\alpha \left[\sin\beta - (\tan^2\beta)^{\frac{1}{2}}\cos\beta\right]\right) \tag{4.138}$$

$\underline{D}(M_cP_c)$ :

$$D_x(M_cP_c) = -\tfrac{1}{2} V_{c1s} \left[ \tfrac{1}{2} - q\,(\tan^2\beta)^{\frac{1}{2}} \right] \tag{4.139}$$

$$D_y(M_cP_c) = -\tfrac{1}{2} V_{c2s} \left[ \tfrac{1}{2} - q\,(\tan^2\beta)^{\frac{1}{2}} \right] \tag{4.140}$$

<u>Null Images</u> :

$\underline{D}(01)$ :

$$D_x(01) = \tfrac{1}{2} V_{c1s} \tag{4.141}$$

$$D_y(01) = \tfrac{1}{2} V_{c2s} \tag{4.142}$$

$\underline{D}(12)$ :

$$D_x(12) = \tfrac{1}{2} p V_{c2s} \tag{4.143}$$

$$D_y(12) = -\tfrac{1}{2} p V_{c1s} \tag{4.144}$$

$\underline{D}(23)$ :

$$D_x(23) = \tfrac{1}{2} V_{c1s} ( 1 - p \tan\alpha ) \tag{4.145}$$

$$D_y(23) = \tfrac{1}{2} \; V_{c2s} \; ( 1 + p \cot\alpha ) \tag{4.146}$$

$\underline{D}(34)$ :

$$D_x(34) = - \tfrac{1}{2} \; V_{c1s} \; ( 1 + p \tan\alpha ) \tag{4.147}$$

$$D_y(34) = - \tfrac{1}{2} \; V_{c2s} \; ( 1 - p \cot\alpha ) \tag{4.148}$$

$\underline{D}(41)$ :

$$D_x(41) = \tfrac{1}{2} \, p \; V_{c2s} \tag{4.149}$$

$$D_y(41) = - \tfrac{1}{2} \, p \; V_{c1s} \tag{4.150}$$

$\underline{D}(10)$ :

$$D_x(10) = - \tfrac{1}{2} \; V_{c1s} \tag{4.151}$$

$$D_y(10) = - \tfrac{1}{2} \; V_{c2s} \tag{4.152}$$

A specialized image having shape parameters $p = 1/2$, $q = 1/8$, elevation angle equal to $\pi/6$ and advancing angle equal to $\pi/4$ , is shown in Fig.(4.22).

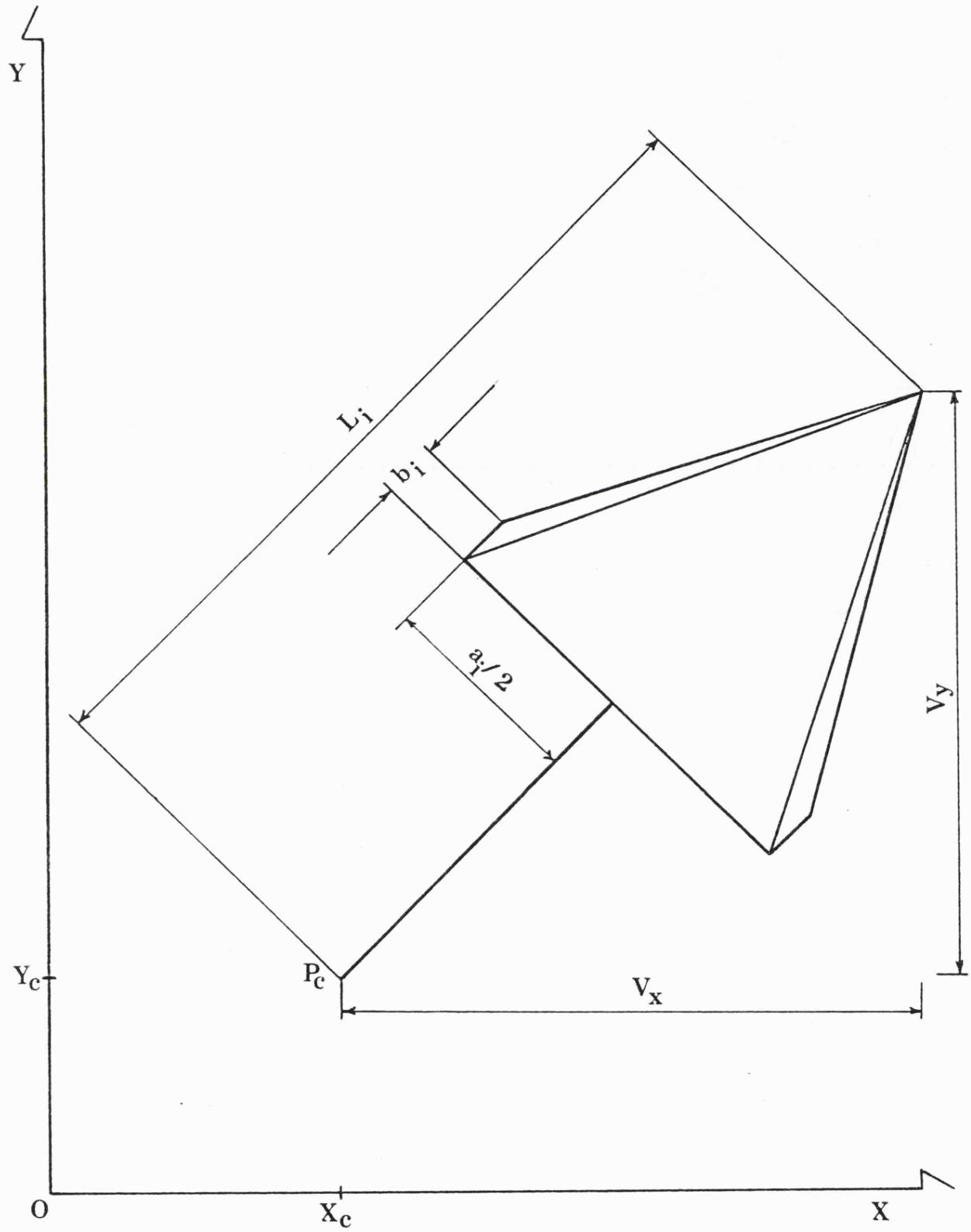


FIG. 4.22 SPECIALIZED IMAGE

The picture shows a specialized image with shape parameters $p = 1/2$ and $q = 1/8$. The advancing angle is $\alpha = \tan^{-1}(V_y/V_x) = \pi/4$. The angle of elevation is $\beta = \sin^{-1}(b_i/qL_i) = \pi/6$.

### 4.8.10 FIRST EXAMPLES

Two simplified experimental versions of routines coded in Fortran – VECT2 and VECT3 – using the proposed vector representation for 2-dimensional and 3-dimensional fields respectively , have been employed to produce arrow assembly diagrams based on the first propagating modes of a typical rectangular waveguide*. Those first examples of arrow assembly diagrams have been generated in order to access and discuss the usefulness of the proposed representation. Although some modifications in the coding have been introduced later to give to the user an extended control over the vector images , the basic structure of the experimental routines has been kept in the final version.

The generation of the diagrams is accomplished by first reading in the data specifying the rectangular waveguide geometry (ratio between the narrower and the broader cross-section sides) , the plane section where the fields are to be calculated over an user specified regular distribution of nodal points ( three cutting possibilities are available corresponding to sampling the waveguide field by planes which are parallel to one of the xy, xz and yz co-ordinate planes) and then proceeding to calculate the waveguide field at every nodal point through the analytical expressions[25]:

TE MODES :

$$E_x = Z_{h,mn} H_y \tag{4.153}$$

---

* Other rectangular waveguide geometries have also been investigated.

$$E_y = - Z_{h,mn} \; H_x \tag{4.154}$$

$$E_z = 0 \tag{4.155}$$

$$H_x = \mathrm{Re}\left( i \frac{\beta_{mn} \, m \, \pi}{a \, k^2_{c,mn}} \sin\left(\frac{m \, \pi x}{a}\right) \cos\left(\frac{n \, \pi y}{b}\right) \exp.i \, (\omega t - \beta_{mn} z)\right) \tag{4.156}$$

$$H_y = \mathrm{Re}\left( i \frac{\beta_{mn} \, n \, \pi}{b \, k^2_{c,mn}} \cos\left(\frac{m \, \pi x}{a}\right) \sin\left(\frac{n \, \pi y}{b}\right) \exp.i \, (\omega t - \beta_{mn} z)\right) \tag{4.157}$$

$$H_z = \mathrm{Re}\left( \cos\left(\frac{m \, \pi x}{a}\right) \cos\left(\frac{n \, \pi y}{b}\right) \exp.i \, (\omega t - \beta_{mn} z)\right) \tag{4.158}$$

<u>TM MODES</u> :

$$E_x = \mathrm{Re}\left( - i \frac{\beta_{mn} \, m \, \pi}{a \, k^2_{c,mn}} \cos\left(\frac{m \, \pi x}{a}\right) \sin\left(\frac{n \, \pi y}{b}\right) \exp.i(\omega t - \beta_{mn} z)\right) \tag{4.159}$$

$$E_y = \mathrm{Re}\left( - i \frac{\beta_{mn} \, m \, \pi}{b \, k^2_{c,mn}} \sin\left(\frac{m \, \pi x}{a}\right) \cos\left(\frac{n \, \pi y}{b}\right) \exp.i(\omega t - \beta_{mn} z)\right) \tag{4.160}$$

$$E_z = \mathrm{Re}\left( \sin\left(\frac{m \, \pi x}{a}\right) \sin\left(\frac{n \, \pi y}{b}\right) \exp.i \, (\omega t - \beta_{mn} z)\right) \tag{4.161}$$

$$H_x = - \frac{E_y}{Z_{e,mn}} \tag{4.162}$$

$$H_y = \frac{E_x}{Z_{e,mn}} \tag{4.163}$$

$$H_z = 0 \tag{4.164}$$

In eq.(4.153) to eq.(4.164) $E_x$, $E_y$ and $E_z$ are the electric field components, $H_x$, $H_y$ and $H_z$ the magnetic field components and a and b the broader and the narrower cross-section sides length respectively.

The quantities $Z_{h,mn}$ and $Z_{e,mn}$ are the wave impedance for $TE_{mn}$ and $TM_{mn}$ modes respectively whereas $k_{c,mn}$ is the cut-off wave-number and $\beta_{mn}$ the propagation function for the mode being considered. They are given by:

$$Z_{h,mn} = \frac{k_0}{\beta_{mn}} Z_0 \tag{4.165}$$

$$Z_{e,mn} = \frac{\beta_{mn}}{k_0} Z_0 \tag{4.166}$$

$$k_{c,mn} = \left[ \left( \frac{m\pi}{a} \right)^2 + \left( \frac{n\pi}{b} \right)^2 \right]^{\frac{1}{2}} \tag{4.167}$$

$$\beta_{mn} = \left( k_0^2 - k_{c,mn}^2 \right)^{\frac{1}{2}} \tag{4.168}$$

The quantities $k_0$ and $Z_0$ are the free-space wave-number and the free-space impedance, given by

$$k_0 = \omega (\mu \varepsilon)^{\frac{1}{2}} \tag{4.169}$$

$$Z_0 = (\mu / \varepsilon)^{\frac{1}{2}} \tag{4.170}$$

where $\omega$ is the angular frequency of the propagating wave, $\mu$ the permeability and $\varepsilon$ the permittivity of the lossless isotropic homogeneous medium which completely fills the waveguide. Also, in order to perform the calculations, the phase in which the field is frozen in time has been set to

$$\omega t = \frac{\pi}{2} \tag{4.171}$$

Once the fields have been obtained at every mesh point the program divides each field component by the corresponding maximum component found in the plane sample, and so, for each field, the maximum component equals the unity. Finally, the field values at each point are used to generate the arrow assembly diagrams. The frequency of the propagating wave for which the diagrams are constructed has been chosen by convenience to be $\sqrt{5}$ times the cut-off frequency of the mode under consideration.

A detailed description of the program developed to generate the examples below is given in Appendix 5. The diagram parameters in all waveguide field display examples are:

$$p = 0.500 \tag{4.172}$$

$$q = 0.125 \tag{4.173}$$

4.8.10.1 TRANSVERSE FIELD DIAGRAMS

Diagrams displaying the transverse electromagnetic fields for $TE_{10}$, $TM_{11}$ and $TM_{21}$ modes in a typical rectangular waveguide are presented in Fig.(4.23), Fig.(4.24) and Fig.(4.25).

Comparison of Fig.(4.1) and Fig.(4.2) with Fig.(4.23) shows that the field intensity variations along the cross-section are pictorially better described by the arrow assembly diagram than by the conventional field line diagram. Also, comparison between Fig.(4.4) and Fig.(4.23) and Fig.(4.5) and Fig.(4.24) shows that, for these two types of automatic generated (computerized) pictures, the arrow assembly diagrams can be advantageously used to describe the field behaviour.

Finally, it was found that by moving the arrows in such way that the calculation point $P_c$ is made coincident with the point where the tail intercepts the arrow head and by superimposing the waveguide boundary, as shown, the diagram presentation format is improved.

4.8.10.2 NON-TRANSVERSE FIELDS

The non-transverse fields corresponding to Fig.(4.23) to Fig.(4.25) are presented in Fig.(4.26) to Fig.(4.28), respectively. Because those fields are 3-dimensional, they cannot be displayed by means of the conventional field line diagrams nor by a single auto-

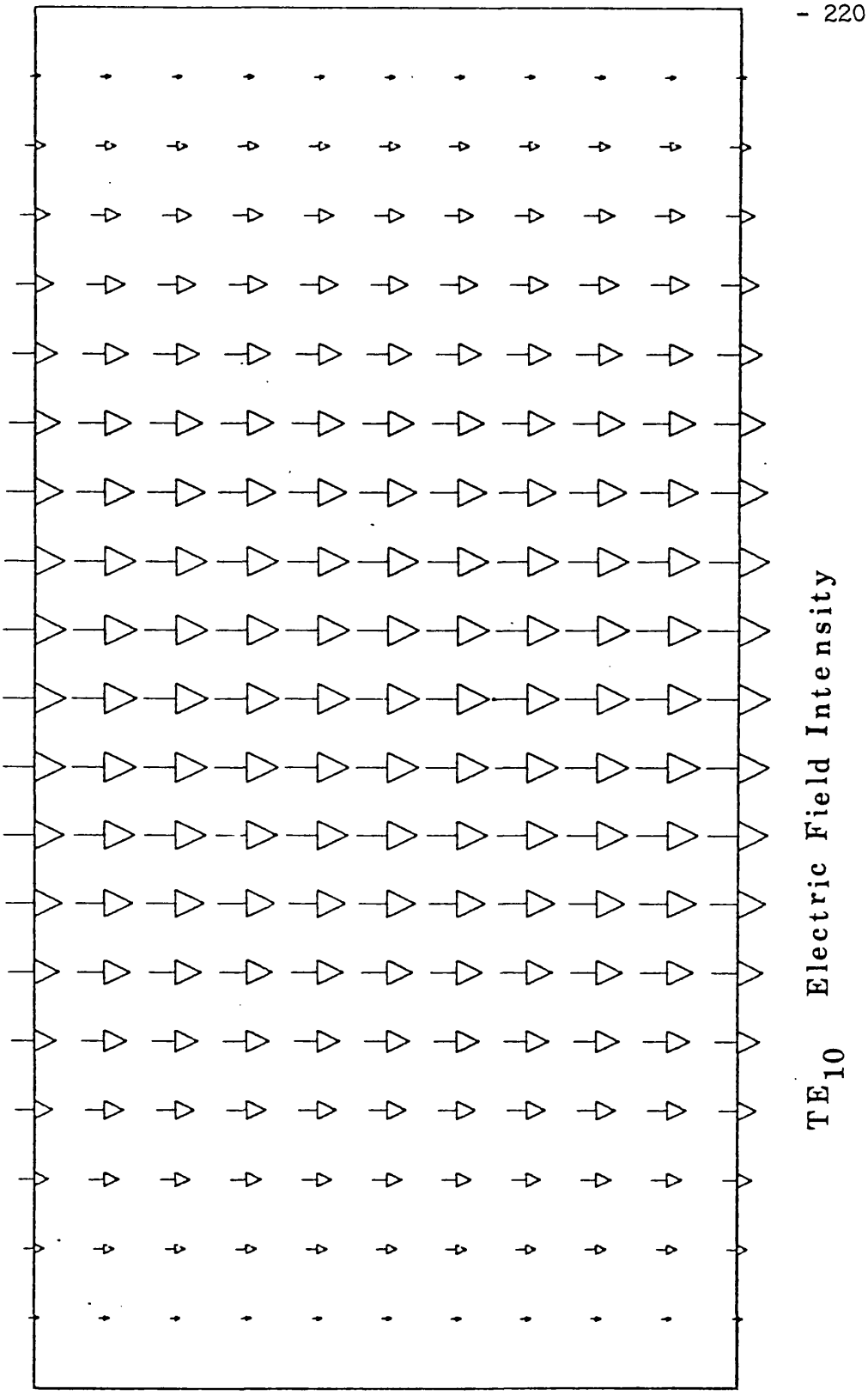


FIG. 4.23 $TE_{10}$ TRANSVERSE FIELD DISPLAY.

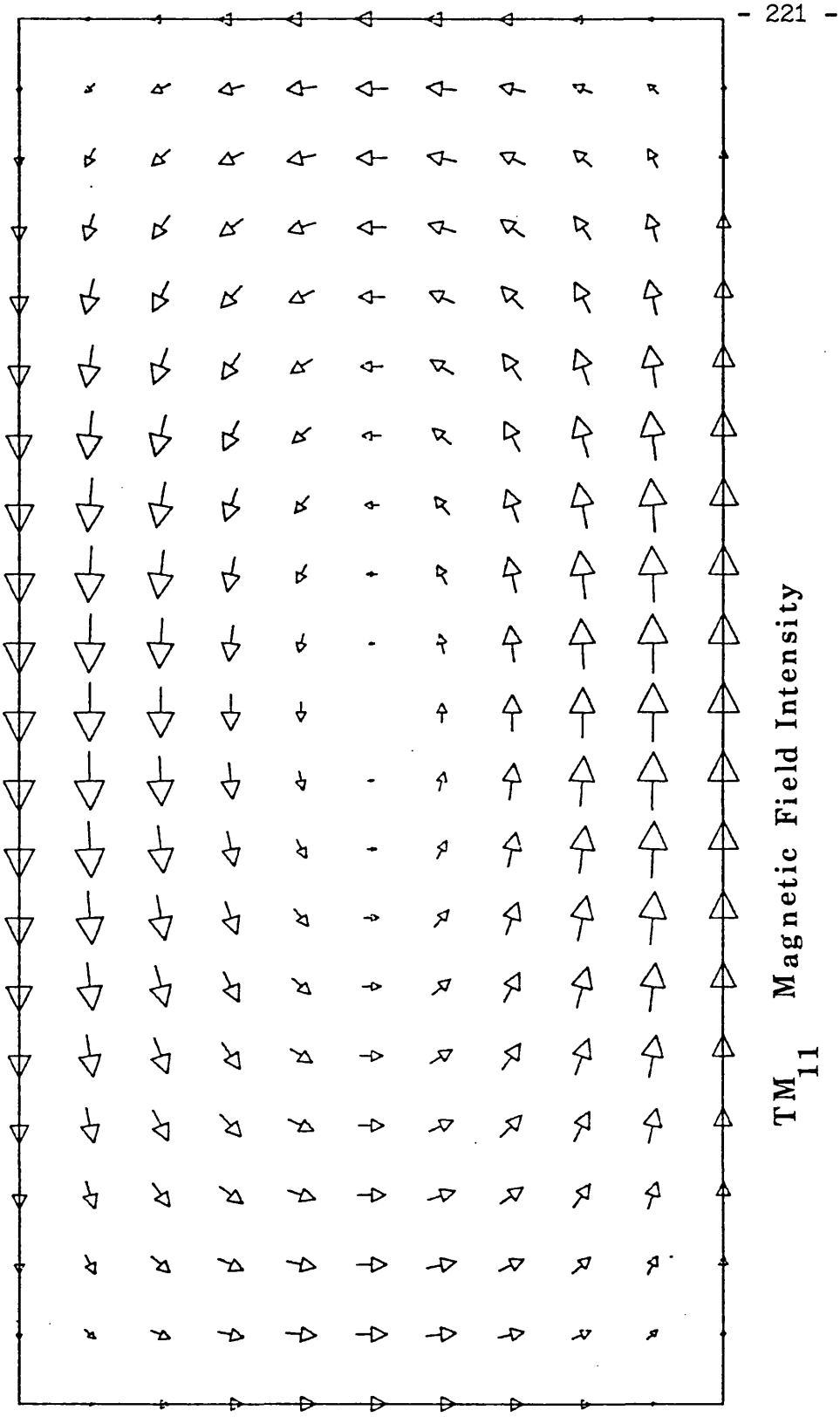


FIG. 4.24 $TM_{11}$ TRANSVERSE FIELD DISPLAY

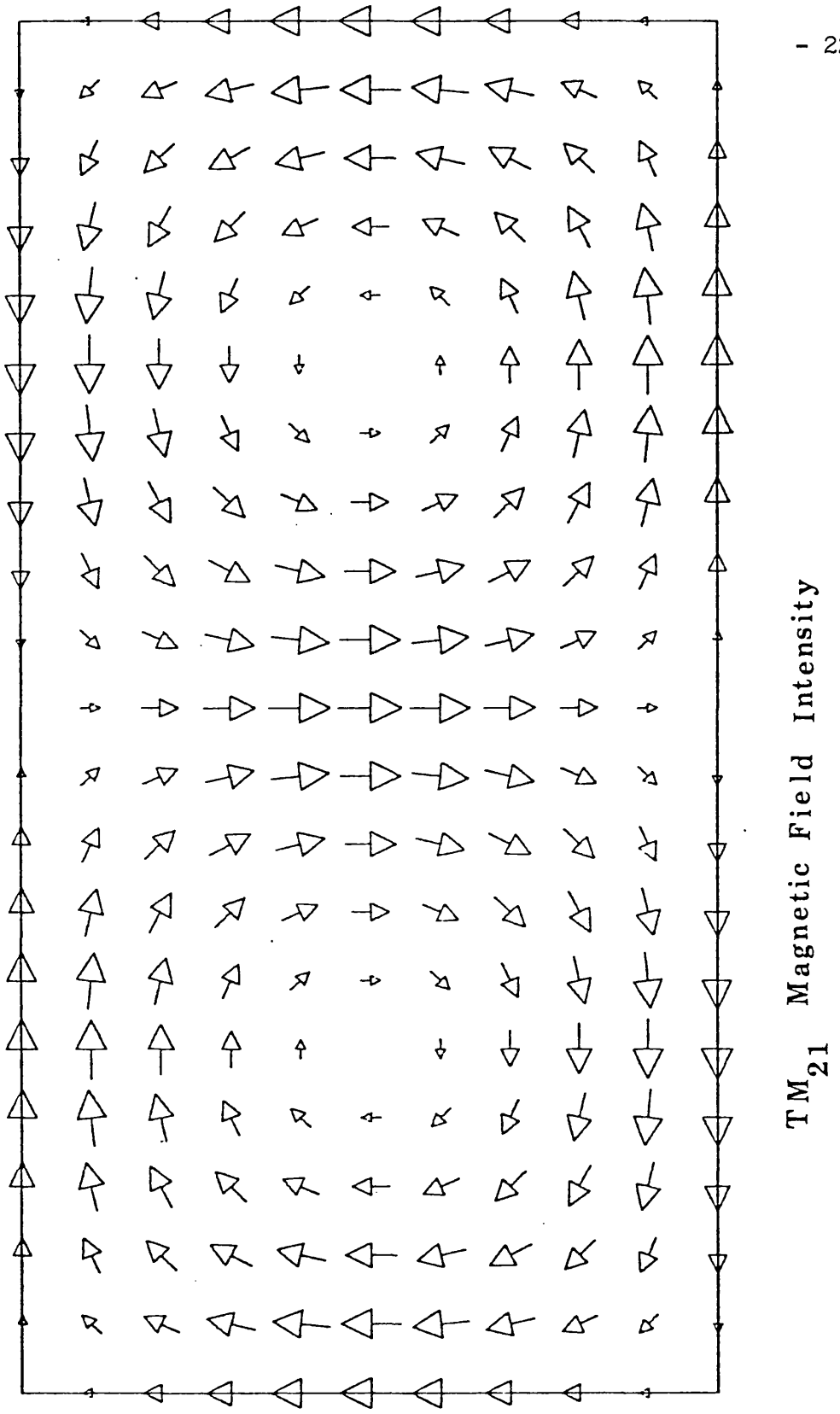


FIG. 4.25 $TM_{21}$ TRANSVERSE FIELD DISPLAY

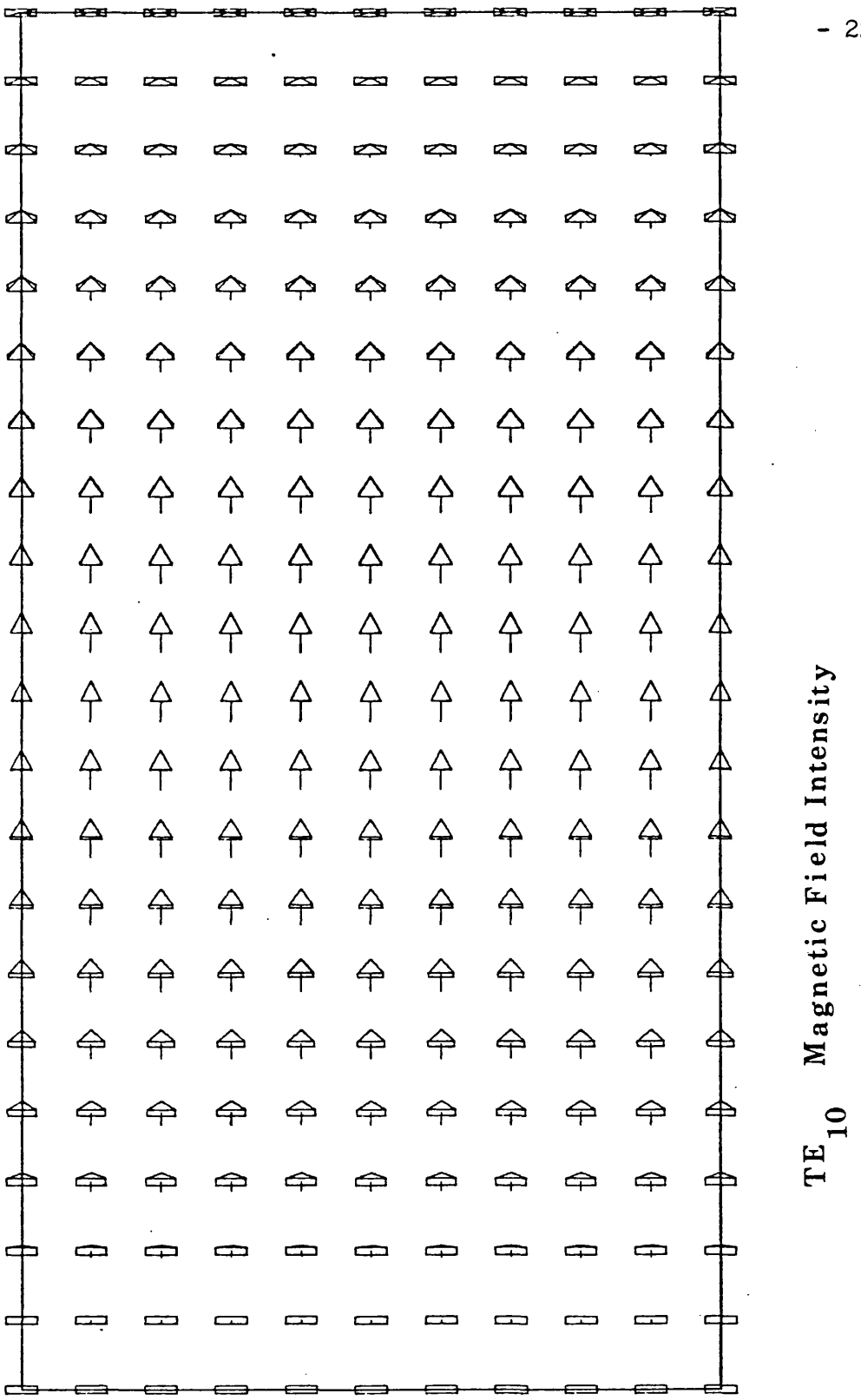


FIG. 4.26 $TE_{10}$ NON-TRANSVERSE FIELD DISPLAY

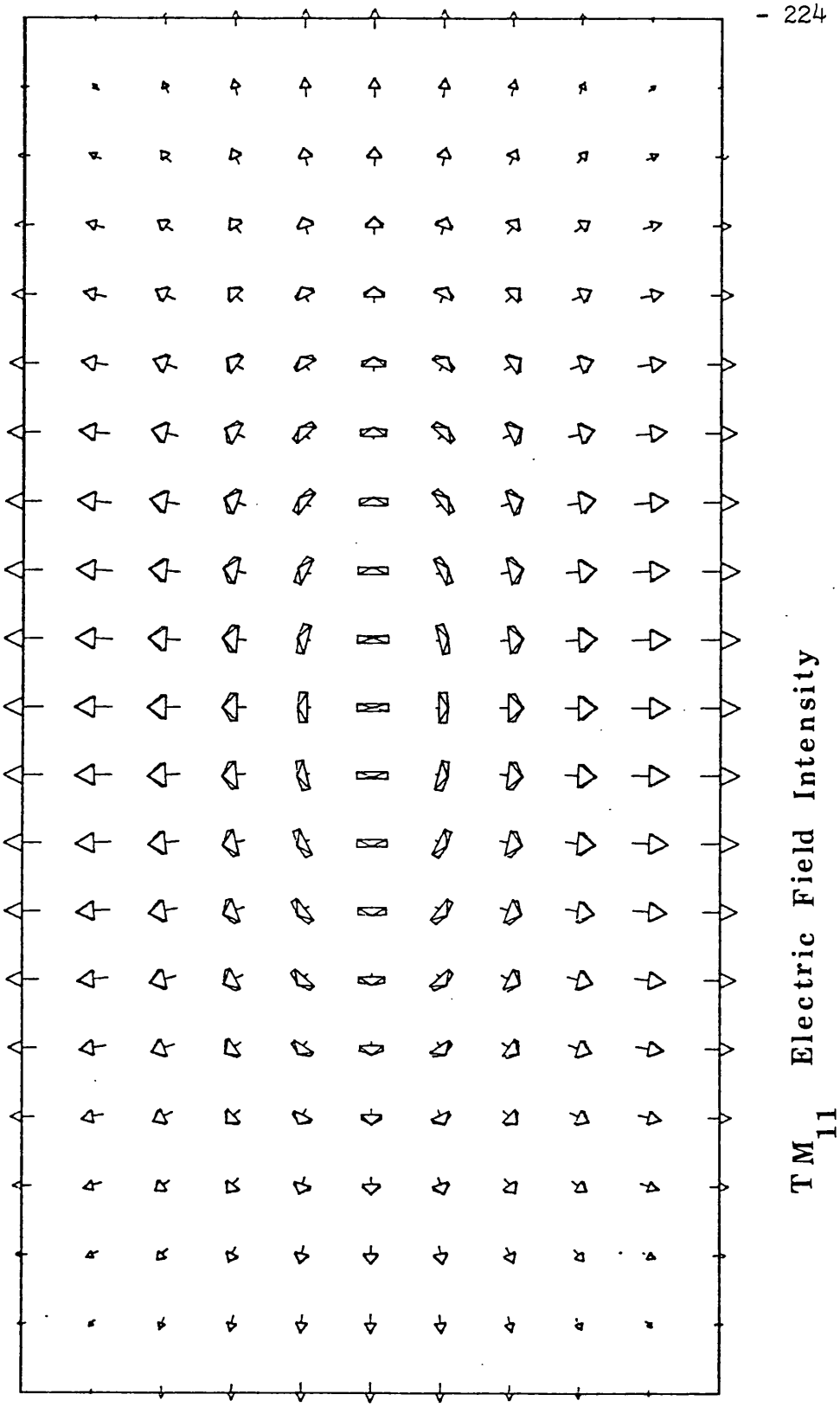


FIG. 4.27 $TM_{11}$ NON-TRANSVERSE FIELD DISPLAY

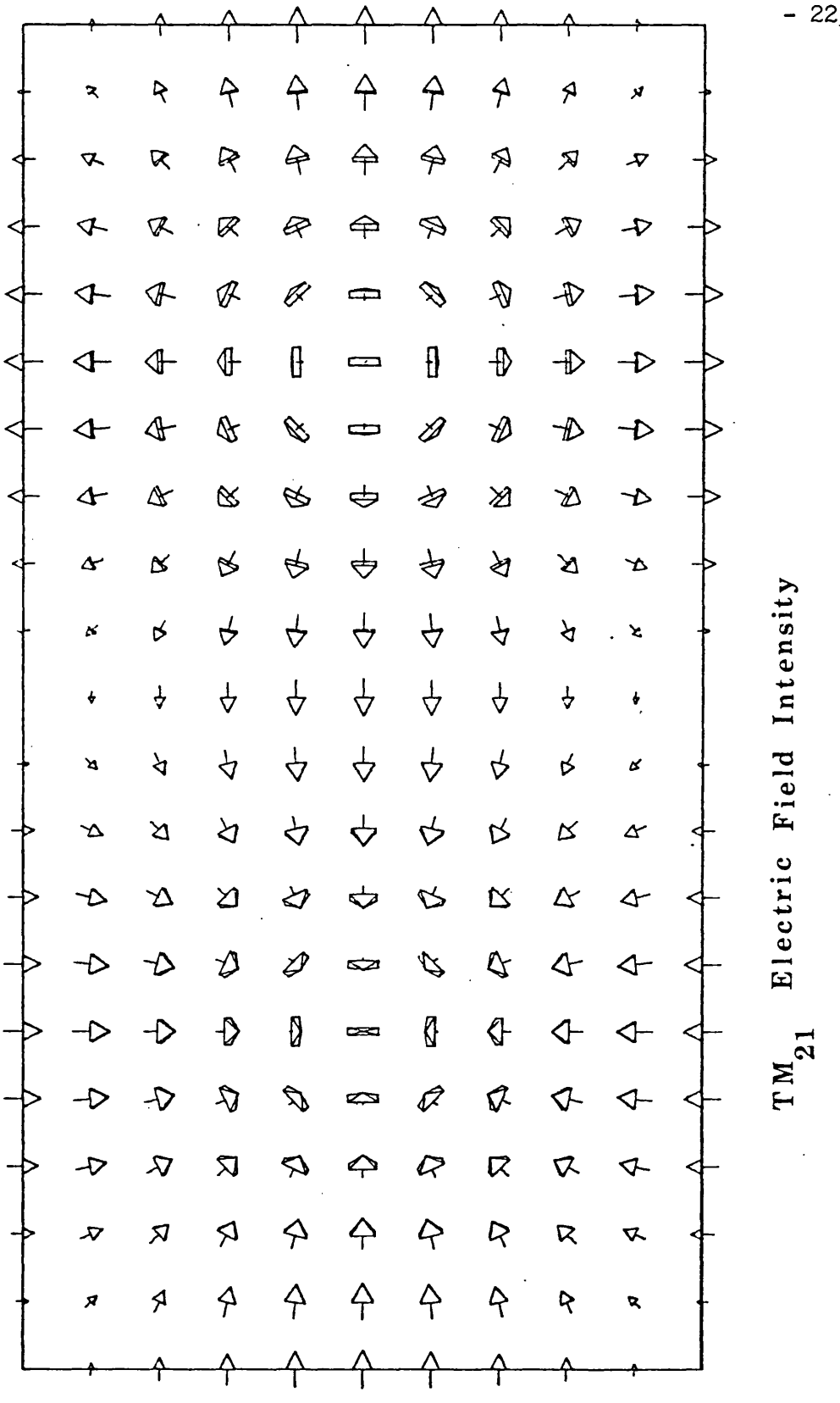


FIG. 4.28 $TM_{21}$ NON-TRANSVERSE FIELD DISPLAY

matic generated contour diagram.

The examples presented here are the first accurate graphic description of non-transverse waveguide fields on a plane transverse to the direction of power flow, by means of single diagrams.

The intensity of the non-transverse field at every mesh point (intersection of tail and arrow head) is given by the length of the pyramid base, a. It is measured in terms of the maximum field component on the plane sample with a scale factor equal to the first diagram parameter, p , in the form:

$$M = p\, a_i \tag{4.174}$$

The angle of elevation can be measured at each mesh point through the expression:

$$\beta = \tan^{-1} \left( q^{-1} \frac{b_i}{L_i} \right) \tag{4.175}$$

where $b_i$ and $L_i$ are the base width and total image length on the image plane respectively, and q the second diagram parameter , (see Fig.(4.22)). The angle of elevation $\beta$ is positive when the point of contact tail-head is hidden and negative otherwise.

4.8.10.3 <u>ELECTRIC AND MAGNETIC FIELDS</u>

The diagrams presented in Fig.(4.23) to Fig.(4.28) can be superimposed to produce an arrow assembly displaying both the electric and the magnetic fields.

Although the number of arrows become doubled and the complexity of the picture is increased, such diagrams have the advantage of showing the basic characteristics of the electromagnetic vectors, as for instance, their perpendicularity at each point and the encircling of the electric field by the magnetic field. Each field can be identified in the diagrams by its behaviour at the cross-section boundary. Mode type and mode numbers can be obtained from the diagrams by observing the field intensity variations along the cross-section sides. Also, colour has been used to facilitate the identification of the fields. Red is used to display non-transverse fields while black has been selected for transverse fields.

Examples of superimposed field patterns are presented in Fig. (4.29) and Fig.(4.30). In those pictures the nodal point where the fields have been calculated , $P_c$, coincides with the tail end.

### 4.8.10.4 POLARIZATION

The diagram in Fig.(4.31) represents the magnetic field of the $TE_{10}$ mode on a plane sample, one wavelength long, which has been taken parallel to the broader cross-section walls. The circular polarization of the magnetic field can be observed along the columns indicated in the picture.

### 4.8.10.5 PHASE RELATIONSHIPS, LONGITUDINAL VARIATIONS AND THE PSEUDO INCREASE IN FIELD INTENSITY EFFECT

Phase relationships between the electromagnetic vectors in the waveguide can be displayed by changing the angle in eq.(4.171) or,in the case of transverse plane samples, by taking successive plane

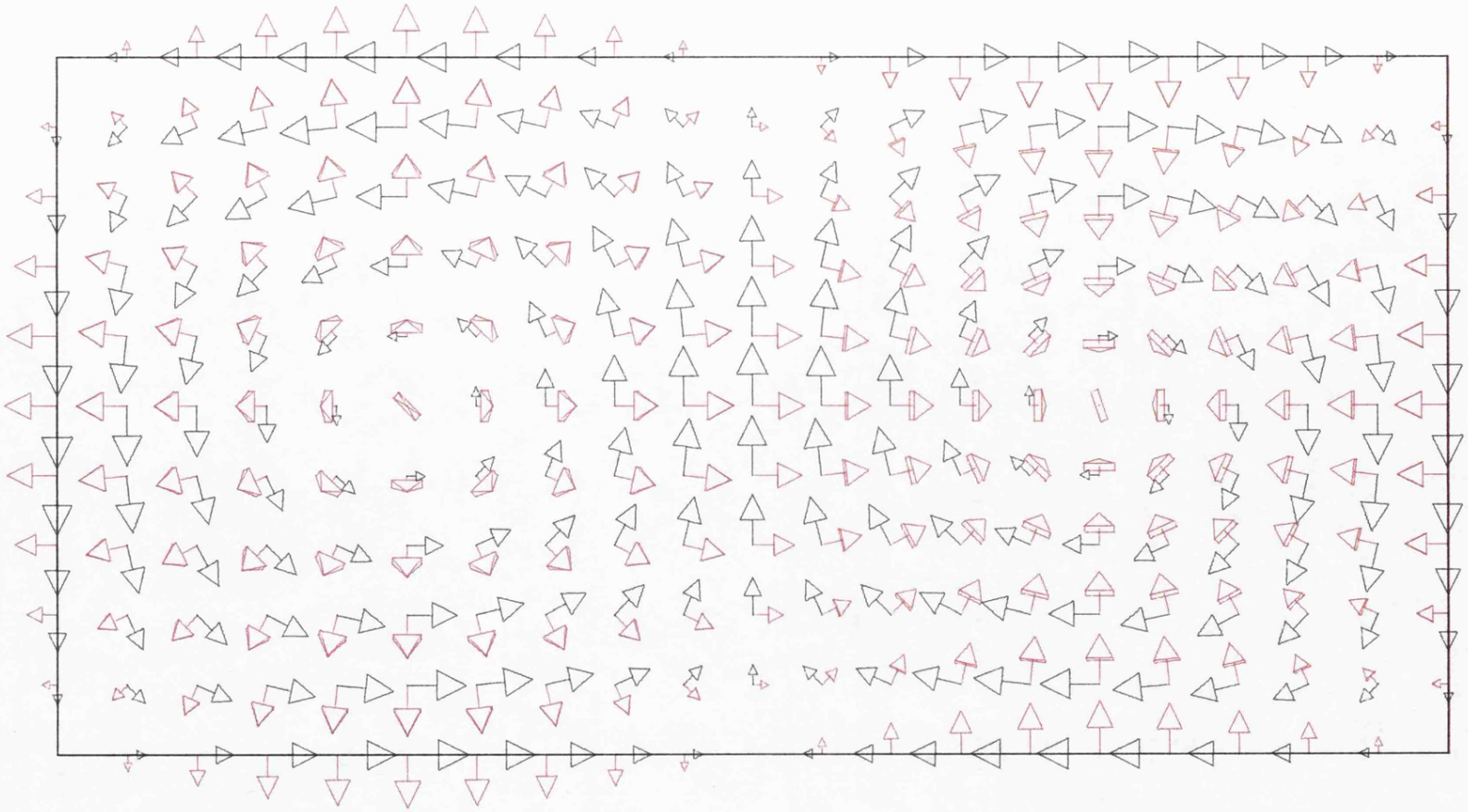

FIG. 4.29 $TM_{21}$ ELECTROMAGNETIC FIELD DISTRIBUTION DISPLAY

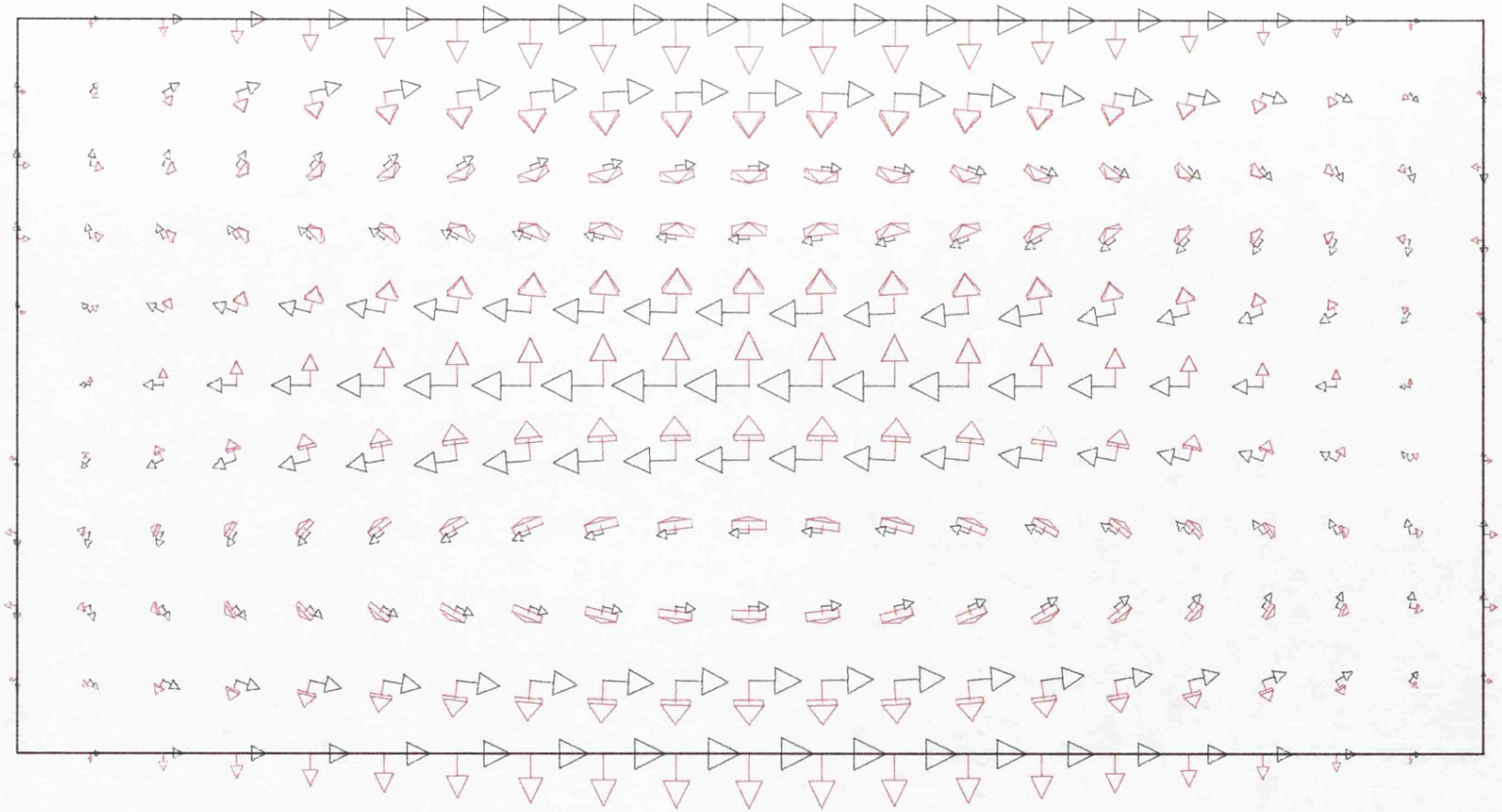

FIG. 4.30 $TM_{12}$ ELECTROMAGNETIC FIELD DISTRIBUTION DISPLAY

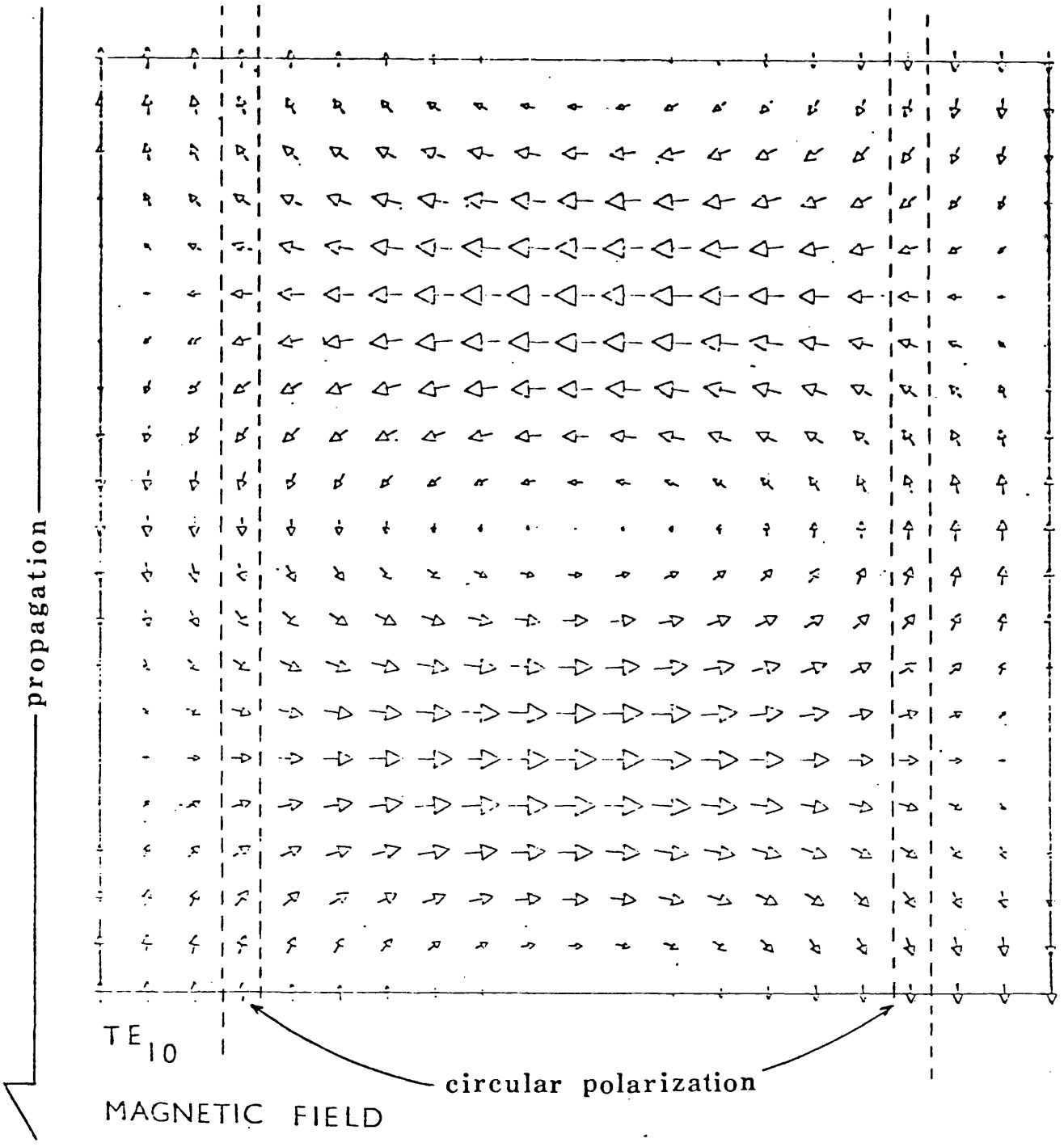


FIG. 4.31 CIRCULAR POLARIZATION

The circular polarization of the magnetic field of the $TE_{10}$ mode is noticeable in the indicated regions.

samples along the propagation direction. An example of the latter procedure involving the $TE_{11}$ and the $TM_{11}$ field distribution for the waveguide in Fig.(4.32) are shown in Fig.(4.33) to Fig.(4.38).

Observation of these pictures shows that the transverse fields are linearly polarized since their direction is constant along the propagation. The size of the representative arrows is constant in this case because the normalization with respect to the greatest vector component on the plane sample has been accomplished for each diagram. It need not be necessarily so.

The non-transverse fields,however, show over the cross-section an alternate phase behaviour along the wavelength. Note that the pseudo increase in field intensity effect does not persist since the field varies from diagram to diagram. The sinusoidal variation of the field intensity along the wavelength can be observed by taking longitudinal plane samples (parallel to the narrower cross-section sides) of the field distribution. The diagram in Fig.(4.39) exemplifies this procedure with a longitudinal plane sample in the middle of the guide for the electric field of the $TE_{10}$ mode.

## 4.9 VISUAL APPROXIMATION TO FIELD LINES

It can be seen from the diagrams presented in this work that one of the advantages of the arrow assembly diagrams in field plotting is that they always give an immediate visual approximation of the field line diagram of the vector field under consideration.

It is not possible, however , to get a visual approximation of the arrow assembly diagrams by contemplating the corresponding field line diagrams.

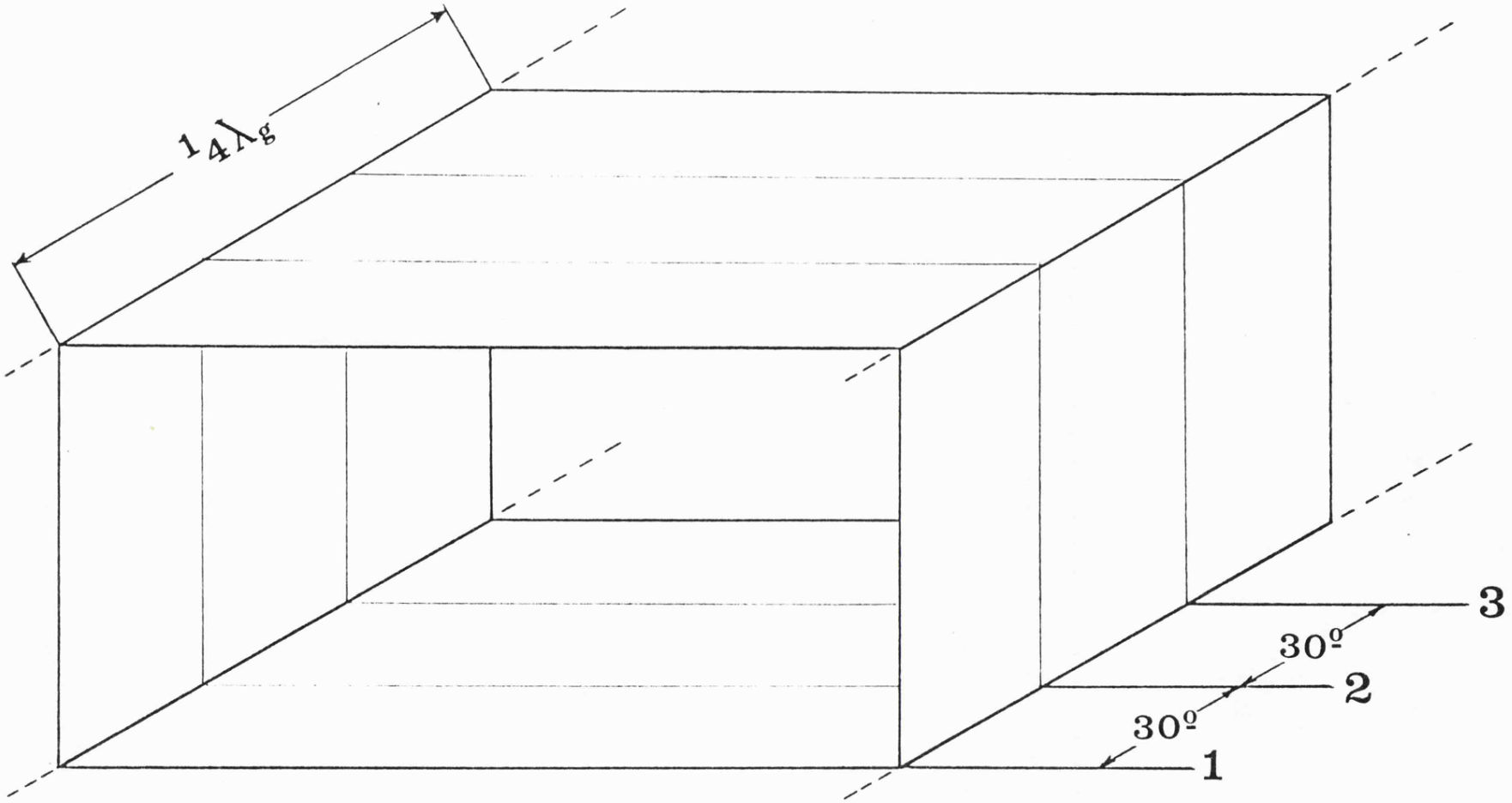


FIG. 4.32 PLANE SAMPLES IN A RECTANGULAR WAVEGUIDE

Typical rectangular waveguide where the samples of the $TE_{11}$ and $TM_{11}$ field distributions having $30^{\circ}$ phase difference are taken.

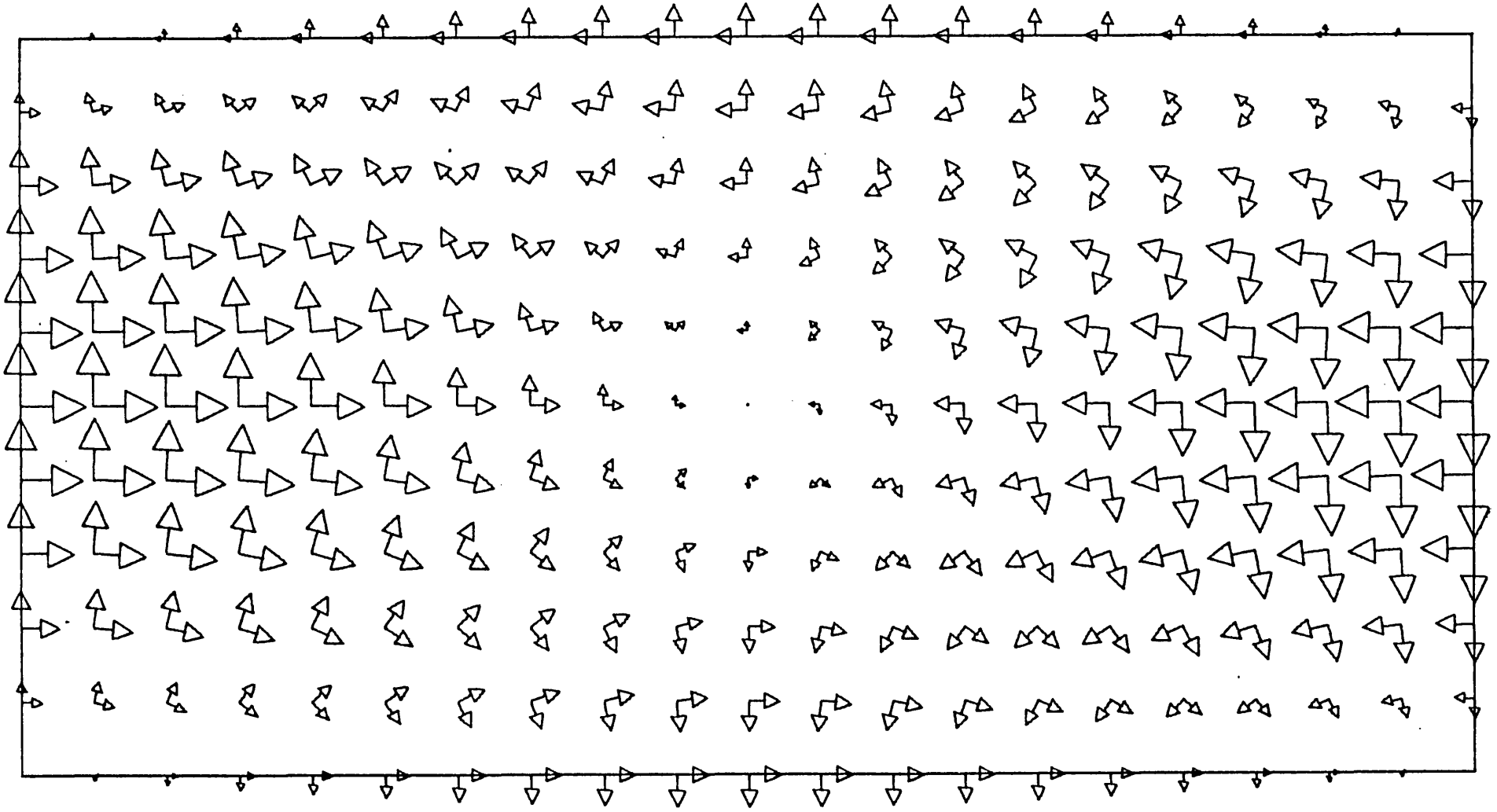

FIG. 4.33 RECTANGULAR WAVEGUIDE SAMPLE SEQUENCE

Sample No. 1 of the field distribution of the $TE_{11}$ mode. Note that the magnetic field has low intensity at waveguide corners.

1

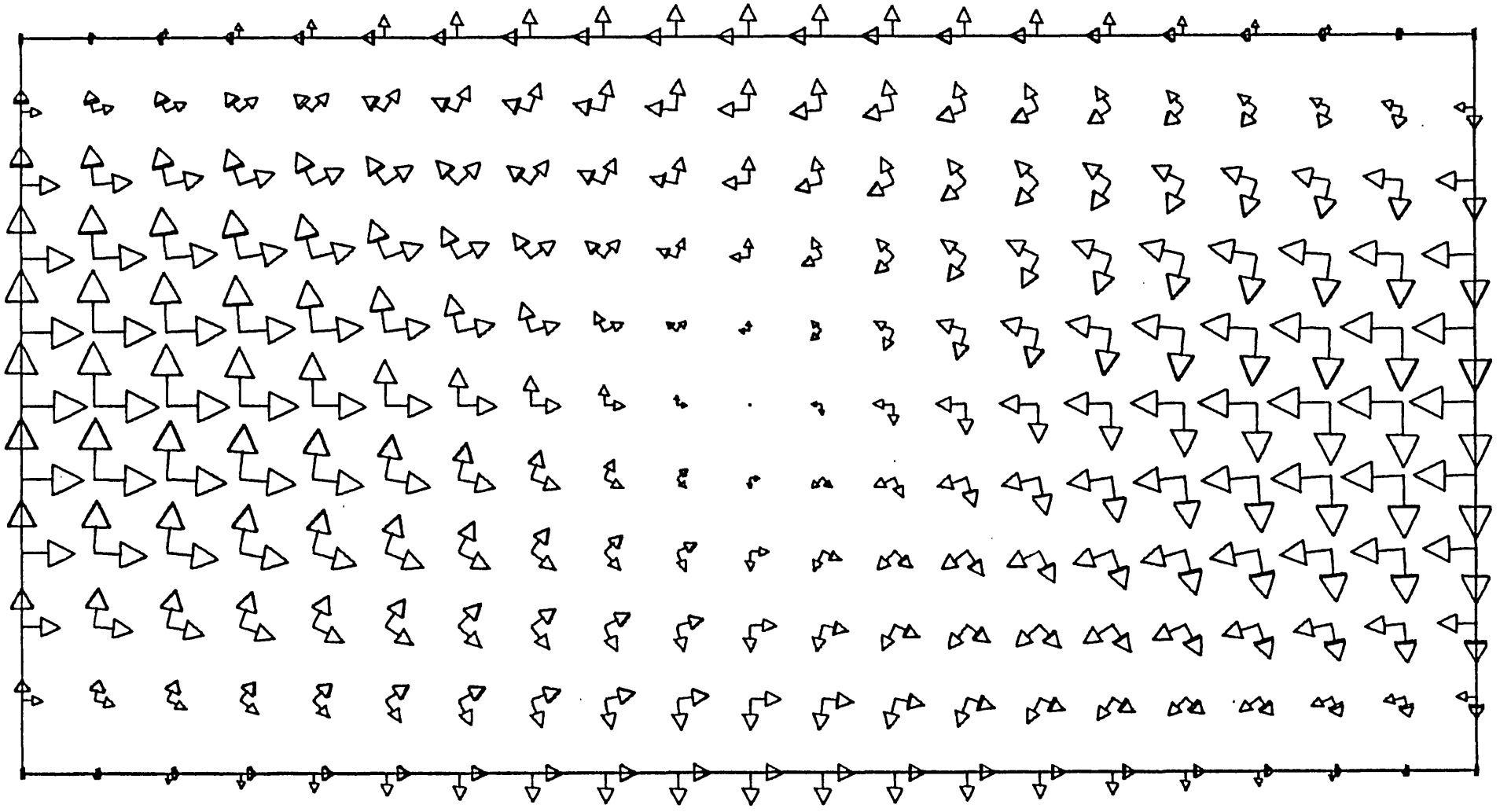

FIG. 4.34 RECTANGULAR WAVEGUIDE SAMPLE SEQUENCE

Sample No. 2 of the field distribution of the $TE_{11}$ mode. The intensity of the magnetic field is increasing at waveguide corners.

2

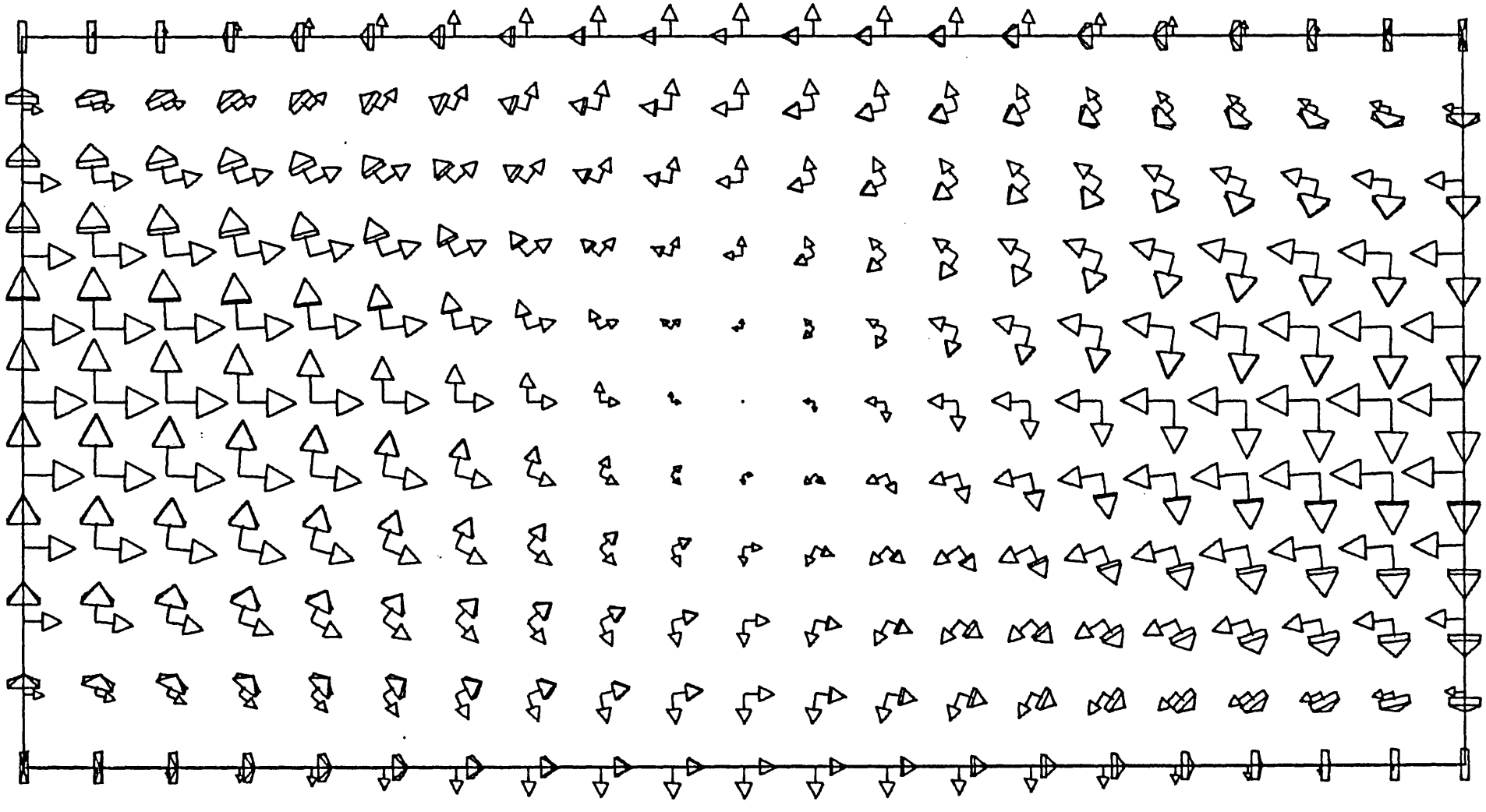

FIG. 4.35 RECTANGULAR WAVEGUIDE SAMPLE SEQUENCE

Sample No. 3 of the field distribution of the $TE_{11}$ mode. The magnetic field is intense at waveguide corners for this phase of propagation.

3

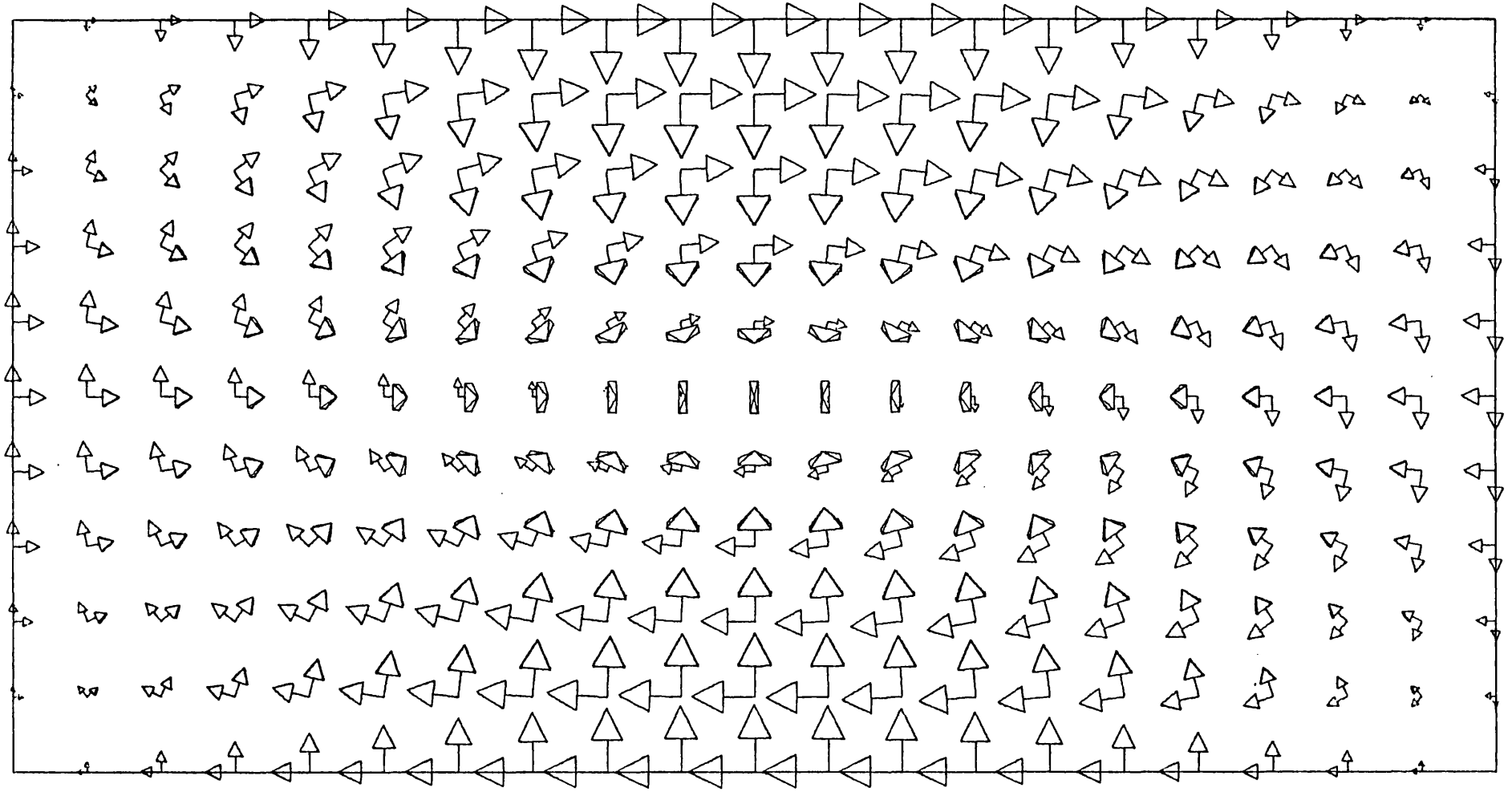

FIG. 4.36 RECTANGULAR WAVEGUIDE SAMPLE SEQUENCE

Sample No. 1 of the field distribution of the $TM_{11}$ mode. Note that the electric field is intense in the waveguide centre region.

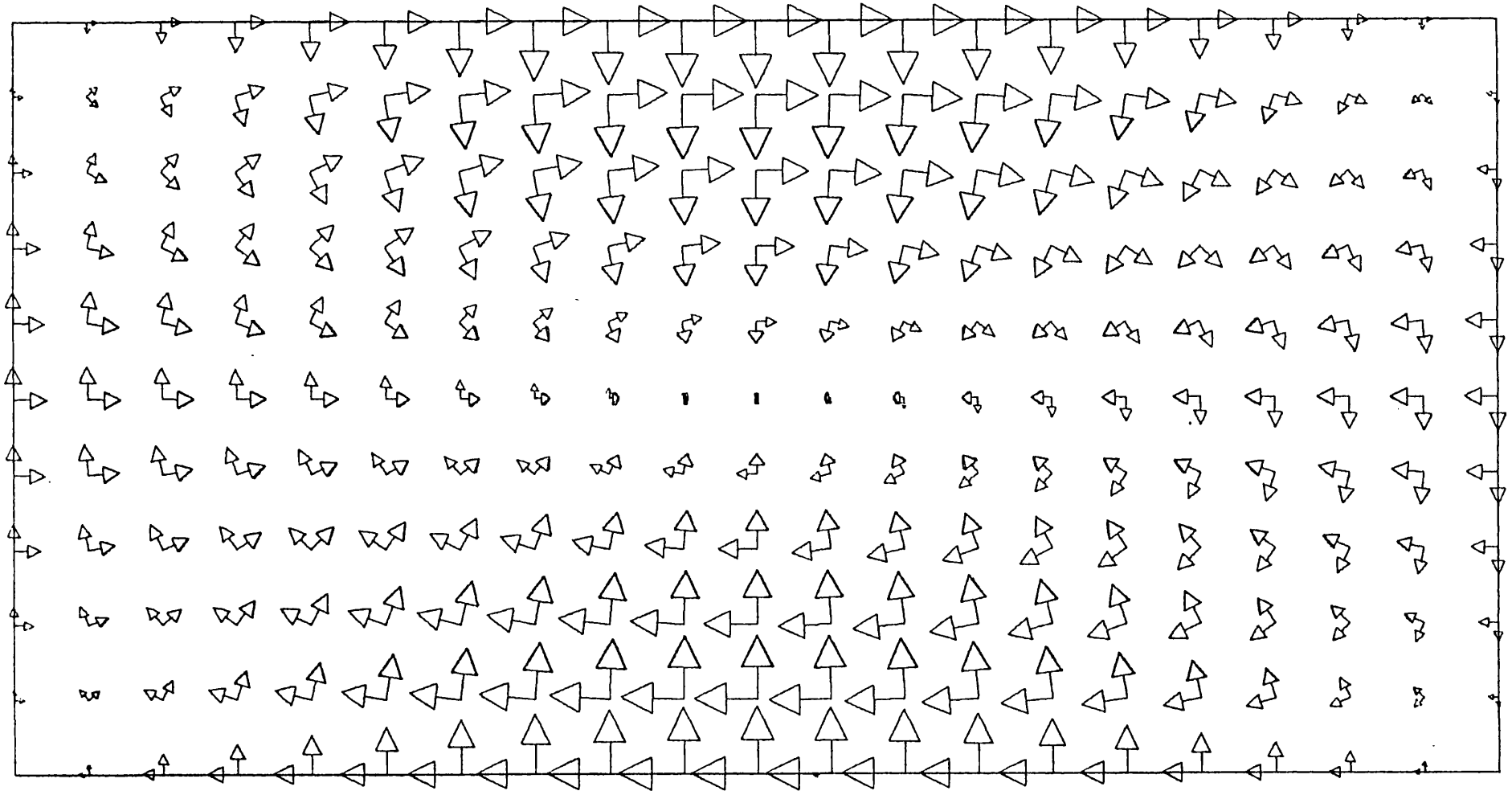

FIG. 4.37 RECTANGULAR WAVEGUIDE SAMPLE SEQUENCE

Sample No. 2 of the field distribution of the $TM_{11}$ mode. The field intensity in the waveguide centre region has decreased.

2

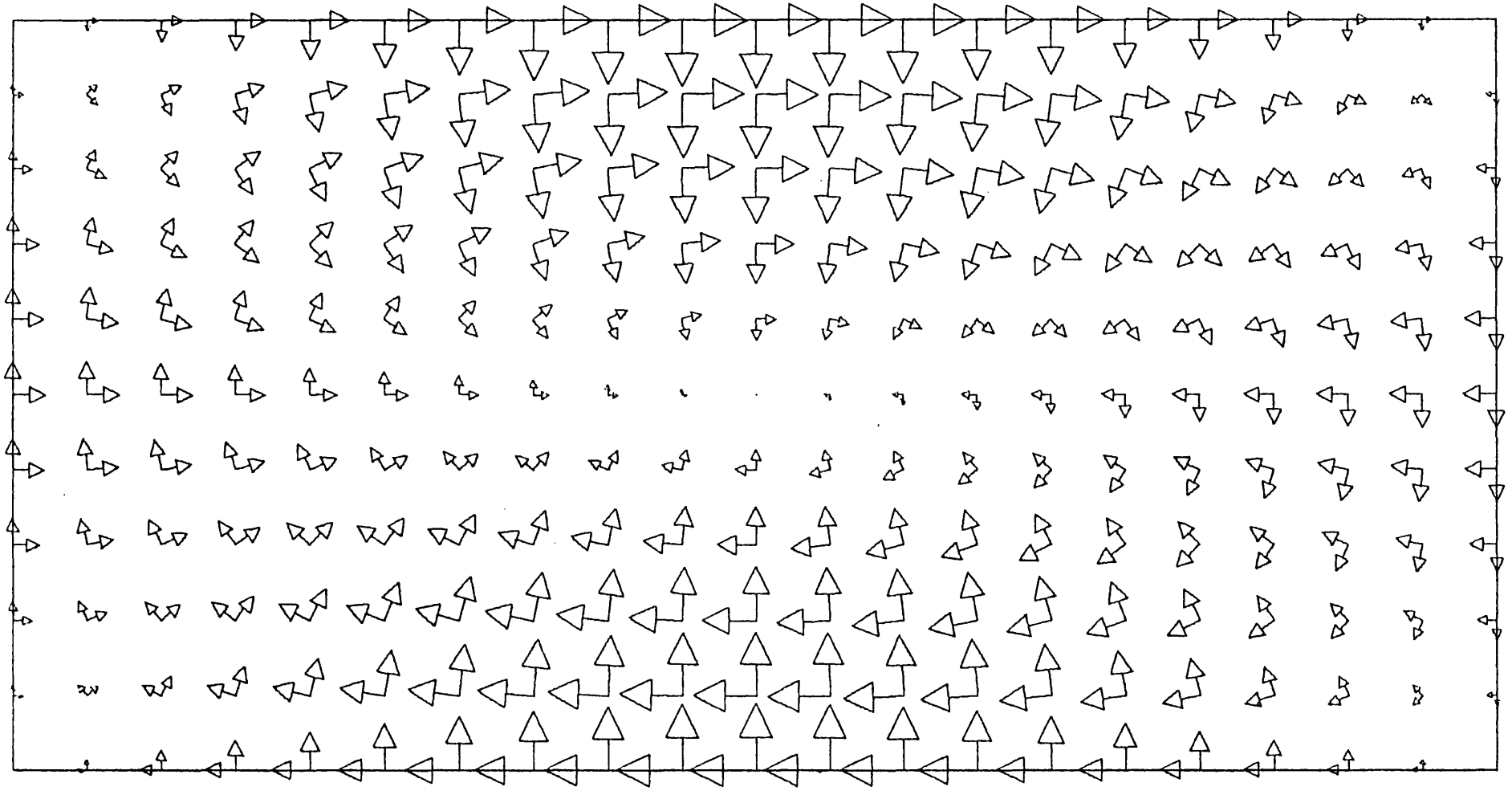

FIG. 4.38 RECTANGULAR WAVEGUIDE SAMPLE SEQUENCE

Sample No. 3 of the field distribution of the $TM_{11}$ mode. The field is now weak in the waveguide centre region.

3

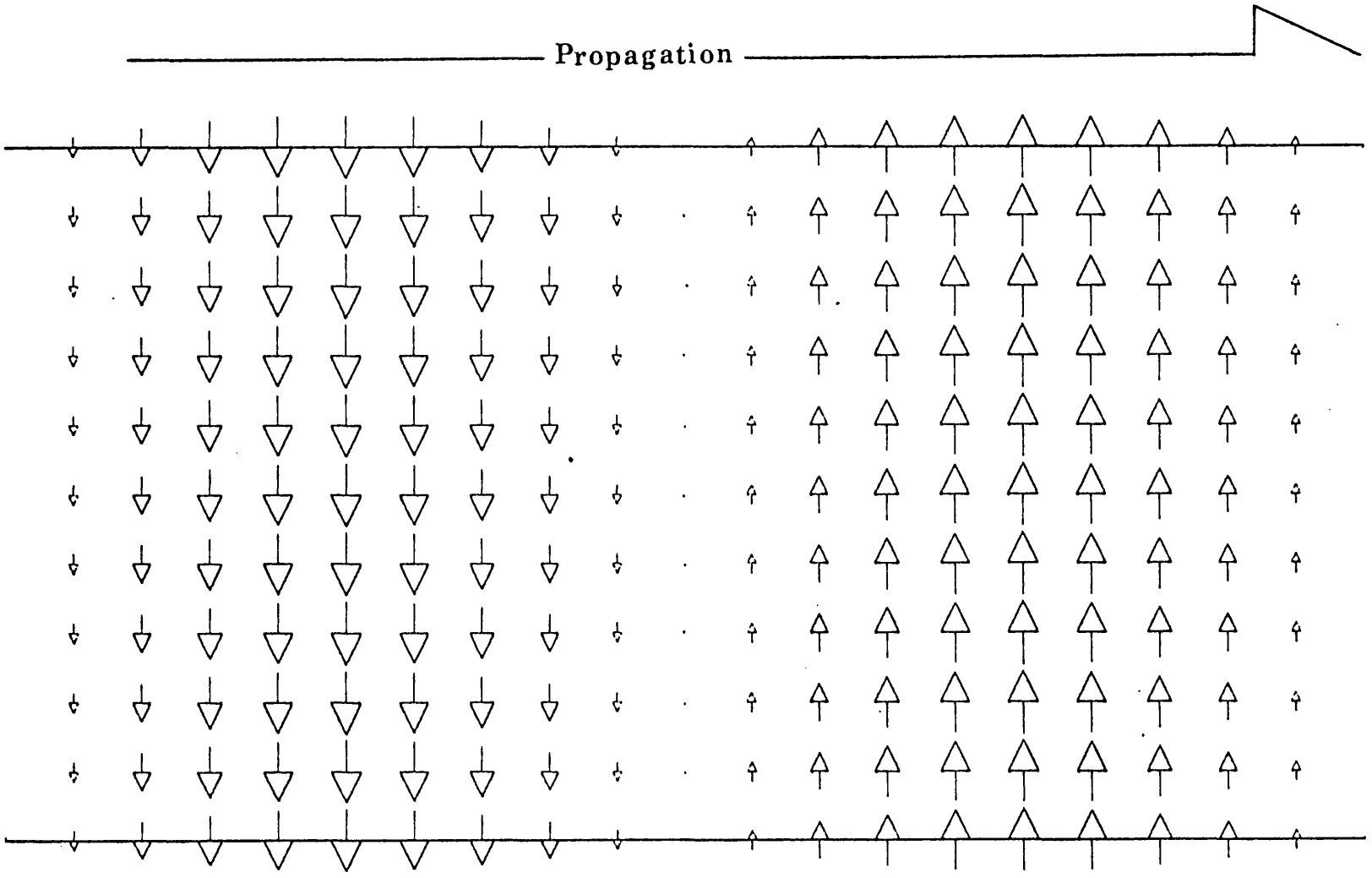


FIG. 4.39 FIELD BEHAVIOUR ALONG THE LONGITUDINAL DIRECTION

Sinusoidal variation of the field intensity along the wavelength.

## 4.10 DYNAMIC DIAGRAMS

The fields displayed on the image plane are calculated for a given value of the product $\omega t$. By recalculating the fields for several values of the variable t , a set of diagrams showing the fields dependence on time can be generated. If those diagrams are copied onto a film, a dynamical description of the field behaviour on the sampling plane can be obtained. Experiences with dynamic diagrams based on the field patterns shown during this chapter are now under development at Leicester University Engineering Department.

In this case, a careful choice of the frequency for which the diagrams are produced facilitates the interpretation of the non-transverse fields. This is so because, if a balance between the transverse and the longitudinal components of the field is not established, the diagrams may produce comparatively small images of vectors for which the magnitude of the angle of elevation is high. In order to establish a convenient diagram generation frequency consider the general expressions for the transverse and longitudinal components of the general waveguide fields (obtained from eq.(2.138) to eq.(2.145)) given respectively by:

$$\underline{V}_{Tn}^{(j)} = i\,\beta_n\,\nabla_T\,G_n^{(j)} \tag{4.176}$$

$$V_{Ln}^{(j)} = k_{cn}^2\,G_n^{(j)} \tag{4.177}$$

$$(j = 1,2)$$

where the general propagation function $\gamma_n$ has been replaced by $i\,\beta_n$ to indicate that only propagating waves are being considered.

The moduli of the maximum field components $V_T$ and $V_L$ can be written, considering eq.(4.176) and eq.(4.177), in the form:

$$V_T = \beta_n \left| \nabla_T G_n^{(j)} \right| \max \tag{4.178}$$

$$V_L = k_{cn}^2 \left| G_n^{(j)} \right| \max \tag{4.179}$$

A convenient pictorial balance is obtained when points displaying vector components with maximum intensity in any direction have the same image size associated to them. In this case, $V_T$ and $V_L$ become equal and the propagation function $\beta_n$ is given by

$$\beta_n = \frac{k_{cn}^2 \left| G_n^{(j)} \right| \max}{\left| \nabla_T G_n^{(j)} \right| \max} \tag{4.180}$$

Defining the normalized propagating frequency, $f_n$ by

$$f_n = \frac{k_0}{k_{cn}} \tag{4.181}$$

and considering that

$$\beta_n = k_{cn} (f_n^2 - 1)^{\frac{1}{2}} \tag{4.182}$$

the convenient normalized frequency for dynamical diagrams is written

in the form:

$$f_n = \left[ 1 + k_{cn}^2 \left( \frac{G_n^{(j)} \quad max}{\nabla_T \, G_n^{(j)} \quad max} \right)^2 \right]^{\frac{1}{2}} \tag{4.183}$$

For a rectangular waveguide the balance between the transverse and longitudinal components of the field is obtained when

$$\frac{\beta_n \, \pi}{B \, k_{cn}^2} \approx 1 \tag{4.184}$$

where B is the narrower cross-section side length. Therefore, for that particular geometry, the normalized frequency for the generation of dynamic diagrams can be chosen to be

$$f_n \approx \left[ 1 + k_{cn}^2 \left( \frac{B}{\pi} \right)^2 \right]^{\frac{1}{2}} \tag{4.185}$$

An illustrative example of a sequence of pictures which can be used to produce a dynamical display of the field behaviour of the $TM_{11}$ mode in accordance with eq.(4.185) is shown in Fig.(4.40) to Fig.(4.52). Note that the normalization is not accomplished at each plane sample in order to show the dynamic variation of the field intensity. The diagrams presented cover one wavelength and have a $30^{\circ}$ difference in phase.

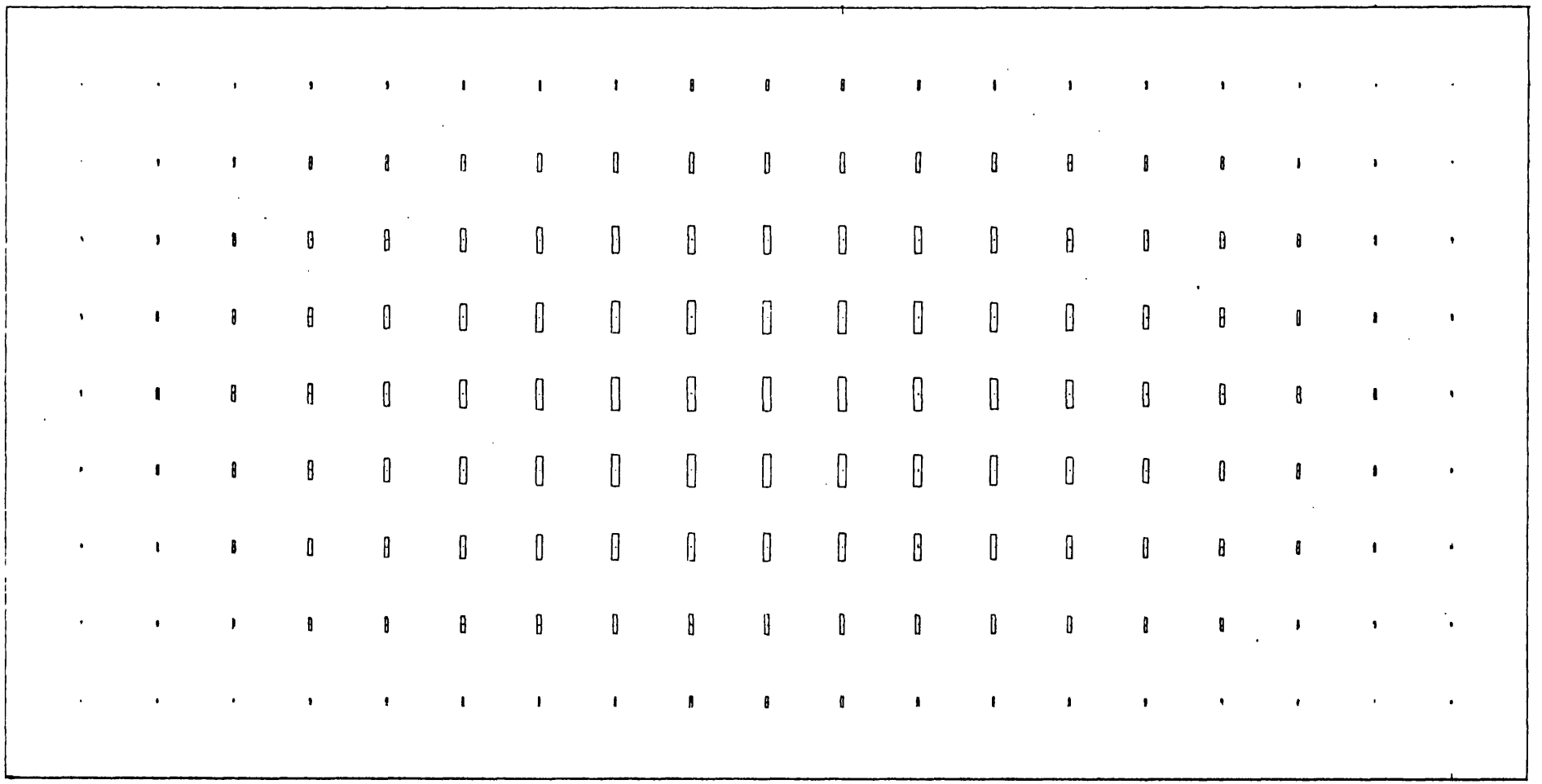

FIG. 4.40 DYNAMIC DISPLAY SEQUENCE

Field distribution for the $TM_{11}$ mode. Reference angle along the wavelength equal to $0^{\circ}$.

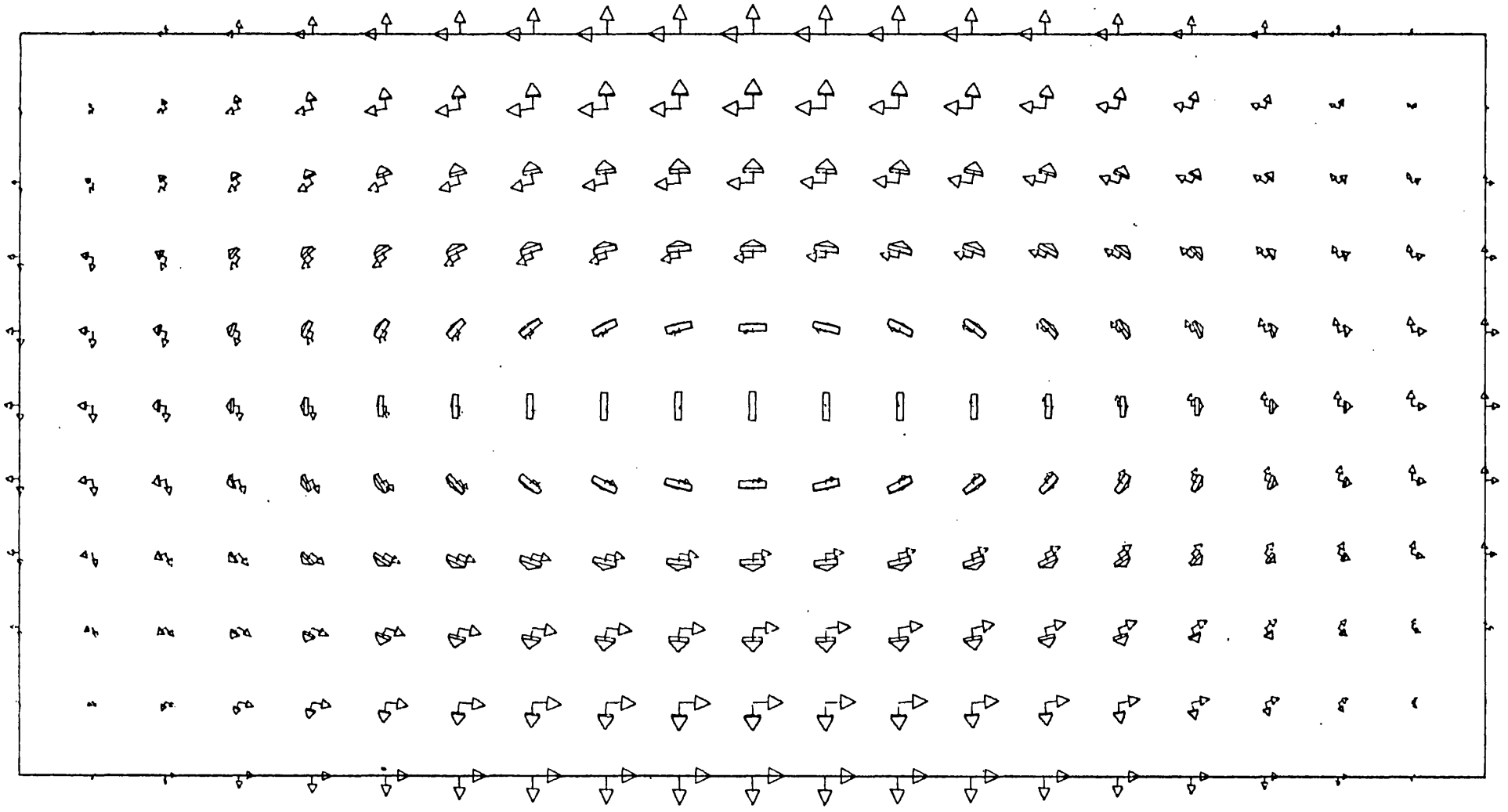

FIG. 4.41 DYNAMIC DISPLAY SEQUENCE

Field distribution for the $TM_{11}$ mode. Reference angle along the wavelength equal to $30^{\circ}$.

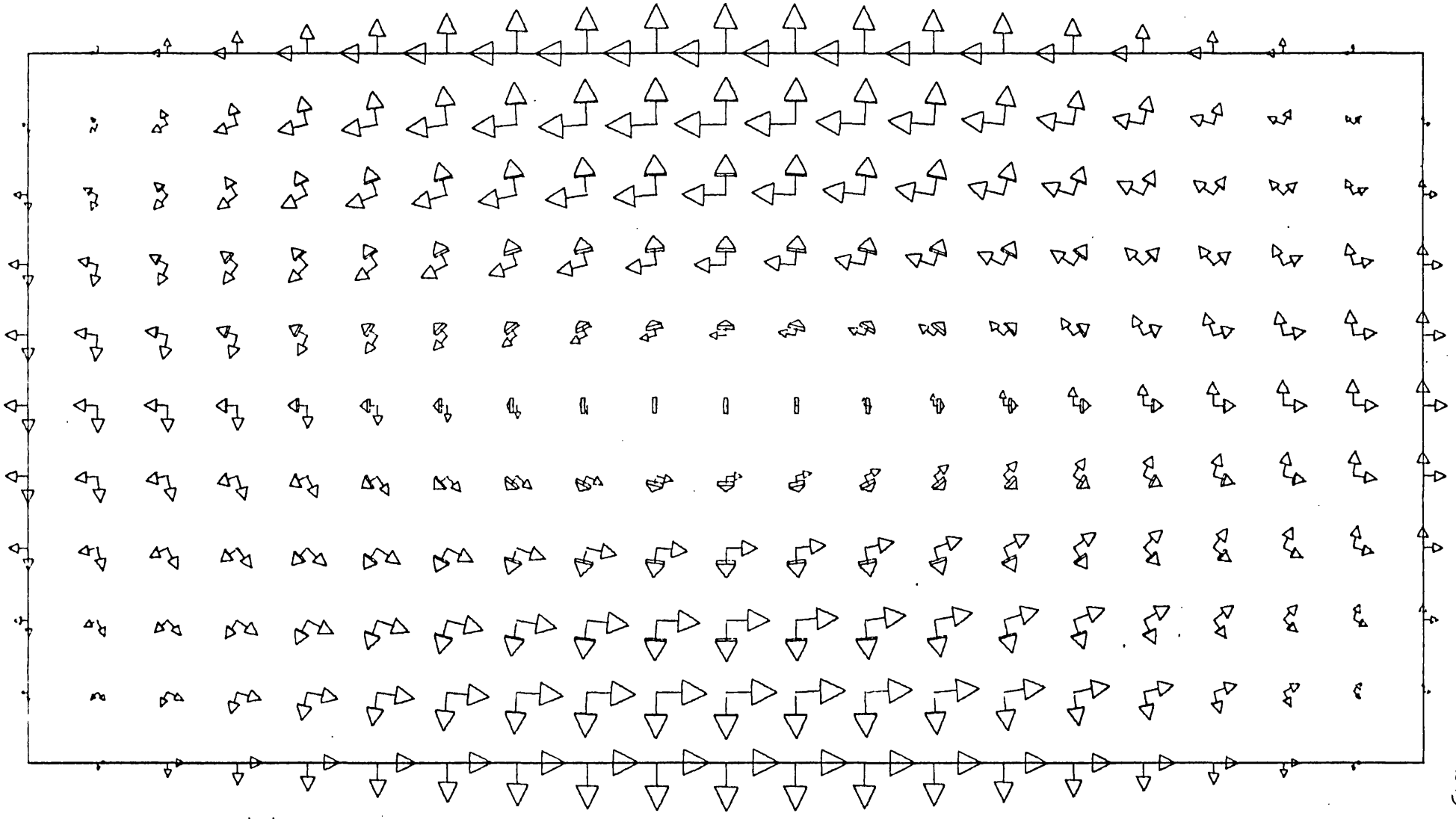

FIG. 4.42 DYNAMIC DISPLAY SEQUENCE

Field distribution for the $TM_{11}$ mode. Reference angle along the wavelength equal to $60^{\circ}$.

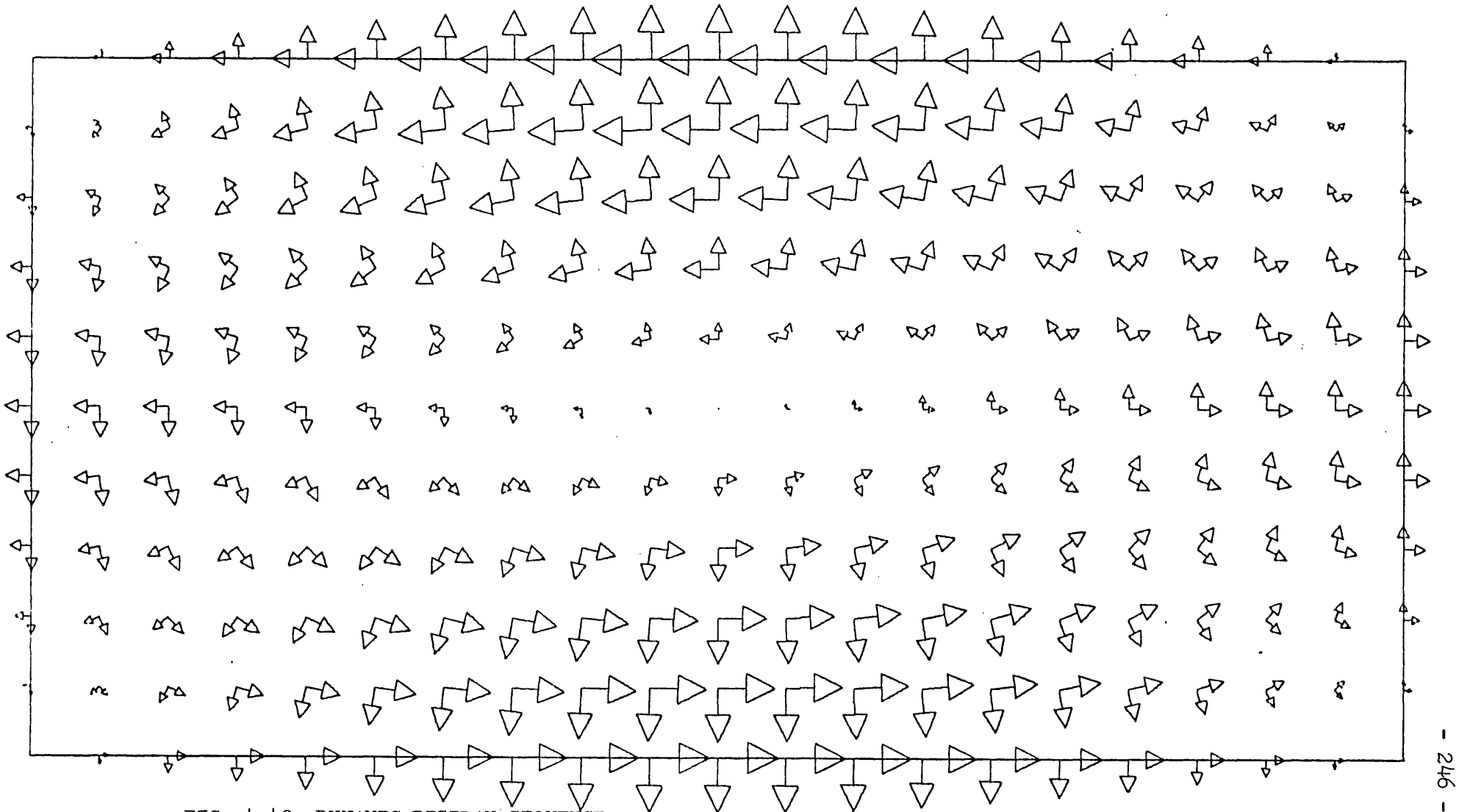

FIG. 4.43 DYNAMIC DISPLAY SEQUENCE

Field distribution for the $TM_{11}$ mode. Reference angle along the wavelength equal to $90^{\circ}$.

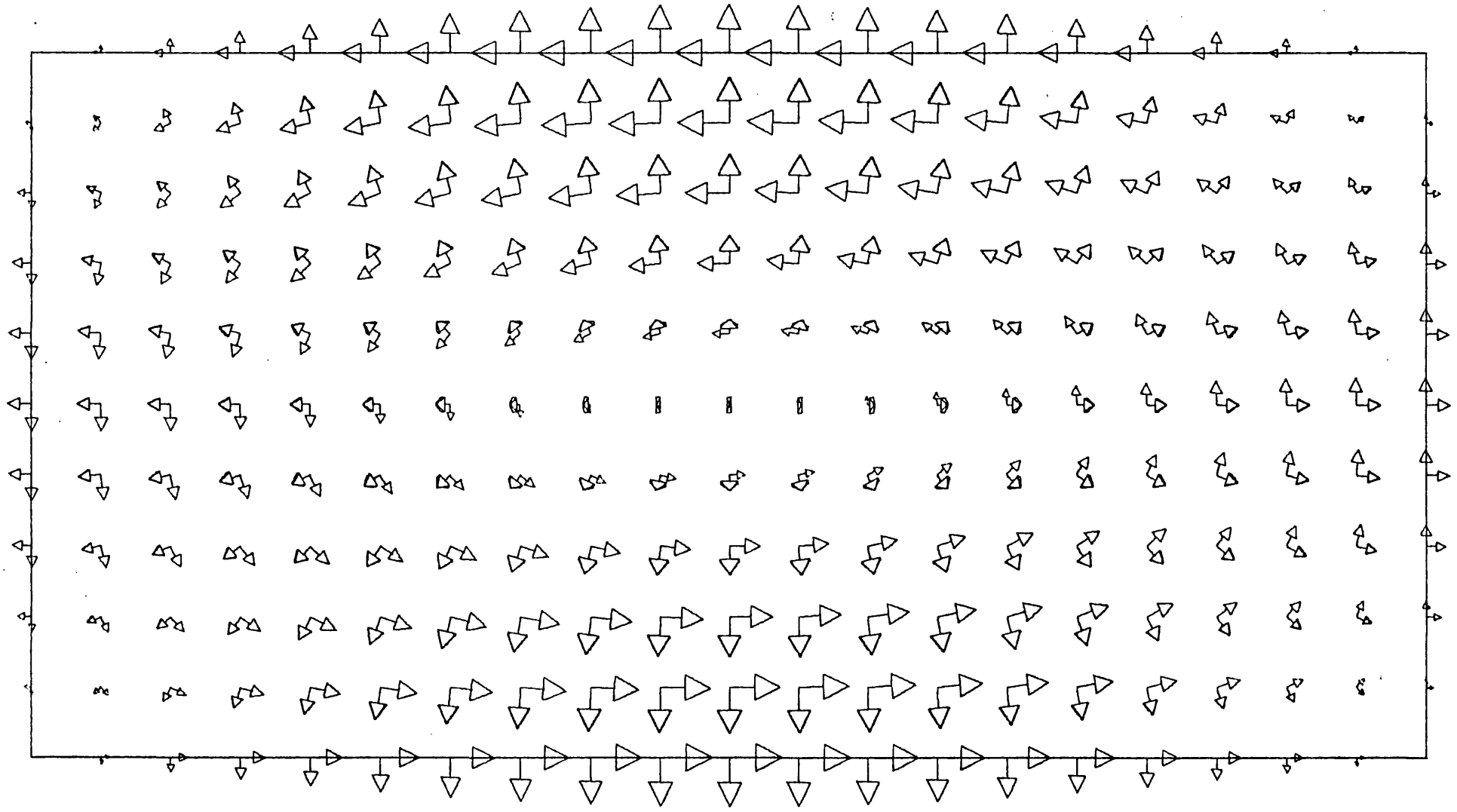

FIG. 4.44 DYNAMIC DISPLAY SEQUENCE

Field distribution for the $TM_{11}$ mode. Reference angle along the wavelength equal to $120^{\circ}$.

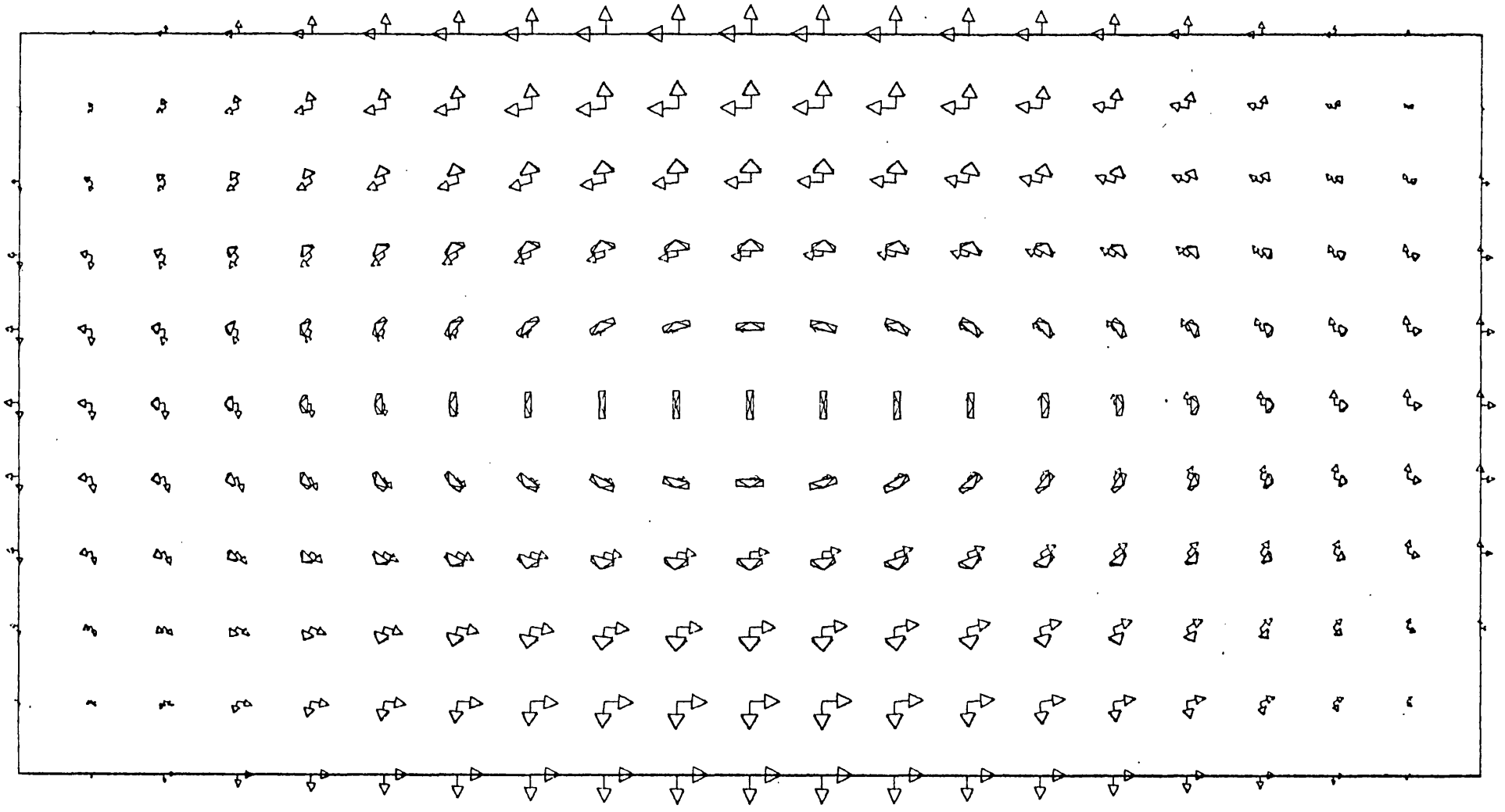

FIG. 4.45 DYNAMIC DISPLAY SEQUENCE

Field distribution for the $TM_{11}$ mode. Reference angle along the wavelength equal to $150^{\circ}$.

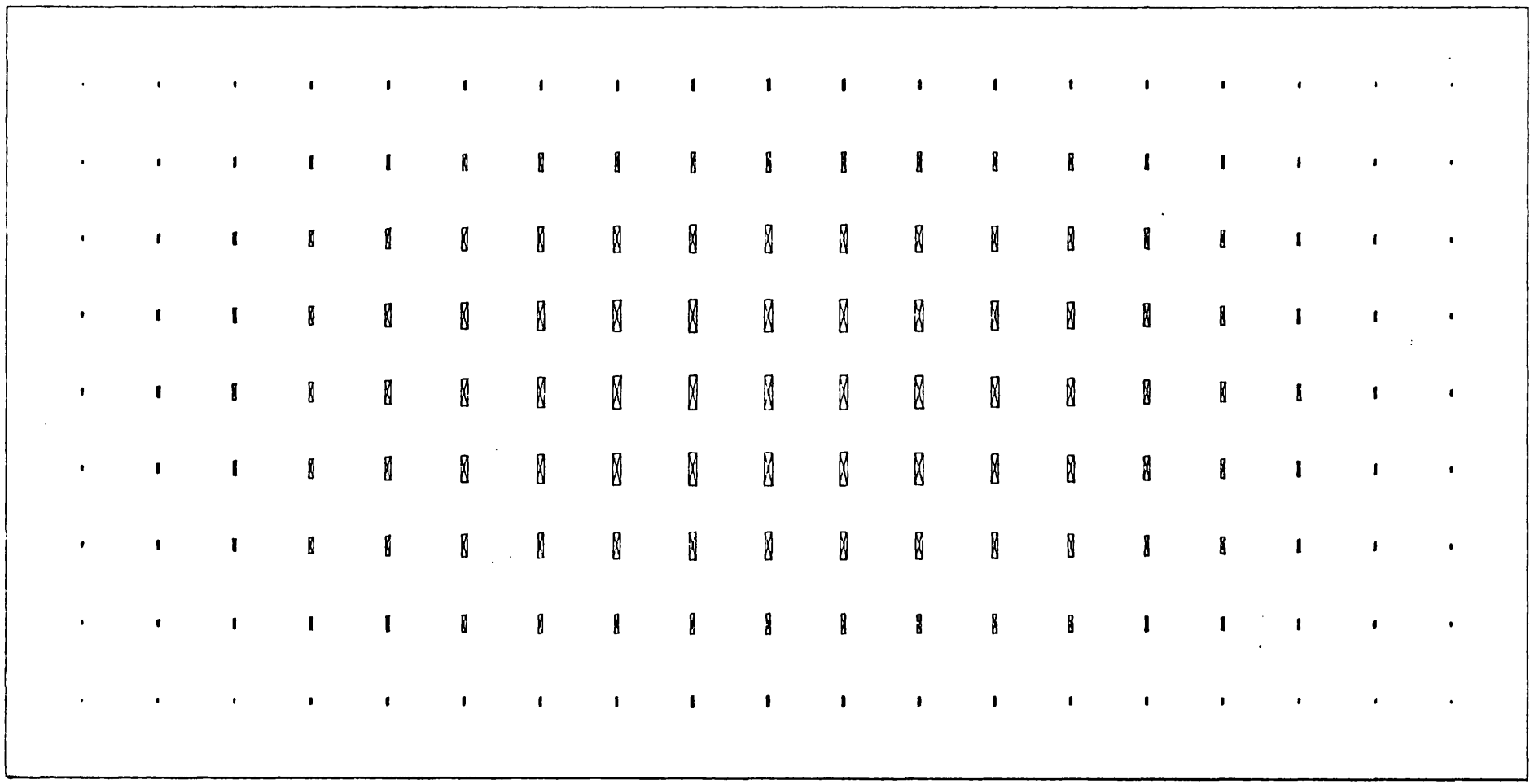

FIG. 4.46 DYNAMIC DISPLAY SEQUENCE

Field distribution for the $TM_{11}$ mode. Reference angle along the wavelength equal to $180^{\circ}$.

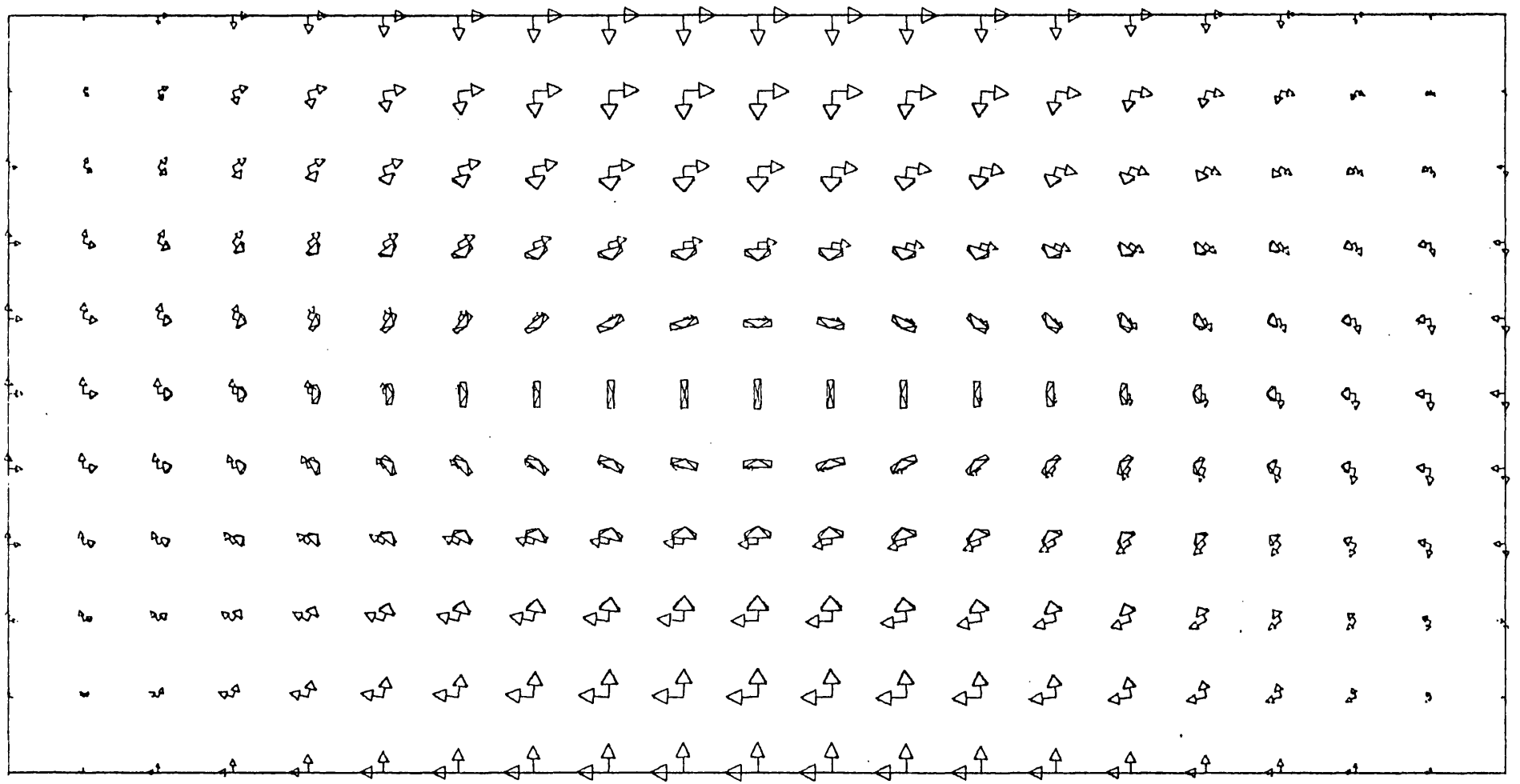

FIG. 4.47 DYNAMIC DISPLAY SEQUENCE

Field distribution for the $TM_{11}$ mode. Reference angle along the wavelength equal to $210^{\circ}$.

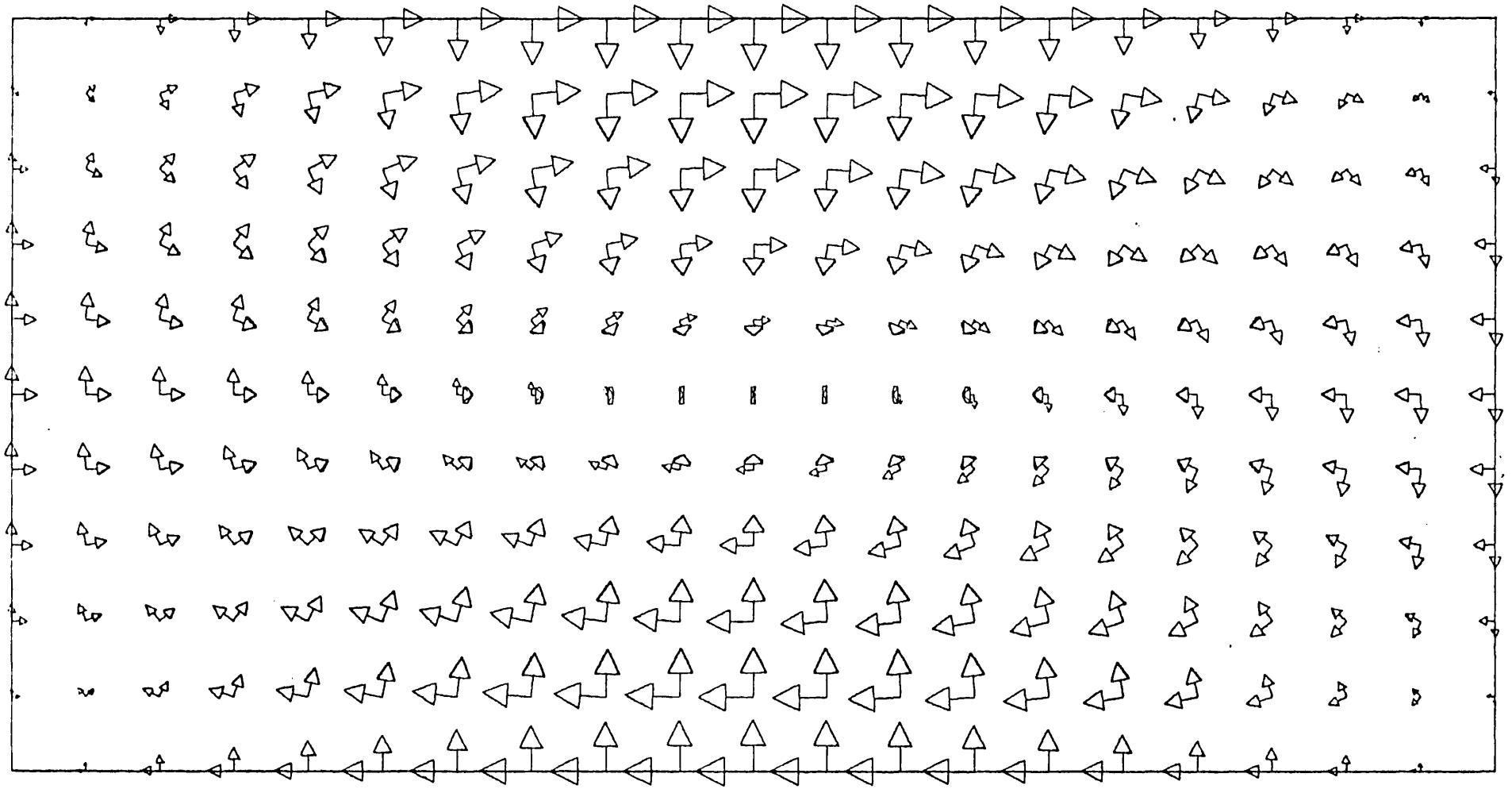

FIG. 4.48 DYNAMIC DISPLAY SEQUENCE

Field distribution for the $TM_{11}$ mode. Reference angle along the wavelength equal to $240^{\circ}$.

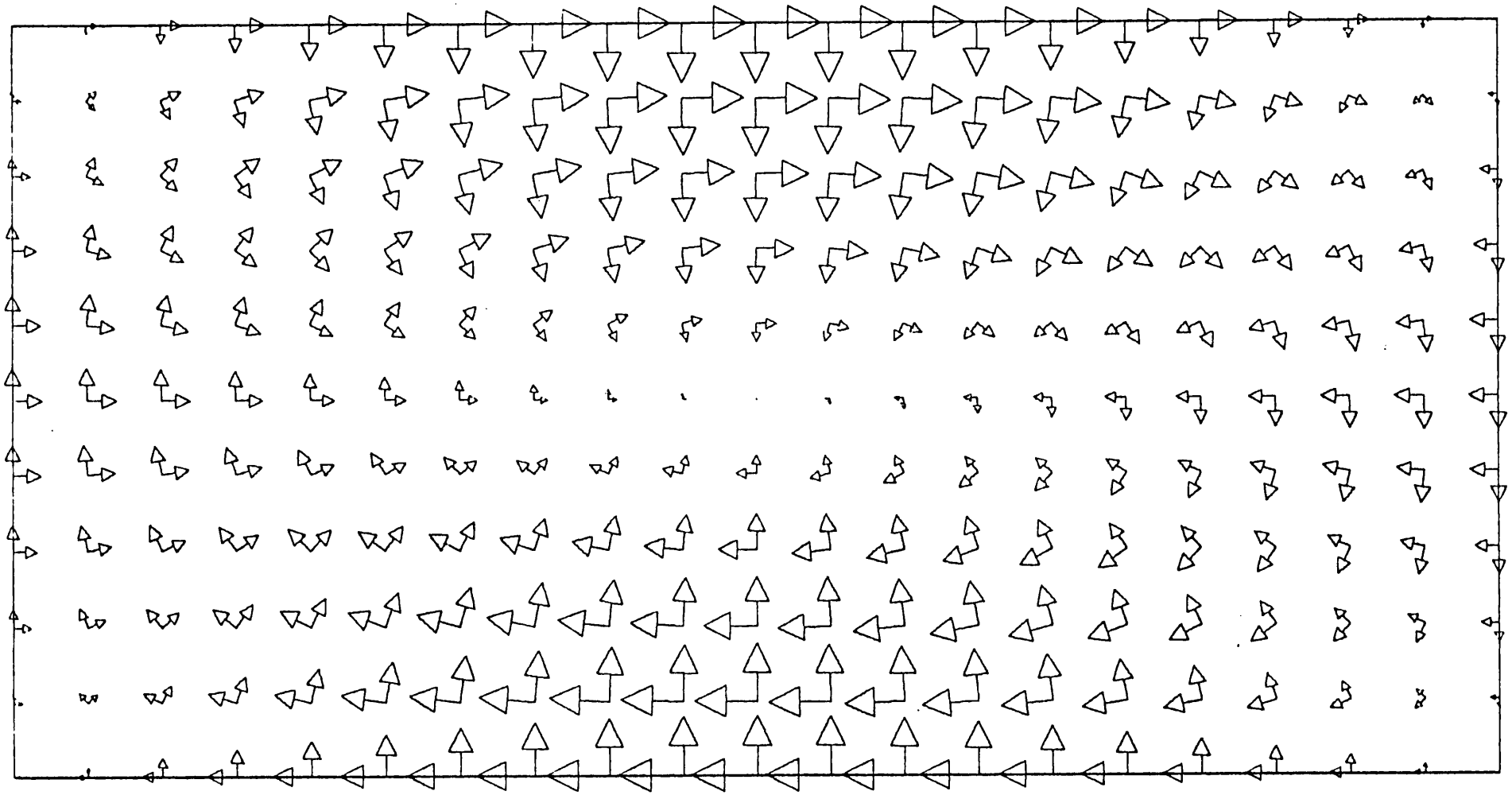

FIG. 4.49 DYNAMIC DISPLAY SEQUENCE

Field distribution for the $TM_{11}$ mode. Reference angle along the wavelength equal to $270^{\circ}$.

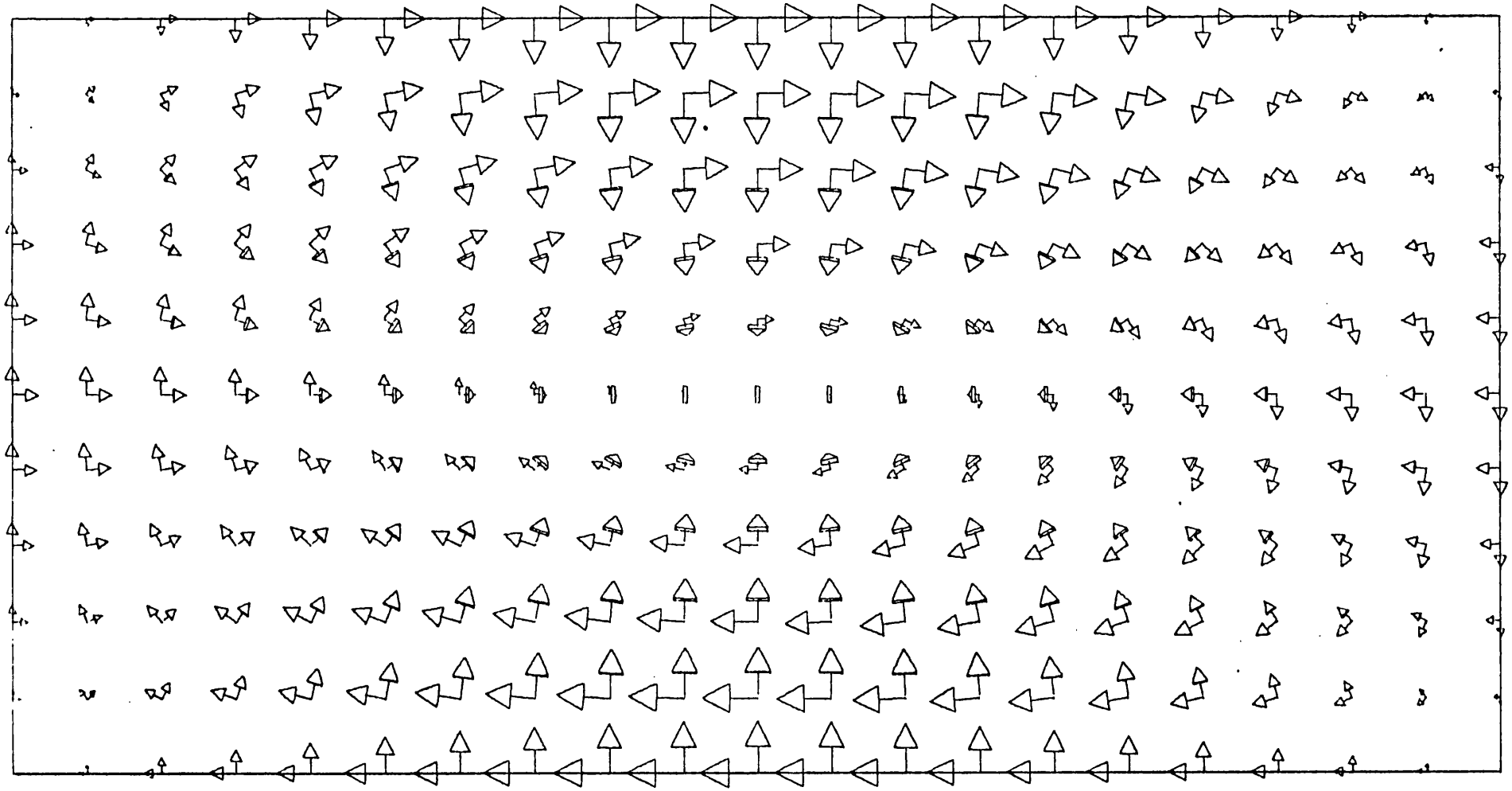

FIG. 4.50 DYNAMIC DISPLAY SEQUENCE

Field distribution for the $TM_{11}$ mode. Reference angle along the wavelength equal to $300^{o}$.

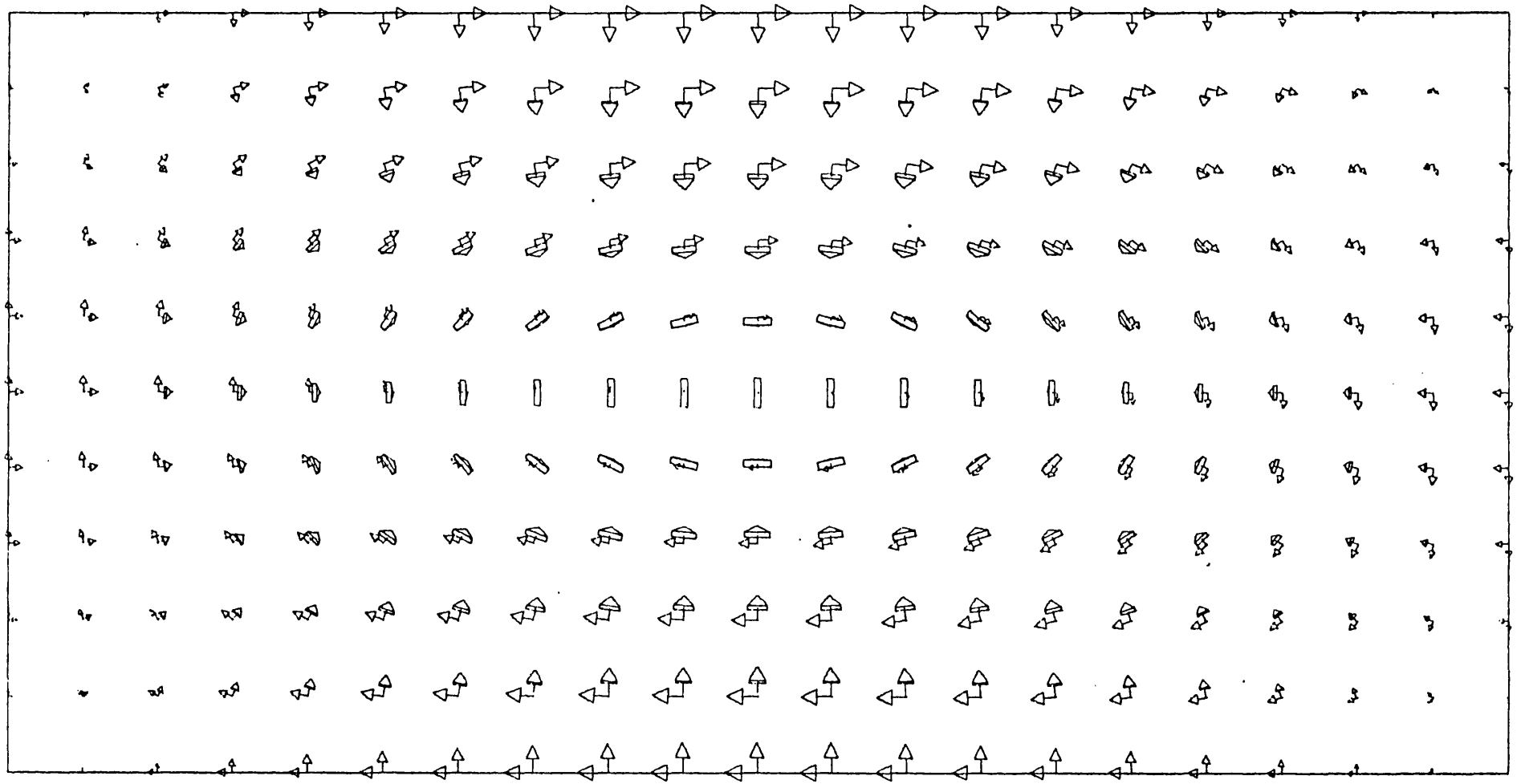

FIG. 4.51 DYNAMIC DISPLAY SEQUENCE

Field distribution for the $TM_{11}$ mode. Reference angle along the wavelength equal to $330^{o}$.

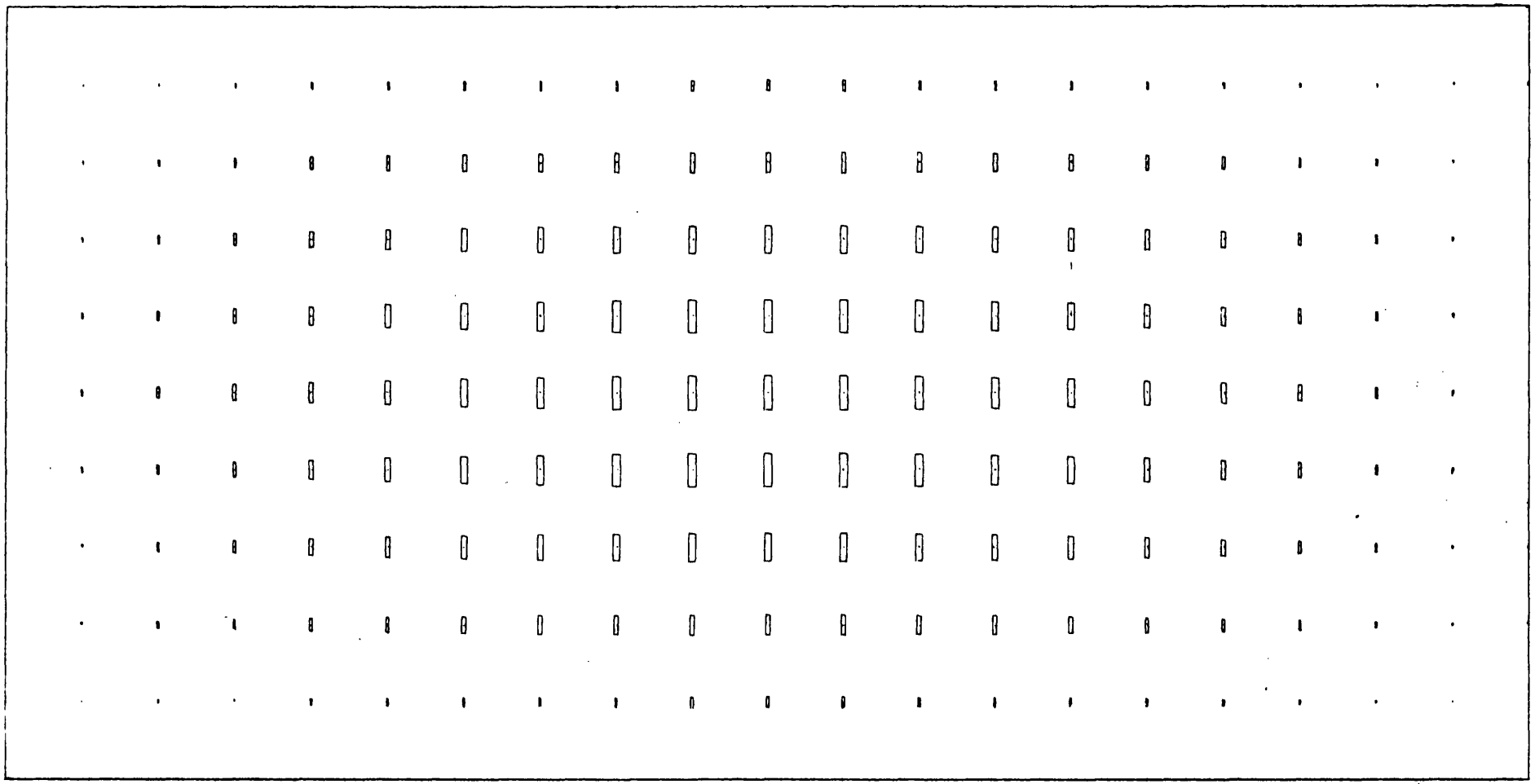

FIG. 4.52 DYNAMIC DISPLAY SEQUENCE

Field distribution for the $TM_{11}$ mode. Reference angle long the wavelength equal to $360^{o}$.

## 4.11 REPRESENTATION OF GENERAL VOLUME FIELDS

The arrow assembly diagrams presented in the previous examples depicted fields which are calculated on given reference planes. In order to produce diagrams of fields which are defined over a volume, the same technique is applied. First , plane samples are taken in the volume and then arrow assembly diagrams are generated as before for each plane sample.

The only difference between the technique used in the previous examples and the one corresponding to fields defined over an entire 3-dimensional region occurs in the field normalization. Now, instead of normalizing the field components with respect to the maximum field component on the plane sample , as in the previous cases, the maximum existing field component in the volume is used to normalize each plane sample. The number of diagrams it may become necessary to produce in order to obtain a reasonable description of the field behaviour inside a volume, by means of plane samples , depends on the way in which the nodal points are distributed in the region and on the complexity of the vector field itself. For instance, regions showing geometric symmetry and supporting relatively simple field distributions can, in some cases, be well described by using only 3 plane samples, taken in parallel to the xy, yz and xz planes, respectively. More complicated fields may require a greater number of plane sections to become pictorially evident.

Examples of the latter type of field are shown in Fig.(4.54)to Fig.(4.64) and in Fig.(4.66) to Fig.(4.71). The first set of diagrams represents the electric field inside the one-port microwave junction, shown in Fig.(4.53), when the reference plane is excited by the main guide dominant $TE_{10}$ mode. In order to obtain the field

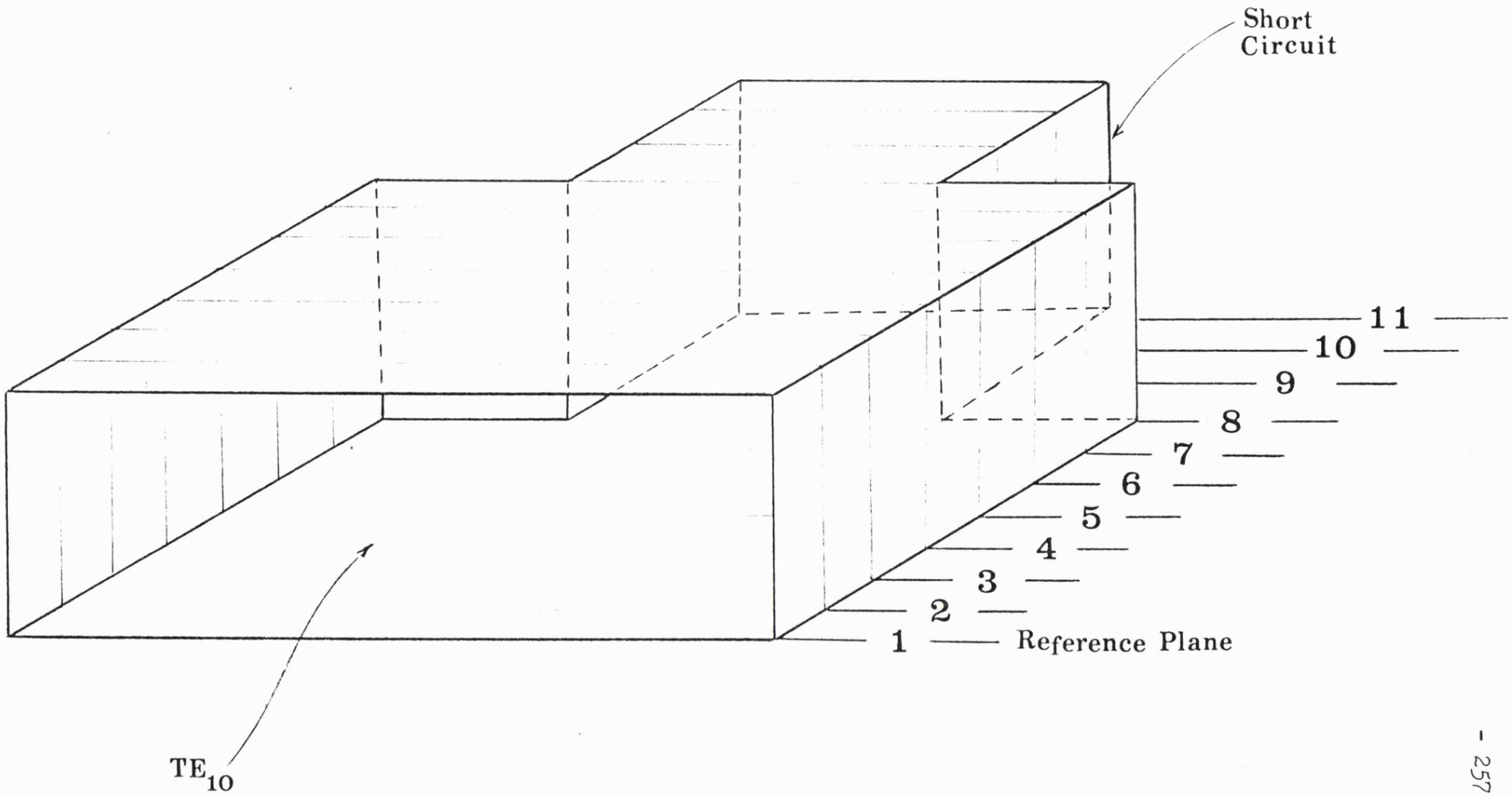


FIG. 4.53 MICROWAVE JUNCTION AND SAMPLING PLANES.

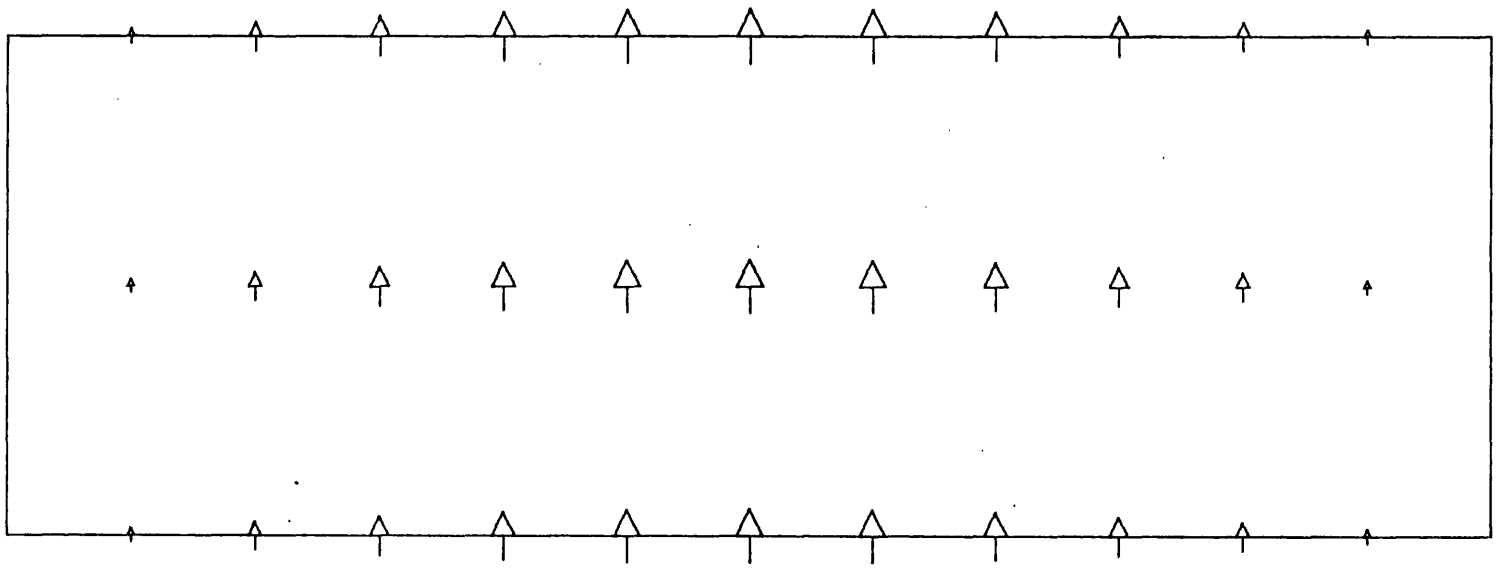

1

FIG. 4.54 PLANE SAMPLE

Sample No. 1 of the microwave junction of Fig.(4.53). The $TE_{10}$ electric driving field is shown.

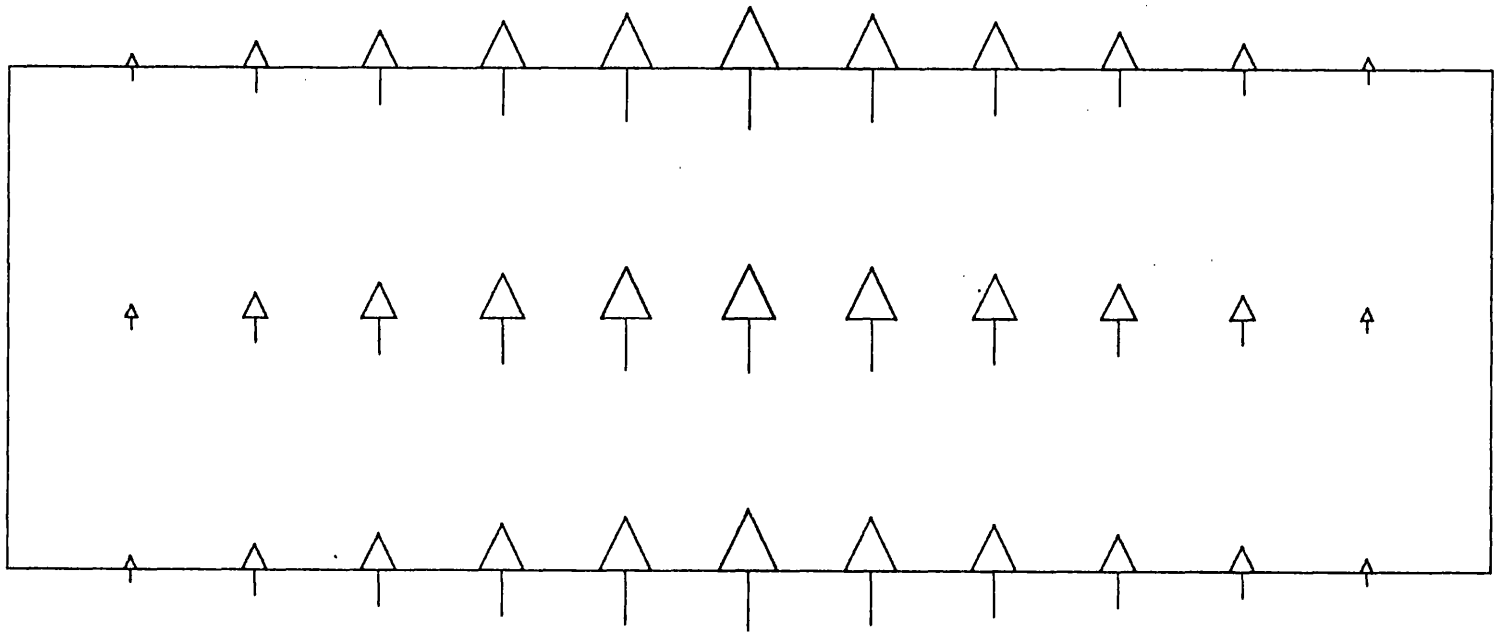

2

FIG. 4.55 PLANE SAMPLE

Sample No. 2 of the electric field inside the microwave junction of Fig. (4.53).

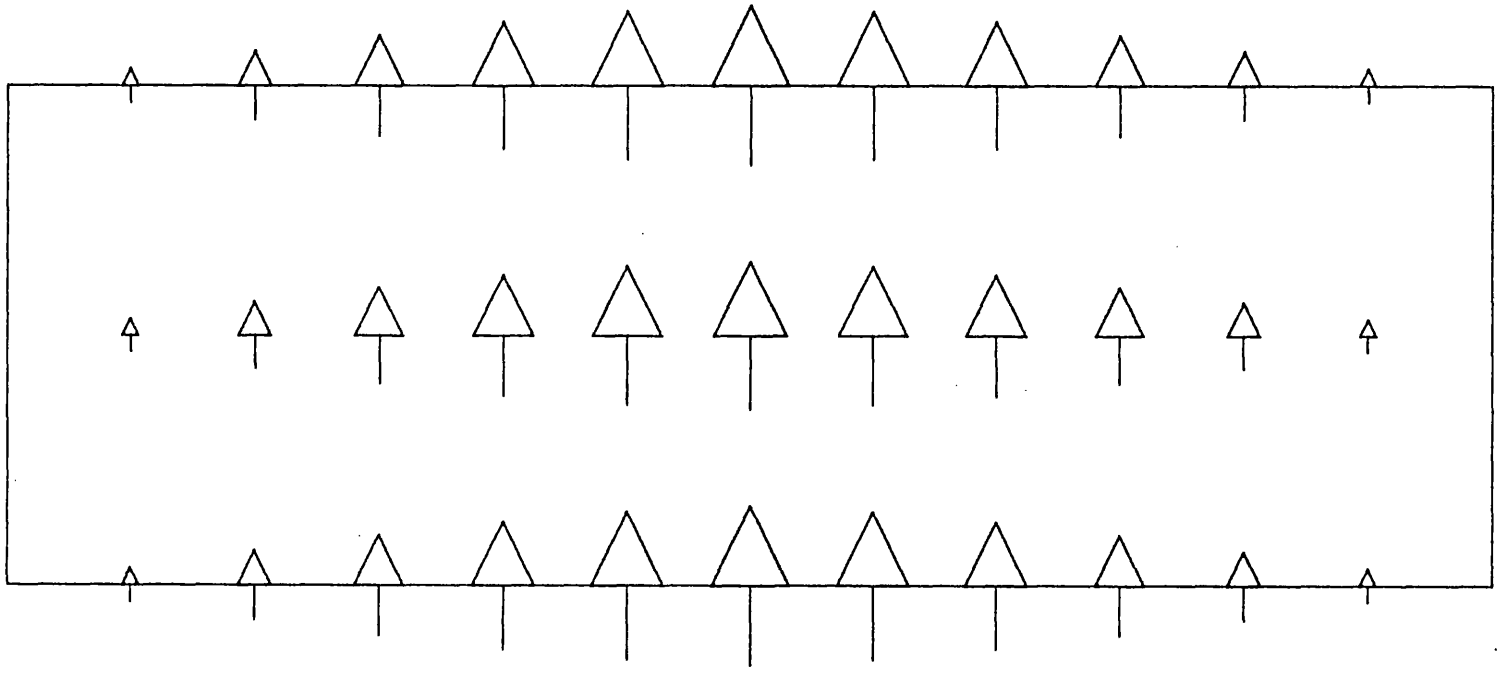

3

FIG. 4.56 PLANE SAMPLE

Sample No. 3 of the electric field inside the microwave junction of Fig.(4.53).

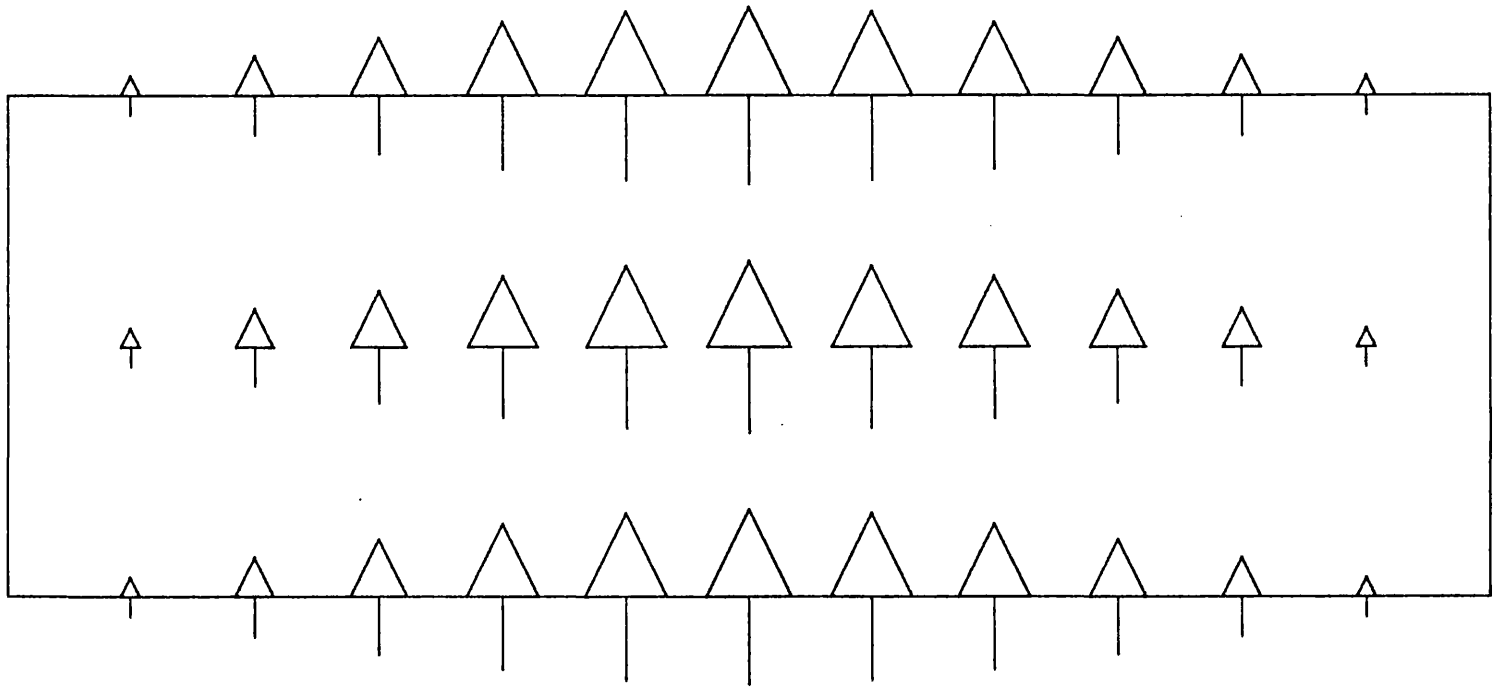

4

FIG. 4.57 PLANE SAMPLE

Sample No. 4 of the electric field inside the microwave junction of Fig.(4.53).

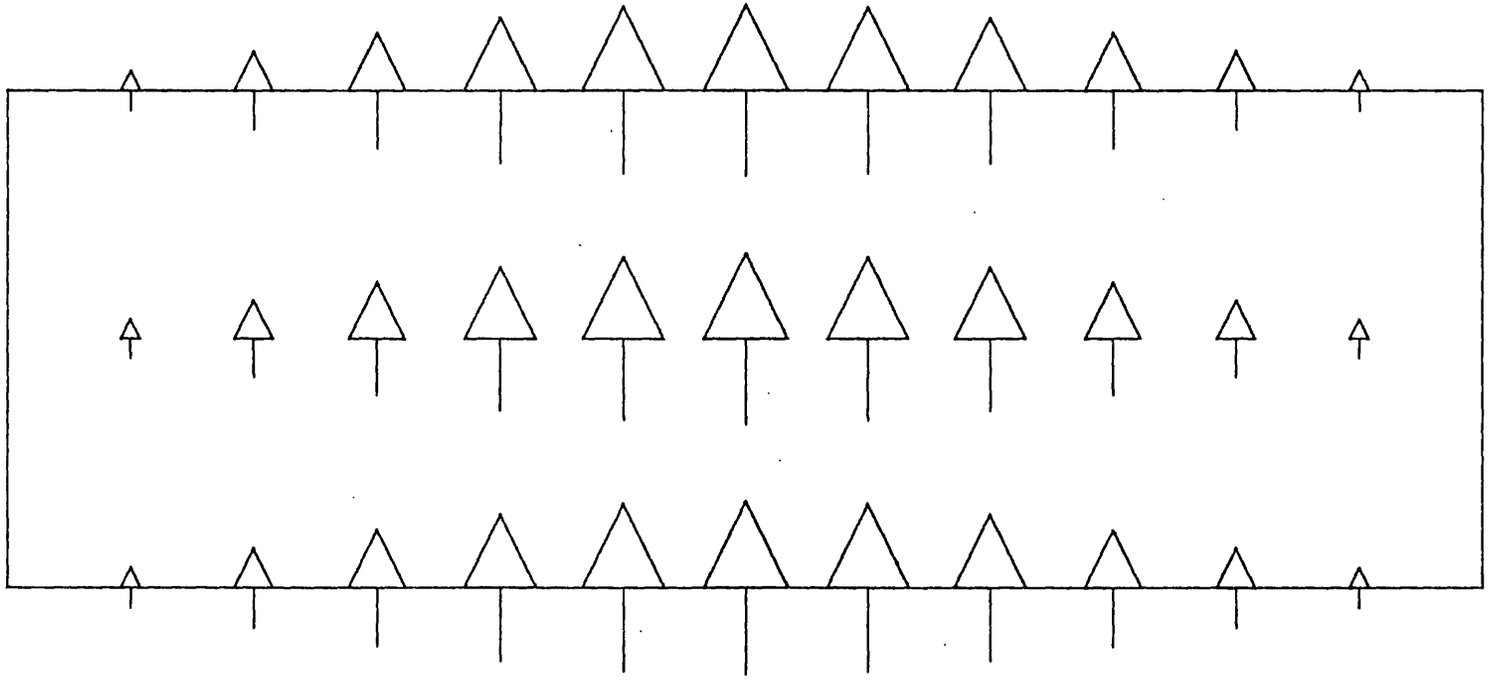

5

FIG. 4.58 PLANE SAMPLE

Sample No. 5 of the electric field inside the microwave junction of Fig.(4.53).

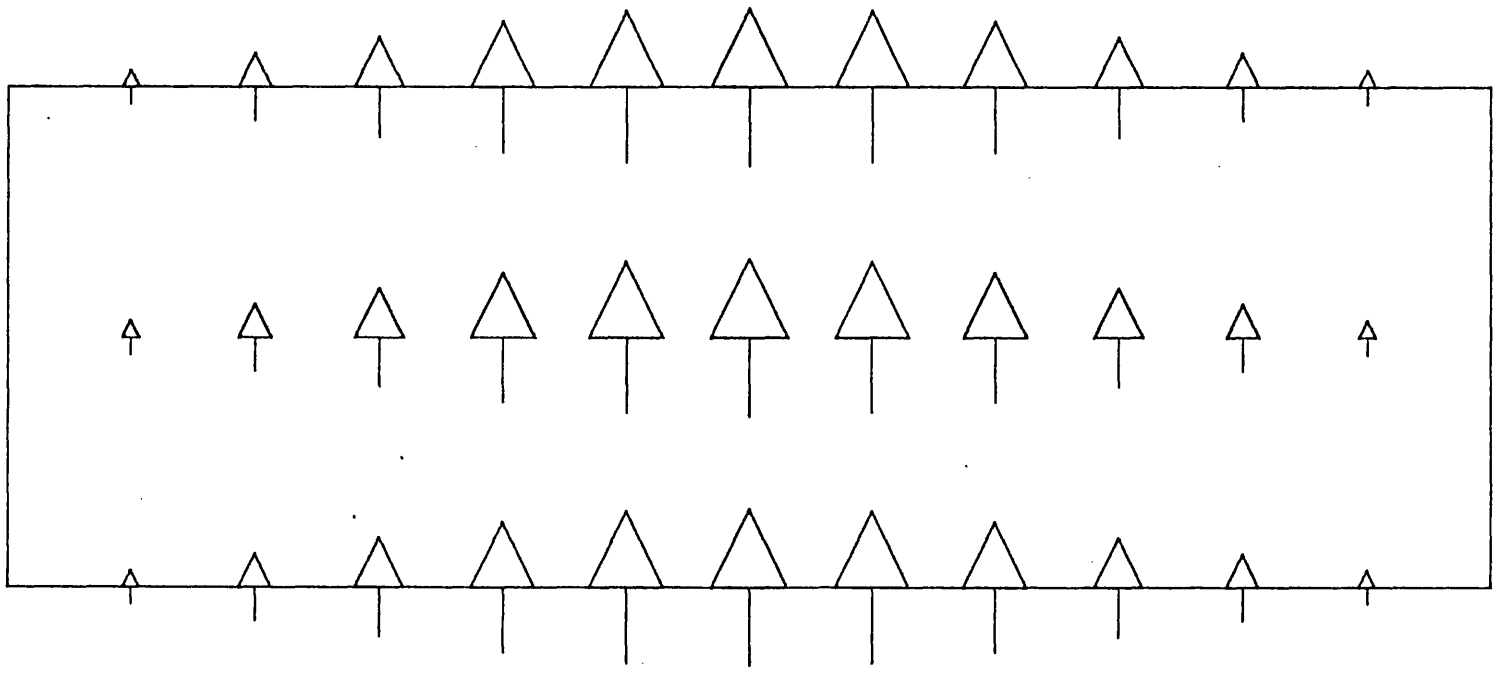

6

FIG. 4.59 PLANE SAMPLE

Sample No. 6 of the electric field inside the microwave junction of Fig.(4.53).

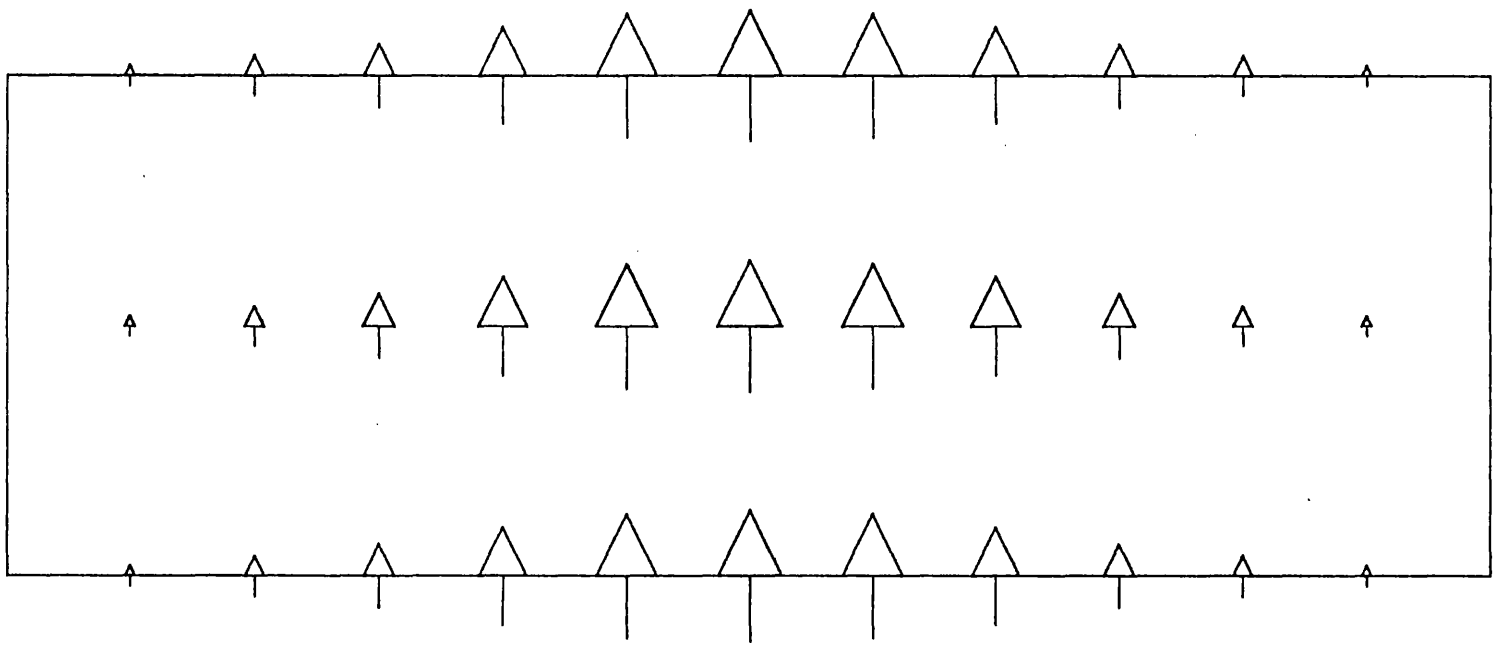

7

FIG. 4.60 PLANE SAMPLE

Sample No. 7 of the electric field inside the microwave junction of Fig.(4.53).

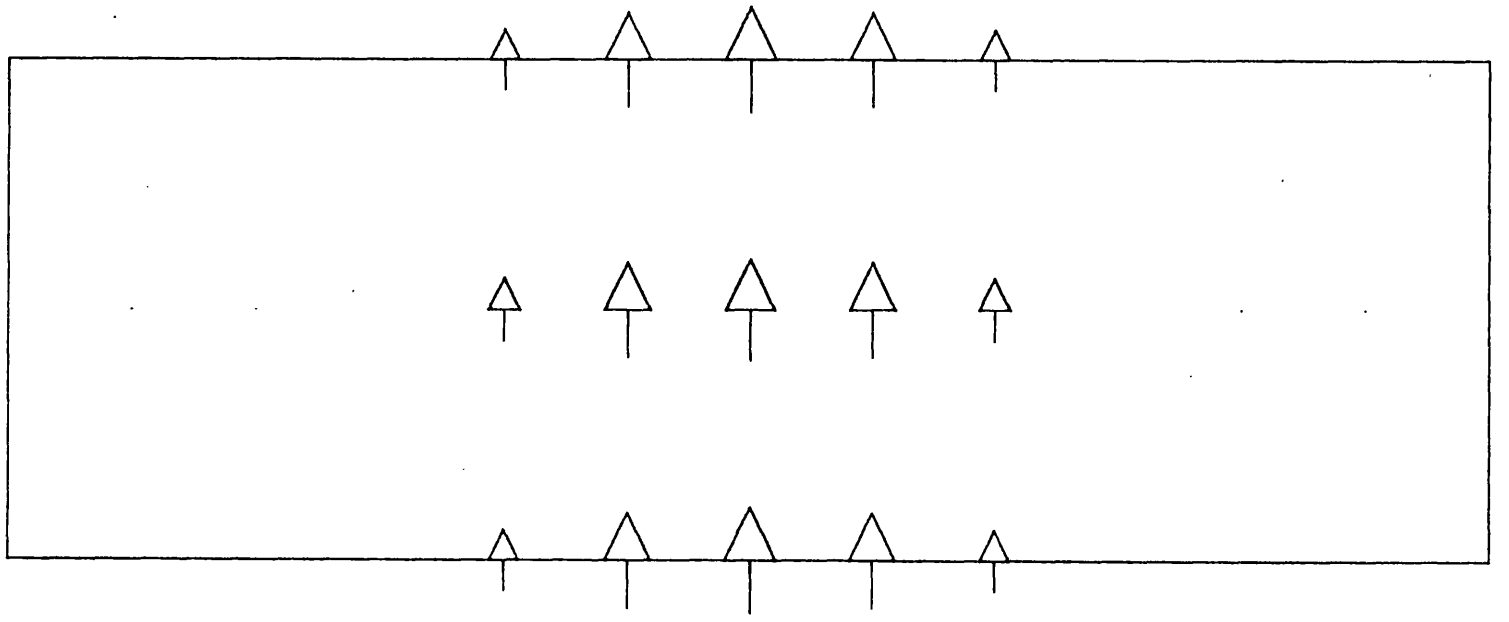

8

FIG. 4.61 PLANE SAMPLE

Sample No. 8 of the electric field inside the microwave junction of Fig.(4.53).

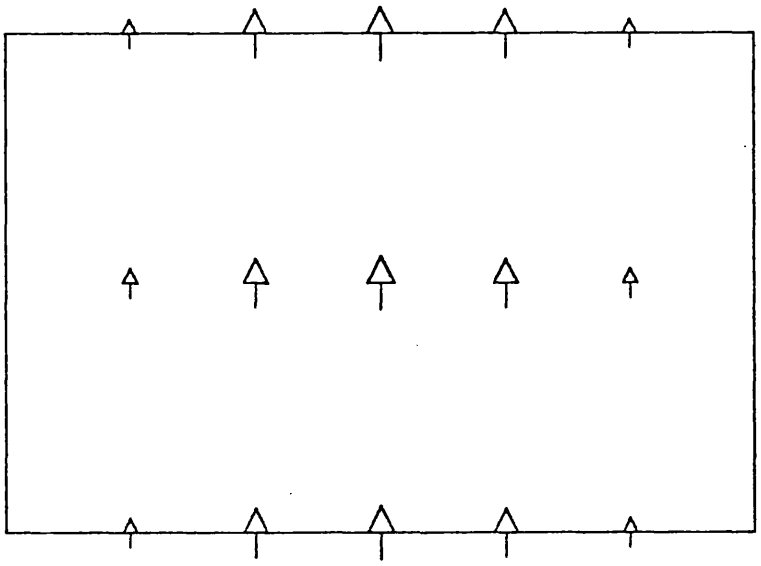

9

FIG. 4.62 PLANE SAMPLE

Sample No. 9 of the electric field (inside the narrower guide) of the microwave junction of Fig.(4.53).

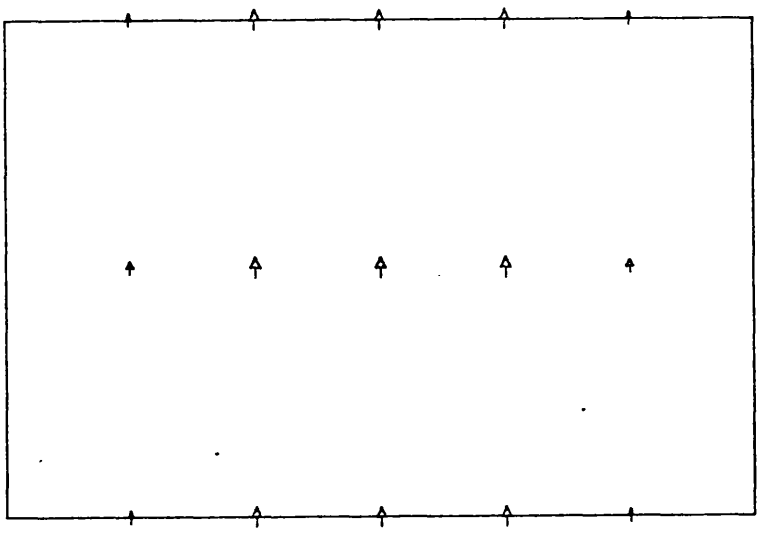

10

FIG. 4.63 PLANE SAMPLE

Sample No. 10 of the electric field inside the microwave junction of Fig.(4.53).

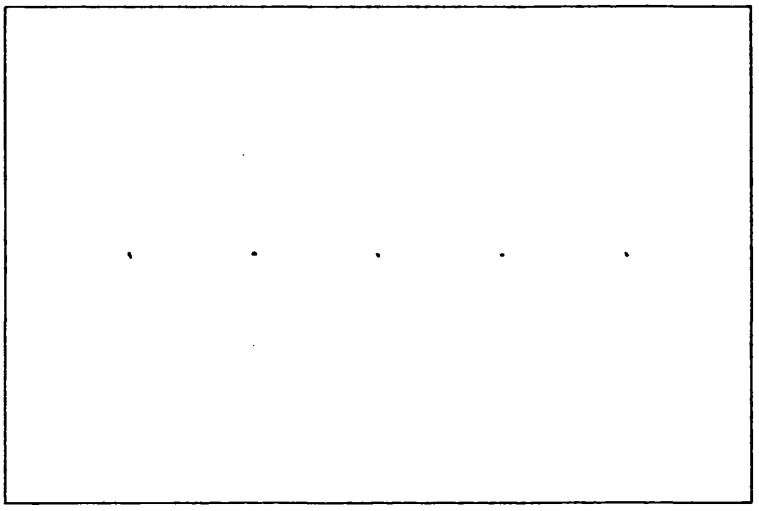

11

FIG. 4.64 PLANE SAMPLE

Sample No. 11 of the electric field on the short circuit plate terminating the microwave junction of Fig.(4.53).

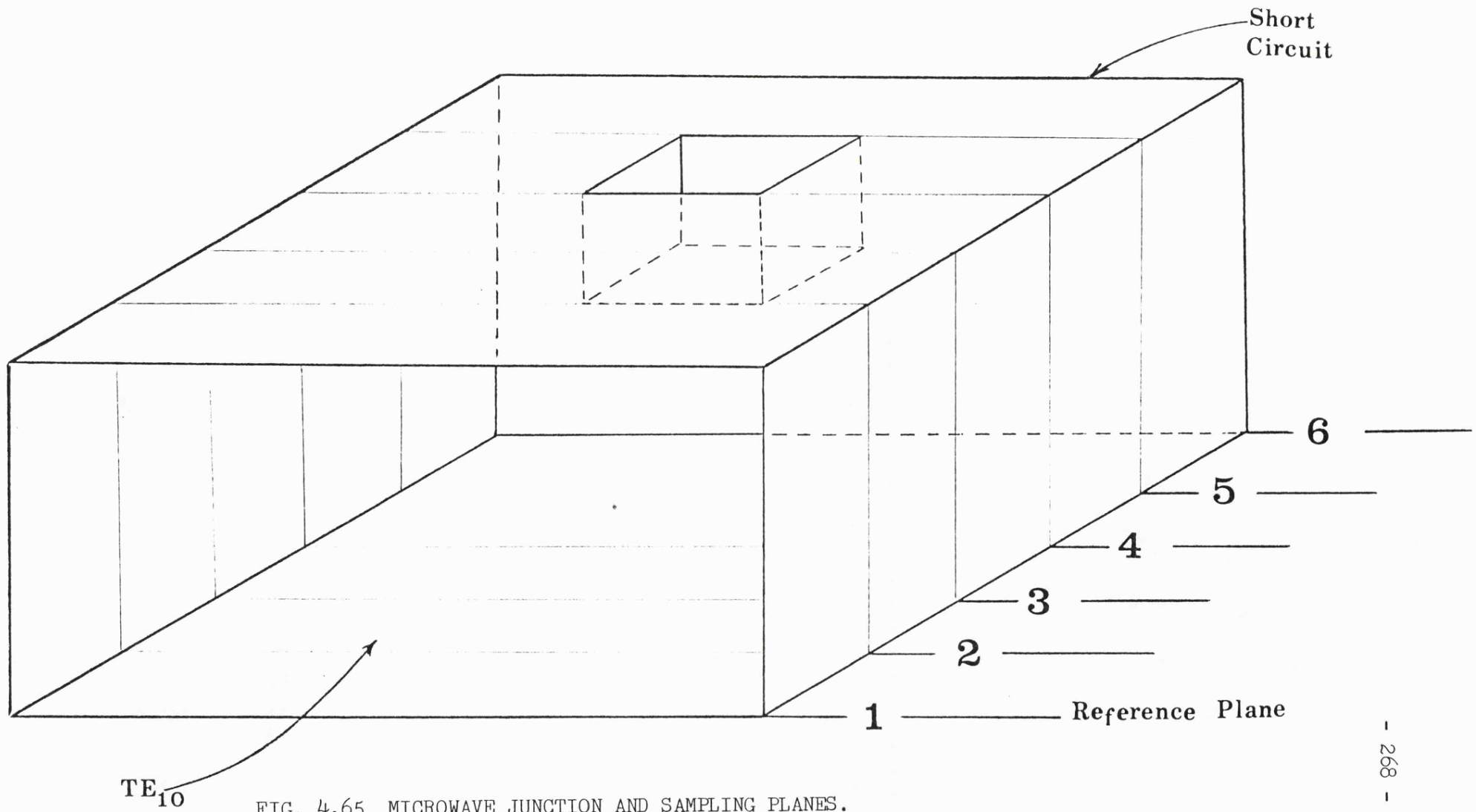


FIG. 4.65 MICROWAVE JUNCTION AND SAMPLING PLANES.

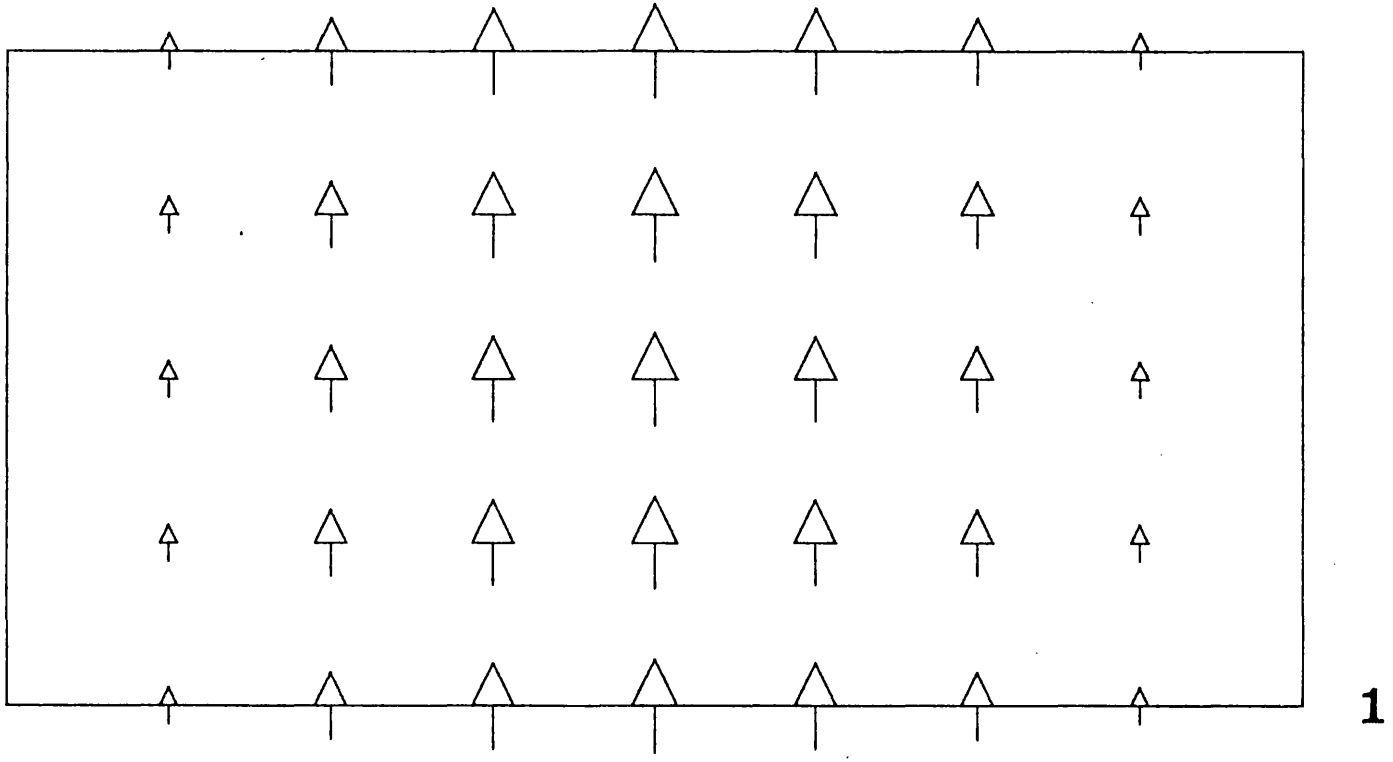


FIG. 4.66 PLANE SAMPLE

$TE_{10}$ field (electric) on the reference plane (sample No. 1) of the microwave junction in Fig.(4.65).

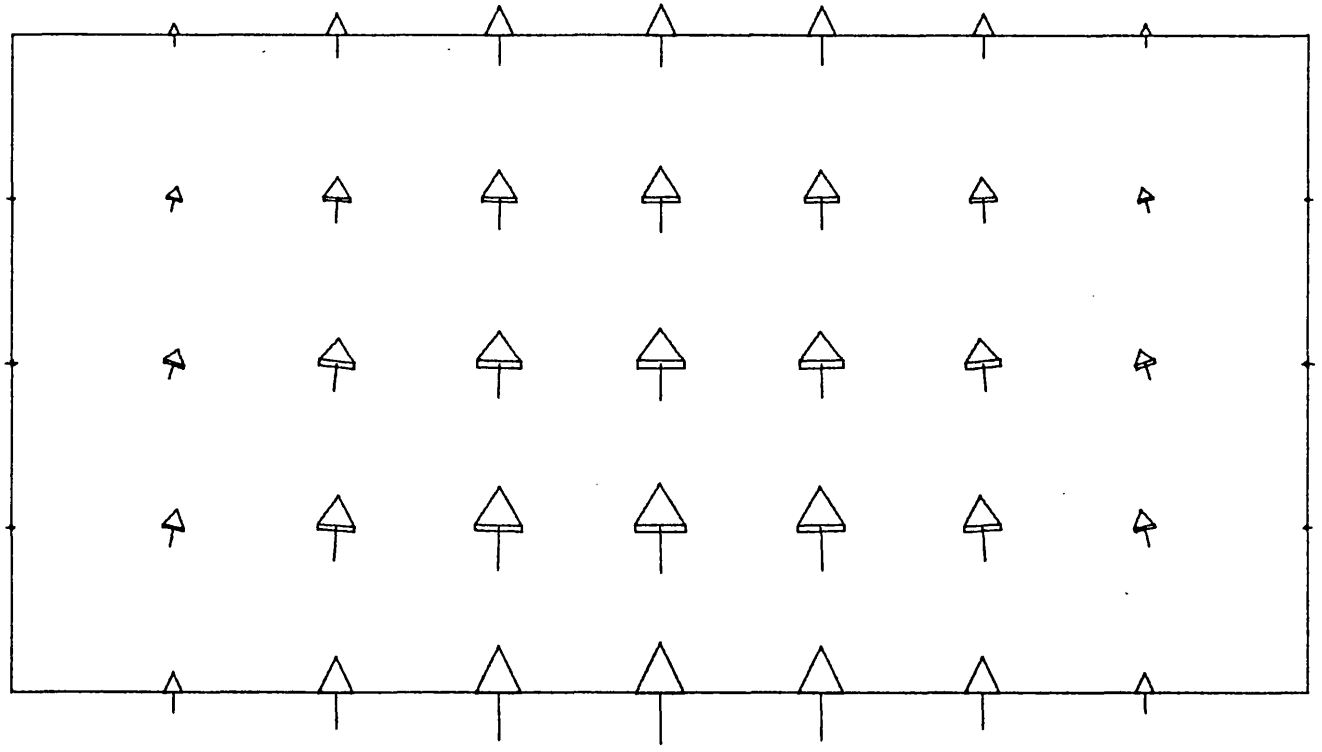

2

FIG. 4.67 PLANE SAMPLE

Sample No. 2. Note the inclination of the electric field vectors towards the rectangular post of the junction of Fig.(4.65).

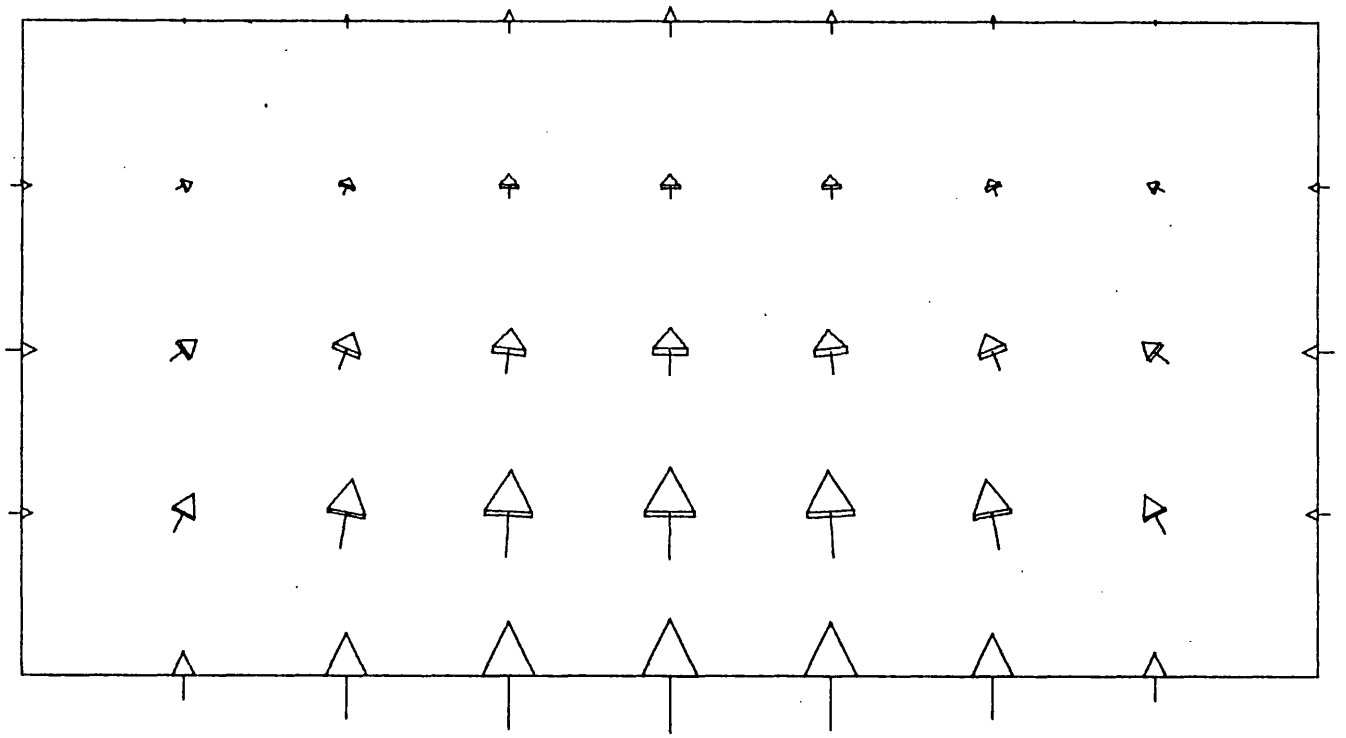

3

FIG. 4.68 PLANE SAMPLE

Sample No. 3 of the electric field inside the microwave junction of Fig.(4.65).

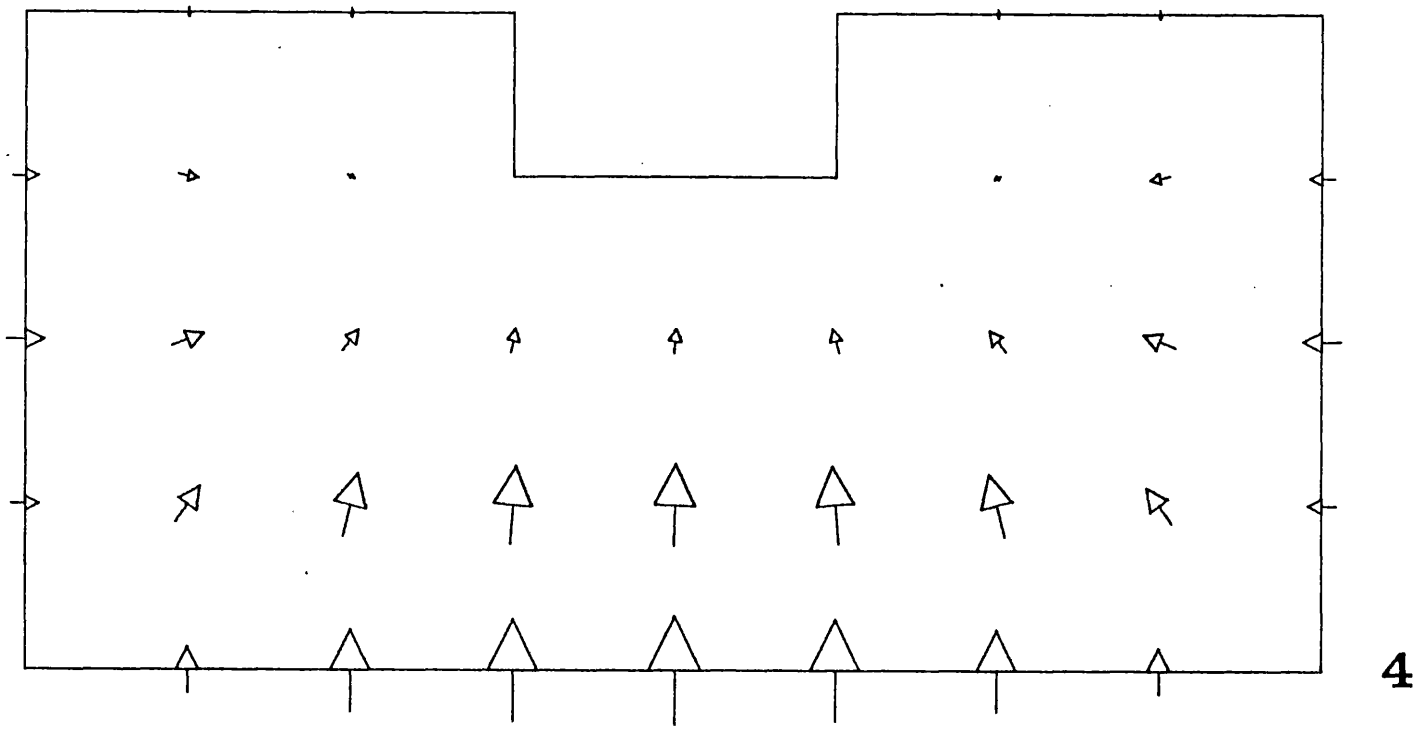


FIG. 4.69 PLANE SAMPLE

Sample No. 4 of the electric field inside the microwave junction of Fig.(4.65).

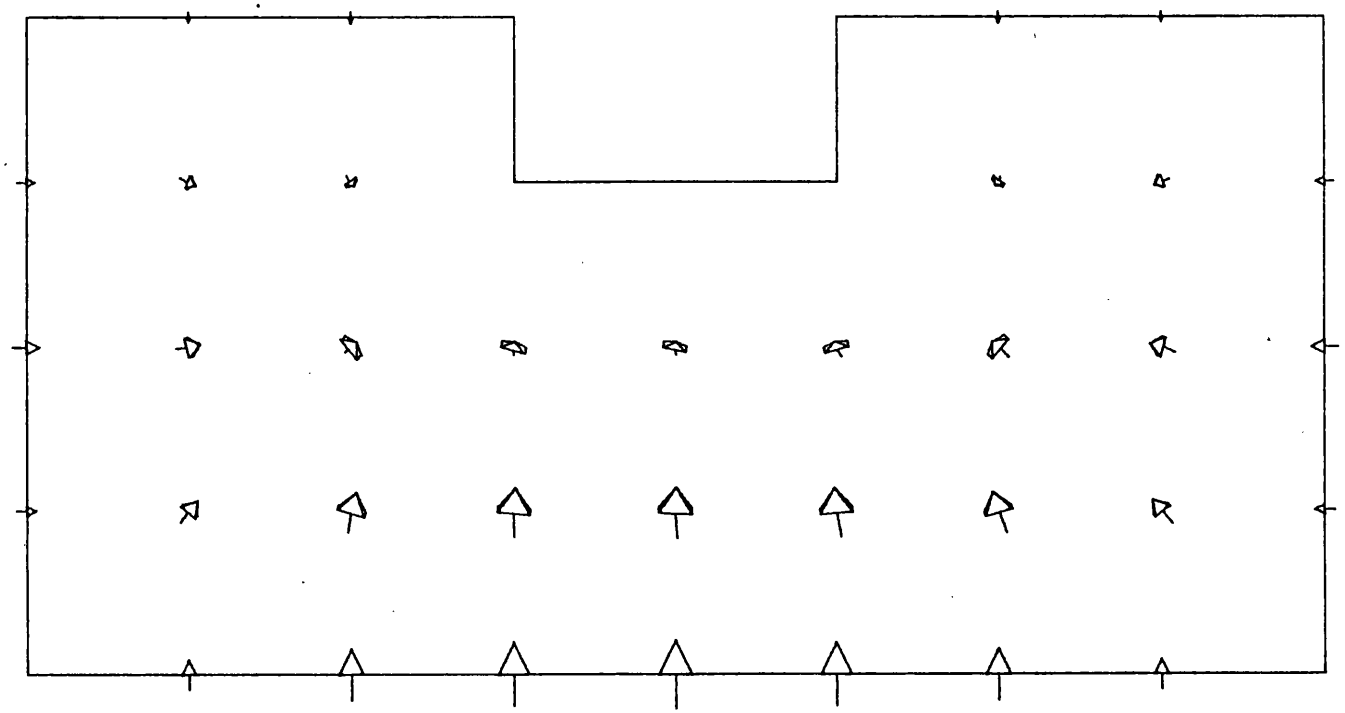

5

FIG. 4.70 PLANE SAMPLE

Sample No. 5 of the electric field inside the microwave junction of Fig.(4.65). Because of the rectangular post, the electric field inclinates towards the propagation direction, as shown.

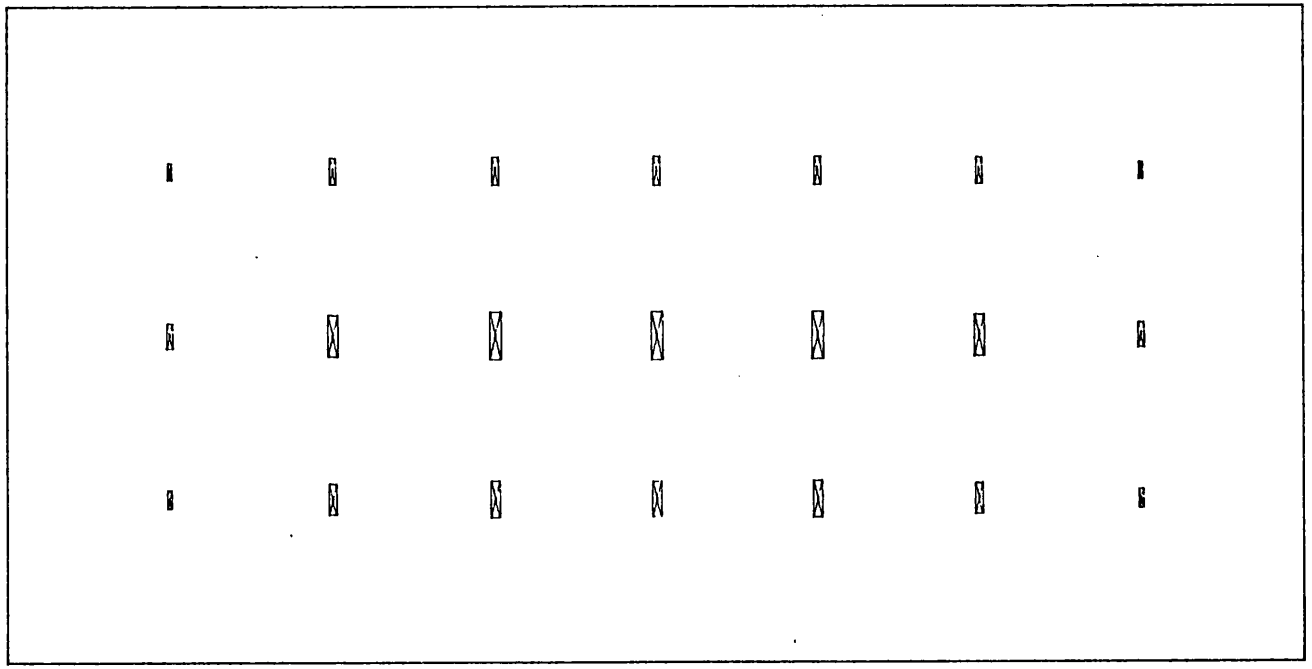

6

FIG. 4.71 PLANE SAMPLE

Sample No. 6 of the electric field on the short circuit terminating the microwave junction of Fig.(4.65). Note the $TM_{11}$ like field distribution on the short plate generated by the perturbation of the guide geometry.

values, the volume of the junction has been divided into elementary hexahedra and the vector field components at each element vertex (nodal points) calculated through a vector variational finite element technique. The field calculation has been performed by Maile and Ferrari at Cambridge University Engineering Department and the arrow assembly diagrams produced by the author at Leicester University. The standing wave pattern inside the junction is noticeable through the diagrams.

The second set of pictures corresponds to the electric field distribution inside the one-port microwave junction shown in Fig.(4.65) obtained under conditions similar to those used for the first junction. In both sets of diagrams, only transverse plane samples have been used to produce the graphic image of the field distribution although other plane samples could have been chosen.

## 4.12 FIELD INFORMATION FROM THE SCALAR NODAL VALUE DISTRIBUTION

As shown in Chapter 2, the electromagnetic field distribution inside a general cross-section waveguide can be obtained through the generating function of the mode under consideration and its gradient. When the waveguide has been numerically analysed by the finite element method,instead of having a closed form of the generating function in which to perform the differentiation, the calculation of the gradient must be carried out over a set of scalar values distributed over the cross-section.

While the analytical process of differentiating functions which are given in closed form is a well ruled process in which a closed form of result is always obtained, the process of differentiating

over a set of numerical values may not give satisfactory results. This happens because the numerical differentiation is , in general, unstable unless for nodal distributions describing an analytic complex variable function[86][87]. Here, the state of the art is such that one should not look for the best technique to apply in all cases but adopt the realistic view point that any process which gives sufficiently accurate results with a reasonable efficiency is good enough for the problem in hand.

There are in the literature, several propositions which can be used for differentiating a function through a set of representative nodal values[69][88][89][90][91]. In general , those propositions interpolate the numeric distribution without taking into account the nature of the technique by which the representative nodal values have been obtained. There are also excellent published works which utilize the actual characteristics of the high-order finite element method[92][93] in order to perform the numerical differentiation consistently.

It is beyond the scope of this work to describe and experiment with the known methods of obtaining numerical derivatives in order to produce some enlightening evidence or to search for a more general process. This certainly is a topic for future development in connection with the technique of generating arrow assembly diagrams.

Because the problem being considered in this thesis consists of obtaining a visual approximation for the electromagnetic field distribution inside waveguides such that a clear understanding of the physical behaviour of the guiding structure becomes possible, simple differentiation techniques can be used.

To illustrate this point , consider the application of the centred difference formula[94]

$$\frac{\delta}{\delta x^i} f(x^1, x^2)\Big|_{f=f_0} = \frac{1}{2h^i}(f_r - f_l) \qquad (4.186)$$

where $2h^i$ is the distance in the $x^i$ direction between the nodal values $f_r$ and $f_l$ which are immediately to the right and to the left (or above and below) of the central point $f_0$ for which the derivative is calculated; to the nodal distribution in Map.(3.21) ($TE_{10}$ mode; typical rectangular waveguide).The results are presented in Map.(4.1) and Map.(4.2) where the derivatives on the cross-section narrower sides have been obtained by applying the specific boundary conditions.

To obtain the expressions for the field distribution we recast eq.(2.138) to eq.(2.141), in the modified form:

$$k_{cn}^{-1}\,\underline{H}_{zn} = \underline{u}_z\,\mathrm{Re}\Big(k_{cn}\,G_n^{(2)}\exp.\big(i\,[\omega t - [f_n^2 - 1]^{\frac{1}{2}}\,z'\big)\Big) \qquad (4.187)$$

$$k_{cn}^{-1}\,\underline{H}_{Tn} = \mathrm{Re}\Big(i\,[f_n^2 - 1]^{\frac{1}{2}}\,\nabla_T\,G_n^{(2)}\exp.\big(i\,[\omega t - [f_n^2 - 1]^{\frac{1}{2}}\,z'\big)\Big) \qquad (4.188)$$

$$\beta_n^{-1}\,\underline{E}_{Tn} = \mathrm{Re}\Big(-i\,\frac{Z_0\,f_n}{[f_n^2 - 1]^{\frac{1}{2}}}\,\underline{u}_z \times \nabla_T G_n^{(2)}\exp.\big(i\,[\omega t - [f_n^2 - 1]^{\frac{1}{2}}\,z'\big)\Big) \qquad (4.189)$$

| | | | | | | |
|---|---|---|---|---|---|---|
| 0.00 | 1.75 | 3.03 | 3.50 | 3.03 | 1.75 | 0.00 |
| 0.00 | 1.75 | 3.03 | 3.50 | 3.03 | 1.75 | 0.00 |
| 0.00 | 1.75 | 3.03 | 3.50 | 3.03 | 1.75 | 0.00 |
| 0.00 | 1.75 | 3.03 | 3.50 | 3.03 | 1.75 | 0.00 |
| 0.00 | 1.75 | 3.03 | 3.50 | 3.03 | 1.75 | 0.00 |
| 0.00 | 1.75 | 3.03 | 3.50 | 3.03 | 1.75 | 0.00 |
| 0.00 | 1.75 | 3.03 | 3.50 | 3.03 | 1.75 | 0.00 |

MAP 4.1 : X-Component of $\nabla_T G_{10}$ obtained from the nodal values distribution in Map.(3.21).

| | | | | | | |
|---|---|---|---|---|---|---|
| 0.00 | 0.00 | 0.00 | 0.00 | 0.00 | 0.00 | 0.00 |
| 0.00 | 0.00 | 0.00 | 0.00 | 0.00 | 0.00 | 0.00 |
| 0.00 | 0.00 | 0.00 | 0.00 | 0.00 | 0.00 | 0.00 |
| 0.00 | 0.00 | 0.00 | 0.00 | 0.00 | 0.00 | 0.00 |
| 0.00 | 0.00 | 0.00 | 0.00 | 0.00 | 0.00 | 0.00 |
| 0.00 | 0.00 | 0.00 | 0.00 | 0.00 | 0.00 | 0.00 |
| 0.00 | 0.00 | 0.00 | 0.00 | 0.00 | 0.00 | 0.00 |

MAP 4.2 : Y-Component of $\nabla_T G_{10}$ obtained from the nodal values distribution in Map.(3.21). The repeated values 0.00 are shown for convenience in the presentation of the example.

where $Z_0 = (\mu/\varepsilon)^{\frac{1}{2}} \approx 120\,\pi$ Ohms.

Taking the real part in eq.(4.187) to eq.(4.189) we get , explicitly:

$$k_{cn}^{-1}\,\underline{H}_{zn} = k_{cn}\cos[\omega t - (f_n^2 - 1)^{\frac{1}{2}}\,z']\,\underline{u}_z\,G_n^{(2)} \qquad (4.190)$$

$$k_{cn}^{-1}\,\underline{H}_{Tn} = -\,(f_n^2 - 1)^{\frac{1}{2}}\sin[\omega t - (f_n^2 - 1)^{\frac{1}{2}}\,z']\,\nabla_T\,G_n^{(2)} \qquad (4.191)$$

$$\beta_n^{-1}\,E_{Tn} = \frac{Z_0\,f_n}{(f_n^2 - 1)^{\frac{1}{2}}}\sin[\omega t - (f_n^2 - 1)^{\frac{1}{2}}\,z']\,\underline{u}_z \times \nabla_T G_n^{(2)} \qquad (4.192)$$

Using eq.(4.190) to eq.(4.192) the vector components at each node of a plane sample can be calculated at a given frequency ($f_n$) for the specific $TE_{10}$ mode ($k_c$) at a frozen phase ($\omega t$).

For the present example let transverse plane samples be considered and also, make

$$\omega t = \frac{\pi}{2} \qquad (4.193)$$

$$f_n = \sqrt{5} \qquad (4.194)$$

The particular broader cross-section side length chosen (Appendix 3) is such that the cut-off wave-number for the $TE_{10}$ mode is:

$$k_{cn} = \frac{\pi}{2} \qquad (4.195)$$

Substituting eq.(4.193) to eq.(4.195) into eq.(4.190) to eq.(4.192) we get :

$$\underline{H}_{zn} = \underline{u}_z \frac{\pi^2}{4} \sin(2\ z')G_n^{(2)} \tag{4.196}$$

$$\underline{H}_{Tn} = -\pi \cos(2\ z')\nabla_T\ G_n^{(2)} \tag{4.197}$$

$$\underline{E}_{Tn} = 60\sqrt{5}\ \pi\beta_n \cos(2\ z')\ \underline{u}_z \times \nabla_T\ G_n^{(2)} \tag{4.198}$$

The maximum absolute valued component of the transverse electric field occurs for

$$z' = \tfrac{1}{2} n\ \pi \tag{4.199}$$

$$(n = 0,1,2,\ldots)$$

and is given by:

$$\left| \underline{E}_{Tn} \right|_{max} = 60\sqrt{5}\ \pi\beta_n \left| \nabla_T\ G_n^{(2)} \right|_{max} \tag{4.200}$$

Similarly for the magnetic field, according to Map.(3.21) and Map.(4.1) , we have

$$\frac{\pi^2}{4} \left| G_n^{(2)} \right|_{max} > \pi \left| \nabla_T\ G_n^{(2)} \right|_{max} \tag{4.201}$$

Therefore, the maximum absolute valued magnetic field component can be written in the form:

$$\left| \underline{H}_{zn} \right|_{max} = \frac{\pi^2}{4} \left| G_n^{(2)} \right|_{max} \tag{4.202}$$

The normalized field components $\underline{h}_{zn}$, $\underline{h}_{Tn}$ and $\underline{e}_{Tn}$ , can now be written according to eq.(4.196) to eq.(4.198) and eq.(4.200) and eq.(4.202) in the form:

$$\underline{h}_{zn} = \left[ \underline{u}_z \frac{G_n^{(2)}}{\left| G_n^{(2)} \right|_{max}} \right] \sin 2 z' \tag{4.203}$$

$$\underline{h}_{Tn} = - \left[ \frac{4}{\pi} \frac{\nabla_T G_n^{(2)}}{\left| G_n^{(2)} \right|_{max}} \right] \cos 2 z' \tag{4.204}$$

$$\underline{e}_{Tn} = \left[ \frac{{}_T G_n^{(2)}}{\left| \nabla_T G_n^{(2)} \right|_{max}} \times \underline{u}_z \right] \cos 2 z' \tag{4.205}$$

Knowing the nodal value distribution of Map.(3.21) and the transverse gradient distributions of Map.(4.1) and Map.(4.2), the normalized vector component distributions in Map.(4.3) to Map.(4.7), which correspond to the terms between brackets in eq.(4.203) to eq.(4.204), are obtained.

| | | | | | | |
|---|---|---|---|---|---|---|
| -1.00 | -0.87 | -0.50 | 0.00 | 0.50 | 0.87 | 1.00 |
| -1.00 | -0.87 | -0.50 | 0.00 | 0.50 | 0.87 | 1.00 |
| -1.00 | -0.87 | -0.50 | 0.00 | 0.50 | 0.87 | 1.00 |
| -1.00 | -0.87 | -0.50 | 0.00 | 0.50 | 0.87 | 1.00 |
| -1.00 | -0.87 | -0.50 | 0.00 | 0.50 | 0.87 | 1.00 |
| -1.00 | -0.87 | -0.50 | 0.00 | 0.50 | 0.87 | 1.00 |
| -1.00 | -0.87 | -0.50 | 0.00 | 0.50 | 0.87 | 1.00 |

MAP 4.3 : Distribution of the normalized $h_z$ component (eq.(4.203)) for the $TE_{10}$ mode in a typical waveguide.

| | | | | | | |
|---|---|---|---|---|---|---|
| 0.00 | 0.00 | 0.00 | 0.00 | 0.00 | 0.00 | 0.00 |
| 0.00 | 0.00 | 0.00 | 0.00 | 0.00 | 0.00 | 0.00 |
| 0.00 | 0.00 | 0.00 | 0.00 | 0.00 | 0.00 | 0.00 |
| 0.00 | 0.00 | 0.00 | 0.00 | 0.00 | 0.00 | 0.00 |
| 0.00 | 0.00 | 0.00 | 0.00 | 0.00 | 0.00 | 0.00 |
| 0.00 | 0.00 | 0.00 | 0.00 | 0.00 | 0.00 | 0.00 |
| 0.00 | 0.00 | 0.00 | 0.00 | 0.00 | 0.00 | 0.00 |

MAP 4.4 : Distribution of the normalized $h_y$ component for the $TE_{10}$ mode in a typical waveguide (eq.(4.204)). The repeated zeros are shown for illustrative purposes only.

| | | | | | | |
|---|---|---|---|---|---|---|
| 0.00 | 0.32 | 0.55 | 0.64 | 0.55 | 0.32 | 0.00 |
| 0.00 | 0.32 | 0.55 | 0.64 | 0.55 | 0.32 | 0.00 |
| 0.00 | 0.32 | 0.55 | 0.64 | 0.55 | 0.32 | 0.00 |
| 0.00 | 0.32 | 0.55 | 0.64 | 0.55 | 0.32 | 0.00 |
| 0.00 | 0.32 | 0.55 | 0.64 | 0.55 | 0.32 | 0.00 |
| 0.00 | 0.32 | 0.55 | 0.64 | 0.55 | 0.32 | 0.00 |
| 0.00 | 0.32 | 0.55 | 0.64 | 0.55 | 0.32 | 0.00 |

MAP 4.5 : Distribution of the normalized $h_x$ component (eq.(4.204)) for the $TE_{10}$ mode in a typical waveguide.

| | | | | | | |
|---|---|---|---|---|---|---|
| 0.00 | 0.00 | 0.00 | 0.00 | 0.00 | 0.00 | 0.00 |
| 0.00 | 0.00 | 0.00 | 0.00 | 0.00 | 0.00 | 0.00 |
| 0.00 | 0.00 | 0.00 | 0.00 | 0.00 | 0.00 | 0.00 |
| 0.00 | 0.00 | 0.00 | 0.00 | 0.00 | 0.00 | 0.00 |
| 0.00 | 0.00 | 0.00 | 0.00 | 0.00 | 0.00 | 0.00 |
| 0.00 | 0.00 | 0.00 | 0.00 | 0.00 | 0.00 | 0.00 |
| 0.00 | 0.00 | 0.00 | 0.00 | 0.00 | 0.00 | 0.00 |

MAP 4.6 : Distribution of the normalized $e_x$ component (eq.(4.205)) for the $TE_{10}$ mode in a typical waveguide. The repeated zeros are shown for illustrative purposes only.

| | | | | | | |
|---|---|---|---|---|---|---|
| 0.00 | -0.50 | -0.87 | -1.00 | -0.87 | -0.50 | 0.00 |
| 0.00 | -0.50 | -0.87 | -1.00 | -0.87 | -0.50 | 0.00 |
| 0.00 | -0.50 | -0.87 | -1.00 | -0.87 | -0.50 | 0.00 |
| 0.00 | -0.50 | -0.87 | -1.00 | -0.87 | -0.50 | 0.00 |
| 0.00 | -0.50 | -0.87 | -1.00 | -0.87 | -0.50 | 0.00 |
| 0.00 | -0.50 | -0.87 | -1.00 | -0.87 | -0.50 | 0.00 |
| 0.00 | -0.50 | -0.87 | -1.00 | -0.87 | -0.50 | 0.00 |

MAP 4.7 : Distribution of the normalized $e_y$ component (eq.(4.205)) for the $TE_{10}$ mode in a typical waveguide.

Once the normalized vector component distributions have been calculated, the displaying plane along the propagation direction is determined by setting the value of the z' co-ordinate. The vector imaging routine can now be used to generate the arrow assembly diagram. Diagrams for $z' = \pi/8$ are presented in Fig.(4.72-a,b and c). The diagrams parameters are, in this case,

$$p = 1.00 \tag{4.206}$$

(Electric Field)

and

$$p = 0.250 \quad ; \quad q = 0.125 \tag{4.207}$$

(Magnetic Field)

Field patterns corresponding to other waveguide modes can be obtained by following a procedure similar to the one outlined in the above example.

## 4.13 DIRECT CALCULATION OF THE VECTOR COMPONENT DISTRIBUTIONS OF GENERAL CROSS-SECTION WAVEGUIDES

The process of differentiating over a set of nodal values becomes unnecessary when a vector finite element formulation is used in order to calculate the vector components on the cross-section of arbitrary shaped waveguides. In this case, the vector components to be used in the imaging routine are directly available and the arrow diagrams can be generated in a straightforward manner.

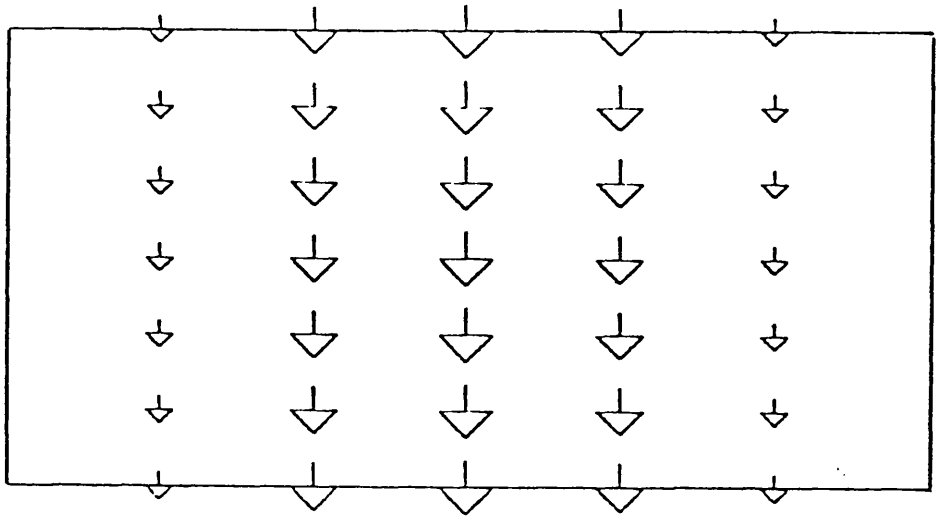

(a) Electric Field

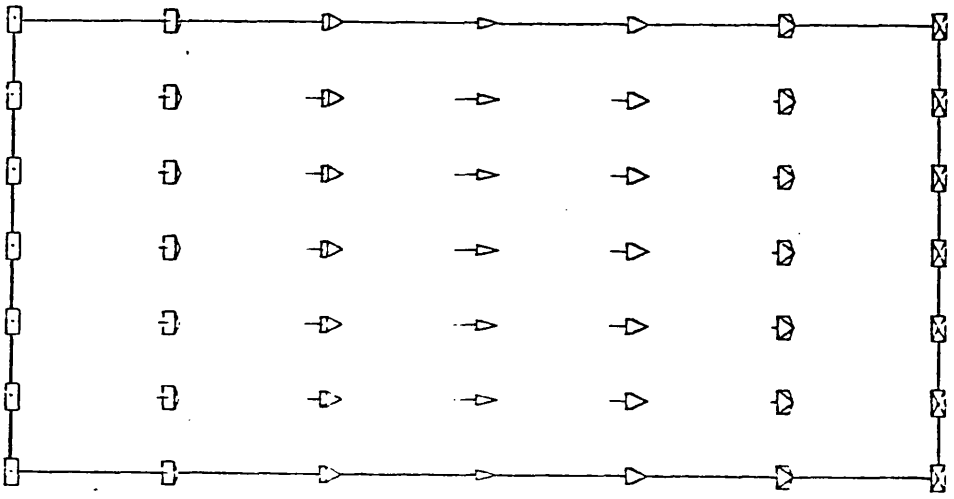

(b) Magnetic Field

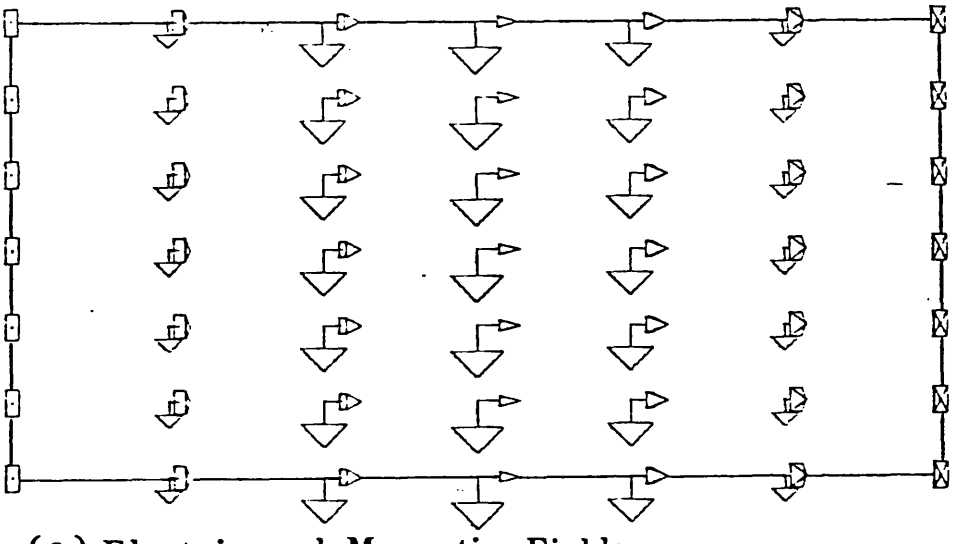

(c) Electric and Magnetic Fields

FIG. 4.72 $TE_{10}$ FIELD DISTRIBUTION FROM THE NODAL VALUES

A finite element technique capable of producing vector components on the cross-section of arbitrary shaped waveguides has been reported at McGill University - Canada - by Konrad[50] in his Ph.D. thesis and related articles have been recently published[51] [52]. Also, a computer program has been written[50] in order to perform the proposed vector finite element analysis and results of specific waveguide propagation problems obtained.

During this research work in Leicester, we did not have the opportunity of using either Konrad's program or its results in order to generate arrow assembly diagrams. In fact, the program if available, would be excessively big to run in the Leicester University Computer. However, it appeared from the study of Konrad's work that the use of the imaging routine proposed here, in order to generate arrow assembly diagrams from his program output, could be done with the same simplicity as for the vector component results obtained by Maile and Ferrari at Cambridge University.

# CHAPTER 5

# CONCLUSION

## 5.1 CRITIQUE

The research project reported in this thesis consisted of the author's investigation into the computation of electromagnetic field distributions in waveguides and their display by computer graphics. It involved the study of the variational approach to waveguide propagation together with the application of the finite element method to the extremization of the waveguide functional. These subjects have of course received extensive treatment elsewhere, and references are supplied in the bibliography.

Our research also involved the study of graphic techniques commonly used for the representation of waveguide fields. This, in its turn, involved the discussion of their applicability to numerically evaluated results. The inadequacy of the conventional field line diagrams to electrodynamical situations such as guided wave propagation is fully characterized. The difficulties with the contour-map technique are discussed. A method for displaying computer evaluated vector fields via graphic terminals and plotters has been developed and is presented in detail. Examples of its application to waveguide propagation problems including 3-D waveguide discontinuity

fields are given. As far as one knows , this subject has not been previously dealt with. In effect, very few references on the matter of computerized display of vector fields could be collected, and no parallel development found, in the relevant literature.

## 5.2 RESULTS

The results presented in this thesis are of both a theoretical and a practical nature. The theoretical results have been obtained by studying the variational approach to waveguide propagation and the finite element method for the extremization of the waveguide functional. They are the derivation of the waveguide scalar functional from the least action principle presented in Chapter 2 and the comparative results between the first-order finite element nodal equation and the five-point finite difference operator shown in Chapter 3. The first enabled the author to formulate a unified presentation of the waveguide propagation theory directed towards the numerical analysis of waveguides. This is relevant for the systematic understanding of the finite element analysis of waveguides within the field theory context of microwave engineering.The second illustrates the algebraic distributions of nodal values obtained with the finite element and finite difference formulations and their resemblance to the exact nodal value distributions in rectangular waveguides. In fact, the finite difference and finite element techniques are nowadays well known, and the references describing the applications of either technique to waveguide propagations copious. It now appears unlikely that an aspect of the subject will be found where new and decisive results are required.

The practical results consist of the rectangular waveguide field patterns present in Chapter 4 together with the dynamical rectangular waveguide field displays being experimentally produced at the Department of Engineering of the University of Leicester. Here, it might be thought desirable to have diagrams for other waveguide cross-sections produced.This could have been done through the analytical expressions of the field configuration for the commonly used circular and elliptical cross-section waveguides. The ridged and other cross-section geometries could have been analysed through the scalar program package, and diagrams could have been produced. It was decided , however , that a comprehensive set of diagrams involving a particularly suitable waveguide geometry would be preferable to the repetition of the same technique to several cross-section geometries. In the latter case , the examples would have to be presented parsimoniously if the number of diagrams in this thesis were to be kept within reasonable bounds. Furthermore, their generation would consume, in straightforward but long programming, part of the inherently limited time available for this research project.

## 5.3 FUTURE DEVELOPMENTS

Field patterns and dynamic field displays for waveguide geometries other than rectangular could certainly be produced, and their usefulness in microwave engineering investigated.On the other hand, research on 3-D vector finite element techniques for investigating the solution of essentially 3-dimensional microwave problems will probably produce numerical results suitable to the application

of the proposed field pattern displays. The numerical solution of this kind of problem can only be carried out on large computers but, once the results are made available, the vector field imaging technique can be employed, presumably without difficulties. Works dealing with vector finite element methods for 3-D waveguide problems are referenced in the text.

The generation of field patterns and dynamic displays from finite element results of hybrid propagation in microstrip lines [95] appears to be another promising area for future application.In this case, both the electric and the magnetic field intensities are , in general, non-transverse and the computer print-outs difficult to interpret[60][61]. The generation of accurate field patterns for hybrid propagation will depend on the ability to differentiate the generating function nodal value distributions. Several techniques for numerical differentiation appear in the literature , and a full investigation of the application of those techniques in connection with the generation of field patterns could be carried out.In fact, the problem of finding a stable general process for numerical differentiation of the nodal value distributions obtained as computer solutions for Helmholtz equation remains unsolved. A solution for this problem would be highly desirable not only in connection with the generation of field patterns but also in other areas of applied electromagnetics. Finally, because the vector imaging method developed during this work is general and only microwave fields have been considered, one can assume that it will eventually be applied to other branches of engineering.

# APPENDIX 1

## INTEGRATION OF EQ.(3.39) AND THE ANGULAR FORM OF THE COEFFICIENTS $k_{0j}$ AND $k_{1j}$

### A1.1 INTEGRATION OF EQ.(3.39)

The integration of eq.(3.39) over the element area using the geometry of Fig.(3.3) is long and tedious. However, by resorting to a local co-ordinate system, as shown in Fig.(A1.1), much of the algebraic work during the integration can be avoided. In order to illustrate this point and to present a proof of the somewhat surprising result given by eq.(3.40) the integration will be carried out here.

Considering the geometry of Fig.(A1.1), we have:

$$x_{0j} = 0 \tag{A1.1}$$

$$y_{0j} = 0 \tag{A1.2}$$

$$x_{1j} = x_{2j} = h_j \tag{A1.3}$$

$$y_{2j} - y_{1j} = b_j \tag{A1.4}$$

$$A_j = \frac{1}{2} h_j b_j \tag{A1.5}$$

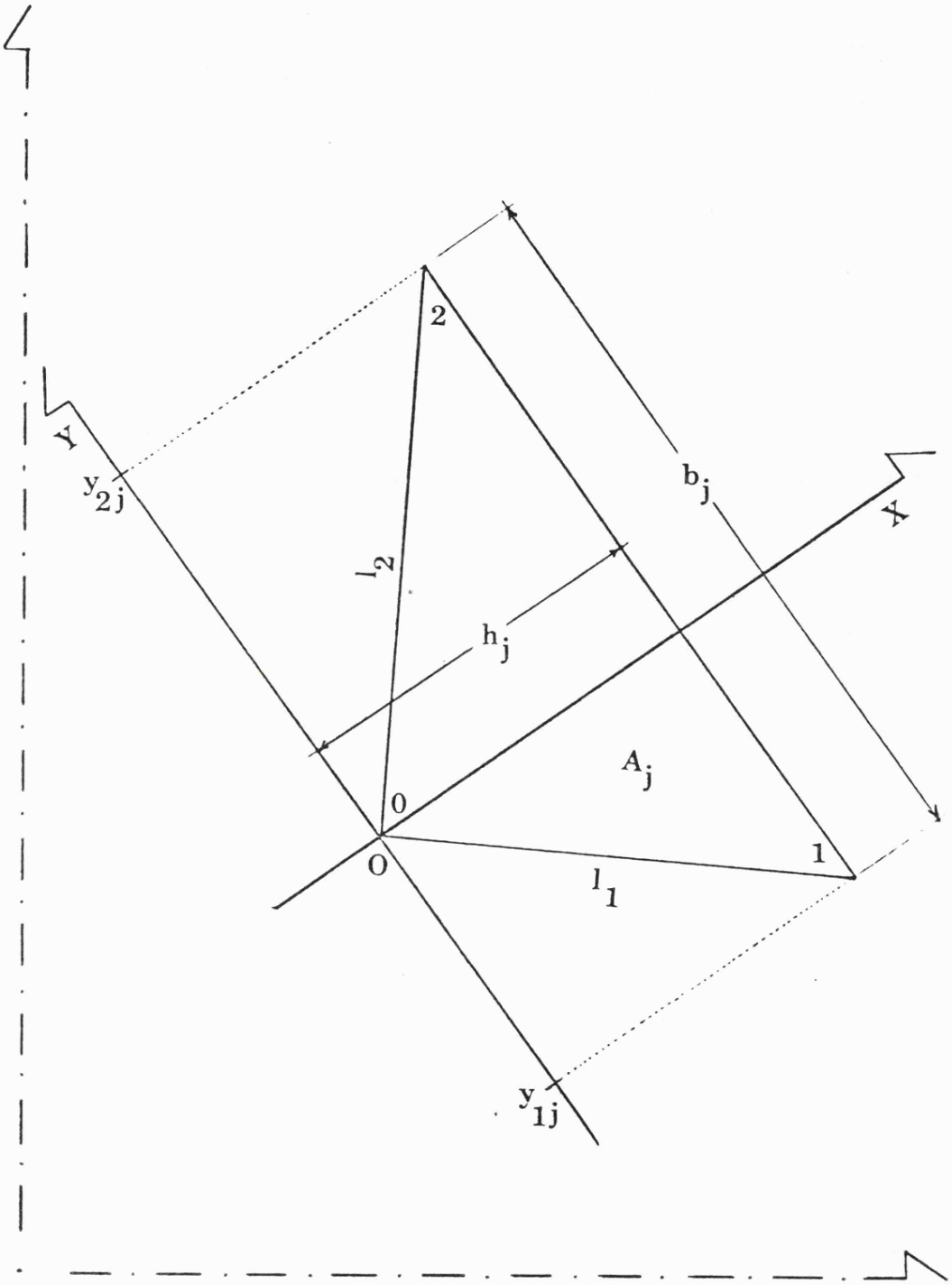


FIG. A1.1 LOCAL CO-ORDINATE SYSTEM FOR INTEGRATION OF EQ.(3.39)

Expanding eq.(3.39) and substituting eq.(A1.1) to eq.(A1.2) , we get:

$$G_{Mn}^{ej} \frac{\delta}{\delta G_{0j}} G_{Mn}^{ej} = \frac{1}{4A_j^2} G_{0j}(2A_j - b_j x)^2 + G_{1j}(y_{2j}x - x_{2j}y)(2A_j b_j x)$$

$$- G_{2j}(y_{1j}x - x_{1j}y)\ (2A_j - b_j x) \qquad (A1.6)$$

Defining

$$K_0 = (2A_j - b_j x)^2 = 4\ A_j^2 + b_j^2 x - 4\ A_j b_j x \qquad (A1.7)$$

$$K_1 = (y_{2j}x - x_{2j}y)\ (2A_j - b_j x) = 2\ y_{2j}A_j x - b_j y_{2j} x^2$$

$$- 2\ x_{2j}A_j y + b_j x_{2j} xy \qquad (A1.8)$$

$$K_2 = -\ (y_{1j}x - x_{1j}y)\ (2A_j - b_j x) = -\ 2\ y_{1j}A_j x - b_j y_{1j} x^2$$

$$- 2\ x_{1j}A_j y + b_j x_{1j} xy \qquad (A1.9)$$

it is noted that the following integrals are to be evaluated over the area defined by $A_j$ :

$$I_1 = \iint_{A_j} x\ dS \qquad (A1.10)$$

$$I_2 = \iint_{A_j} y \, dS \tag{A1.11}$$

$$I_3 = \iint_{A_j} xy \, dS \tag{A1.12}$$

$$I_4 = \iint_{A_j} x^2 \, dS \tag{A1.13}$$

For the particular geometry chosen the limiting curves $l_1$ and $l_2$ are given by:

$$l_1 \; ) \quad y = \frac{y_{1j}}{h_j} x \tag{A1.14}$$

$$l_2 \; ) \quad y = \frac{y_{2j}}{h_j} x \tag{A1.15}$$

therefore, the integrals $I_1 \ldots I_4$ are of the form

$$I = \int_0^h \left( \int_{l_2}^{l_1} f(x,y) \, dy \right) dx \tag{A1.16}$$

$$(l_1 = y = (y_{2j} / h_j)x \; )$$

$$(l_2 = y = (y_{1j} / h_j)x \; )$$

For $I_1$, $f(x,y) = x$ , so :

$$I_1 = \frac{1}{3} b_j h_j^2 \tag{A1.17}$$

For $I_2$ , $f(x,y) = y$ , then :

$$I_2 = \frac{1}{6} b_j c_j h_j \tag{A1.18}$$

where,

$$c_j = y_{1j} + y_{2j} \tag{A1.19}$$

For $I_3$ , $f(x,y) = xy$ , thus :

$$I_3 = \frac{1}{8} b_j c_j h_j \tag{A1.20}$$

Finally, for $f(x,y) = x^2$ we have :

$$I_4 = \frac{1}{4} b_j h_j^3 \tag{A1.21}$$

Once the foregoing results have been obtained, substitution into the corresponding functions $K_i$ and some manipulation gives:

$$\iint_{A_j} K_0 \, dS = \frac{2}{3} A_j^3 \tag{A1.22}$$

$$\iint_{A_j} K_1 \, dS = \frac{1}{3} A_j^3 \tag{A1.23}$$

$$\iint_{A_j} K_2 \, dS = \frac{4}{3} A_j^3 \tag{A1.24}$$

Therefore, we have:

$$\iint_{A_j} G_{Mn}^{ej} \frac{\delta}{\delta G_{0j}} G_{Mn}^{ej} \, dS = \sum_i G_{ij} \iint K_i \, dS$$

$$= \frac{1}{6} A_j \left[G_{0j} + \frac{1}{2}(G_{1j} + G_{2j})\right] \tag{A1.25}$$

Comparison of eq.(A1.25) with eq.(3.34) gives eq.(3.40) which can be written in the form:

$$\sum_{j=1}^{m} \iint_{A_j} G_{Mn}^{ej} \frac{\delta}{\delta G_{0j}} G_{Mn}^{ej} = \sum_{j=1}^{m} \left[k_{3j} G_{0j} + k_{12j}(G_{1j} + G_{2j})\right] \tag{A1.26}$$

where

$$k_{3j} = \frac{1}{3} A_j \tag{A1.27}$$

$$k_{12j} = \frac{1}{2} k_{3j} = \frac{1}{6} A_j \tag{A1.28}$$

as defined in eq.(3.41) and eq.(3.42).

## A1.2 ANGULAR FORM OF THE COEFFICIENTS $k_{ij}$

Considering the co-ordinates of the element vertices in Fig. (A1.2) the coefficients $k_{ij}$ are calculated by applying eq.(3.31) to eq.(3.33), in the form:

$$k_{0j} = \frac{1}{2A_j}(x_{2j} - x_{1j})^2 = \frac{(x_{2j} - x_{1j})^2}{(x_{2j} - x_{1j})y_{0j}} = \frac{x_{2j}}{y_{0j}} - \frac{x_{1j}}{y_{0j}} \tag{A1.29}$$

$$k_{1j} = - \frac{x_{2j}(x_{2j} - x_{1j})}{2A_j} = \frac{x_{2j}(x_{2j} - x_{1j})}{(x_{2j} - x_{1j})y_{0j}} = - \frac{x_{2j}}{y_{0j}} \tag{A1.30}$$

Refering to Fig.(A1.2) and applying the geometric properties of a triangle, the angular form of the coefficients $k_{ij}$ of eq.(3.45) and eq.(3.46) are finally obtained:

$$k_{0j} = \sum_{i=1}^{2} \operatorname{cotg}\theta_{ij} \tag{A1.31}$$

$$k_{ij} = \operatorname{cotg}\theta_{ij} \tag{A1.32}$$

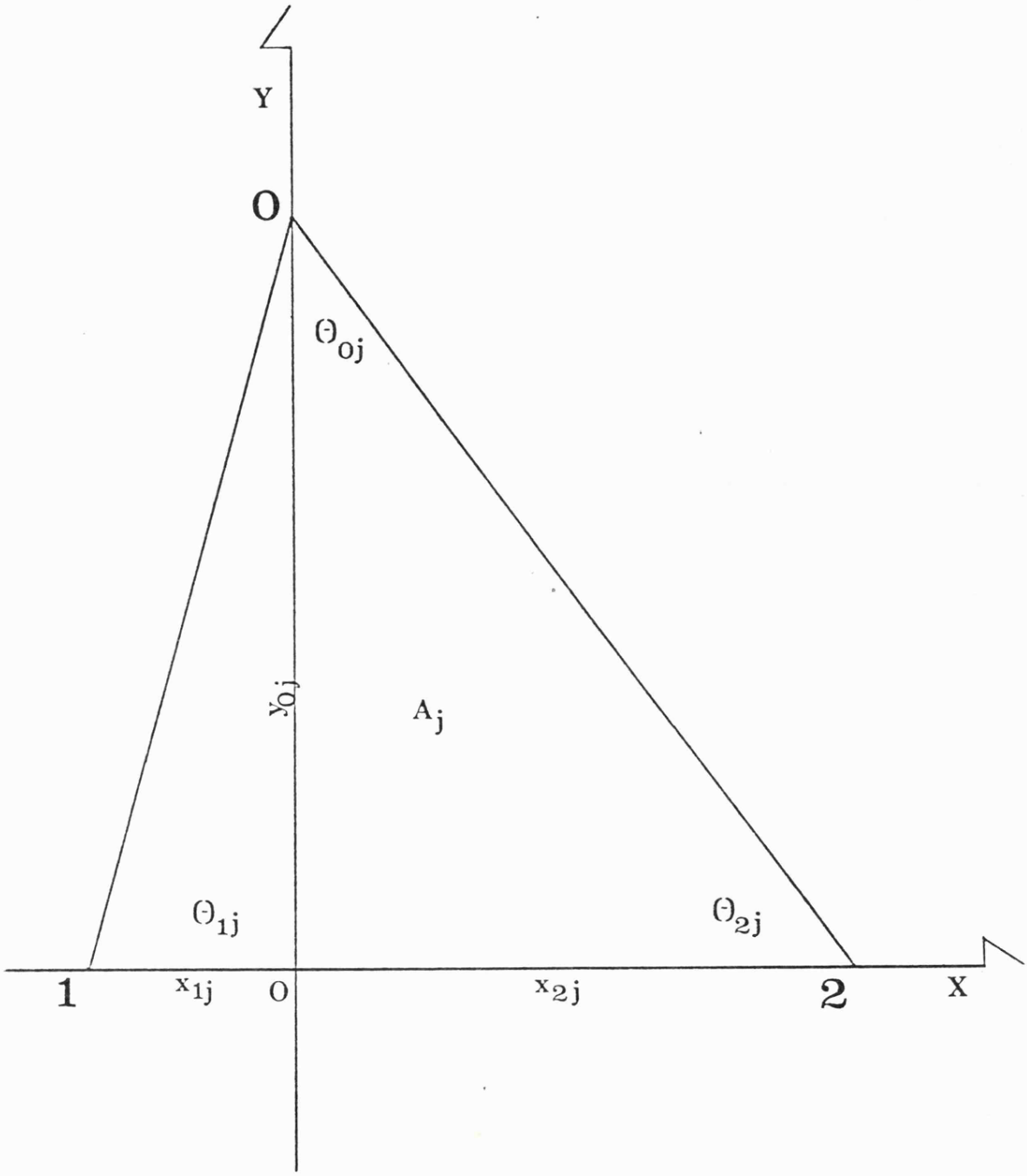


FIG. A1.2 VERTICES AND ANGLES OF AN ELEMENT

Geometry used for the derivation of the angular form of coefficients $k_{0j}$ and $k_{1j}$ .

# APPENDIX 2

## PROGRAM DESCRIPTION : MXSNEX

### A2.1 PURPOSE

MXSNEX calculates the central node values of the generating functions for TE and TM modes of propagation inside a typical rectangular waveguide using the five point finite difference formula (eq.(3.77)), the finite element formula (eq.(3.78))and the symmetric finite element formula (eq.(3.79))over an equispaced mesh. The program does not solve the waveguide by finite difference nor by finite element techniques. Instead, it uses the analytical values of the generating function calculated at each node in the neighbourhood of a given node to estimate the value of the generating function at that node. The central node value estimation is performed separately, using each one of the above formulae at a time, per complete cross-section. The program generates maps of the estimated central node value distribution for each formula and also prints the percentual error of each estimated value when compared with its analytical counterpart .

MXSNEX has been formulated to provide a simple numerical experimentation with the foregoing mentioned formulae in order to illustrate their dependence on mesh length and on mode pattern complexity.

A2.2 DESCRIPTION

A rectangular cross-section having the ratio of the narrower to the broader sides equal to $\frac{1}{2}$ is firstly divided by MXSNEX into a regular mesh consisting of (IM + 1) vertical lines or columns and (JM + 1) horizontal lines or rows. See Fig.(3.5), Chapter 3, paragraph (3.10.1). The numbering of rows and columns starts with the number 1 and finishes respectively with the numbers ICOL and ILIN which are program variables depending on the number of divisions on the broader side given by program variable IDIV. The program variable IDIV determines the mesh length to be used in the calculations and therefore establishes the total number of nodal points over the cross-section.

Once the rectangular waveguide cross-section has been divided into a regular mesh, the program reads information about the propagating mode to be considered and then proceeds to calculate the nodal values at each mesh node using the analytical expression for the generating function for the mode under consideration (Chapter 3, paragraph (3.10.1)). An array containing the obtained analytical node values is generated and stored and a map of the analytical node values distribution printed out in matrix form.

Having obtained the analytical values of the generating function at each node the program re-estimates the central node values at each of the mesh points by substituting for the neighbouring nodes their analytical values and using at a time , per complete cross-section , the finite difference formula , the finite element formula and the symmetric finite element formula , respectively. After performing the calculations for each formula , an estimated

node value distribution array and a percentual error distribution array obtained by comparing the estimated values with their analytical values are generated and printed out in matrix form.

## A2.3 INPUT VARIABLES

The input for the program consists of:

a) a variable specifying the number of experiments, that is , the number of executions to be performed after loading;

b) variables specifying the number of divisions on the broader cross-section side and the mode of propagation.

The inputs variables are defined, by reading order, in table T (A2.1).

## A2.4 TIMING

The average running time of the program is around 1.0 sec. per experiment and the compilation time using the FTN compiler around 5.0 seconds.

## A2.5 STORAGE

The programs utilizes 3 variable dimensioned arrays defined as one (40,20) array plus four (40,20) arrays ; the latter being equivalenced into two locations.

## A2.6 EXAMPLE

A $TE_{10}$ mode sequence of matrices is generated by the following card deck:

| NAME | FORMAT | PURPOSE |
|---|---|---|
| NEX | I2 | Number of experiments to be performed per run*. |
| IDIV | I2 | Number of divisions on the broader cross-section side. |
| IWAV | I1 | Wave type of the propagation<br>IWAV = 1 for $TE_{M,N}$ modes<br>IWAV = 2 for $TM_{M,N}$ modes |
| M<br>N | 2I1 | First mode index<br>Second mode index |

TABLE T A2.1 : Input variables in the program MXSNEX.

* If NEX > 1 the data sequence for each experiment must start with the value of variable IDIV

```
JOB CARD.
USER,USERNAME,PASSWORD.
CHARGE,DEPARTMENT,PROJECT.
FTN.
LGO.
END OF RECORD CARD.
PROGRAM MXSNEX(INPUT,OUTPUT,...
:
SUBROUTINE MAPGN(IWAV...
:
SUBROUTINE MAPFD(ICOL,...
:
SUBROUTINE MAPFE(ICOL,...
:
SUBROUTINE MAPFES(ICOL,...
:
SUBROUTINE MAPA(XVALOR,...
END OF RECORD CARD.
```

(i) 01

(ii) 10

(iii) 110

END OF INFORMATION CARD.

(i) One experiment

(ii) 10 divisions on the broader cross-section side

(iii) $TE_{10}$ mode of propagation.

## A2.7 OUTPUT FORMAT

The program has been provided with WRITE statements(SUBROUTINE MAPA) capable of printing out matrices resulting from the division

of the broader cross-section side in 10,14 and 18 parts.If different broader cross-section side divisions are used and the variable IDIV is less than 39 the FORMAT statements in MAPA must be changed accordingly. For a number of divisions greater than 39 the FORMAT statements in MAPA and the DIMENSION statements in MXSNEX must be changed.

## A2.8 PROGRAM ORGANIZATION

The program consists of a main routine calling five subroutines to perform the operations indicated in table T (A2.2).

## A2.9 METHOD

A complete description of the method used in the calculations together with the interpretation of the output matrices is presented in Chapter 3 (paragraph (3.10) to paragraph (3.10.4)).

## A2.10 PROGRAM AVAILABILITY

The program is available at Leicester University Engineering Department.

| NAME | PURPOSE |
|---|---|
| MXSNEX | Main routine. |
| MAPGN | Calculates the analytical node value distribution. |
| MAPFD | Estimates the central node values using the finite difference formula and calculates the percentual error at each estimated node. |
| MAPFE | Same as MAPFD but using the finite element formula. |
| MAPFES | Same as MAPFD but using the symmetric finite element formula. |
| MAPA | Prints out the result of the calculations in matrix form. |

TABLE T A2.2 : Routines in the program MXSNEX.

# APPENDIX 3

## SCALAR FINITE ELEMENT PROGRAM PACKAGE (CAMBRIDGE VERSION) : EXAMPLES OF ACCESS AND USE FROM LEICESTER

### A3.1 PURPOSE

Appendix 3 describes the use of a scalar finite element program package (Cambridge version via telephone link from Leicester ) to obtain the nodal values of the generating function of the first propagating TE and TM modes (Map.(2.21) to Map.(2.23)) of a typical rectangular waveguide.

### A3.2 FINITE ELEMENT MODEL OF THE CROSS-SECTION

The typical rectangular waveguide cross-section having the ratio of the narrower to the broader sides equal to $\frac{1}{2}$ has been divided into two sixth-order elements as shown in Fig.(A3.1). The numbered points in the figure are the nodal points defining the geometry of the model, that is, the waveguide cross-section and its division into finite elements. The numbers along the element sides are the constraints to be applied to the nodal points to be generated by the program pacakage along each side. Sides having associated constraint number equal to zero have free nodes. This means that the program will calculate their nodal values. If constraint zero

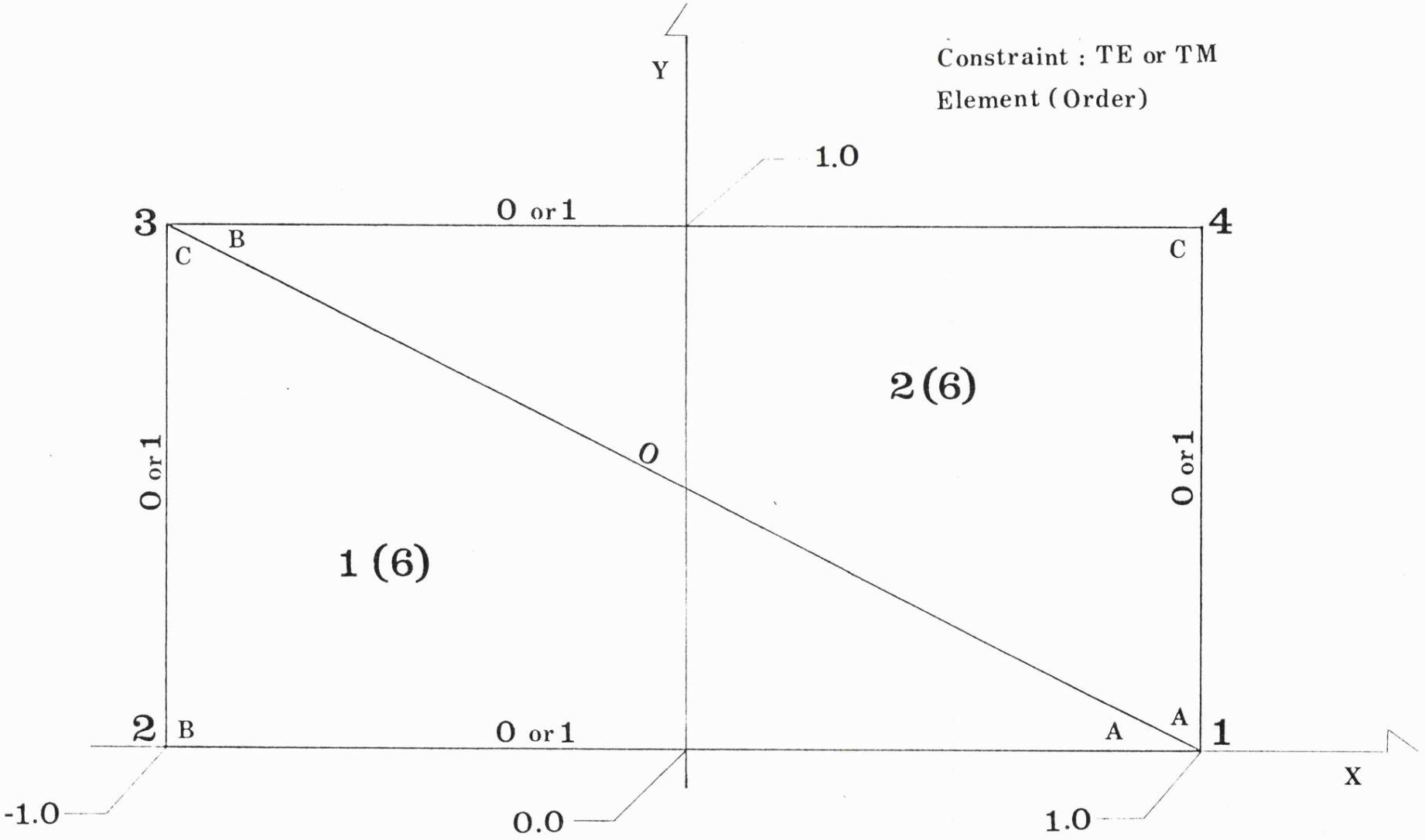


FIG. A3.1 : FINITE ELEMENT DIVISION OF THE CROSS-SECTION

sides are on the boundary (TE modes) , the nodal values calculated by the program package will satisfy the boundary condition

$$\frac{\delta G_n}{\delta_n} = 0 \qquad \text{(on the boundary)} \tag{A3.1}$$

where $G_n$ is the mode generating function. Sides having associated constraint number equal to the unity have fixed nodal values and any node on constraint one sides, will be given zero nodal value when the Helmholtz equation is solved. Those nodes are placed on the cross-section boundary for TM modes such that the boundary condition

$$G_n = 0 \tag{A3.2}$$

where $G_n$ is again the mode generating function,is satisfied.The constraint conditions on element sides of waveguide cross-section finite element models are summarized in tables T(A3.1) and T(A3.2).

The individual element vertex identification letters ( A,B and C ) are shown in Fig.(A3.1) together with the element identification number and approximation order.

## A3.3 INPUT TABLES

The program input concerning the finite element model of the cross-section contains information about:

(i) Scale factors of the x and y axes;

(ii) Node identification numbers and co-ordinates;

(iii) Element identification numbers , approximation order, vertices A,B and C, constraints to be applied on element sides and the relative permittivity of the medium contained by the element.

According to Fig.(A3.1) the required information can be organized, in the present case, as in table T(A3.3) to table T(A3.6).

## A3.4 SOLUTION SPECIFICATION

The last data entry specifies how many eigenvalues in an increasing value order and respective eigenvectors are required in the program output. This information is given by entering a positive real number with its integer part equal to the number of eigenvalues and eigenvectors required. The positive real number is preceeded by space (blank) for TE modes and by 0.0 for TM modes which are, in both cases, followed by a double slash ( // ). See examples.

## A3.5 OPTION CARD (END OF DATA RECORD)

The "PUNCH" option card is intended to produce the output results on punched cards. This option was not effective for jobs submitted from Satelite-1-Leicester because only the card reader and the line printer were operational in the link. However, the "PUNCH" card has been used in the examples presented here to indicate to the program the end of the data record. See reference below* for other possible option cards.

---

* ASIS-NAPS Document No. NAPS-01604

ASIS NATIONAL AUXILIARY PUBLICATIONS SERVICE, N.Y.

## A3.6 COMPUTERIZED MODEL OF THE CROSS-SECTION

Receiving the information contained in table T(A3.1) to table T(A3.6), the program package automatically generates the node distribution inside the elements according to the specified order of polynomial approximation. Later, a map showing the approximate location of the nodes over the cross-section is output via line printer. The nodes assembled by the program package are numbered in accordance with an order depending on processing convenience which may produce node identification numbers which do not coincide with the original numbering of nodes as given in the input.

The cross-section model of the typical rectangular waveguide with complete element mode distributions is shown in Fig.(A3.2) ; where it is assumed that the element vertices have their identification numbers unaltered when assembled by the program.

## A3.7 INPUT ORGANIZATION, FORMAT AND DEFAULTS

The input deck is organized in the Cambridge version similarly to the original input data layout presented in table T(A3.8) with the spaces compressed to a slash ( / ). The defaults used by the program are shown in table T(A3.8).

## A3.8 JOB SUBMISSION FROM LEICESTER

A complete deck for job submission* to the Cambridge computer from Leicester consists of the following cards:

---

* The program must be available in compiled form in the user's disc file at Cambridge Computer Laboratory.

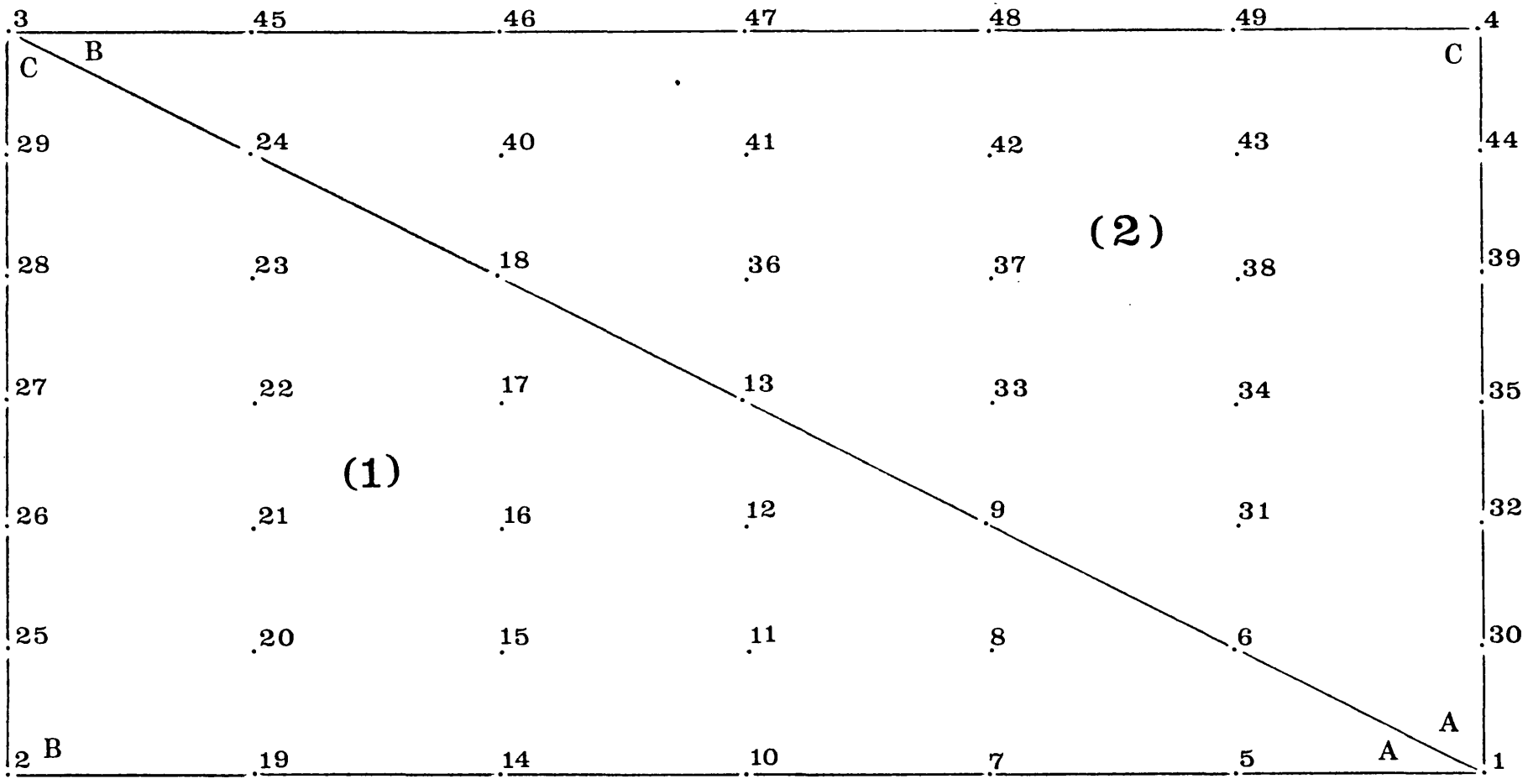


FIG. A3.2 : NODAL DISTRIBUTION ON THE CROSS-SECTION

(i) JOB/bUSERNAME/bPROJECTNUMBER/bJOBTITLE

ROUTE/bLEICESTER

(ii) TIME/bMN/bSECONDS

PHX

FILE/bFROM/b%H# /bTO/b&A/FB

```
DATA IN COMPRESSED FORM START-
ING WITH THE TITLE CARD    AND
FINISHING WITH THE    SOLUTION
SPECIFICATION CARD FOLLOWED BY
THE OPTION CARD.
(See examples).
```

C/bUSERNAME.PROGRAM(FORMAT)/bFROM/b&A/bTO/bUSERNAME.DATA/FB

USERNAME.LINK(GO)(FT05F001=USERNAME.DATA,FT06F001=C,

FT07F001=£)/*EOF

(i) USERNAME and PROJECTNUMBER are assigned to the user when registered with Cambridge Computer Laboratory.

JOBTITLE is the user's identification of the job being submitted.

(ii) MN is the time parameter in seconds.

All the cards are punched from column 1 and /b represents a space.

## A3.9 DISC USAGE

The compiled form of the program package needs approximately 10 discs tracks to be filed.

## A3.10 ERROR INDICATOR

Should an error occur during the execution, the error indicator variable MISTAK is set accordingly. The value of the variable MISTAK is printed out together with other program statistics.

The possible values of the variable MISTAK and respective error indications are given in table T(A3.9).

## A3.11 EXAMPLES

The outputs of the examples below are attached to the present description.

### A3.11.1 CARD DECK FOR THE FIRST 5 TE MODES OF THE TYPICAL RECTANGULAR WAVEGUIDE

```
JOB/bMLXS/b4643/bTE/bMODES.
ROUTE/bLEICESTER
TIME/b10/bSECONDS
PHX
FILE/bFROM/b%H#/bTO/b&A/FB
(i)   RECTANGULAR/bWAVEGUIDE/bTE/bMODES
(ii)  1/1.0/0.0
      2/-1.0/0.0
      3/-1.0/1.0
      4/1.0/1.0
(iii)/b/b/b.......b......b.....b....b/b/b
(iv)  6/1/2/3
      /1/3/4
```

(v) ƀƀƀ..... ...ƀ....ƀ....ƀ...ƀƀ

(vi) ƀ//5.0

(vii) PUNCH

```
C ƀMLXS.PROGRAM(FORMAT)ƀFROMƀ&AƀTOƀMLXS.DATA/FB
MLXS.LINK(GO)(FT05F001=MLXS.DATA,FT06F001=*C,FT07F001=£)
```

(viii)/*EOF

(i) Title card

(ii) Cards originated from table T(A3.4)

(iii) Blank card separating the cards originated from table T(A3.4) from the cards originated from table T(A3.5)

(iv) Cards originated from table T(A3.5)

(v) Blank card separating the cards originated from table T(A3.5) from the cards originated from table T(A3.7)

(vi) Solution specification card.

(vii) End of the data record. (Option card)

(viii)End of file card.

A3.11.2 CARD DECK FOR THE FIRST 5 TM MODES OF THE TYPICAL RECTANGULAR WAVEGUIDE

```
JOB/bMLXS/b4643/bTM/bMODES.
ROUTE/bLEICESTER
TIME/b10/bSECONDS
PHX
FILE/bFROM/b%H#/bTO/b&A/FB
RECTANGULAR/bWAVEGUIDE/bTM/bMODES
1/1.0/0.0
2/-1.0/0.0
3/-1.0/1.0
4/1.0/1.0
/b/b/b..... ...../b....../b....../b....../b/b
6/1/2/3/1/1
/1/3/4//1/1
/b/b/b..... ...../b....../b....../b....../b/b
0.0//5.0
PUNCH

C/bMLXS.PROGRAM(FORMAT)/bFROM/b&A/bTO/bMLXS.DATA/FB
MLXS.LINK(GO)(FT05F001=MLXS.DATA,FT06F001=*C,FT07F001=£)
/*EOF
```

TABLE T A3.1 :

| SIDES ON BOUNDARY | | |
|---|---|---|
| MODES | TE | TM |
| CONSTRAINT | 0 | 1 |

TABLE T A3.2 :

| SIDES INSIDE CROSS-SECTION | | |
|---|---|---|
| MODES | TE | TM |
| CONSTRAINT | 0 | 0 |

TABLE T A3.3 :

| SCALE FACTOR | |
|---|---|
| HORIZONTAL (x) | 1.0 |
| VERTICAL (y) | 1.0 |

TABLE T A3.4 :

| NODE IDENTIFICATION AND POSITIONING | | |
|---|---|---|
| NUMBER | X CO-ORD. | Y CO-ORD. |
| 1 | 1.0 | 0.0 |
| 2 | -1.0 | 0.0 |
| 3 | -1.0 | 1.0 |
| 4 | 1.0 | 1.0 |

TABLE T A3.5 :

| ELEMENT IDENTIFICATION AND PROPERTIES - TE MODES | | | | | | | | |
|---|---|---|---|---|---|---|---|---|
| NUMBER | ORDER | VERTICES | | | CONSTRAINTS | | | REL.PERM. |
| | | A | B | C | AB | BC | AC | |
| 1 | 6 | 1 | 2 | 3 | 0 | 0 | 0 | 1.0 |
| 2 | 6 | 1 | 3 | 4 | 0 | 0 | 0 | 1.0 |

TABLE T A3.6 :

| ELEMENT IDENTIFICATION AND PROPERTIES - TM MODES | | | | | | | | |
|---|---|---|---|---|---|---|---|---|
| NUMBER | ORDER | VERTICES | | | CONSTRAINTS | | | REL.PERM. |
| | | A | B | C | AB | BC | AC | |
| 1 | 6 | 1 | 2 | 3 | 1 | 1 | 0 | 1.0 |
| 2 | 6 | 1 | 3 | 4 | 0 | 1 | 1 | 1.0 |

TABLE T A3.7 :

## D A T A  C A R D S :

| CARDS | DATA | COLUMNS | FORMAT |
|---|---|---|---|
| CARD \1 | ↑*↑ (STAR) | \1 | A1 |
| | TITLE | \8-\47 | 40A1 |
| | HORIZONTAL SCALE | \56-\63 | F8.2 |
| | VERTICAL SCALE | \72-\79 | F8.2 |
| DATA CARDS BELONGING TO THE FIRST PART OF DATA SET | ↑ ↑ (BLANK) | \1 | A1 |
| | POINT NO. | \13-\17 | I5 |
| | HORIZONTAL COORDINATE | \32-\48 | F17.5 |
| | VERTICAL COORDINATE | \63-\79 | F17.5 |
| BLANK CARD | | | |
| DATA CARDS BELONGING TO THE SECOND PART OF DATA SET | ↑ ↑ (BLANK) | \1 | A1 |
| | ORDER 'N' | \5 | I1 |
| | VERTEX A | \18-\22 | I5 |
| | VERTEX B | \26-\30 | I5 |
| | VERTEX C | \34-\38 | I5 |
| | CONSTRAINT ON SIDE A•B | \49 | I1 |
| | CONSTRAINT ON SIDE B•C | \55 | I1 |
| | CONSTRAINT ON SIDE A•C | \61 | I1 |
| | MATERIAL PROP. | \70-\80 | F11.5 |
| BLANK CARD | | | |
| LAST CARD OF A DATA SET | POTENTIALS 'VOLT(1-9)' | \1-\72 | 9F8.3 |
| | TYPE OF EQUATION | \73-\80 | F8.3 |
| OPTION CARD | OPTION WORD(S) | \1-\6 OR<br>\7-\12 | A1,5X<br>A1,5X |

TABLE T A3.8 :

| | DEFAULT CONDITIONS* |
|---|---|
| 1 | If the first element to be read is to be of first order then "N" does not have to be specified; it is taken automatically as one. |
| 2 | If more elements are of the same order then it is sufficient to specify the first one; the rest are automatically assigned the value of "N" from the previous one. |
| 3 | Free points have a constraint number of zero assigned to them hence they do not have to be specified. |
| 4 | If the permittivity used is that of empty space then it does not have to be specified; it will automatically be taken as one. |
| 5 | If there is more than one element which has the same relative permittivity then it has to be specified only once; the rest of the elements are automatically assigned the value of permittivity from the previous elements. |
| 6 | If the horizontal and vertical scale factors are not specified then they are automatically taken to be unity. |

---

* For a complete description of default conditions (also applying to the solution of Laplace's and Poisson's equations) see:
ASIS-NAPS Document No. NAPS-01604.

TABLE T A3.9 :

| | ERROR INDICATOR : VARIABLE "MISTAK"* |
|---|---|
| VALUE | INDICATION |
| 0 | Program successifully executed. |
| 1 | One of the element areas is zero. |
| 2 | Error when reading the first data card (Title). |
| 3 | Error encountered in the first card after the title card. |
| 4 | The data card on which the point numbers and co-ordinates are read in are not in order or one is missing or the data card has been mispunched and the wrong number was read in. |
| 5 | The second portion of the data card set which should contain the element specifications are missing and there are no more data sets to be read in. |
| 6 | The element order is negative or greater than 6. |
| 7 | An error condition was encountered in the data transfer. |
| 8 | An error condition was encountered in the data transfer. |
| 9 | The second portion of data card set is missing. |
| 10 | An error condition was encountered in the data transfer. |
| 11 | End read; no more data cards. |
| 12 | The string preceeding the solution specification in the solution specification card is not 0.0// or (blank)//. |
| 13 | "N FREE" equals zero or "N FREE" greater than the specified size "LNGT". See program statistics. |
| 14 | All nodes are free nodes. It is not necessarily an error indication. |

| | ERROR INDICATOR : VARIABLE "MISTAK"* |
|---|---|
| VALUE | INDICATION |
| 15 | One of the constraint numbers has been wiped out due to incorrect problem formulation. |
| 16 | There is a total of only two points or less. The program cannot be used for problems which do not have at least one triangle. |
| 17 | Data error. |
| 18 | "LENGTH" is greater than "LONGST".See program statistics. |
| 19 | "INDIC" greater than "LNVTX". See program statistics. |
| 20 | A blank card is missing in the data set. |
| 21 | "NSU" is greater than "LNGT". See program statistics. |

---

* For a detailed description of the error indications by variable "MISTAK" see : ASIS-NAPS Document No. NAPS-01604.

```
HASP-II***HASP-II.....START JOB  394.....1.52.12 PM 31 MAY 78....POST MLXS...J0394MLXS.............................HASP-
HASP-II***HASP-II.....START JOB  394.....1.52.12 PM 31 MAY 78....POST MLXS...J0394MLXS.............................HASP-
HASP-II***HASP-II.....START JOB  394.....1.52.12 PM 31 MAY 78....POST MLXS...J0394MLXS.............................HASP-
HASP-II***HASP-II.....START JOB  394.....1.52.12 PM 31 MAY 78....POST MLXS...J0394MLXS.............................HASP-
HASP-II***HASP-II.....START JOB  394.....1.52.12 PM 31 MAY 78....POST MLXS...J0394MLXS.............................HASP-
HASP-II***HASP-II.....START JOB  394.....1.52.12 PM 31 MAY 78....POST MLXS...J0394MLXS.............................HASP-

 *JOB  394 **** V=.46209 U=3232.1 W=138.99 P=14.011 S=20 M=6411.0 N=6411.0 *******
 *JOB  394 *USERID LAST USED 23 MAY 78 13.40****THIS JOB SUBMITTED 23 MAY 78 13.4:*
L*JOB  394 CPU USED  0.39 DISC USED  0.41


                                   ***************************************************
                                   * 16.5.78  SPSS VERSION 7 - SEE INFO.NEW FOR DETAILS.*
                                   ***************************************************

     0.90 RESOURCE UNITS --      4 CARDS READ --      346 LINES PRINTED --      0 CARDS PUNCHED --   0.03 MINUTES EXECUT


TYPE ,RESULTS1

FILE FROM %H$ TO &A/FB
C MLXS.PROGRAM(FORMAT) FROM &A TO MLXS.DATA/FB
ERROR STATE RC= 8
** OUTPUT TO MLXS.DATA/FB
MLXS.LINK(GO)(FT05F001=MLXS.DATA,FT06F001=*C,FT07F001=£)

                          **** RECTANGULAR WAVEGUIDE TE MODES          ****

                                SCALE =      1.00     HORIZONTAL
                                SCALE =      1.00     VERTICAL


                                  *** INPUT POINT LIST ***

                        POINT        HORIZONTAL      VERTICAL
                         NO.         COORDINATE      COORDINATE

                          1.           1.00000         0.0
                          2.          -1.00000         0.0
                          3.          -1.00000         1.00000
                          4.           1.00000         1.00000

                          **** RECTANGULAR WAVEGUIDE TE MODES          ****
```

*** INPUT ELEMENT LIST ***

| TRIANGLE NO. | ORDER N | VERTICES: A | B | C | CONSTRAINTS A⊥B | B⊥C | A⊥C | MATERIAL PROPERTY (PERMITTIVITY) |
|---|---|---|---|---|---|---|---|---|
| 1. | 6 | 1 | 2 | 3 | 0 | 0 | 0 | 1.00000 |
| 2. | 6 | 1 | 3 | 4 | 0 | 0 | 0 | 1.00000 |

**** RECTANGULAR WAVEGUIDE TE MODES ****

*** ASSEMBLED POINT LIST ***

| POINT NO. | HORIZONTAL COORDINATE | VERTICAL COORDINATE | POINT NO. | HORIZONTAL COORDINATE | VERTICAL COORDINATE | POINT NO. | HORIZONTAL COORDINATE | VERTICAL COORDINATE |
|---|---|---|---|---|---|---|---|---|
| 1. | 1.00000 | 0.0 | 18. | -0.33333 | 0.66667 | 35. | 1.00000 | 0.50000 |
| 2. | -1.00000 | 0.0 | 19. | -0.66667 | 0.0 | 36. | 0.0 | 0.66667 |
| 3. | -1.00000 | 1.00000 | 20. | -0.66667 | 0.16667 | 37. | 0.33333 | 0.66667 |
| 4. | 1.00000 | 1.00000 | 21. | -0.66667 | 0.33333 | 38. | 0.66667 | 0.66667 |
| 5. | 0.66667 | 0.0 | 22. | -0.66667 | 0.50000 | 39. | 1.00000 | 0.66667 |
| 6. | 0.66667 | 0.16667 | 23. | -0.66667 | 0.66667 | 40. | -0.33333 | 0.83333 |
| 7. | 0.33333 | 0.0 | 24. | -0.66667 | 0.83333 | 41. | 0.0 | 0.83333 |
| 8. | 0.33333 | 0.16667 | 25. | -1.00000 | 0.16667 | 42. | 0.33333 | 0.83333 |
| 9. | 0.33333 | 0.33333 | 26. | -1.00000 | 0.33333 | 43. | 0.66667 | 0.83333 |
| 10. | 0.0 | 0.0 | 27. | -1.00000 | 0.50000 | 44. | 1.00000 | 0.83333 |
| 11. | 0.0 | 0.16667 | 28. | -1.00000 | 0.66667 | 45. | -0.66667 | 1.00000 |
| 12. | 0.0 | 0.33333 | 29. | -1.00000 | 0.83333 | 46. | -0.33333 | 1.00000 |
| 13. | 0.0 | 0.50000 | 30. | 1.00000 | 0.16667 | 47. | 0.0 | 1.00000 |
| 14. | -0.33333 | 0.0 | 31. | 0.66667 | 0.33333 | 48. | 0.33333 | 1.00000 |
| 15. | -0.33333 | 0.16667 | 32. | 1.00000 | 0.33333 | 49. | 0.66667 | 1.00000 |
| 16. | -0.33333 | 0.33333 | 33. | 0.33333 | 0.50000 | | | |
| 17. | -0.33333 | 0.50000 | 34. | 0.66667 | 0.50000 | | | |

**** RECTANGULAR WAVEGUIDE TE MODES ****

*** ASSEMBLED ELEMENT LIST ***

| TRIANGLE NO. | ORDER N | POINT NO. 1 OR 16 | POINT NO. 2 OR 17 | POINT NO. 3 OR 18 | POINT NO. 4 OR 19 | POINT NO. 5 OR 20 | POINT NO. 6 OR 21 | POINT NO. 7 OR 22 | POINT NO. 8 OR 23 | POINT NO. 9 OR 24 | POINT NO. 10 OR 25 | POINT NO. 11 OR 26 | POINT NO. 12 OR 27 | POINT NO. 13 OR 28 | POINT NO. 14 | POINT NO. 15 |
|---|---|---|---|---|---|---|---|---|---|---|---|---|---|---|---|---|
| 1. | 6 | 1* | 5 | 6 | 7 | 8 | 9 | 10 | 11 | 12 | 13 | 14 | 15 | 16 | 17 | 18 |
| | | 19 | 20 | 21 | 22 | 23 | 24 | 2* | 25 | 26 | 27 | 28 | 29 | 3* | | |
| 2. | 6 | 1* | 6 | 30 | 9 | 31 | 32 | 13 | 33 | 34 | 35 | 18 | 36 | 37 | 38 | 39 |
| | | 24 | 40 | 41 | 42 | 43 | 44 | 3* | 46 | 46 | 47 | 48 | 49 | 4* | | |

********** (N,B: POINT NUMBERS MARKED WITH AN ASTERISK INDICATE VERTICES.) **********

**** RECTANGULAR WAVEGUIDE TE MODES ****

*** DIMENSIONS OF THE PROBLEM ***

| | | | |
|---|---|---|---|
| ERROR CODE: | "MISTAK" | = | 14 |
| NO. OF FIXED POTENTIALS: | "NFIX" | = | 0 |
| NO. OF FREE POTENTIALS: | "NFREE" | = | 49 |
| TOTAL NO. OF POINTS: | "NSUM" | = | 49 |
| PERMISSIBLE NO. OF POINTS: | "LNGT" | = | 215 |
| NO. OF TRIANGULAR ELEMENTS: | "NELMT" | = | 2 |
| REQUIRED "S"-MATRIX: | "LENGTH" | = | 1225 |
| AVAILABLE "S"-MATRIX: | "LONGST" | = | 9000 |
| NO. OF ENTRIES IN "NVTX": | "INDIC" | = | 57 |
| AVAILABLE "NVTX" SIZE: | "LNVTX" | = | 1000 |

*** MAP OF THE ASSEMBLED POINTS ***

| | | | | | | |
|---|---|---|---|---|---|---|
| 3 | 45 | 46 | 47 | 48 | 49 | 4 |
| 29 | 24 | 40 | 41 | 42 | 43 | 44 |
| 28 | 23 | 18 | 36 | 37 | 38 | 39 |

| | | | | | | |
|---|---|---|---|---|---|---|
| 27 | 22 | 17 | 13 | 33 | 34 | 35 |
| 26 | 21 | 16 | 12 | 9 | 31 | 32 |
| 25 | 20 | 15 | 11 | 8 | 6 | 30 |
| 2 | 19 | 14 | 10 | 7 | 5 | 1 |

**** RECTANGULAR WAVEGUIDE TE MODES ****

```
*****************************
*                           *
* WAVENUMBER =  0.140421E-01 *
*                           *
*****************************
```

*** LIST OF POINTS WITH FREE POTENTIALS ***

| POINT NO. | FREE POTENTIAL | POINT NO. | FREE POTENTIAL | POINT NO. | FREE POTENTIAL |
|---|---|---|---|---|---|
| 1. | 0.495512E+01 | 18. | 0.494791E+01 | 35. | 0.495448E+01 |
| 2. | 0.494438E+01 | 19. | 0.494539E+01 | 36. | 0.495007E+01 |
| 3. | 0.494568E+01 | 20. | 0.494554E+01 | 37. | 0.495190E+01 |
| 4. | 0.495378E+01 | 21. | 0.494569E+01 | 38. | 0.495313E+01 |
| 5. | 0.495472E+01 | 22. | 0.494578E+01 | 39. | 0.495371E+01 |
| 6. | 0.495446E+01 | 23. | 0.494600E+01 | 40. | 0.494791E+01 |
| 7. | 0.495239E+01 | 24. | 0.494609E+01 | 41. | 0.495016E+01 |
| 8. | 0.495244E+01 | 25. | 0.494455E+01 | 42. | 0.495173E+01 |
| 9. | 0.495218E+01 | 26. | 0.494487E+01 | 43. | 0.495267E+01 |
| 10. | 0.494957E+01 | 27. | 0.494503E+01 | 44. | 0.495340E+01 |
| 11. | 0.494973E+01 | 28. | 0.494520E+01 | 45. | 0.494582E+01 |
| 12. | 0.494972E+01 | 29. | 0.494539E+01 | 46. | 0.494794E+01 |
| 13. | 0.494988E+01 | 30. | 0.495511E+01 | 47. | 0.495026E+01 |
| 14. | 0.494734E+01 | 31. | 0.495393E+01 | 48. | 0.495135E+01 |
| 15. | 0.494735E+01 | 32. | 0.495500E+01 | 49. | 0.495216E+01 |
| 16. | 0.494736E+01 | 33. | 0.495196E+01 | | |
| 17. | 0.494747E+01 | 34. | 0.495355E+01 | | |

**** RECTANGULAR WAVEGUIDE TE MODES ****

```
*****************************
*                           *
* WAVENUMBER =  0.157076E+01 *
*                           *
*****************************
```

*** LIST OF POINTS WITH FREE POTENTIALS ***

| POINT NO. | FREE POTENTIAL | POINT NO. | FREE POTENTIAL | POINT NO. | FREE POTENTIAL |
|---|---|---|---|---|---|
| 1. | 0.699778E+01 | 18. | -0.350264E+01 | 35. | 0.699766E+01 |
| 2. | -0.700220E+01 | 19. | -0.606504E+01 | 36. | -0.257438E-02 |
| 3. | -0.700366E+01 | 20. | -0.606515E+01 | 37. | 0.349658E+01 |
| 4. | 0.699715E+01 | 21. | -0.606530E+01 | 38. | 0.605965E+01 |
| 5. | 0.605999E+01 | 22. | -0.606521E+01 | 39. | 0.699795E+01 |
| 6. | 0.605939E+01 | 23. | -0.606527E+01 | 40. | -0.350218E+01 |
| 7. | 0.349523E+01 | 24. | -0.606538E+01 | 41. | -0.164253E-02 |
| 8. | 0.349524E+01 | 25. | -0.700233E+01 | 42. | 0.349725E+01 |
| 9. | 0.349560E+01 | 26. | -0.700284E+01 | 43. | 0.605985E+01 |
| 10. | -0.635326E-02 | 27. | -0.700321E+01 | 44. | 0.699769E+01 |
| 11. | -0.602130E-02 | 28. | -0.700329E+01 | 45. | -0.606584E+01 |
| 12. | -0.489274E-02 | 29. | -0.700333E+01 | 46. | -0.350221E+01 |
| 13. | -0.368464E-02 | 30. | 0.699748E+01 | 47. | -0.106519E-02 |
| 14. | -0.350423E+01 | 31. | 0.605961E+01 | 48. | 0.349766E+01 |
| 15. | -0.350409E+01 | 32. | 0.699751E+01 | 49. | 0.605950E+01 |
| 16. | -0.350347E+01 | 33. | 0.349615E+01 | | |
| 17. | -0.350275E+01 | 34. | 0.605959E+01 | | |

**** RECTANGULAR WAVEGUIDE TE MODES ****

```
*****************************
*                           *
* WAVENUMBER =  0.314156E+01 *
*                           *
*****************************
```

*** LIST OF POINTS WITH FREE POTENTIALS ***

| POINT NO. | FREE POTENTIAL | POINT NO. | FREE POTENTIAL | POINT NO. | FREE POTENTIAL |
|---|---|---|---|---|---|
| 1. | -0.314334E+01 | 18. | 0.156558E+01 | 35. | 0.312356E+01 |
| 2. | -0.314243E+01 | 19. | -0.470066E+01 | 36. | 0.163889E-01 |
| 3. | 0.938927E+01 | 20. | -0.386157E+01 | 37. | 0.156516E+01 |
| 4. | 0.938790E+01 | 21. | -0.156778E+01 | 38. | 0.469710E+01 |
| 5. | -0.470001E+01 | 22. | 0.156410E+01 | 39. | 0.625556E+01 |
| 6. | -0.386113E+01 | 23. | 0.469705E+01 | 40. | 0.385926E+01 |
| 7. | -0.783177E+01 | 24. | 0.699054E+01 | 41. | 0.231023E+01 |
| 8. | -0.699285E+01 | 25. | -0.230335E+01 | 42. | 0.385893E+01 |
| 9. | -0.469896E+01 | 26. | -0.954611E-02 | 43. | 0.699076E+01 |
| 10. | -0.938018E+01 | 27. | 0.312261E+01 | 44. | 0.654911E+01 |
| 11. | -0.854104E+01 | 28. | 0.625600E+01 | 45. | 0.782946E+01 |

| | | | | | |
|---|---|---|---|---|---|
| 12. | -0.624706E+01 | 29. | 0.854941E+01 | 46. | 0.469829E+01 |
| 13. | -0.311524E+01 | 30. | -0.230333E+01 | 47. | 0.314937E+01 |
| 14. | -0.783167E+01 | 31. | -0.156759E+01 | 48. | 0.469795E+01 |
| 15. | -0.699262E+01 | 32. | -0.978082E-02 | 49. | 0.782964E+01 |
| 16. | -0.469870E+01 | 33. | -0.156651E+01 | | |
| 17. | -0.156687E+01 | 34. | 0.156529E+01 | | |

**** RECTANGULAR WAVEGUIDE TE MODES ****

```
*****************************
*                           *
* WAVENUMBER =  0.314161E+01 *
*                           *
*****************************
```

*** LIST OF POINTS WITH FREE POTENTIALS ***

| POINT NO. | FREE POTENTIAL | POINT NO. | FREE POTENTIAL | POINT NO. | FREE POTENTIAL |
|---|---|---|---|---|---|
| 1. | -0.939857E+01 | 18. | 0.470945E+01 | 35. | -0.625631E+01 |
| 2. | -0.939700E+01 | 19. | -0.627532E+01 | 36. | 0.781195E+01 |
| 3. | -0.311554E+01 | 20. | -0.585482E+01 | 37. | 0.470934E+01 |
| 4. | -0.311403E+01 | 21. | -0.470503E+01 | 38. | -0.156385E+01 |
| 5. | -0.627621E+01 | 22. | -0.313515E+01 | 39. | -0.468548E+01 |
| 6. | -0.585556E+01 | 23. | -0.156472E+01 | 40. | 0.585934E+01 |
| 7. | -0.263324E-02 | 24. | -0.415125E+00 | 41. | 0.896190E+01 |
| 8. | 0.418095E+00 | 25. | -0.897651E+01 | 42. | 0.585939E+01 |
| 9. | 0.156833E+01 | 26. | -0.782685E+01 | 43. | -0.413562E+00 |
| 10. | 0.310028E+01 | 27. | -0.625697E+01 | 44. | -0.353489E+01 |
| 11. | 0.352111E+01 | 28. | -0.468652E+01 | 45. | 0.533115E-02 |
| 12. | 0.467128E+01 | 29. | -0.353692E+01 | 46. | 0.627997E+01 |
| 13. | 0.624176E+01 | 30. | -0.897741E+01 | 47. | 0.938258E+01 |
| 14. | -0.194340E-02 | 31. | -0.470543E+01 | 48. | 0.628007E+01 |
| 15. | 0.418083E+00 | 32. | -0.782752E+01 | 49. | 0.728018E-02 |
| 16. | 0.156870E+01 | 33. | 0.313908E+01 | | |
| 17. | 0.313882E+01 | 34. | -0.313437E+01 | | |

**** RECTANGULAR WAVEGUIDE TE MODES ****

```
*****************************
*                           *
* WAVENUMBER =  0.351240E+01 *
*                           *
*****************************
```

*** LIST OF POINTS WITH FREE POTENTIALS ***

| POINT NO. | FREE POTENTIAL | POINT NO. | FREE POTENTIAL | POINT NO. | FREE POTENTIAL |
|---|---|---|---|---|---|
| 1. | -0.991372E+01 | 18. | -0.247097E+01 | 35. | -0.244510E-02 |
| 2. | 0.990315E+01 | 19. | 0.857396E+01 | 36. | -0.327406E-02 |
| 3. | -0.991866E+01 | 20. | 0.742506E+01 | 37. | 0.246970E+01 |
| 4. | 0.989795E+01 | 21. | 0.428717E+01 | 38. | 0.428458E+01 |
| 5. | -0.856879E+01 | 22. | 0.374795E-02 | 39. | 0.494825E+01 |

| | |
|---|---|
| 6. | -0.742808E+01 |
| 7. | -0.494806E+01 |
| 8. | -0.428064E+01 |
| 9. | -0.246656E+01 |
| 10. | 0.745402E-02 |
| 11. | 0.969935E-02 |
| 12. | 0.134743E-02 |
| 13. | -0.453341E-02 |
| 14. | 0.495497E+01 |
| 15. | 0.428987E+01 |
| 16. | 0.247340E+01 |
| 17. | -0.249114E-03 |
| 23. | -0.428635E+01 |
| 24. | -0.743354E+01 |
| 25. | 0.857541E+01 |
| 26. | 0.495028E+01 |
| 27. | -0.299422E-02 |
| 28. | -0.495402E+01 |
| 29. | -0.857250E+01 |
| 30. | -0.856859E+01 |
| 31. | -0.428304E+01 |
| 32. | -0.495154E+01 |
| 33. | 0.127554E-04 |
| 34. | 0.411063E-02 |
| 40. | -0.428808E+01 |
| 41. | 0.181228E-02 |
| 42. | 0.428335E+01 |
| 43. | 0.742014E+01 |
| 44. | 0.857102E+01 |
| 45. | -0.857505E+01 |
| 46. | -0.495666E+01 |
| 47. | -0.167769E-02 |
| 48. | 0.494749E+01 |
| 49. | 0.856809E+01 |

```
HASP-II***HASP-II.....START JOB    45.....1.59.21 PM 31 MAY 78....POST MLXS...J0045MLXS.............................HASP-
HASP-II***HASP-II.....START JOB    45.....1.59.21 PM 31 MAY 78....POST MLXS...J0045MLXS.............................HASP-
HASP-II***HASP-II.....START JOB    45.....1.59.21 PM 31 MAY 78....POST MLXS...J0045MLXS.............................HASP-
HASP-II***HASP-II.....START JOB    45.....1.59.21 PM 31 MAY 78....POST MLXS...J0045MLXS.............................HASP-
HASP-II***HASP-II.....START JOB    45.....1.59.21 PM 31 MAY 78....POST MLXS...J0045MLXS.............................HASP-
HASP-II***HASP-II.....START JOB    45.....1.59.21 PM 31 MAY 78....POST MLXS...J0045MLXS.............................HASP-

 *JOB    45 **** V=.50580 U=3702.5 W=347.21 P=41.643 S=20 M=16493 N=16493 **********
 *JOB    45 *USERID LAST USED 23 MAY 78 14.52****THIS JOB SUBMITTED 23 MAY 78 14.53*
L*JOB    45 CPU USED  0.41 DISC USED  0.31


                                   ***************************************************
                                   * 16.5.78  SPSS VERSION 7 - SEE INFO.NEW FOR DETAILS.*
                                   ***************************************************

     0.88 RESOURCE UNITS --      4 CARDS READ --      343 LINES PRINTED --      0 CARDS PUNCHED --   0.05 MINUTES EXECUT


TYPE .RESULTS2

FILE FROM %HS TO &A/FB
C MLXS.PROGRAM(FORMAT) FROM &A TO MLXS.DATA/FB
ERROR STATE RC= 8
** OUTPUT TO MLXS.DATA/FB
MLXS.LINK(GO)(FT05F001=MLXS.DATA,FT06F001=*C,FT07F001=£)

                          **** RECTANGULAR WAVEGUIDE TM MODES          ****

                                SCALE =      1.00     HORIZONTAL
                                SCALE =      1.00     VERTICAL


                                  *** INPUT POINT LIST ***

                          POINT        HORIZONTAL       VERTICAL
                           NO.         COORDINATE       COORDINATE

                            1.           1.00000          0.0
                            2.          -1.00000          0.0
                            3.          -1.00000          1.00000
                            4.           1.00000          1.00000

                          **** RECTANGULAR WAVEGUIDE TM MODES          ****
```

*** INPUT ELEMENT LIST ***

| TRIANGLE NO. | ORDER N | VERTICES: A | B | C | CONSTRAINTS A⊥B | B⊥C | A⊥C | MATERIAL PROPERTY (PERMITTIVITY) |
|---|---|---|---|---|---|---|---|---|
| 1. | 6 | 1 | 2 | 3 | 1 | 1 | 0 | 1.00000 |
| 2. | 6 | 1 | 3 | 4 | 0 | 1 | 1 | 1.00000 |

**** RECTANGULAR WAVEGUIDE TM MODES ****

*** ASSEMBLED POINT LIST ***

| POINT NO. | HORIZONTAL COORDINATE | VERTICAL COORDINATE | POINT NO. | HORIZONTAL COORDINATE | VERTICAL COORDINATE | POINT NO. | HORIZONTAL COORDINATE | VERTICAL COORDINATE |
|---|---|---|---|---|---|---|---|---|
| 1. | 0.66667 | 0.16667 | 18. | 0.66667 | 0.50000 | 35. | -1.00000 | 0.16667 |
| 2. | 0.33333 | 0.16667 | 19. | 0.0 | 0.66667 | 36. | -1.00000 | 0.33333 |
| 3. | 0.33333 | 0.33333 | 20. | 0.33333 | 0.66667 | 37. | -1.00000 | 0.50000 |
| 4. | 0.0 | 0.16667 | 21. | 0.66667 | 0.66667 | 38. | -1.00000 | 0.66667 |
| 5. | 0.0 | 0.33333 | 22. | -0.33333 | 0.83333 | 39. | -1.00000 | 0.83333 |
| 6. | 0.0 | 0.50000 | 23. | 0.0 | 0.83333 | 40. | 1.00000 | 0.16667 |
| 7. | -0.33333 | 0.16667 | 24. | 0.33333 | 0.83333 | 41. | 1.00000 | 0.33333 |
| 8. | -0.33333 | 0.33333 | 25. | 0.66667 | 0.83333 | 42. | 1.00000 | 0.50000 |
| 9. | -0.33333 | 0.50000 | 26. | 1.00000 | 0.0 | 43. | 1.00000 | 0.66667 |
| 10. | -0.33333 | 0.66667 | 27. | -1.00000 | 0.0 | 44. | 1.00000 | 0.83333 |
| 11. | -0.66667 | 0.16667 | 28. | -1.00000 | 1.00000 | 45. | -0.66667 | 1.00000 |
| 12. | -0.66667 | 0.33333 | 29. | 1.00000 | 1.00000 | 46. | -0.33333 | 1.00000 |
| 13. | -0.66667 | 0.50000 | 30. | 0.66667 | 0.0 | 47. | 0.0 | 1.00000 |
| 14. | -0.66667 | 0.66667 | 31. | 0.33333 | 0.0 | 48. | 0.33333 | 1.00000 |
| 15. | -0.66667 | 0.83333 | 32. | 0.0 | 0.0 | 49. | 0.66667 | 1.00000 |
| 16. | 0.66667 | 0.33333 | 33. | -0.33333 | 0.0 | | | |
| 17. | 0.33333 | 0.50000 | 34. | -0.66667 | 0.0 | | | |

**** RECTANGULAR WAVEGUIDE TM MODES ****

*** ASSEMBLED ELEMENT LIST ***

| TRIANGLE NO. | ORDER N | POINT NO. 1 OR 16 | POINT NO. 2 OR 17 | POINT NO. 3 OR 18 | POINT NO. 4 OR 19 | POINT NO. 5 OR 20 | POINT NO. 6 OR 21 | POINT NO. 7 OR 22 | POINT NO. 8 OR 23 | POINT NO. 9 OR 24 | POINT NO.10 OR 25 | POINT NO.11 OR 26 | POINT NO.12 OR 27 | POINT NO.13 OR 28 | POINT NO.14 | POINT NO.15 |
|---|---|---|---|---|---|---|---|---|---|---|---|---|---|---|---|---|
| 1. | 6 | 26* | 30 | 1 | 31 | 2 | 3 | 32 | 4 | 5 | 6 | 33 | 7 | 8 | 9 | 10 |
| | | 34 | 11 | 12 | 13 | 14 | 15 | 27* | 35 | 36 | 37 | 38 | 39 | 28* | | |
| 2. | 6 | 26* | 1 | 40 | 3 | 16 | 41 | 6 | 17 | 18 | 42 | 10 | 19 | 20 | 21 | 43 |
| | | 15 | 22 | 23 | 24 | 25 | 44 | 28* | 45 | 46 | 47 | 48 | 49 | 29* | | |

********** (N.B: POINT NUMBERS MARKED WITH AN ASTERISK INDICATE VERTICES.) **********

**** RECTANGULAR WAVEGUIDE TM MODES ****

*** DIMENSIONS OF THE PROBLEM ***

| | | |
|---|---|---|
| ERROR CODE: | "MISTAK" = | 0 |
| NO. OF FIXED POTENTIALS: | "NFIX" = | 24 |
| NO. OF FREE POTENTIALS: | "NFREE" = | 25 |
| TOTAL NO. OF POINTS: | "NSUM" = | 49 |
| PERMISSIBLE NO. OF POINTS: | "LNGT" = | 215 |
| NO. OF TRIANGULAR ELEMENTS: | "NELMT" = | 2 |
| REQUIRED "S"-MATRIX: | "LENGTH" = | 325 |
| AVAILABLE "S"-MATRIX: | "LONGST" = | 9000 |
| NO. OF ENTRIES IN "NVTX": | "INDIC" = | 57 |
| AVAILABLE "NVTX" SIZE: | "LNVTX" = | 1000 |

*** MAP OF THE ASSEMBLED POINTS ***

| | | | | | | |
|---|---|---|---|---|---|---|
| 28 | 45 | 46 | 47 | 48 | 49 | 29 |
| 39 | 15 | 22 | 23 | 24 | 25 | 44 |
| 38 | 14 | 10 | 19 | 20 | 21 | 43 |

| | | | | | | |
|---|---|---|---|---|---|---|
| 37 | 13 | 9 | 6 | 17 | 18 | 42 |
| 36 | 12 | 8 | 5 | 3 | 16 | 41 |
| 35 | 11 | 7 | 4 | 2 | 1 | 40 |
| 27 | 34 | 33 | 32 | 31 | 30 | 26 |

**** RECTANGULAR WAVEGUIDE TM MODES ****

*** LIST OF POINTS WITH FIXED POTENTIALS ***

| POINT NO. | FIXED POTENTIAL |
|---|---|
| 26. | 0.0 |
| 27. | 0.0 |
| 28. | 0.0 |
| 29. | 0.0 |
| 30. | 0.0 |
| 31. | 0.0 |
| 32. | 0.0 |
| 33. | 0.0 |
| 34. | 0.0 |
| 35. | 0.0 |
| 36. | 0.0 |
| 37. | 0.0 |
| 38. | 0.0 |
| 39. | 0.0 |
| 40. | 0.0 |
| 41. | 0.0 |
| 42. | 0.0 |
| 43. | 0.0 |
| 44. | 0.0 |
| 45. | 0.0 |

| | |
|---|---|
| 46. | 0.0 |
| 47. | 0.0 |
| 48. | 0.0 |
| 49. | 0.0 |

**** RECTANGULAR WAVEGUIDE TM MODES ****

```
*****************************
*                           *
* WAVENUMBER =  0.351240E+01 *
*                           *
*****************************
```

*** LIST OF POINTS WITH FREE POTENTIALS ***

| POINT NO. | FREE POTENTIAL | POINT NO. | FREE POTENTIAL | POINT NO. | FREE POTENTIAL |
|---|---|---|---|---|---|
| 1. | 0.176223E+01 | 10. | 0.530802E+01 | 19. | 0.612148E+01 |
| 2. | 0.306624E+01 | 11. | 0.176838E+01 | 20. | 0.529881E+01 |
| 3. | 0.530855E+01 | 12. | 0.306255E+01 | 21. | 0.306296E+01 |
| 4. | 0.353780E+01 | 13. | 0.353913E+01 | 22. | 0.306597E+01 |
| 5. | 0.612143E+01 | 14. | 0.306555E+01 | 23. | 0.353781E+01 |
| 6. | 0.706659E+01 | 15. | 0.176183E+01 | 24. | 0.306126E+01 |
| 7. | 0.306148E+01 | 16. | 0.306614E+01 | 25. | 0.176854E+01 |
| 8. | 0.529837E+01 | 17. | 0.612330E+01 | | |
| 9. | 0.612272E+01 | 18. | 0.353972E+01 | | |

**** RECTANGULAR WAVEGUIDE TM MODES ****

```
*****************************
*                           *
* WAVENUMBER =  0.445397E+01 *
*                           *
*****************************
```

*** LIST OF POINTS WITH FREE POTENTIALS ***

| POINT NO. | FREE POTENTIAL | POINT NO. | FREE POTENTIAL | POINT NO. | FREE POTENTIAL |
|---|---|---|---|---|---|
| 1. | 0.343857E+01 | 10. | -0.503076E+01 | 19. | 0.161587E+00 |
| 2. | 0.303982E+01 | 11. | -0.307510E+01 | 20. | 0.518793E+01 |
| 3. | 0.503045E+01 | 12. | -0.534913E+01 | 21. | 0.534902E+01 |
| 4. | -0.124280E+00 | 13. | -0.625719E+01 | 22. | -0.303996E+01 |
| 5. | -0.162221E+00 | 14. | -0.557363E+01 | 23. | 0.123928E+00 |
| 6. | -0.379145E-03 | 15. | -0.343841E+01 | 24. | 0.304111E+01 |
| 7. | -0.304142E+01 | 16. | 0.557376E+01 | 25. | 0.307498E+01 |
| 8. | -0.518838E+01 | 17. | 0.589469E+01 | | |
| 9. | -0.589514E+01 | 18. | 0.625718E+01 | | |

**** RECTANGULAR WAVEGUIDE TM MODES ****

```
*****************************
*                           *
```

```
                    * WAVENUMBER =  0.572757E+01 *
                    *                            *
                    ******************************
```

*** LIST OF POINTS WITH FREE POTENTIALS ***

| POINT NO. | FREE POTENTIAL | POINT NO. | FREE POTENTIAL | POINT NO. | FREE POTENTIAL |
|---|---|---|---|---|---|
| 1. | 0.423555E+01 | 10. | -0.722959E+00 | 19. | -0.575410E+01 |
| 2. | -0.865831E+00 | 11. | 0.343839E+01 | 20. | 0.231068E+00 |
| 3. | -0.723273E+00 | 12. | 0.596811E+01 | 21. | 0.596708E+01 |
| 4. | -0.335910E+01 | 13. | 0.701597E+01 | 22. | -0.865535E+00 |
| 5. | -0.575428E+01 | 14. | 0.639302E+01 | 23. | -0.335889E+01 |
| 6. | -0.669995E+01 | 15. | 0.423569E+01 | 24. | 0.295809E+00 |
| 7. | 0.295854E+00 | 16. | 0.639280E+01 | 25. | 0.343819E+01 |
| 8. | 0.231174E+00 | 17. | -0.199900E+00 | | |
| 9. | -0.199677E+00 | 18. | 0.701574E+01 | | |

**** RECTANGULAR WAVEGUIDE TM MODES ****

```
                    ******************************
                    *                            *
                    * WAVENUMBER =  0.649038E+01 *
                    *                            *
                    ******************************
```

*** LIST OF POINTS WITH FREE POTENTIALS ***

| POINT NO. | FREE POTENTIAL | POINT NO. | FREE POTENTIAL | POINT NO. | FREE POTENTIAL |
|---|---|---|---|---|---|
| 1. | -0.354605E+01 | 10. | 0.511755E+01 | 19. | 0.581980E+01 |
| 2. | -0.552380E+01 | 11. | -0.312949E+01 | 20. | 0.521314E+01 |
| 3. | -0.511807E+01 | 12. | -0.312158E+01 | 21. | 0.312215E+01 |
| 4. | -0.609645E+01 | 13. | -0.778785E-01 | 22. | 0.552322E+01 |
| 5. | -0.581975E+01 | 14. | 0.323249E+01 | 23. | 0.609648E+01 |
| 6. | 0.301600E-04 | 15. | 0.354531E+01 | 24. | 0.529694E+01 |
| 7. | -0.529640E+01 | 16. | -0.323304E+01 | 25. | 0.312996E+01 |
| 8. | -0.521261E+01 | 17. | 0.165592E+00 | | |
| 9. | -0.165525E+00 | 18. | 0.779877E-01 | | |

**** RECTANGULAR WAVEGUIDE TM MODES ****

```
                    ******************************
                    *                            *
                    * WAVENUMBER =  0.707925E+01 *
                    *                            *
                    ******************************
```

*** LIST OF POINTS WITH FREE POTENTIALS ***

| POINT NO. | FREE POTENTIAL | POINT NO. | FREE POTENTIAL | POINT NO. | FREE POTENTIAL |
|---|---|---|---|---|---|

| | | | | | |
|---|---|---|---|---|---|
| 1. | -0.630834E+01 | 10. | -0.475997E+01 | 19. | 0.563315E-02 |
| 2. | -0.490092E+01 | 11. | 0.530906E+01 | 20. | 0.485730E+01 |
| 3. | -0.475958E+01 | 12. | 0.530509E+01 | 21. | 0.530517E+01 |
| 4. | 0.569102E+00 | 13. | 0.213265E+00 | 22. | -0.490135E+01 |
| 5. | 0.612539E-02 | 14. | -0.544626E+01 | 23. | 0.568581E+00 |
| 6. | -0.334489E+00 | 15. | -0.630854E+01 | 24. | 0.528638E+01 |
| 7. | 0.528674E+01 | 16. | -0.544601E+01 | 25. | 0.530906E+01 |
| 8. | 0.485761E+01 | 17. | -0.116345E+00 | | |
| 9. | -0.116381E+00 | 18. | 0.213469E+00 | | |

# APPENDIX 4

## ORTHOGONAL PROJECTION OF A POINT ONTO A PLANE

### A4.1 GEOMETRY

The geometric configuration used to determine the expressions for the co-ordinates of the orthogonal projection, W', of a general point, W, onto the projection plane $(x_s, y_s)$ is shown in Fig.(A4.1). The projection is made along the $z_s$ direction.The system $(x_v, y_v, z_v)$ is the system where the point W is originally defined. The position of this system related to the projection system $(x_s, y_s, z_s)$ is determined by the distance $\ell$ between the origins of the two systems and by the angles $\alpha$ , $\beta$ , and $\gamma$ , as shown in Fig.(A4.1).The system $(x'_v, y'_v, z'_v)$ is an auxiliary system having the $x'_v$ axis parallel to the projecting plane. The angle $\gamma$ , therefore, corresponds to the rotation angle as defined in Section (4.8.2). By construction, the angles $\alpha$ and $\beta$ correspond respectively to the advancing and elevation angles, also defined in Section (4.8.2). The system $(x'_s, y'_s)$is another auxiliary system having its origin on the orthogonal projection of the origin of the systems $(x_v, y_v, z_v)$ and $(x'_v, y'_v, z'_v)$, and its axes $x'_s$ and $y_s$ ,consist of the orthogonal projection of the axes $x'_v$ and $y_v$, respectively. Finally, a third auxiliary system $(x''_s, y''_s)$ is defined, also with its origin on the point $O'_v$ , but

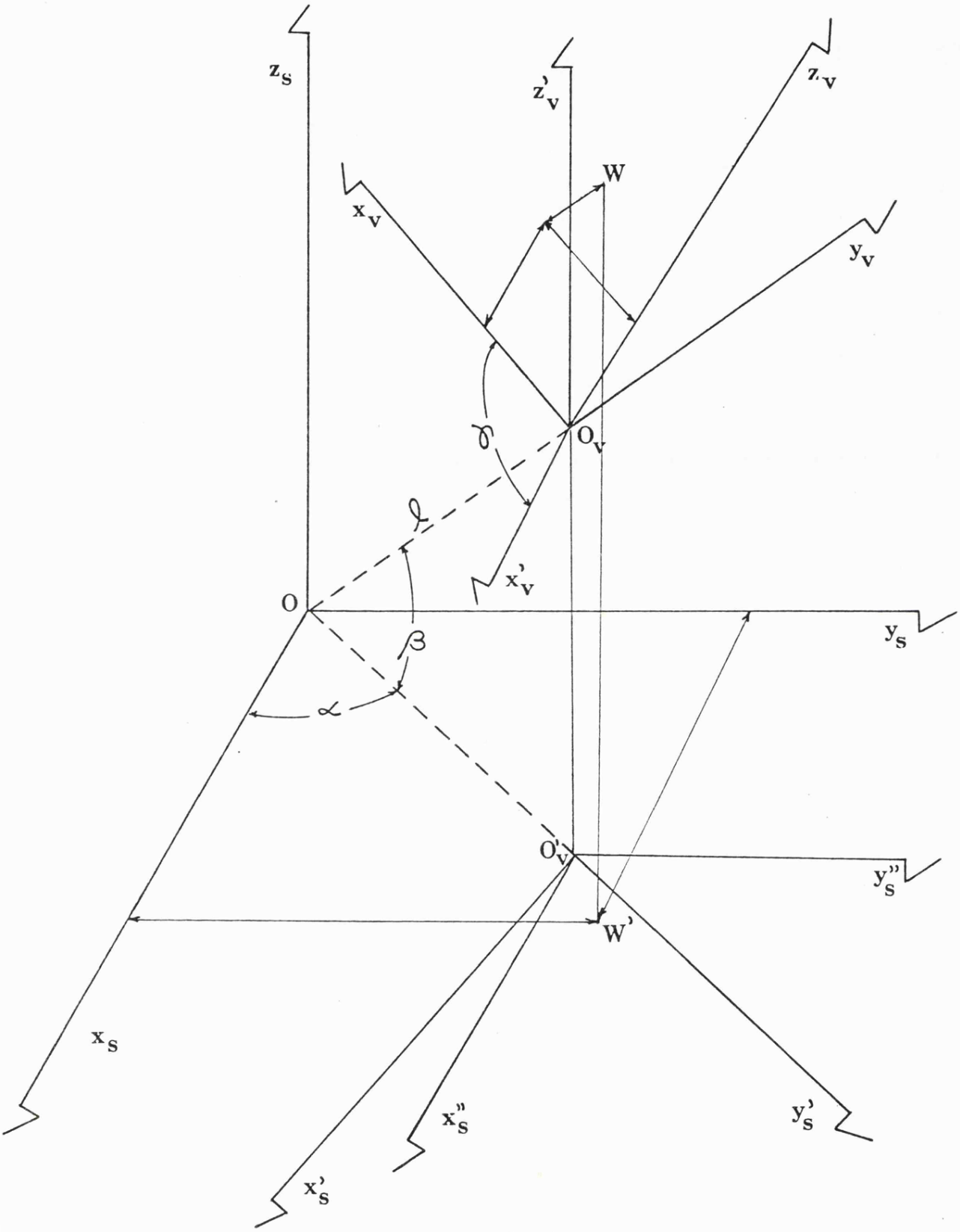


FIG. A4.1 : ORTHOGONAL PROJECTION

Geometry for the determination of the orthogonal projection of the arbitrary point W onto the plane $(x_s, y_s)$

having axes parallel to the projecting axes $(x_s, y_s)$.

A4.2 CO-ORDINATES OF THE POINT $W(x_v, y_v, z_v)$ IN THE SYSTEM $(x'_v, y'_v, z'_v)$

The auxiliary system $(x'_v, y'_v, z'_v)$ is obtained by rotating the system $(x_v, y_v, z_v)$ through an angle $\gamma$ about the $y_v$ axis. The co-ordinates of the point $W(x_v, y_v, z_v)$ in the rotated system are given by:

$$x'_v = x_v \cos\gamma - z_v \sin\gamma \tag{A4.1}$$

$$y'_v = y_v \tag{A4.2}$$

$$z'_v = x_v \sin\gamma + z_v \cos\gamma \tag{A4.3}$$

A4.3 CO-ORDINATES OF THE PROJECTION OF THE POINT $W(x'_v, y_v, z'_v)$ IN THE SYSTEM $(x'_s, y'_s)$

Similarly, the co-ordinates of the projection of the point $W(x'_v, y_v, z'_v)$ on the projecting plane, related to the system $(x'_s, y'_s)$ with its origin on the orthogonal projection of the point $O_v$, are given by:

$$x'_s = x'_v \tag{A4.4}$$

$$y'_s = y_v \cos\beta \tag{A4.5}$$

$$x'_s (z_v) = 0 \tag{A4.6}$$

$$y'_s \ (z_v) = \pm \ z_v \ \sin\beta \qquad (A4.7)$$

Equations (A4.6) and (A4.7) are necessary to represent explicitly the projection of all co-ordinates $z_v$ , because of the elimination of one variable through the process of projecting.

Substitution of equation (A4.1), (A4.2) and (A4.3) into equations (A4.4) to (A4.7) yields:

$$x'_s = x_v \ \cos\gamma - z_v \ \sin\gamma \qquad (A4.8)$$

$$y'_s = y_v \ \cos\beta \qquad (A4.9)$$

$$x'_s \ (z_v) = 0 \qquad (A4.10)$$

$$y'_s \ (z_v) = -(x_v \ \sin\gamma + z_v \ \cos\gamma \ ) \sin\beta \qquad (A4.11)$$

A4.4 <u>CO-ORDINATES OF THE POINT</u> $W(x'_s, y'_s)$ <u>IN THE SYSTEM</u> $(x''_s, y''_s)$

Applying a transformation of co-ordinates, from system $(x'_s, y'_s)$ to the system $(x''_s, y''_s)$, it is possible to write equations (A4.8) to (A4.11) in the form:

$$x''_s = x'_s \ \sin\alpha + y'_s \ \cos\alpha \qquad (A4.12)$$

$$y''_s = - x'_s \ \cos\alpha + y'_s \ \sin\alpha \qquad (A4.13)$$

$$x''_s \ (z_v) = y'_s \ (z_v) \ \cos\alpha \qquad (A4.14)$$

$$y_s''(z_v) = y_s'(z_v) \sin\alpha \qquad (A4.15)$$

Substitution of equations (A4.8) to (A4.11) into equations (A4.12) to (A4.15) leads to:

$$x_s'' = x_v \sin\alpha \cos\gamma + y_v \cos\alpha \cos\beta - z_v \sin\alpha \sin\gamma \qquad (A4.16)$$

$$y_s'' = - x_v \cos\alpha \cos\gamma + y_v \cos\alpha \cos\beta + z_v \cos\alpha \sin\gamma \qquad (A4.17)$$

$$x_s''(z_v) = - x_v \cos\alpha \sin\beta \sin\gamma - z_v \cos\alpha \sin\beta \cos\gamma \qquad (A4.18)$$

$$y_s''(z_v) = - x_v \sin\alpha \sin\beta \sin\gamma - z_v \sin\alpha \sin\beta \cos\gamma \qquad (A4.19)$$

## A4.5 ORTHOGONAL PROJECTION CO-ORDINATES

Once equations (A4.16) to (A4.19) have been obtained, the expressions for the co-ordinates of the orthogonal projection or orthogonal image of the point W can be obtained by shifting the system $(x_s'', y_s'')$ onto the system $(x_s, y_s)$. This gives:

$$x_s = \ell \cos\alpha \cos\beta + x_v \sin\alpha \cos\gamma + y_v \cos\alpha \cos\beta - z_v \sin\alpha \sin\gamma \qquad (A4.20)$$

$$y_s = \ell \sin\alpha \cos\beta - x_v \cos\alpha \cos\gamma + y_v \cos\alpha \cos\beta + z_v \cos\alpha \sin\gamma \qquad (A4.21)$$

$$x_s(z_v) = \ell \cos\alpha \cos\beta - x_v \cos\alpha \sin\beta \sin\gamma - z_v \cos\alpha \sin\beta \cos\gamma \tag{A4.22}$$

$$y_s(z_v) = \ell \sin\alpha \cos\beta - x_v \sin\alpha \sin\beta \sin\gamma - z_v \sin\alpha \sin\beta \cos\gamma \tag{A4.23}$$

Considering that, according to equations (A4.18) and (A4.19) all $z_v$ co-ordinates will project on a straight line passing on the projection of the point $(x_v, y_v, 0)$ with an inclination equal to the complement of the angle $\alpha$ , the expressions for $x_s(z_v)$ and $y_s(z_v)$ can be included in the expressions for $x_s$ and $y_s$ . Thus , equations (A4.20) to (A4.23) can be finally written in the form:

$$\begin{aligned} x\,(W) = {} & x_v\,(\sin\alpha \cos\gamma - \cos\alpha \sin\beta \sin\gamma) \\ & + (\ell + y_v) \cos\alpha \cos\beta \\ & - z_v(\sin\alpha \sin\gamma + \cos\alpha \sin\beta \cos\gamma) \end{aligned} \tag{A4.24}$$

$$\begin{aligned} y\,(W) = {} & - x_v(\cos\alpha \cos\gamma + \sin\alpha \sin\beta \sin\gamma) \\ & + (\ell + y_v) \sin\alpha \cos\beta \\ & + z_v(\cos\alpha \sin\gamma - \sin\alpha \sin\beta \cos\gamma) \end{aligned} \tag{A4.25}$$

# APPENDIX 5

## PROGRAM DESCRIPTION : MXSGUIA

### A5.1 PURPOSE

MXSGUIA generates rectangular waveguide field diagrams for TE and TM propagating modes.

### A5.2 VERSIONS

The program is available in 4 versions. Those versions are obtained at Leicester University by calling the procedure files MXSI, MXSII, MXSIII and MXSIV. The first version is the basic version from which the other versions derive. The versions produce the following outputs:

MXSI : Separate plotting of the electric and magnetic field intensities using current plotting paper.

MXSII : Superposition of the electric and magnetic field plottings using two colours (red and black) on current plotting paper.

MXSIII: Extended version of MXSI with halved mesh length and wide plotting paper.

MXSIV : Extended version of MXSII with halved mesh length and wide plotting paper.

## A5.3 DESCRIPTION

The generation of a rectangular waveguide field diagram by means of any of the previous program versions is accomplished in the following steps:

i) Generation of guide geometry: Based on a cross-section selection by the user, MXSGUIA creates a sample of the rectangular waveguide and divides that sample, regularly, into several perpendicular sections. See Fig.(A5.1).

ii) Field calculations: After receiving information about the propagating mode and the section to be displayed, the program calculates the field values at the intersections of the displaying section with all the other orthogonal sections. (Point P in Fig.(A5.1)).

iii) Field normalization and filtering: The values of the electric and magnetic field components at each point are divided by the maximum absolute valued component in the respective field arrays. Any resulting component having magnitude less than .01 of the magnitude of the largest value of field component is approximated to zero.

iv) Field plotting: A 3D arrow is associated with each field value at each point and its orthogonal image onto the displaying plane plotted. The cross-section and a picture identification number are also drawn. See Fig.(A5.2) for output format and plotter mapping.

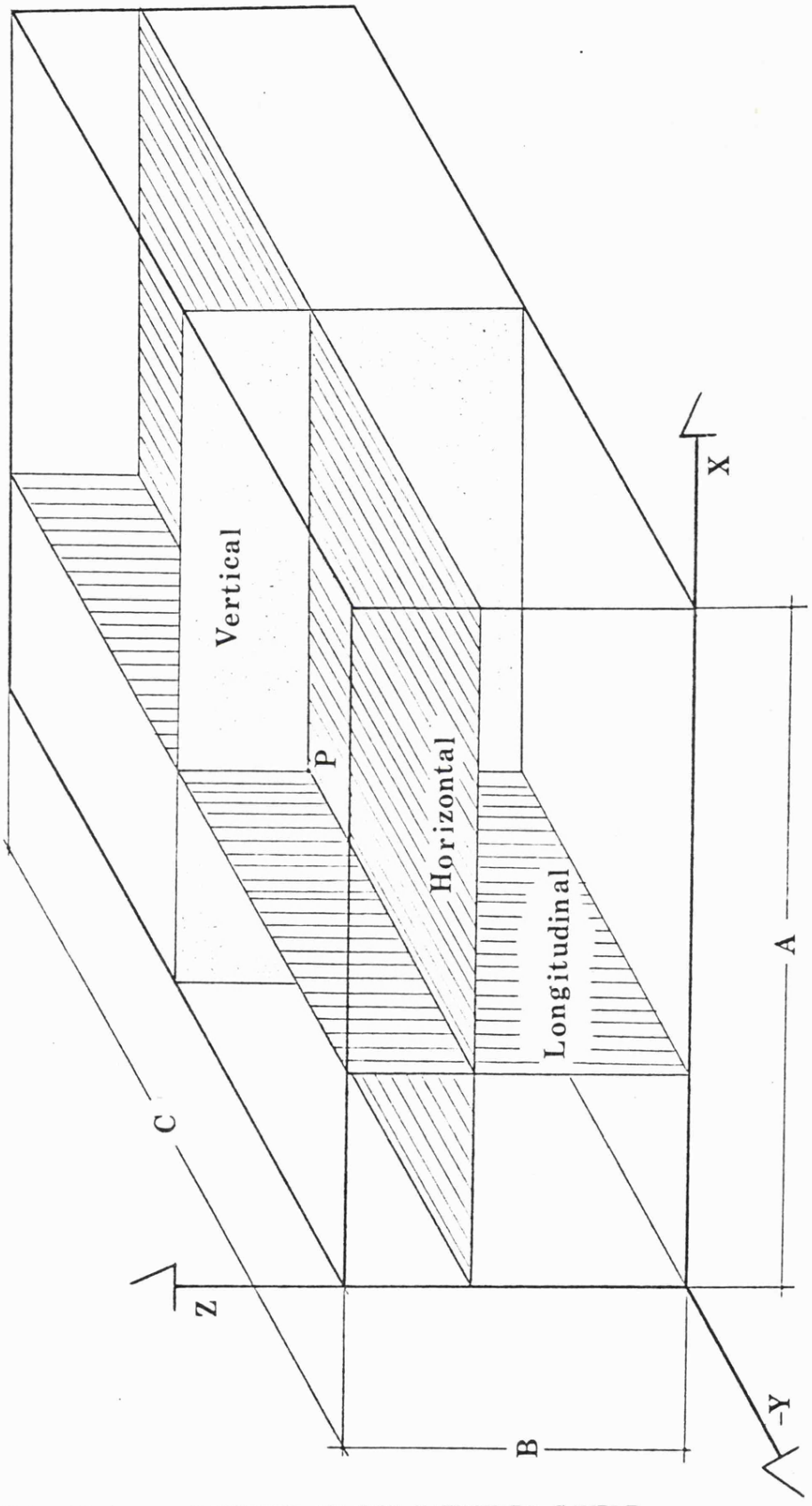


Waveguide cutting planes

FIG. A5.1 : GEOMETRY OF THE WAVEGUIDE SAMPLE

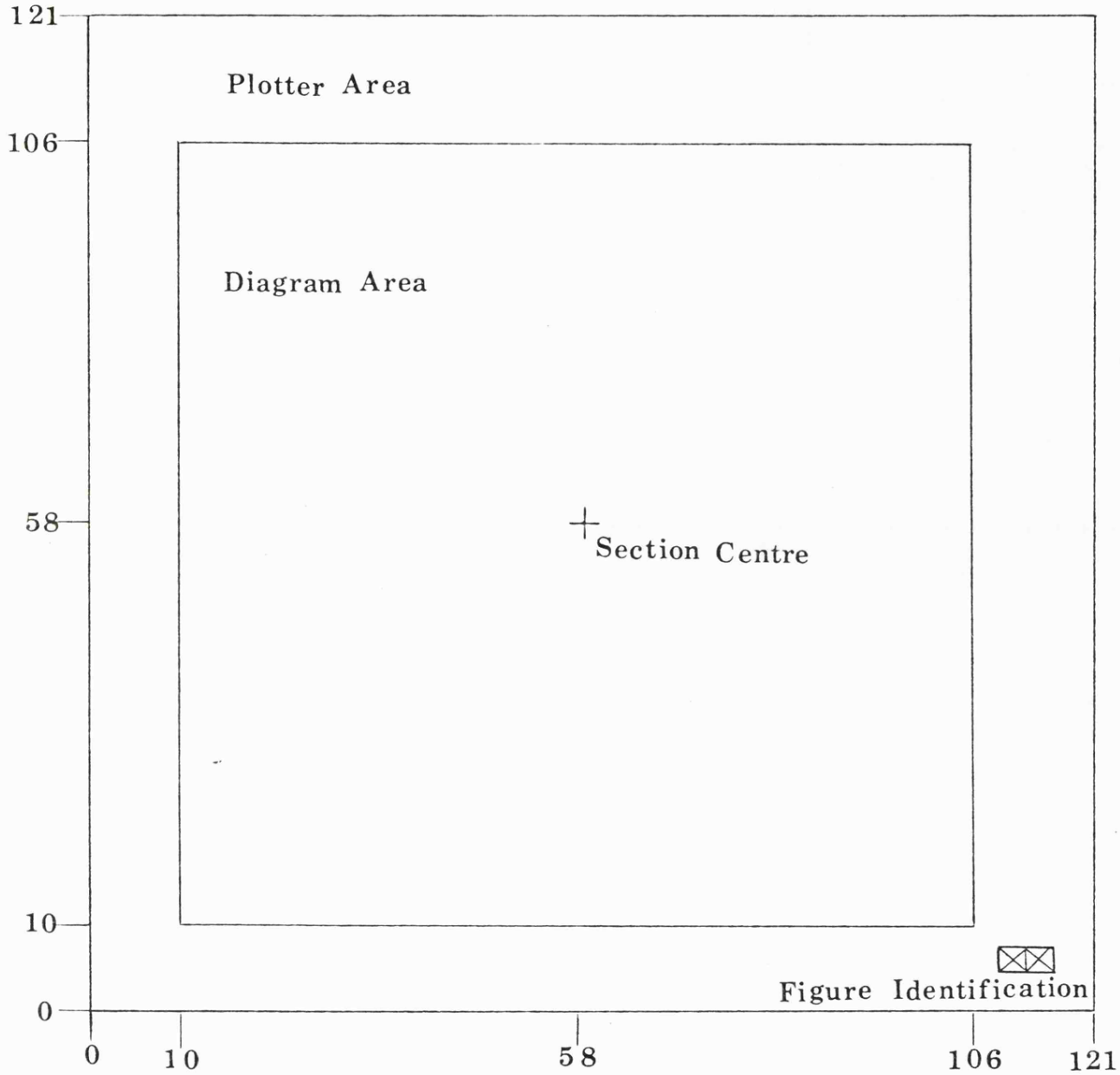


FIG. A5.2 : OUTPUT FORMAT AND MAPPING

## A5.4 INPUT VARIABLES

The input data consists of one control variable (NPLAN) and variables specifying the mode of propagation and the cross-section to be displayed. They are given, by reading order in Table T(A5.1).

The maximum value of the variable IORD = IORDM depends on the variables SHAPE and CUT accoridng to the version being used,as shown in Table T(A5.2).

## A5.5 ERROR INDICATOR

Should the variable IORD accidentally be chosen such that the displaying section is placed outside the waveguide sample boundaries, the program stops and prints:

"DISPLAYING PLANE OF FIG(IDENTIFICATION NUMBER) OUTSIDE WAVEGUIDE"
"EXECUTION DISCONTINUED"
or,
"FIRST DISPLAYING PLANE OUTSIDE WAVEGUIDE"
"EXECUTION DISCONTINUED"

## A5.6 TIMING

See dayfiles DFI, DFII, DFIII and DFIV for typical running and plotting times (UCPT) for each version.

## A5.7 STORAGE

The program uses 5 arrays with (50,50) dimension. No variable dimensioned array is used.

| NAME | VALUE | PURPOSE | FORMAT |
|---|---|---|---|
| NPLAN | | Indicates the number of cross-sections to be displayed during the complete running of the program | I1 |
| SHAPE | | Determines one of the following waveguide cross-sections(Fig.(A5.1) | I1 |
| | 1 | (B/A) = $\frac{1}{4}$ | |
| | 2 | (B/A) = $\frac{1}{3}$ | |
| | 3 | (B/A) = $\frac{1}{2}$ | |
| | 4 | (B/A) = $\frac{2}{3}$ | |
| | 5 | (B/A) = $\frac{3}{4}$ | |
| | 6 | (B/A) = 1 | |
| WAVE | | Indicates TE or TM propagation | I1 |
| | 1 | TE modes | |
| | 2 | TM modes | |
| M,N | | Mode indexes | 2I1 |
| CUT | | Type of cross-section to be displayed | I1 |
| | 1 | Vertical | |
| | 2 | Horizontal | |
| | 3 | Longitudinal | |
| IORD | 0..... .IORDM | Indicates the order of the plane to be displayed, counting from the origin | I2 |

TABLE T A5.1 : INPUT VARIABLES (MXSGUIA)

| SHAPE | CUT | IORDM<br>MXSI<br>MXSII | IORDM<br>MXSIII<br>MXSIV |
|---|---|---|---|
| 1 | 1 | 20 | 40 |
| | 2 | 5 | 10 |
| | 3 | 20 | 40 |
| 2 | 1 | 20 | 40 |
| | 2 | 6 | 12 |
| | 3 | 20 | 40 |
| 3 | 1 | 20 | 40 |
| | 2 | 10 | 20 |
| | 3 | 20 | 40 |
| 4 | 1 | 20 | 40 |
| | 2 | 12 | 24 |
| | 3 | 20 | 40 |
| 5 | 1 | 20 | 40 |
| | 2 | 15 | 30 |
| | 3 | 20 | 40 |
| 6 | 1 | 20 | 40 |
| | 2 | 20 | 40 |
| | 3 | 20 | 40 |

TABLE T A5.2 : VARIABLES SHAPE, CUT and IORDM

```
    FULL  DAYFILE,  78/05/12, 14.48.34,*14.45.14* PAGE    1
14.45.14.MXSJ17.
14.45.15.USER,MXS,
14.45.15.CHARGE,ENGG,ENEL.
14.45.19.CALL,MXSI.
14.45.22.*
14.45.22.*
14.45.22.*    RECTANGULAR WAVEGUIDE DIAGRAMS
14.45.22.*    E AND H FIELDS
14.45.22.*
14.45.22.*
14.45.22.GET,MXSBAG.
14.45.30.GET,MXSNUM.
14.45.30.GET,MXSRWG.
14.45.39.GET,MXSRWH.
14.45.40.ATTACH,CGHOST/UN=LIBS.
14.45.44.LDSET,LIB=CGHOST.
14.45.44.LDSET,LIB=MXSBAG.
14.45.44.LDSET,LIB=MXSNUM.
14.45.44.LDSET,LIB=MXSRWG.
14.45.44.LDSET,LIB=MXSRWH.
14.45.44.MXSGUIA.
14.47.24.   CM LWA+1 = 61302B, LOADER USED  766000B
14.47.39.     STOP
14.47.39.      6.631 CP SECONDS EXECUTION TIME
14.47.39.EXEC,CCPROC.
14.47.40.CALL,CCPROC.
14.47.41.ATTACH,CGPABS/UN=LIBS.
14.47.41.FILE,TAPE98,RT=F,BT=C.
14.47.43.CGPABS(DR=WIDTH,PA=PAPER,PE=PENS,PR=PRIO
14.47.43.R)
14.47.45. *CLUL  CALCOMP PLOTTER POST PROCESSOR
14.48.32. *CLUL FRAMES USED    0000000000000004
14.48.33.UCPQ, 10.
14.48.33.UCPL,        .831METR.
14.48.33.UCPT,       9.882MINS.
14.48.33.     STOP
14.48.33.     19.722 CP SECONDS EXECUTION TIME
14.48.34.GOTO,99.
14.48.34.99,DAYFILE.
```

DFI : TYPICAL DAYFILE (MXSI)

```
    FULL  DAYFILE,  78/05/12, 14.50.13.*14.45.14* PAGE     1

14.45.14.MXSJ18.
14.45.17.USER,MXS,,
14.45.17.CHARGE,ENGG,ENEL.
14.45.21.CALL,MXSII.
14.45.23.*
14.45.23.*
14.45.23.*    RECTANGULAR WAVEGUIDE DIAGRAMS
14.45.23.*    EH FIELDS
14.45.23.*
14.45.23.*
14.45.23.GET,MXSBAG.
14.45.32.GET,MXSNUM.
14.45.33.GET,MXSRWG.
14.45.35.GET,MXSRWF.
14.45.36.ATTACH,CGHOST/UN=LIBS.
14.45.36.LDSET,LIB=CGHOST.
14.45.36.LDSET,LIB=MXSBAG.
14.45.36.LDSET,LIB=MXSNUM.
14.45.36.LDSET,LIB=MXSRWG.
14.45.36.LDSET,LIB=MXSRWF.
14.45.36.MXSGUIA.
14.49.21.  CM LWA+1 = 61447B, LOADER USED  77000B
14.49.36.     STOP
14.49.36.      6.624 CP SECONDS EXECUTION TIME
14.49.36.EXEC,CCPROC.
14.49.37.CALL,CCPROC.
14.49.37.ATTACH,CGPABS/UN=LIBS.
14.49.38.FILE,TAPE98,RT=F,BT=C.
14.49.38.CGPABS(DR=WIDTH,PA=PAPER,PE=PENS,PR=PRIO
14.49.38.R)
14.49.40. *CLUL  CALCOMP PLOTTER POST PROCESSOR
14.50.11. *CLUL FRAMES USED    0000000000000003
14.50.11.UCPQ, 10.
14.50.11.UCPL,        .449METR.
14.50.11.UCPT,      9.747MINS.
14.50.12.     STOP
14.50.12.      19.618 CP SECONDS EXECUTION TIME
14.50.12.GOTO,99.
14.50.13.99,DAYFILE.
```

DFII : TYPICAL DAYFILE (MXSII)

```
    FULL  DAYFILE.  78/05/23. 13.01.26.*12.57.14* PAGE     1

12.57.14.MXSJN4,T222.
12.57.16.USER,MXS,.
12.57.18.CHARGE,ENGG,ENEL.
12.57.22.CALL,MXSIII.
12.57.23.*
12.57.23.*
12.57.23.*     RECTANGULAR WAVEGUIDE DIAGRAMS
12.57.23.*     E AND H FIELDS
12.57.23.*     WIDE PAPER
12.57.23.*
12.57.23.*
12.57.24.GET,MXSVCT.
12.57.25.GET,MXSBAG.
12.57.27.GET,MXSNUM.
12.57.31.GET,MXSRNG.
12.57.33.GET,MXSRNJ.
12.57.36.ATTACH,CGHOST/UN=LIBS.
12.57.37.LDSET,LIB=CGHOST.
12.57.37.LDSET,LIB=MXSVCT.
12.57.37.LDSET,LIB=MXSBAG.
12.57.37.LDSET,LIB=MXSNUM.
12.57.37.LDSET,LIB=MXSRNG.
12.57.37.LDSET,LIB=MXSRNJ.
12.57.37.MXSGUIA.
12.58.00.   CM LWA+1 = 613323, LOADER USED  767000B
12.59.07.      STOP
12.59.07.      15.157 CP SECONDS EXECUTION TIME
12.59.07.EXEC,CGPROD(WIDTH=WIDE)
12.59.09.CALL,CGPROD(WIDTH=WIDE)
12.59.09.ATTACH,CGPABS/UN=LIBS.
12.59.10.FILE,TAPE96,RT=F,BT=S.
12.59.14.CGPABS(DR=WIDE,PA=PAPER,PE=PENS,PR=PRIOR
12.59.14.)
12.59.35. *CLUL  CALCOMP PLOTTER POST PROCESSOR
13.01.24. *CLUL FRAMES USED    0000000000000004
13.01.24.UCPO, 15.
13.01.24.UCPL,       1.766 METR.
13.01.24.UCPT,      25.062 INS.
13.01.25.      STOP
13.01.25.      48.072 CP SECONDS EXECUTION TIME
13.01.25.GOTO,99.
13.01.26.99,DAYFILE.
```

DFIII : TYPICAL DAYFILE (MXSIII)

```
FULL  DAYFILE.  73/05/23. 13.46.57.*13.42.46* PAGE     1

13.42.46.MXSJW6,T222.
13.42.47.USER,MXS,.
13.42.47.CHARGE,ENGG,ENEL.
13.42.51.CALL,MXSIV.
13.42.53.*
13.42.53.*
13.42.53.*    RECTANGULAR WAVEGUIDE DIAGRAMS
13.42.53.*    EH FIELDS.
13.42.53.*    WIDE PAPER
13.42.53.*
13.42.53.*
13.42.53.GET,MXSVCT.
13.42.55.GET,MXSBAG.
13.42.56.GET,MXSNUM.
13.42.57.GET,MXSRNG.
13.42.58.GET,MXSRWI.
13.43.00.ATTACH,CGHOST/UN=LIBS.
13.43.02.LDSET,LIB=CGHOST.
13.43.02.LDSET,LIB=MXSVCT.
13.43.02.LDSET,LIB=MXSBAG.
13.43.02.LDSET,LIB=MXSNUM.
13.43.02.LDSET,LIB=MXSRNG.
13.43.02.LDSET,LIB=MXSRWI.
13.43.02.MXSGUIA.
13.43.46.   CM LWA+1 = 514778, LOADER USED  77100B
13.44.17.     STOP
13.44.17.     15.494 CP SECONDS EXECUTION TIME
13.44.17.EXEC,CGPROG(WIDTH=WIDE)
13.44.19.CALL,CGPROG(WIDTH=WIDE)
13.44.21.ATTACH,CGPABS/UN=LIBS.
13.44.22.FILE,TAPE99,RT=F,DT=9.
13.44.25.CGPABS(DR=WIDE,PA=PAPER,PE=PENS,PR=PRIOR
13.44.25.)
13.44.27. *CDCL  CALCOMP PLOTTER POST PROCESSOR
13.46.53. *CDCL FRAMES USED     0000000000000003
13.46.53.UCPQ, 15.
13.46.53.UCPL,        .915METR.
13.46.53.UCPT,      23.9394MS.
13.46.55.     STOP
13.46.55.     51.408 CP SECONDS EXECUTION TIME
13.46.55.GOTO,99.
13.46.57.99,DAYFILE.
```

DFIV : TYPICAL DAYFILE (MXSIV)

## A5.8 EXAMPLES

### A5.8.1 $TE_{10}$ MODE

This example shows the separated plotting of the electric and magnetic field intensities corresponding to the dominant $TE_{10}$ mode in a rectangular waveguide with the ratio of the narrower to the broader cross-section sides equal to $\frac{1}{2}$.

```
JOBCARD.
USER,USERNAME,PASSWORD.
CHARGE,DEPARTMENT,PROJECT.
CALL,MXSI.
END OF RECORD CARD.
```

(i) 1

(ii) 3

(iii) 1

(iv) 10

(v) 1

(vi) 01

END OF INFORMATION CARD.

(i) Number of cross-sections to be displayed

(ii) Choice of waveguide cross-section

(iii) Selection of TE modes

(iv) Mode indexes

(v) Vertical cross-section

(vi) Selection of the first cross-section after the origin.

### A5.8.2 $TM_{11}$ MODE

Separated diagrams of the electric and magnetic intensities for the first propagating TM mode ($TM_{11}$) in the waveguide of example 1 are generated by this example.

```
JOBCARD.
USER,USERNAME,PASSWORD.
CHARGE,DEPARTMENT,PROJECT.
CALL,MXSI.
END OF RECORD CARD.
1
3
2
11
1
04
END OF INFORMATION CARD.
```

### A5.8.3 $TM_{21}$ MODE

This job produces a two-colour (black and red) diagram with superposition of the electric and magnetic field imtensities for the $TM_{21}$ mode, in the same waveguide.

```
JOBCARD.
USER,USERNAME,PASSWORD.
CHARGE,DEPARTMENT,PROJECT.
CALL,MXSII.
END OF RECORD CARD.
```

1

3

2

21

1

04

END OF INFORMATION CARD.

## A5.9 FURTHER COMMENTS

The wide paper versions MXSIII and MXSIV must be used with care since they have large running and plotting times.

The maximum number of cross-sections to be displayed per run equals 9 and corresponds to, approximately, 1 hour of plotter dedication using current paper.

When more than one waveguide section (NPLAN $\neq$ 1) are to be displayed the data corresponding to each section must start from the variable SHAPE.

## A.5.10 PROGRAM ORGANIZATION

The program consists of one main program MXSGUIA, (available in four versions) calling several auxiliary routines, as shown in Fig.(A5.3). The purpose and the relocatable libraries containing the routines are given in Table T(A5.3).

## A5.11 METHOD

The vector intensities are calculated using the analytical solutions for the electric and magnetic field intensities at a signal

| NAME | PURPOSE | LIBRARY |
|---|---|---|
| MXSGUIA | Main program. Initialization and diagram control. Basic Version. | MXSRWH |
| | Superposition of diagrams. | MXSRWF |
| | Extended MXSRWH version. | MXSRWJ |
| | Extended MXSRWF version. | MXSRWI |
| INICIO | Initialization of variables CUT and WAVE. | MXSRWG |
| REWDE | Read in program data. | MXSRWG |
| REWGE | Generation of waveguide sample. | MXSRWG |
| REWAN | Field calculations. | MXSRWG |
| NORM 2 | Normalization and filtering of transverse field intensities. | MXSNUM |
| NORM 3 | Normalization and filtering of non-transverse field intensities. | MXSNUM |
| PDP 2 | Displaying of transverse field intensities and cross-section boundaries. | MXSRWG |
| PDP 3 | Displaying of non-transverse fields intensities and cross-section boundaries. | MXSRWG |
| QUADRO | Picture identification. | MXSRWG |
| CC935 | | |
| MOVBY2 | Basic graphic routines interfacing GHOST | |
| LINBY2 | graphic package.These routines are not load- | MXSBAG |
| MOVTO2 | ed when the GINO-F graphic package is used. | |
| LINTO2 | | |
| VECT 2 | Experimental 2D vector imaging routine. | MXSVCT |
| VECT 3 | Experimental 3D vector imaging routine. | MXSVCT |

TABLE T A5.3 : PROGRAM ORGANIZATION

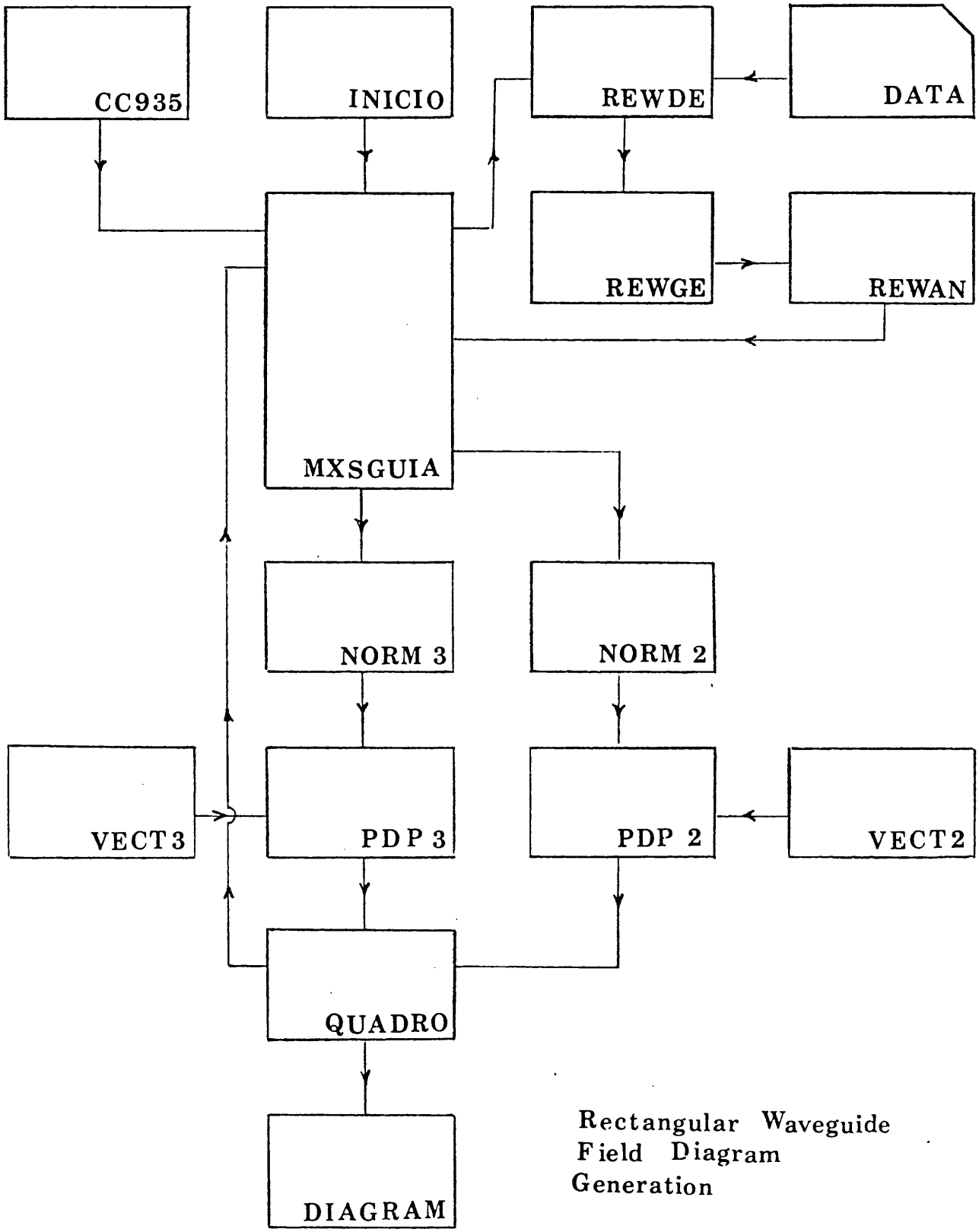


FIG. A5.3 : PROGRAM ORGANIZATION

frequency $\sqrt{5}$ times the cuttoff frequency of the mode being considered as described in Chapter 4. In the waveguide sample geometry used the longitudinal dimension C equals the broader cross-section side, A .

The point of application of a displayed vector image coincides with the point of head and tail intersection for diagrams with separated transverse and longitudinal fields. For diagrams having superimposed fields, the application point coincides with the tail end.

## A5.12 PROGRAM AVAILABILITY

The program is available at Leicester University Engineering Department.

# NOTATION

| | |
|---|---|
| $A$ | Area of a triangle. |
| $A$ | Broader cross-section side length of a typical rectangular waveguide. |
| $A$ | Coefficient |
| $a$ | Broader rectangular waveguide cross-section side length. |
| $a$ | Segment of the 3-dimensional representation of a vector quantity. |
| $\underline{A}$ | General vector function. |
| $\underline{A}$ | Time-harmonic electromagnetic vector potential. |
| $\underline{A}^*$ | Complex conjugate of $\underline{A}$. |
| $A_c$ | Point of the 3-dimensional representation of a vector quantity. |
| $A_c$ | Value of $A(x,y,z)$ at point $P_c$. |
| $A_i$ | Area of a triangle used to determine the area co-ordinates of a point. |
| $a_i$ | Length of an image segment. |
| $a_i^{(d)}$ | Coefficient (d-dimensional model). |
| $a_i^{(k)}$ | Coefficient (d-dimensional model). |
| $a_i^{(r)}$ | Coefficient (d-dimensional model). |

$a_i^{(0)}$ Coefficient (d-dimensional model).

$a_i^{(1)}$ Coefficient (d-dimensional model).

$a_{ij}^{(r)}$ Generic component of a matrix of results.

$a_{ij}^{(1)}$ Generic component of the matrix of results (finite difference formula).

$a_{ij}^{(2)}$ Generic component of the matrix of results (finite element formula).

$a_{ij}^{(3)}$ Generic component of the matrix of results (symmetric finite element formula).

$A_j$ Area of an element.

$a_j^{(k)}$ Coefficient (d-dimensional model).

$A_n$ Amplitude of the $n^{th}$ propagating normal mode.

$\underline{A}(\underline{r})$ Electromagnetic vector potential.

$\underline{A}(\underline{r},t)$ Electromagnetic vector potential.

$A(x,y,z)$ Angular function of the 3 co-ordinates describing the direction of a general vector field.

$a_1$ Coefficient.

$a_2$ Coefficient.

$a_3$ Coefficient

B Narrower cross-section side length of a typical rectangular waveguide.

b Narrower rectangular waveguide cross-section length.

| | |
|---|---|
| $b$ | Segment of the 3-dimensional representation of a vector quantity. |
| $\underline{B}$ | General vector function. |
| $\underline{B}$ | Time-harmonic magnetic flux density. |
| $\underline{B}^*$ | Complex conjugate of $\underline{B}$. |
| $B_c$ | Point of the 3-dimensional representation of a vector quantity. |
| $b_i$ | Length of an image segment. |
| $b_j$ | Triangle base length. |
| $[\ B^e]$ | Gradient of the first-order generating function approximation. |
| $B_n$ | Amplitude of the $n^{th}$ reverse propagating normal mode. |
| $\underline{B}(\underline{r},t)$ | Magnetic flux density. |
| $\underline{B}^*(\underline{r},t)$ | Complex conjugate of $\underline{B}(\underline{r},t)$. |
| $\underline{B}_1$ | Magnetic flux density (medium $M_1$). |
| $\underline{B}_2$ | Magnetic flux density (medium $M_2$). |
| $\underline{B}_{1n}$ | Normal component of $\underline{B}_1$. |
| $\underline{B}_{2n}$ | Normal component of $\underline{B}_2$. |
| $C$ | Boundary of a region S of the cartesian plane. |
| $C$ | Closed curve. |
| $c$ | Light velocity. |
| $c^{(a)}$ | Coefficient. |
| $c^{(b)}$ | Coefficient. |
| $C_c$ | Point of the 3-dimensional representation of a vector quantity. |

| | |
|---|---|
| $c_i$ | Expansion coefficient. |
| $c_\ell$ | Polynomial in triangle area co-ordinates. |
| $C_n$ | Closed curve. |
| $C_n$ | Constant. |
| $c_q$ | Complete polynomial of the N order in generalized volume co-ordinates. |
| $c_q$ | Polynomial in triangle area co-ordinates. |
| CUT | Program variable (MXSGUIA). |
| $C_1$ | Closed curve. |
| d | Distance from the image of the point (a/2,0,0) to the origin of the system $(x'_s, y'_s)$. |
| $\underline{D}$ | Time-harmonic electric flux density. |
| $\underline{D}^*$ | Complex conjugate of $\underline{D}$. |
| $\underline{D}(A_cB_c)$ | Increment to move from point $A_c$ to point $B_c$. |
| $\underline{D}(A_cQ_c)$ | Increment to move from point $A_c$ to point $Q_c$. |
| $\underline{D}(B_cC_c)$ | Increment to move from point $B_c$ to point $C_c$. |
| $\underline{D}(B_cD_c)$ | Increment to move from point $B_c$ to point $D_c$. |
| $D_c$ | Point of the 3-dimensional representation of a vector quantity. |
| $\underline{D}(C_cD_c)$ | Increment to move from point $C_c$ to point $D_c$. |
| $\underline{D}(C_cM_c)$ | Increment to move from point $C_c$ to point $M_c$. |
| $\underline{D}(D_cA_c)$ | Increment to move from point $D_c$ to point $A_c$. |
| $\underline{D}(D_cQ_c)$ | Increment to move from point $D_c$ to point $Q_c$. |

| | |
|---|---|
| $\underline{D}(I_cJ_c)$ | Increment to move from the general picture point $I_c$ to another picture point $J_c$. |
| $d_{i0}$ | Coefficient. |
| $d_{i1}$ | Coefficient. |
| $d_{i2}$ | Coefficient. |
| $dL$ | Line differential. |
| $d_m$ | Minimum detectable distance between two parallel lines on the displaying system. |
| $\underline{D}(M_cP_c)$ | Increment to move from point $M_c$ to point $P_c$. |
| $D_n$ | Constant. |
| $\underline{D}(O_vA_c)$ | Increment to move from point $O_v$ to point $A_c$. |
| $\underline{D}(P_cO_v)$ | Increment to move from point $P_c$to point $O_v$. |
| $\underline{D}(Q_cB_c)$ | Increment to move from point $Q_c$ to point $B_c$. |
| $\underline{D}(Q_cC_c)$ | Increment to move from point $Q_c$ to point $C_c$. |
| $\underline{D}(\underline{r},t)$ | Electric flux density. |
| $\underline{D}^*(\underline{r},t)$ | Complex conjugate of $\underline{D}(\underline{r},t)$ |
| $dS$ | Surface differential. |
| $dV$ | Volume differential. |
| $D_x(A_cB_c)$ | $x_p$ Component of $\underline{D}(A_cB_c)$. |
| $D_x(A_cQ_c)$ | $x_p$ Component of $\underline{D}(A_cQ_c)$. |
| $D_x(B_cC_c)$ | $x_p$ Component of $\underline{D}(B_cC_c)$. |
| $D_x(B_cD_c)$ | $x_p$ Component of $\underline{D}(B_cD_c)$. |
| $D_x(C_cD_c)$ | $x_p$ Component of $\underline{D}(C_cD_c)$. |
| $D_x(C_cM_c)$ | $x_p$ Component of $\underline{D}(C_cM_c)$. |

$D_x(D_cA_c)$ $x_p$ Component of $\underline{D}(D_cA_c)$.

$D_x(D_cQ_c)$ $x_p$ Component of $\underline{D}(D_cQ_c)$.

$D_x(I_cJ_c)$ $x_p$ Component of $\underline{D}(I_cJ_c)$.

$D_x(M_cP_c)$ $x_p$ Component of $\underline{D}(M_cP_c)$.

$D_x(O_vA_c)$ $x_p$ Component of $\underline{D}(O_vA_c)$.

$D_x(P_cO_v)$ $x_p$ Component of $\underline{D}(P_cO_v)$.

$D_x(Q_cB_c)$ $x_p$ Component of $\underline{D}(Q_cB_c)$.

$D_x(Q_cC_c)$ $x_p$ Component of $\underline{D}(Q_cC_c)$.

$D_x(01)$ $x_p$ Component of $\underline{D}(01)$.

$D_x(10)$ $x_p$ Component of $\underline{D}(10)$.

$D_x(12)$ $x_p$ Component of $\underline{D}(12)$.

$D_x(23)$ $x_p$ Component of $\underline{D}(23)$.

$D_x(34)$ $x_p$ Component of $\underline{D}(34)$.

$D_x(41)$ $x_p$ Component of $\underline{D}(41)$

$dx^{(d)}$ Differential of the $d^{th}$ d-dimensional co-ordinate.

$dx^{(1)}$ Differential of the $1^{st}$ d-dimensional co-ordinate.

$dx^{(2)}$ Differential of the $2^{nd}$ d-dimensional co-ordinate.

$D_y(A_cB_c)$ $y_p$ Component of $\underline{D}(A_cB_c)$.

$D_y(A_cQ_c)$ $y_p$ Component of $\underline{D}(A_cQ_c)$.

$D_y(B_cC_c)$ $y_p$ Component of $\underline{D}(B_cC_c)$.

$D_y(B_cD_c)$ $y_p$ Component of $\underline{D}(B_cD_c)$.

$D_y(C_cD_c)$ $y_p$ Component of $\underline{D}(C_cD_c)$.

| | |
|---|---|
| $D_y(C_cM_c)$ | $y_p$ Component of $\underline{D}(C_cM_c)$. |
| $D_y(D_cA_c)$ | $y_p$ Component of $\underline{D}(D_cA_c)$. |
| $D_y(D_cQ_c)$ | $y_p$ Component of $\underline{D}(D_cQ_c)$. |
| $D_y(I_cJ_c)$ | $y_p$ Component of $\underline{D}(I_cJ_c)$. |
| $D_y(M_cP_c)$ | $y_p$ Component of $\underline{D}(M_cP_c)$. |
| $D_y(O_vA_c)$ | $y_p$ Component of $\underline{D}(O_vA_c)$. |
| $D_y(P_cO_v)$ | $y_p$ Component of $\underline{D}(P_cO_v)$. |
| $D_y(Q_cB_c)$ | $y_p$ Component of $\underline{D}(Q_cB_c)$. |
| $D_y(Q_cC_c)$ | $y_p$ Component of $\underline{D}(Q_cC_c)$. |
| $D_y(01)$ | $y_p$ Component of $\underline{D}(01)$. |
| $D_y(10)$ | $y_p$ Component of $\underline{D}(10)$. |
| $D_y(12)$ | $y_p$ Component of $\underline{D}(12)$. |
| $D_y(23)$ | $y_p$ Component of $\underline{D}(23)$. |
| $D_y(34)$ | $y_p$ Component of $\underline{D}(34)$. |
| $D_y(41)$ | $y_p$ Component of $\underline{D}(41)$. |
| $dz$ | $z$ differential. |
| $d_{00}$ | Coefficient. |
| $\underline{D}(01)$ | Increment to move from point 0 to point 1. |
| $d_{01}$ | Coefficient. |
| $d_{02}$ | Coefficient. |
| $\underline{D}_1$ | Electric flux density (Medium $M_1$). |
| $\underline{D}_{1n}$ | Normal component of $\underline{D}_1$. |

| | |
|---|---|
| $\underline{D}(10)$ | Increment to move from point 1 to point 0. |
| $\underline{D}(12)$ | Increment to move from point 1 to point 2. |
| $\underline{D}_2$ | Electric flux density (Medium 2). |
| $\underline{D}_{2n}$ | Normal component of $\underline{D}_2$. |
| $\underline{D}(23)$ | Increment to move from point 2 to point 3. |
| $\underline{D}(34)$ | Increment to move from point 3 to point 4. |
| $\underline{D}(41)$ | Increment to move from point 4 to point 1. |
| $d\beta$ | Phase function differential. |
| $d\Omega$ | Generalized volume differential. |
| $d\omega$ | Angular frequency differential. |
| | |
| $E$ | error |
| $\underline{E}$ | General waveguide electric field intensity. |
| $\underline{E}$ | Time-harmonic electric field intensity. |
| $\underline{E}^*$ | Complex conjugate of $\underline{E}$. |
| $E_L$ | Longitudinal component of $\underline{E}$. |
| $E_L$ | Longitudinal electric field intensity component (Normal modes). |
| $\underline{E}_{Ln}$ | Longitudinal electric field intensity of the $n^{th}$ normal mode. |
| $E_{Ln}^{(3)}$ | Longitudinal electric field intensity component of the $n^{th}$ TM mode. |
| $\underline{E}_n^+$ | Electric field intensity of the $n^{th}$ propagating normal mode. |
| $\underline{E}_n^-$ | Electric field intensity of the $n^{th}$ reverse propagating normal mode. |

| | |
|---|---|
| $e_N^2$ | Error. |
| $\underline{E}_p^{(i)}$ | Electric field intensity of a propagating mode. |
| $\underline{E}_q^{(j)}$ | Electric field intensity of a propagating mode. |
| $\underline{E}(\underline{r})$ | Eletric field intensity. |
| $\underline{E}(\underline{r},t)$ | Eletric field intensity. |
| $\underline{E}^*(\underline{r},t)$ | Complex conjugate of $\underline{E}(\underline{r},t)$. |
| $\underline{E}_T$ | Transverse part of $\underline{E}$. |
| $[\ \underline{E}_T^{(1)}]$ | Set of TEM mode electric field intensities. |
| $[\ \underline{E}_T^{(2)}]$ | Set of TE mode electric field intensities. |
| $[\ \underline{E}_T^{(3)}]$ | Set of TM mode electric field intensities. |
| $[\ \underline{E}_T^{(4)}]$ | Set of electric field intensities. |
| $\underline{E}_{TA}$ | Transverse electric field intensity satisfying the boundary conditions on perfect conducting walls. |
| $\underline{E}_{Ti}$ | General transverse electric field intensity of normal mode waves. |
| $\underline{E}_{Tj}$ | Transverse electric field intensity of the $j^{th}$ mode. |
| $\underline{E}_{Tj}^{(a)}$ | Transverse electric field intensity. |
| $\underline{E}_{Tj}^{(b)}$ | Transverse electric field intensity. |
| $\underline{E}_{Tj}^{(1)}$ | General field within set $[\ \underline{E}_T^{(1)}]$ |
| $\underline{E}_{Tj}^{(2)}$ | General field within set $[\ \underline{E}_T^{(2)}]$ |
| $\underline{E}_{Tj}^{(3)}$ | General field within set $[\ \underline{E}_T^{(3)}]$ |

| | |
|---|---|
| $\underline{E}_{Tm}$ | Transverse electric field intensity of the $m^{th}$ mode. |
| $\underline{E}^*_{Tm}$ | Complex conjugate of $\underline{E}_{Tm}$. |
| $\underline{E}_{Tn}$ | Transverse electric field intensity of the $n^{th}$ mode. |
| $\underline{e}_{Tn}$ | Normalized transverse component of the electric field intensity of the $n^{th}$ mode. |
| $\underline{E}^{(i)}_{Tn}$ | Transverse electric field intensity of the $n^{th}$ mode. |
| $\underline{E}^{(1)}_{Tn}$ | Transverse electric field intensity of the $n^{th}$ TEM mode. |
| $\underline{E}^{(2)}_{Tn}$ | Transverse electric field intensity of the $n^{th}$ TE mode. |
| $\underline{E}^{(3)}_{Tn}$ | Transverse electric field intensity of the $n^{th}$ TM mode. |
| $\underline{E}_{Tp}$ | Transverse electric field intensity of the $p^{th}$ mode. |
| $\underline{E}_{Tq}$ | Transverse electric field intensity of the $q^{th}$ mode. |
| $\underline{E}_T(x,y)$ | Trial transverse electric field intensity function satisfying the boundary conditions. |
| $\underline{E}^{(2)}_T(x,y)$ | Trial transverse electric field intensity - TE modes. |
| $\underline{E}^{(3)}_T(x,y)$ | Trial transverse electric field intensity - TM modes. |
| $\underline{E}_T(0)$ | General transverse electric field intensity satisfying the boundary conditions of the cross-section $z = 0$ . |
| $E_x$ | x Component of the electric field intensity in a rectangular waveguide. |
| $e_x$ | Normalized component of the electric field intensity in the x-direction. |
| $E_y$ | y Component of the electric field intensity in a rectangular waveguide. |

| | |
|---|---|
| $e_y$ | Normalized component of the electric field intensity in the y-direction |
| $E_z$ | z Component of the electric field intensity in a rectangular waveguide. |
| $E_0$ | Arbitrary amplitude constant. |
| $\underline{E}_0$ | Electric field intensity (Normal mode). |
| $\underline{E}_1$ | Electric field intensity (Medium $M_1$). |
| $\underline{E}_{1t}$ | Tangential component of $\underline{E}_1$. |
| $\underline{E}_2$ | Electric field intensity (Medium $M_2$). |
| $\underline{E}_{2t}$ | Tangential component of $\underline{E}_2$. |
| $\underline{E}_\beta$ | Fourier Transform of $\underline{E}(\underline{r})$. |
| $\underline{E}_\beta^*$ | Complex conjugate of $\underline{E}_\beta$. |
| $\underline{E}_{\beta L}$ | Longitudinal component of $\underline{E}_\beta$. |
| $\underline{E}_{\beta T}$ | Transverse component of $\underline{E}_\beta$. |
| % E | Percentual error when estimating central node values. |
| F | Time-harmonic electromagnetic scalar potential. |
| F* | Complex conjugate of F. |
| F(G) | Waveguide scalar functional. |
| $F(G^{(t)})$ | Error functional of the approximation of the solution of Helmholtz equation over the waveguide cross-section. |
| $f_1$ | Node value. |
| $f_n$ | Normalized frequency. |
| $f_r$ | Node value. |

| | |
|---|---|
| $F(\underline{r})$ | Electromagnetic scalar potential. |
| $F(\underline{r},t)$ | Electromagnetic scalar potential. |
| $F^*(\underline{r},t)$ | Complex conjugate of $F(\underline{r},t)$. |
| FT [ ] | Fourier Transform. |
| $\underline{f}(x,y,z)$ | Well behaved vector function of the co-ordinates x,y,and z. |
| $f(x^1,x^2)$ | Scalar function of the variables $x^1$ and $x^2$ . |
| $f_0$ | Central node value. |
| G | D-dimensional generating function. |
| G | Trial scalar function. |
| [ G ] | Global node value finite element matrix. |
| $[\ G^e]$ | Node value element matrix. |
| $G_E^{(2)}$ | Generic approximate TE generating function. |
| $G_i$ | First interval node value. |
| $G_i$ | Node value. |
| $G^{(i)}(x,y)$ | Solution of the homogeneous scalar Helmholtz equation. |
| $G_i^{(2)}(x,y)$ | Generating function of the $i^{th}$ TE mode. |
| $G_{ij}$ | Generic node value. |
| $G_j$ | Node value. |
| $G(j_1,j_2,\ldots j_{d+1})$ | Node values of the d-dimensional element. |
| $G_j^{(2)}(x,y)$ | Generating function of the $j^{th}$ TE mode. |
| $G_k$ | Node value. |
| $G_\ell$ | Node value. |

$G_m^{(2)}(x,y)$ Generating function for the $m^{th}$ TE mode.

$G_m^{(3)}(x,y)$ Generating function for the $m^{th}$ TM mode.

$G_{Mn}(x,y)$ Approximation to the function $G_n(x,y)$.

$G_{Mn}^e$ Generating function expressed as a polynomial in triangle area co-ordinates.

$G_{Mn}^e(x,y)$ Approximation to the function $G_n(x,y)$ inside a first-order element.

$G_{Mn}^{ej}(x,y)$ Generating function inside the $j^{th}$ element.

$G_{mn}^{(2)}$ TE modes generating function for rectangular waveguides.

$G_{mn}^{(3)}$ TM modes generating function for rectangular waveguides.

$G_n(x,y)$ Generic generating function.

$[\ G_n(x,y)]$ Set of functions $G_n(x,y)$.

$G_n^{(i)}(x,y)$ Solution of the homogeneous scalar Helmholtz equation ($n^{th}$ normal mode).

$G_n^{(1)}(x,y)$ Generating function of the $n^{th}$ TEM mode.

$G_n^{(2)}(x,y)$ Generating function of the $n^{th}$ TE mode.

$G_n^{(3)}(x,y)$ Generating function of hte $n^{th}$ TM mode.

$G_p^{(2)}(x,y)$ Degenerate generating function of the $p^{th}$ TE mode.

$G_{pq}^{(2)}(x,y)$ Modified generating function for the $q^{th}$ degenerate TE mode.

$G_{pq}^{(3)}(x,y)$ Modified generating function for the $q^{th}$ degenerate TM mode.

$G_q$ Generic d-dimensional element node value.

$G_q$ Generic higher-order element node value.

$G_q^{(2)}(x,y)$ Degenerate generating function of the $q^{th}$ TE mode.

$G_q^{(3)}(x,y)$ Degenerate generating function of the $q^{th}$ TM mode.

$G_t(F(\underline{r},t))$ General function describing the time domain gauge condition.

$G^{(t)}(x,y)$ Trial function satisfying the boundary conditions.

$G_0$ Central node value.

$G_0$ Constant value of $G_n^{(1)}(x,y)$.

$G_0^{(i)}$ Approximate central node value.

$G_{0j}$ Node value associated with node $N_{0j}$.

$G_{1j}$ Node value.

$G_{2j}$ Node value.

$G\ (F(\underline{r},\omega\ )$ General function describing the frequency domain gauge condition.

h Mesh length.

h Segment of the 3-dimensional representation of a vector quantity.

$\underline{H}$ General waveguide magnetic field intensity.

$\underline{H}$ Time-harmonic magnetic field intensity.

$\underline{H}^*$ Complex conjugate of $\underline{H}$.

$H(G_1,G_2,\ldots G_N)$ Function of the nodal values $G_1,G_2\ldots.G_N$.

$h_j$ Triangle height.

| | |
|---|---|
| $H_L$ | Longitudinal component of H. |
| $H_{Ln}$ | Longitudinal magnetic field intensity of the $n^{th}$ normal mode. |
| $\underline{H}_{Ln}^{(2)}$ | Longitudinal magnetic field intensity of the $n^{th}$ TE mode. |
| $\underline{H}_n^+$ | Magnetic field intensity of the $n^{th}$ propagating normal mode. |
| $\underline{H}_n^-$ | Magnetic field intensity of the $n^{th}$ reverse propagating normal mode. |
| HORZ | Program variable (MXSGUIA). |
| $\underline{H}_p^{(i)}$ | Magnetic field intensity of a propagating mode. |
| $\underline{H}_q^{(j)}$ | Magnetic field intensity of a propagating mode. |
| $\underline{H}_q^{*(j)}$ | Complex conjugate of $\underline{H}_q^{(j)}$. |
| $\underline{H}(\underline{r},t)$ | Magnetic field intensity. |
| $\underline{H}^*(\underline{r},t)$ | Complex conjugate of $\underline{H}(\underline{r},t)$. |
| $\underline{H}_T$ | Transverse part of $\underline{H}$. |
| $\underline{H}_{Tm}$ | Transverse magnetic field intensity of the $m^{th}$ mode. |
| $\underline{H}_{Tn}$ | Transverse magnetic field intensity of the $n^{th}$ mode. |
| $\underline{h}_{Tn}$ | Normalized transverse component of the magnetic field intensity of the $n^{th}$ mode. |
| $\underline{H}_{Tn}^{(i)}$ | Transverse magnetic field intensity of the $n^{th}$ mode. |
| $\underline{H}_{Tn}^{(2)}$ | Transverse magnetic field intensity of the $n^{th}$ TE mode. |
| $\underline{H}_{Tn}^{(3)}$ | Transverse magnetic field intensity of the $n^{th}$ TM mode. |

| | |
|---|---|
| $\underline{H}_T(0)$ | General transverse magnetic field intensity satisfying the boundary conditions on the cross-section z=0 |
| $H_x$ | x Component of the magnetic field intensity in a rectangular waveguide. |
| $h_x$ | Normalized component of the magnetic field intensity in the x-direction |
| $H_y$ | y Component of the magnetic field intensity in a rectangular waveguide. |
| $h_y$ | Normalized component of the magnetic field intensity in the y-direction. |
| $H_z$ | z Component of the magnetic field intensity in a rectangular waveguide. |
| $h_z$ | Normalized component of the magnetic field intensity in the z-direction. |
| $h_{zn}$ | Normalized longitudinal component of the magnetic field intensity of the $n^{th}$ mode. |
| $H_0$ | Part of the waveguide scalar functional associated with the m triangles adjoining node $N_0$. |
| $\underline{H}_0$ | Magnetic field intensity (Normal mode). |
| $H_{01}$ | Part of $H_0$. |
| $H_{02}$ | Part of $H_0$. |
| $H_{01}^0$ | Part of $H_{01}$ depending on the nodal value $G_{0j}$. |
| $H_{02}^0$ | Part of $H_{02}$ depending on the nodal value $G_{0j}$. |
| $\underline{H}_1$ | Magnetic field intensity (Medium $M_1$). |
| $\underline{H}_{1t}$ | Tangential component of $\underline{H}_1$. |

| | |
|---|---|
| $\underline{H}_2$ | Magnetic field intensity (Medium $M_2$). |
| $\underline{H}_{2t}$ | Tangential component of $\underline{H}_2$. |
| | |
| i | Imaginary unity. |
| $I_c$ | General picture point. |
| $I_{cx}$ | $x_p$ Co-ordinate of the point $I_c$. |
| $I_{cy}$ | $y_p$ Co-ordinate of the point $I_c$. |
| ICOL | Program variable (MXSNEX). |
| IDIV | Program variable (MXSNEX). |
| ILIN | Program variable (MXSNEX). |
| IM | Program variable (MXSNEX),(MXSGUIA). |
| $I_{mn}$ | Integral of a typical term appearing (High-order finite element approximations). |
| IORD | Program variable (MXSGUIA). |
| IORDM | Program variable (MXSGUIA). |
| $I_t$ | Time domain action integral. |
| IWAV | Program variable (MXSNEX). |
| $I_1$ | Typical term in the integration of eq.(3.39). |
| $I_2$ | Typical term in the integration of eq.(3.39). |
| $I_3$ | Typical term in the integration of eq.(3.39). |
| $I_4$ | Typical term in the integration of eq.(3.39). |
| | |
| $\underline{J}$ | Time-harmonic electric current density. |
| $\underline{J}^*$ | Complex conjugate of $\underline{J}$. |
| $J_c$ | General picture point. |

| | |
|---|---|
| $J_{cx}$ | $x_p$ Co-ordinate of the point $J_c$. |
| $J_{cy}$ | $y_p$ Co-ordinate of the point $J_c$. |
| $J_M$ | Program variable (MXSNEX),(MXSGUIA). |
| $\underline{J}(\underline{r},t)$ | Electric current density. |
| $\underline{J}^*(\underline{r},t)$ | Complex conjugate of $\underline{J}(r,t)$. |
| $\underline{J}_s$ | Surface current density. |
| K | Integer constant |
| k | Free-space wave-number*. |
| $k_c$ | D-dimensional cut-off wave-number. |
| $k_{cj}$ | Cut-off wave-number of the $j^{th}$ mode. |
| $k_{cm}$ | Cut-off wave-number of the $m^{th}$ mode. |
| $k_{c,mn}$ | Cut-off wave-number of the $TE_{mn}$ or $TM_{mn}$ in a rectangular waveguide. |
| $k_{cn}$ | Cut-off wave-number of the $n^{th}$ mode. |
| $k_{cp}$ | Degenerate cut-off wave-number. |
| $k_{cq}$ | Degenerate cut-off wave-number. |
| $k_{ij}$ | Finite element coefficient. |
| $k_0$ | Finite element coefficient. |
| $k_0$ | Free-space wave-number*. |
| $k_1$ | Finite element coefficient. |

---

* The free-space wave-number is denoted either by k (author's notation) or by $k_0$ (from expressions quoted from reference(25)).

| | |
|---|---|
| $k_{1j}$ | Finite element coefficient. |
| $k_{12j}$ | Finite element coefficient. |
| $k_2$ | Finite element coefficient. |
| $k_{2j}$ | Finite element coefficient. |
| $k_3$ | Finite element coefficient. |
| $k_{3j}$ | Finite element coefficient. |
| | |
| L | Total length of the 3-dimensional representation of a vector quantity. |
| $\ell$ | Segment of the 3-dimensional representation of a vector quantity. |
| $L_g$ | Lagrange function for electromagnetic quantities. |
| $L_g(\underline{E})$ | Lagrange function (Electric field ). |
| $L_g(\underline{E}_\beta)$ | Lagrange function (Fourier Transform of the electric field). |
| $L_i$ | Total length of the frontal image of a vector quantity. |
| $\ell_i$ | Length of an image segment. |
| $l_j$ | Triangle side length. |
| LONG | Program variable (MXSGUIA). |
| | |
| M | Magnitude or intensity of a vector quantity. |
| M | Program variable (MXSNEX),(MXSGUIA). |
| m | Mode index. |
| m | Number of elements adjoining node $N_0$. |
| $M_c$ | Perfect conducting medium. |

| | |
|---|---|
| $M_c$ | Value of M(x,y,z) point $P_c$. |
| $M_c$ | Mobile image point. |
| Mn | Normalizing factor. |
| M(x,y,z) | Scalar function of the 3 co-ordinates describing the intensity of a general vector field. |
| $M(\mu, \varepsilon)$ | Perfect dielectric medium characterized by $\mu$ and $\varepsilon$ . |
| $M_1(\mu_1, \varepsilon_1)$ | Perfect dielectric medium characterized by $\mu_1$ and $\varepsilon_1$. |
| $M_2(\mu_2, \varepsilon_2)$ | Perfect dielectric medium characterized by $\mu_2$ and $\varepsilon_2$. |
| N | Number of element of a model region. |
| N | Order of a polynomial. |
| N | Program variable(MXSNEX),(MXSGUIA). |
| n | Mode index. |
| n | Number of nodes of a d-dimensional element. |
| n | Number of terms of a polynomial. |
| $\underline{n}$ | Unity vector normal to a curve or surface. |
| $[N^e]$ | Shape function. |
| NEX | Program variable (MXSNEX). |
| $N_i$ | Nodal point. |
| $N_i^e(x,y)$ | Component of the shape function. |
| $N_j$ | Nodal point. |
| $N_j^e(x,y)$ | Component of the shape function. |
| $N_k$ | Nodal point. |
| $N_k^e(x,y)$ | Component of the shape function. |
| Nn | Normalizing factor. |

| | |
|---|---|
| NPLAN | Program variable (MXSGUIA). |
| $N_0$ | Central node. |
| $O_v$ | Point of the 3-dimensional representation of a vector quantity. |
| P | Average power flow in a waveguide. |
| p | Arrow assembly diagram parameter. |
| p | Mode index. |
| p | Proportionality factor. |
| $P_c$ | Point of the 3-dimensional representation of a vector quantity. |
| $P_c$ | Point on the sampling plane $\pi$ . |
| $[\ P^e]$ | Matrix describing the polynomial approximation for the generating function. |
| $P_{i,j,k}$ | Generic node of a high-order element. |
| $P_i(s_1)$ | Polynomial of the $i^{th}$ order in the triangle area co-ordinate $s_1$. |
| $P_j(s_2)$ | Polynomial of the $j^{th}$ order in the triangle area co-ordinate $s_2$. |
| $P_{jd+1}(v_{d+1})$ | Polynomial in the generalized volume co-ordinate $v_{d+1}$. |
| $P_{j1}(v_1)$ | Polynomial in the generalized volume co-ordinate $v_1$. |
| $P_{j2}(v_2)$ | Polynomial in the generalized volume co-ordinate $v_2$. |
| $P_k(s_3)$ | Polynomial of the $k^{th}$ order in the triangle area co-ordinate $s_3$. |

$P_m(v_i)$ Polynomial of the $m^{th}$ order in the generic volume co-ordinate $v_i$.

$P_m(z)$ Polynomial of the $m^{th}$ order in z.

$P_n$ Average power flow of each mode propagating in a waveguide.

$P_N^e(s_1,s_2,s_3)$ General N-order polynomial in triangle area co-ordinates.

$P_n^{(2)}$ Average power flow - TE modes.

$P_n^{(3)}$ Average power flow - TM modes.

$P_{pq}^{(i)(j)}$ Average power flow due to the interaction of two non-degenerate propagating modes.

$P(s_1,s_2,s_3)$ Generic point in a triangle (area co-ordinates)

$P_t$ Total average power flow in a waveguide.

$P(v_1,v_2,v_3)$ Generic point in a 3-dimensional element.

$P(x,y)$ Generic point in a triangle (cartesian co-ordinates).

$P(x,y,z)$ Point in a 3-dimensional region.

$P_1$ Vertex of a triangle.

$P_1^e(x,y)$ Complete first-order polynomial defined for each element over the waveguide cross-section.

$P_2$ Vertex of a triangle.

$P_3$ Vertex of a triangle.

Q Finite number

Q Time-harmonic electric charge density.

q Arrow assembly diagram parameter.

| | |
|---|---|
| $q$ | Mode index. |
| $Q^*$ | Complex conjugate of Q. |
| $Q_c$ | Point of the 3-dimensional representation of a vector quantity. |
| $[\ Q^e]$ | High-order element matrices used to decompose the matrix $[\ S^e]$. |
| $[\ Q_i^e]$ | One of the matrices $[\ Q^e]$. |
| $[\ Q^{ij}]$ | Generic element matrix used to decompose the matrix $[S^e]$ (3-dimensional element). |
| $Q(\underline{r},t)$ | Electric charge density. |
| $Q_s$ | Surface charge density. |
| $[\ Q_1^e]$ | One of the matrices $[\ Q_i^e]$ |
| $[\ Q^{12}\ ]$ | One of the matrices $[\ Q^{ij}\ ]$. |
| R | Volume of the 3-dimensional cartesian space. |
| $\underline{r}$ | Position vector. |
| S | Surface. |
| $[\ S\ ]$ | Global finite element matrix. |
| $S_D$ | Subdomain of S. |
| $[\ S^e\ ]$ | Element matrix. |
| SHAPE | Program variable (MXSGUIA). |
| $S_{ij}^e$ | Generic component of $[S^e]$ - first-order element. |
| $S_{\ell q}^e$ | Generic component of $[S^e]$ - high-order and d-dimensional elements. |

| | |
|---|---|
| $S_j$ | One of the surfaces enclosing the volume R. |
| $s_j$ | Generic triangle area co-ordinate. |
| $S_M$ | Model region. |
| $S_n$ | One of the surfaces $S_j$. |
| $s(\underline{r},t)$ | Scalar function of $\underline{r}$ and t (time domain). |
| $s(\underline{r},\omega)$ | Scalar function of $\underline{r}$ and $\omega$ (frequency domain). |
| $s^*(\underline{r},\omega)$ | Complex conjugate of $s(\underline{r},\omega)$. |
| $S_1$ | One of the surfaces $S_j$. |
| $s_1$ | Triangle area co-ordinate. |
| $S_2$ | One of the surfaces $S_j$. |
| $s_2$ | Triangle area co-ordinate. |
| $s_3$ | Triangle area co-ordinate. |
| t | Time. |
| $t_f$ | Time (determined value). |
| $t_i$ | Time (determined value). |
| $[\ T\ ]$ | Global finite element matrix. |
| $[\ T^e\ ]$ | Element matrix. |
| $T^e_{ij}$ | Generic component of $[\ T^e\ ]$ - first-order element. |
| $T^e_{\ell q}$ | Generic component of $[\ T^e\ ]$ - high-order and d-dimensional elements. |
| $\underline{u}_{is}$ | Unity vector along the $i^{th}$ direction in the system $(x_s, y_s, z_s)$. |

| | |
|---|---|
| $\underline{u}_x$ | Unity vector (x direction). |
| $\underline{u}_{xp}$ | Unity vector ($x_p$ direction). |
| $\underline{u}_y$ | Unity vector (y direction). |
| $\underline{u}_{yp}$ | Unity vector ($y_p$ direction). |
| $\underline{u}_z$ | Unity vector (z direction). |
| | |
| V | Volume |
| $\underline{V}$ | Electromagnetic field ($\underline{V} = \underline{E}$ or $\underline{V} = \underline{H}$ ) |
| $\underline{V}$ | General vector field. |
| $\underline{v}$ | General vector function. |
| $\underline{V}_c$ | Vector field at point $P_c$ on the sampling plane $\pi$ . |
| $V_{cis}$ | Component of $V_c$ along the $i^{th}$ direction in the system $(x_s, y_s, z_s)$ |
| $V_{c1s}$ | Component of $V_c$ in the system $(x_s, y_s, z_s)$. |
| $V_{c2s}$ | Component of $V_c$ in the system $(x_s, y_s, z_s)$. |
| $V_{c3s}$ | Component of $V_c$ in the system $(x_s, y_s, z_s)$. |
| $V_e$ | Volume of a 3-dimensional element. |
| VERT | Program variable (MXSGUIA). |
| $v_g$ | Group velocity. |
| $V_i$ | Volume of the $i^{th}$ tetrahedron. |
| $v_i$ | Generalized volume co-ordinate. |
| $V_L$ | Modulus of the maximum longitudinal field component. |
| $\underline{v}_n$ | General transverse field intensity vector. |
| $v_p$ | Phase velocity. |

| | |
|---|---|
| $\underline{v}(\underline{r},t)$ | General vector function of $\underline{r}$ and t (time domain). |
| $\underline{v}(\underline{r},\omega)$ | General vector function of $\underline{r}$ and $\omega$ (frequency domain). |
| $\underline{v}^*(\underline{r},\omega)$ | Complex conjugate of $\underline{v}(\underline{r},\omega)$. |
| $V_T$ | Modulus of the maximum transverse field component. |
| $\underline{v}_T$ | Transverse part of $\underline{v}$. |
| $\underline{v}_T^o$ | Transverse component of v rotated through $(\pi/2)$ rad. |
| W | Arbitrary point of space. |
| W' | Orthogonal image of W on the sampling plane $\pi$ . |
| WAVE | Program variable (MXSGUIA). |
| x | Cartesian co-ordinate. |
| $x_c$ | x Co-ordinate of the point $P_c$. |
| $x^{(d)}$ | D-dimensional co-ordinate. |
| $x^i$ | One of the variables $x^1$ or $x^2$. |
| $x_{i+1}$ | Node co-ordinate. |
| $x_{i+2}$ | Node co-ordinate. |
| $x_p$ | Co-ordinate related to the system associated with the sampling plane $\pi$.(Projection system). |
| $x_p(A_c)$ | $x_p$ Co-ordinate of the orthogonal image of the point $A_c$. |
| $x_p(B_c)$ | $x_p$ Co-ordinate of the orthogonal image of the point $B_c$. |
| $x_p(C_c)$ | $x_p$ Co-ordinate of the orthogonal image of the point $C_c$. |
| $x_p(D_c)$ | $x_p$ Co-ordinate of the orthogonal image of the point $D_c$. |
| $x_p(M_c)$ | $x_p$ Co-ordinate of the orthogonal image of the point $M_c$. |

| | |
|---|---|
| $x_p(O_v)$ | $x_p$ Co-ordinate of the orthogonal image of the point $O_v$. |
| $x_p(P_c)$ | $x_p$ Co-ordinate of the orthogonal image of the point $P_c$. |
| $x_p(Q_c)$ | $x_p$ Co-ordinate of the orthogonal image of the point $Q_c$. |
| $x_p(W)$ | $x_p$ Co-ordinate of the orthogonal image of the point W. |
| $x_p(0)$ | $x_p$ Co-ordinate of the orthogonal image of the point 0. |
| $x_p(1)$ | $x_p$ Co-ordinate of the orthogonal image of the point 1. |
| $x_p(2)$ | $x_p$ Co-ordinate of the orthogonal image of the point 2. |
| $x_p(3)$ | $x_p$ Co-ordinate of the orthogonal image of the point 3. |
| $x_p(4)$ | $x_p$ Co-ordinate of the orthogonal image of the point 4. |
| $x_s$ | x Co-ordinate related to the system associated with the displaying point $P_c$. |
| $x'_s$ | x Co-ordinate of a generic point of an ellipse described by the image of the point (a/2,0,0) on the sampling plane $\pi$. |
| $x_s(W)$ | $x_s$ Co-ordinate of the orthogonal image of the point W. |
| $x_v$ | x Co-ordinate related to the system associated with the vector quantity $\underline{V}_c$. |
| $x_{0j}$ | Node co-ordinate. |
| $x_1$ | Triangle vertex co-ordinate. |
| $x^{(1)}$ | D-dimensional co-ordinate. |
| $x_{1j}$ | Node co-ordinate. |
| $x_2$ | Triangle vertex co-ordinate. |
| $x^{(2)}$ | D-dimensional co-ordinate. |
| $x_{2j}$ | Node co-ordinate. |
| $x_3$ | Triangle vertex co-ordinate. |

| | |
|---|---|
| $y$ | Cartesian co-ordinate. |
| $y_c$ | y Co-ordinate of the point $P_c$. |
| $y_{i+1}$ | Node co-ordinate. |
| $y_{i+2}$ | Node co-ordinate. |
| $y_p$ | Co-ordinate related to the system associated with the sampling plane $\pi$ .(Projection system). |
| $y_p(A_c)$ | $y_p$ Co-ordinate of the orthogonal image of the point $A_c$. |
| $y_p(B_c)$ | $y_p$ Co-ordinate of the orthogonal image of the point $B_c$. |
| $y_p(C_c)$ | $y_p$ Co-ordinate of the orthogonal image of the point $C_c$. |
| $y_p(D_c)$ | $y_p$ Co-ordinate of the orthogonal image of the point $D_c$. |
| $y_p(M_c)$ | $y_p$ Co-ordinate of the orthogonal image of the point $M_c$. |
| $y_p(O_v)$ | $y_p$ Co-ordinate of the orthogonal image of the point $O_v$. |
| $y_p(P_c)$ | $y_p$ Co-ordinate of the orthogonal image of the point $P_c$. |
| $y_p(Q_c)$ | $y_p$ Co-ordinate of the orthogonal image of the point $Q_c$. |
| $y_p(W)$ | $y_p$ Co-ordinate of the orthogonal image of the point W. |
| $y_p(0)$ | $y_p$ Co-ordinate of the orthogonal image of the point 0. |
| $y_p(1)$ | $y_p$ Co-ordinate of the orthogonal image of the point 1. |
| $y_p(2)$ | $y_p$ Co-ordinate of the orthogonal image of the point 2. |
| $y_p(3)$ | $y_p$ Co-ordinate of the orthogonal image of the point 3. |
| $y_p(4)$ | $y_p$ Co-ordinate of the orthogonal image of the point 4. |
| $y_s$ | y Co-ordinate related to the system associated with the displaying point $P_c$. |
| $y'_s$ | y Co-ordinate of a generic point of an ellipse described by the image of the point $(a/2,0,0)$ on the sampling plane $\pi$. |

| | |
|---|---|
| $y_s(W)$ | $y_s$ Co-ordinate of the orthogonal image of the point W. |
| $y_v$ | y Co-ordinate related to the system associated with the vector quantity $\underline{V}_c$. |
| $y_{0j}$ | Node co-ordinate. |
| $y_1$ | Triangle vertex co-ordinate. |
| $y_{1j}$ | Node co-ordinate. |
| $y_2$ | Triangle vertex co-ordinate. |
| $y_{2j}$ | Node co-ordinate. |
| $y_3$ | Triangle vertex co-ordinate. |
| z | Cartesian co-ordinate. |
| z' | Modified z co-ordinate ($z' = k_{cn}\ z$). |
| $Z_{e,mn}$ | Wave impedance for $TM_{mn}$ modes*. |
| $Z_{h,mn}$ | Wave impedance for $TE_{mn}$ modes*. |
| $Z_n$ | Wave impedance of the $n^{th}$ normal mode in waveguides. |
| $Z_n^{(i)}$ | General expression for the wave impedance. |
| $Z_n^{(2)}$ | Wave impedance - TE modes*. |
| $Z_n^{(3)}$ | Wave impedance - TM modes*. |
| z | z Co-ordinate related to the system associated with the sampling plane $\pi$ . (Projection system). |

---

* The wave impedances for TE and TM modes are denoted by either $Z_n^{(2)}$ and $Z_n^{(3)}$ (author's notation) or by $Z_{h,mn}$ and $Z_{e,mn}$ . (See reference (25)).

| | |
|---|---|
| $z_s$ | z Co-ordinate related to the system associated with the displaying point $P_c$. |
| $z_v$ | z Co-ordinate related to the system associated with the vector quantity $\underline{V}_c$. |
| $Z_0$ | Free-space impedance. |
| $z_1$ | Given value of z. |
| $z_2$ | Given value of z. |
| | |
| $\alpha$ | Advancing angle. |
| $\alpha$ | Error distribution variable. |
| | |
| $\beta$ | Elevating angle. |
| $\beta$ | Phase function. |
| $\beta_c$ | Critical angle (Specialized images). |
| $\beta_{c+}$ | Critical angle (General positive images). |
| $\beta_{c-}$ | Critical angle (General negative images). |
| $\beta_j$ | Phase function of the $j^{th}$ propagating mode. |
| $\beta_{mn}$ | Phase function ($TE_{mn}$ or $TM_{mn}$ modes). |
| $\beta_n$ | Phase function of the $n^{th}$ propagating mode. |
| $\beta_p$ | Phase function of the $p^{th}$ propagating mode. |
| $\beta_q$ | Phase function of the $q^{th}$ propagating mode. |
| | |
| | Small angle. |
| | |
| $\gamma$ | Propagation function. |
| $\gamma$ | Rotation angle. |

| | |
|---|---|
| $\gamma_i$ | Propagation function of the $i^{th}$ mode. |
| $\gamma(\underline{E}_T)$ | Propagation function (variational). |
| $\gamma_n$ | Propagation function of the $n^{th}$ mode. |
| $\Delta$ | Generalized volume of the d-dimensional element. |
| $\delta$ | Dirac function |
| $\delta\underline{A}$ | Small variation in $\underline{A}$. |
| $\delta_A I$ | Small variation of I due to a small variation in $\underline{A}(\underline{r},\ )$ |
| $\delta\underline{E}_T$ | Small variation in $\underline{E}_T$. |
| $\delta F$ | Small variation in F. |
| $\delta F(G^{(t)})$ | Small variation of $F(G^{(t)})$. |
| $\delta_F I$ | Small variation of I due to a small variation in $F(\underline{r},\ )$ |
| $\delta G_n^{(i)}(x,y)$ | Small variation of $G_n^{(i)}(x,y)$. |
| $\varepsilon$ | Permittivity. |
| $\varepsilon_1$ | Permittivity (Medium $M_1$). |
| $\varepsilon_2$ | Permittivity (Medium $M_2$). |
| $\theta$ | Angle. |
| $\theta_i$ | Angle at a triangle vertex. |
| $\theta_{ij}$ | Angle at a vertex $N_{ij}$. |
| $\theta_j$ | Angle at a triangle vertex. |
| $\theta_k$ | Angle at a triangle vertex. |

| | |
|---|---|
| $\lambda$ | Angle |
| $\lambda_{cn}$ | Cut-off wavelength of the $n^{th}$ normal mode. |
| $\lambda_g$ | Guided wavelength. |
| $\mu$ | Permeability. |
| $\mu_1$ | Permeability (Medium $M_1$). |
| $\mu_2$ | Permeability (Medium $M_2$). |
| $\sigma_{i,j,k}$ | Polynomial coefficient. |
| $\sigma(j_1, j_2, \ldots j_{d+1})$ | Polynomial coefficient of the d-dimensional finite element model. |
| $\omega$ | Angular frequency. |

## BIBLIOGRAPHY

1. F.L.NG
"Tabulation of methods for the numerical solution of the hollow waveguide problem"
IEEE Trans. Microwave Theory Tech.,Vol.MTT-22, pp 322-329, 1974.

2. H. MOTZ
"Calculation of the electromagnetic field, frequency and circuit parameters of high-frequency resonator cavities"
Jour. Inst. Electr. Engr.,Vol.93, Pt.III, pp 335-343, 1946.

3. J.H. COLLIN and P. DALY
"Calculation for guided electromagnetic waves using finite difference methods"
Jour. Electron. Control, Vol.14, pp 361-380, 1963.

4. M.J. BEAUBIEN and A. WEXLER
"Unequal-arm finite difference operators in the positive-definite overrelaxation (PDSOR) algorithm"
IEEE Trans. Microwave Theory Tech.,Vol. MTT-18, pp 1132-1149,1970.

5. P. SILVESTER and Z.J. CSENDES
"Numerical modeling of passive microwave devices"
IEEE Trans. Microwave Theory Tech,. Vol. MTT-22, pp 190-201, 1974.

6. J.B.DAVIES and C.A. MUILWYK
"Numerical solution of uniform hollow waveguides with boundaries of arbitrary shape"
Proc. IEE, Vol.113, pp 277-284, 1966.

7. R. COURANT
"Variational methods for the solution of problems of equilibrium and vibrations"
Bull. Amer. Math. Soc., Vol.49, pp 1-23, 1943.

8. P.L.ARLETT, A.K. BAHRANI and O.C.ZIENKIEWICZ
"Application of finite elements to the solution of Helmholtz equation"
Proc. IEE, Vol.115, pp 1762-1766, 1968.

9. S. AHMED and P. DALY
"Waveguide solutions by the finite-element method"
The Radio and Elecrtonic Engr., Vol.38, pp 217-223, 1969.

10. P. SILVESTER
"Finite-element solution of homogeneous waveguide problems"
Alta Freq. (Numero Speciale), Vol.38, pp 313-317, 1969.

11. A. KONRAD and P. SILVESTER
"Scalar finite-element program package for two-dimensional field problems"
IEEE Trans. Microwave Theory Tech., Vol. MTT-19, pp 952-954, 1971.

12. K. MORISHITA and N. KUMAGAI
"Unified approach to the derivation of variational expressions for electromagnetic fields"
IEEE Trans. Microwave Theory Tech., Vol. MTT-25, pp 34-40, 1977

13. K. KUROKAWA
"An introduction to the theory of microwave circuits"
Ch. 3, Academic Press, 1969.

14. K. KUROKAWA
"Electromagnetic waves in waveguides with wall impedance"
IRE Trans. Microwave Theory Tech., Vol. MTT-10, pp 314-320, 1962.

15. K KUROKAWA
"The expansions of electromagnetic fields in cavities"
IRE Trans. Microwave Theory Tech., Vol. MTT-6, pp 178-187, 1958.

16. W. KINSNER and E.D. TORRE
"An iterative approach to the finite-element method in field problems"
IEEE Trans. Microwave Theory Tech., Vol. MTT-22, pp 221-228, 1974.

17. Z.J. CSENDES and P. SILVESTER
"FINPLT : A finite element field plotting program"
IEEE Trans. Microwave Theory Tech., Vol. MTT-20, pp 294-295, 1972.

18. P.M. MORSE and H. FESHBACH
"Methods of theoretical physics"
Pt. II, Ch. 9, McGraw-Hill, 1953.

19. M. DECRETON
"Calcul des champs electromagnetiques par la method des elements finis"
Bull. ASE, Vol. 64, pp 1196-1203, 1973.

20. A WEXLER
"Computation of electromagnetics fields"
IEEE Trans. Microwave Theory Tech., Vol. MTT-17, pp 416-439, 1969.

21. W.J. ENGLISH
"Vector variational solutions of inhomogeneously loaded cylindrical waveguide structures"
IEEE Trans. Microwave Theory Tech., Vol. MTT-19, pp 9-18, 1971.

22. R.F. HARRINGTON
"Time-harmonic electromagnetic fields"
Ch. 7, McGraw-Hill, 1961.

23. A.D. BERK
"Variational principles for electromagnetic resonators and waveguides"
IRE Trans. Antennas Propag., Vol. AP-4, pp 104-111, 1956.

24. L.D.LANDAU and E. LIFSHITZ
"Classical theory of fields"
Ch. 2 and Ch. 4, Addison-Wesley, 1951.

25. R.E. COLLIN
"Foundations for microwave engineering"
Ch. 2, McGraw-Hill, 1966.

26. R.E. COLLIN
"Field theory of guided waves"
Ch. 5, McGraw-Hill, 1960.

27. R.W.P. KING
"Transmission line theory"
McGraw-Hill, 1955.

28. A.J. BADEN FULLER
Private communication, Dec. 1977.

29. J. VAN BLADEL
"Expandibility of a waveguide field in terms of normal modes"
Jour. Appl. Phys., Vol. 22, pp 68-69, 1951.

30. J.B. DAVIES
"Review of methods for numerical solution of the hollow waveguide problem"
Pro. IEE, Vol. 119, pp 33-37, 1972.

31. J.H. BRAMBLE and M. ZLAMAL
"Triangular elements in the finite element method"
Math. Comp., Vol. 24, pp 809-820, 1970.

32. O.C. ZIENKIEWICZ
"The finite element method in Engineering Science"
McGraw-Hill, 1971.

33. R.D. COOK
"Concepts and applications of finite element analysis"
John Wiley and Sons, 1974.

34. P. TONG
"Simplex elements of $C^0$ continuity with varying polynomial degrees"
Int. Jour. Num. Meth. Eng., Vol.11, pp 27-38, 1977.

35. P. SILVESTER
"A general high-order finite element waveguide analysis program"
IEEE Trans. Microwave Theory Tech., Vol. MTT-17, pp 204-210, 1969.

36. G.L. MAILE
"The application of an electromagnetic finite element method to waveguide discontinuity problems"
Seminar on numerical method in electromagnetic problems.
University Engineering Department, Cambridge, 1977.

37. P.C. DUNNE

"Complete polynomial displacement fields for finite element methods"

Jour. R. Aeronaut. Soc., Vol. 72, pp 245-246, 1968.

38. A.R.S. PONTER

"The application of dual minimum theorems to the finite element solution of potential problems with special reference to seepage"

Int. Jour. Num. Meth. Eng., Vol. 4, pp 85-93, 1972.

39. E. KREYZIG and C.C. de OLIVEIRA

"Matematica Superior"

Ch. 7, Livros Tecnicos e Cientificos Ed., Rio de Janeiro, 1969.

40. S.S. KUO

"Computer applications of numerical methods"

Ch. 9, Addison-Wesley, 1972.

41. P. SILVESTER

"High-order polynomial triangular finite elements for potential problems"

Int. Jour. Eng. Sci., Vol. 7, pp 849-861, 1969.

42. C.E. SPRINGER

"Geometry and analysis of projective spaces"

Ch. 5, W.H. Freeman and Co., 1964.

43. A.D. MCAULAY
"Variational finite-element solution for dissipative waveguides and transportation application"
IEEE Trans. Microwave Theory Tech., Vol. MTT-25, pp 382-392, 1977

44. A.D. MCAULAY
"The finite element solution of dissipative electromagnetic surface waveguide"
Int. Jour. Num. Eng., Vol. 11, pp 11-25, 1977.

45. P. SILVESTER
"Tetrahedral polynomial finite elements for the Helmholtz equation"
Int. Jour. Num. Meth. Eng., Vol. 4, pp 405-413, 1972.

46. P. DALY and J.D. HELPS
"Exact finite element solutions to the Helmholtz equation"
Int. Jour. Num. Meth. Eng., Vol. 6, pp 529-542, 1973.

47. P. DALY
"Polar geometry waveguides by finite element methods"
IEEE Trans. Microwave Theory Tech., Vol. MTT-22, pp 202-209, 1974.

48. P. DALY
"Finite elements for field problems in cylindrical co-ordinates"
Int. Jour. Num. Meth. Eng., Vol. 6, pp 169-178, 1973.

49. R.L. FERRARI and G.L. MAILE
"Three dimensional finite element method for solving electromagnetic problems"
Electron. Lett., Vol. 14, pp 467-468, 1978.

50. A. KONRAD
"Triangular finite elements for vector fields in electromagnetics"
Ph.D. Thesis, McGill University, Canada, 1974.

51. A. KONRAD
"Vector variational formulation of electromagnetic fields in anisotropic media"
IEEE Trans. Microwave Theory Tech., Vol. MTT-24, pp 553-559, 1976.

52. A. KONRAD
"High-order triangular finite elements for electromagnetic waves in anisotropic media"
IEEE Trans. Microwave Theory Tech., Vol. MTT-25, pp 353-360, 1977.

53. A. CLEMENT-JONES
"An introduction to algebraic geometry"
Ch. 1, Clarendon Press, Oxford, 1912.

54. D.U. VON ROSENBERG
"Methods for numerical solution of partial differential equations"
American Elsevier Publishing Co., 1969.

55. G.E. FORSYTHE and W.R. WASOW
"Finite-difference methods for partial differential equations"
Ch. 3, John Wiley and Sons, 1965.

56. A.M. WINSLOW
"Numerical solution of the quasilinear Poisson equation in a nonuniform triangle mesh"
Jour. Comp. Phys., Vol.2, pp 149-172, 1967.

57. N. MARCUVITZ
"Waveguide Handbook"
Ch. 2, McGraw-Hill, 1951.

58. M.A. EISENBERG and L.E. MALVERN
"On finite element integration in natural co-ordinates"
Int. Jour. Num. Meth. Eng., Vol. 7, pp 574-575, 1974.

59. G.C. BEST
"Helpful formulas for integrating polynomials in three dimensions"
Math. Comp., Vol. 18, pp 310-312, 1964.

60. J.S. HORNSBY and A.GOPINATH
"Numerical analysis of a dielectric-loaded waveguided with a micro-strip line - Finite difference methods"
IEEE Trans. Microwave Theory Tech., Vol. MTT-17, pp 684-690, 1969.

61. D.G. CORR and J.B. DAVIES
"Computer analysis of the fundamental and higher-order modes in a single and coupled microstrip"
IEEE Trans. Microwave Theory Tech., Vol. MTT-20, pp 669-677, 1972.

62. S. RAMO, J.R. WHINNERY and T. VAN DUZER
"Fields and waves in communication electronics"
John Wiley and Sons Ltd., 1967.

63. Sir JAMES JEANS
"The mathematical theory of electricity and magnetism"
Cambridge University Press, 1925.

64. A. J. BADEN FULLER
"Microwaves"
Pergamon Press, 1969.

65. D.H. MCLAIN
"Drawing contours from arbitrary data points"
Comp. Jour., Vol. 17, pp 318-324, 1974.

66. K.W. BRODLIE
"Subroutine DWLSQ1"
Leicester University Computer Laboratory, 1977.

67. M.A. SABIN
"A review of methods for contouring scattered data"
IMA Simposium on Mathematical Methids in Computer Graphics and Design, 1978.

68. D.H. MCLAIN
"Interpolation methods for erroneous data"
IMA Simposium on Mathematical Methods in Computer Graphics and Design, 1978.

69. A. RALSTON and P. RABINOWITZ
"A first course in numerical analysis"
McGraw-Hill Book Co., 1978.

70. P. SILVESTER
"Symmetric quadrature formulae for simplexes"
Math. Comp., Vol. 24, pp 95-100, 1970.

71. Z.J. CSENDES and P. SILVESTER
"Numerical solution of dielectric loaded waveguides : I - Finite Element Analysis"
IEEE Trans. Microwave Theory Tech., Vol. MTT-18, pp 1124-1131,1970.

72. Z.J. CSENDES and P. SILVESTER
"Numerical solution of dielectric loaded waveguides : II - Modal Approximation Technique"
IEEE Trans. Microwave Theory Tech., Vol. MTT-19, pp 504-509, 1971.

73. A. KONRAD
"Linear accelerator cavity field calculation by the finite element method"
IEEE Trans. Nucl. Sci., Vol. NS-20, pp 802-808, 1973.

74. A. KONRAD and P. SILVESTER
"A finite element program package for axisymmetric scalar field problems"
Comp. Phys. Comm., Vol. 5, pp 437-455, 1973.

75. P. SILVESTER and A. KONRAD
"Axisymmetric triangular finite elements for the scalar Helmholtz equation"
Int. Jour. Num. Meth. Eng., Vol. 5, pp 481-497, 1973.

76. A. KONRAD and P. SILVESTER
"Triangular finite elements for the generalized Bessel equation of order m"
Int. Jour. Num. Meth. Eng., Bol. 7, pp 43-55, 1973.

77. A. KONRAD and P. SILVESTER
"A finite element program package for axisymmetric vector field problems"
Comp. Phys. Comm., Vol. 9, pp 193-204, 1975.

78. E.V.D. GLAZIER and M.R.L. LAMONT
"Transmission and propagation"
Services Textbook of Radio, Vol. 5, HMSO, 1958.

79. B. LAX and K.J. BUTTON
"Microwave ferrites and ferrimagnetics"
McGraw-Hill Book Co., 1962.

80. M.L.X. dos SANTOS
"Medida de caracteristicas de ferritas em microondas"
M.Sc. Thesis, ITA, Brazil, 1974.

81. W.J. ENGLISH
"A computer-oriented vector variational solution of loaded rectangular waveguides"
SIAM Jour. Appl. Math., Vol. 21, pp 461-468, 1971.

82. W.J. ENGLISH and F.J. YOUNG
"An E vector variational formulation of the Maxwell's equations for cylindrical waveguide problems"
IEEE Trans. Microwave Theory Tech., Vol. MTT-19, pp 40-46, 1971.

83. A.A. LALOUX, R.J.M. GOVAERTS and A.S. VANDER VORST
"Application of a variation-iteration method to waveguides with inhomogeneous lossy loads"
IEEE Trans. Microwave Theory Tech., Vol. MTT-22, pp 229-236, 1974.

84. D. BEEMAN and J. BOSWELL
"Program WAVGDS"
( CAD Group, Leicester University Engineering Department)

85. A.J. BADEN FULLER
"Engineering field theory"
Pergamon Press, 1973.

86. J.N. LYNESS and C.B. MOLER
"Numerical differentiation of analytic functions"
SIAM Jour. Num. Anal., Vol. 22, pp 202-210, 1967.

87. J.N. LYNESS
"ENTCAF and ENTCRE : Evaluation of normalized Taylor coefficients of an analytic function"
Comm. ACM, Vol. 14, pp 669-675, 1971.

88. Z. KOPAL
"Numerical Analysis"
Ch. 3, Chapman and Hall Ltd., 1955.

89. F.T. KROGH
"Efficient algorithms for polynomial interpolation and numerical differentiation"
Math. Comp., Vol. 24, pp 185-190, 1970.

90. R.B. GUENTHER and E.L. ROETMAN
"Some observations on interpolation in higher dimensions"
Math. Comp., Vol. 24, pp 517-522, 1970.

91. A.C.R. NEWBERY
"Trigonometric interpolation and curve-fitting"
Math. Comp., Vol. 24, pp 869-876, 1970.

92. P. SILVESTER and C.R.S. HASLAM
"Magnetotelluric modelling by the finite element method"
Geoph. Prosp., Vol. 20, pp 872-891, 1972.

93. P. SILVESTER and A. KONRAD

"Analysis of transformer leakage phenomena by high-order finite elements"

IEEE Trans. Power Appar. Syst., Vol. PAS-92, pp 1843-1852, 1973.

94. M. ABRAMOWITZ and I.A. STEGUN

"Handbook of mathematical functions"

Ch. 25, Dover Publications Inc., 1970.

95. P. DALY

"Hybrid-mode analysis of microstrip by finite-element methods"

IEEE Trans. Microwave Theory Tech., Vol. MTT-19, pp 19-25, 1971.